An-Najah National University

Faculty of Graduate Studies

USING ULTRA-HIGH PERFORMANCE CONCRETE FOR ELIMINATING SOFT AND WEAK STORY IRREGULARITIES IN SPECIAL REINFORCED CONCRETE MOMENT RESISTING FRAMED STRUCTURES

By

Ali Mohammad Sharawneh

Supervisors

Dr. Mahmoud M.S Dwaikat

Dr. Monther Dwaikat

This Thesis is Submitted in Partial Fulfillment of the Requirements for the Degree of Master of Structural Engineering, Faculty of Graduate Studies, An-Najah National University, Nablus- Palestine.

2022

USING ULTRA-HIGH PERFORMANCE CONCRETE FOR ELIMINATING SOFT AND WEAK STORY IRREGULARITIES IN SPECIAL REINFORCED CONCRETE MOMENT RESISTING FRAMED STRUCTURES

By

Ali Mohammad Sharawneh

This thesis was Defended Successfully on 27/2/2022 and Approved by

Defense Committee Member	**Signature**
-Dr. Mahmoud M.S Dwaikat / Supervisor	…………………….
-Dr. Monther Dwaikat / Co-Supervisor	…………………….
-Dr. Abdulsamee Halahal/ External Examiner	…………………….
-Dr. Munther D. Ibrahim/ Internal Examiner	…………………….

Dedication

This work is dedicated to:

The sake of Allah, my creator who gave me strength for everyday life.

My great teacher Mohammed “May Allah bless and grant him”, who taught us the purpose of life.

My homeland Palestine, the symbol of sacrifice.

My parents, who have always loved me unconditionally this document are heartily dedicated to my mother.

My dearest wife, who makes it possible for me to complete this work.

My family, who help me to be who I am.

My friends, who encouraged me.

My colleagues in the Ministry of public works and housing, who support me.

All the people in my life who touch my heart, I dedicate this work.

Acknowledgment

Primarily, I would like to express my gratitude to Allah for being able to complete this document, then I would like to thank my supervisors, Dr. Mahmoud M.S Dwaikat and Dr. Monther Dwaikat who gave me the opportunity to undertake such great challenging work, I am grateful to them for their guidance, encouragement, understanding and insightful support in the development process.

Last but not least I would like to sincere acknowledgment to all those whom I might have missed mentioning above who have helped me in this work.

May the almighty God richly bless all of you.

Declaration

I, the undersigned, declare that I submitted the thesis entitled:

USING ULTRA-HIGH PERFORMANCE CONCRETE FOR ELIMINATING SOFT AND WEAK STORY IRREGULARITIES IN SPECIAL REINFORCED CONCRETE MOMENT RESISTING FRAMED STRUCTURES

I declare that the work provided in this thesis, unless otherwise referenced, is the researcher's own work, and has not been submitted elsewhere for any other degree or qualification.

Student's Name: **Ali Mohammad Sharawneh**

Signature:

Date: **2022/02/27**

Table of Contents

Table of Figures

Lists of Tables

List of Appendices

USING ULTR- HIGH PERFORMANCE CONCRETE FOR ELIMINATING SOFT AND WEAK STORY IRREGULARITIES IN SPECIAL REINFORCED CONCRETE MOMENT RESISTING FRAMED STRUCTURES

By
Ali Mohammad Sharawneh
Supervisor
Dr. Mahmoud M.S Dwaikat
Co-Supervisor
Dr. Monther Dwaikat

Abstract

Multistory buildings are common in Palestine and sometimes are built with a ground floor that has an open space or is higher than the rest floors for commercial purposes. Therefore, the soft and weak story irregularities may occur on the ground floor. This research aims to eliminate the soft or weak story irregularities in the design stage without affecting the architectural requirements by changing the columns material from normal strength concrete (NSC) to ultra-high performance concrete (UHPC) in the soft or weak story.

To quantify the effect of the material switch from NSC to UHPC on the column strength and stiffness, a parametric study using sectional stress analysis is performed. Overall, 216 NSC and UHPC columns cross-sections are analyzed under the following parameters: axial load levels, longitudinal reinforcement ratio, cross-section width, and cross-section depth to width ratio.

The effectiveness of using UHPC on the column stiffness is studied where the change in the flexural rigidity is represented using the ratio of the effective flexural rigidity (EI_e) of UHPC columns to NSC columns. Also, the validity of cracking analysis modifiers of NSC columns is established for UHPC columns.

The effectiveness of using UHPC on the column strength is investigated using the ratio of the moment capacity of the UHPC columns to NSC columns. After that, the adequacy of the column shear capacity is checked, and found that the lateral strength of the UHPC column is still controlled by the moment strength.

Moreover, regression analysis is performed for the parametric study results to create equations that predict the increase in the sectional stiffness and strength of the columns.

Finally, a 3D sway special moment-resisting framed building is used as a case study to confirm the sectional analysis results and to investigate the frame's overall behavior before and after using UHPC in the soft/weak story columns. The frame is designed according to ASCE7-16 and ACI318-19 and has both an extremely soft story and weak story irregularities on the ground floor. Nonlinear static analysis (pushover) is performed for the frame using SAP2000. The frame analysis results agree well with the parametric study results. In addition, the overall behavior of the frame is enhanced when the UHPC is used since the displacement and the plastic hinges do not concentrate on the soft/weak story.

In summary, switching the columns material in the soft/weak story from NSC to UHPC can be safely used to eliminate the soft/weak stories irregularities at the design stage without changing the architectural or functional restriction.

Keywords: vertical irregularity, stiffness, strength, soft story, weak story, flexural moment rigidity, XTRACT, cracking analysis modifiers, ultra-high performance concrete (UHPC), plastic hinge, nonlinear static (pushover).

Chapter One

Introduction

1.1 General Background

Earthquakes are natural disasters with unpredictable occurrences and effects. Earthquakes are the vibrational motion generated under the ground surface by natural events such as tectonic movements, volcanic events, and collapses of cavities, or by artificial events like explosions. The relative movements of the tectonic plates at the earth's crust explain 90% of the earthquakes phenomena (Duggal, 2013, Armouti, 2008, Alnajajra, 2017).

Most of the earthquake losses are caused by the collapse of buildings, which leads to material and human losses. A devastating earthquake occurred in Palestine in 1927 and destroyed many buildings resulting in many deaths (SASPARM Project, 2014, Shehadah, 2017).

Most buildings support gravity loads safely without considering lateral loads, although these buildings might not be capable of resisting lateral loads like earthquakes (Alnajajra, 2017). Reinforced concrete buildings must have lateral force resisting systems to resist earthquakes and to provide a continuous load pattern for the seismic forces (Moehle, 2015).

The lateral force resisting system represents all structural elements considered in the seismic design (ASCE, 2016). The lateral force resisting system includes vertical elements that transfer the load to the ground including the shear wall, braced frame, and moment-resisting frames. The lateral force is distributed among the vertical elements through the horizontal elements such as the slab diaphragm (Taranath, 2004). The lateral force resisting systems for concrete structures are grouped to the shear wall, moment resting frame, and combination of them (Taranath, 2009).

A building is more vulnerable to failure when an irregularity exists. Building design codes usually classify the irregularities of buildings into two main categories; vertical and horizontal irregularities. Soft and weak story irregularities are types of vertical irregularities, and it is considered the main reason for the collapse of many buildings during earthquakes. For example, 725 buildings from 1215 were destroyed in the 1999 Izmit earthquake due to the soft and weak story irregularities (Kirac et al., 2011).

In Palestine, many buildings are built with an open space floor on the ground floor without including masonry and infill walls for different purposes such as car parking or other commercial purposes. In addition, the height of the ground floor is usually greater than the rest building floors. These types of buildings lead to soft/weak stories irregularities on the ground floors due to reducing story stiffness and strength. This type of soft/ weak story in the building is becoming a traditional building style in our locality. Figure 1 displays a building with soft/weak story irregularities in Ramallah city.

Figure 1:

A building with soft/weak story irregularities in Ramallah city.

Ultra-High Performance Concrete (UHPC) is a new generation of cementitious materials that have a better performance compared to normal and high-strength concretes in mechanical properties, durability, and other properties. UHPC has been continuously developed to turn it into a regular technology in both fields of construction and retrofitting.

UHPC material has excellent mechanical properties such as high compressive strength, improved tensile strength, modulus of elasticity, compressive ductility, shear strength, and excellent bond and confinement characteristics. These features encourage using UHPC in the design of earthquake-resistant moment frame members. The failure of UHPC is different totally from the typical failure modes in the flexural concrete members of moment frames. The confinement improvement, bar stability, and preventing premature concrete distress are achieved when UHPC are used. Therefore using UHPC enhances the resistance to strong seismic forces (Chao et al., 2016).

1.2 Problem Statement

Some of the common vertical irregularities are caused by abrupt changes in the stiffness and strength of consecutive stories and these are called soft story and weak story irregularities, respectively. Generally, stiffness and strength are related, therefore the soft and the weak story almost exist together (Sadashiva et al., 2012, Chopra, 2012).

The variation of stiffness or strength between the soft or weak story and the adjacent above floors comes due to many reasons. The base floor is usually used as parking or for other commercial purposes, therefore it is built as an open space without infill or masonry walls in contrast to the rest of the above floors. Also, for commercial usage, the base floor may be built higher than the rest of the floors (Kirac et al., 2011). In addition, the soft or weak story irregularity can exist due to reducing the number or the area of the section of the vertical elements of the lateral resisting system in the soft or weak story mainly due to architectural requirements (Guevara-Perez, 2012).

Simplified codes methods of analysis of the story with a soft or weak story irregularity do not represent the correct behavior of the building during the earthquake (Valmundsson et al., 1997, Varadharajan et al., 2013, Villaverde, 1991, Thuat, 2011). The stiffness and strength of the masonry and infill walls are usually neglected in the design and considered as non-structural elements and only their weight is considered in the seismic design of the building in Palestine. These non-structural elements may have a considerable effect on the seismic response of the building (Chandrahas et al., 2017).

The weak story may lead to a total collapse of the structure although the upper stories of the structure may remain in an elastic state. This is because of the concentration of displacement in the soft/weak story which leads to an increase in the rotation demands at the columns in the irregular story more than their rotational capacity, leading to poor distribution of plastic hinges and energy absorption mechanisms. Also, collapse may be due to instability of the building (P-Delta effect) with large displacement concentrated at the soft/weak story level and the high gravity loads from the upper floors (Chandrahas et al., 2017, Mezzi et al., 2005, Guevara-Perez, 2012). Several researchers have studied the behavior of the soft and weak stories and many collapses of the soft-story buildings have occurred in the past. Most building design codes have requirements for maximum stiffness and strength differences between adjacent floors.

It is mostly architectural or functional requirements that lead to soft/weak story irregularities. The prevalence of soft/weak story irregularities in Palestine necessitates a structural solution that does not negate or disfunction the architectural requirements of having an open space garage for instance.

Different techniques were used to increase the stiffness and strength of existing soft and weak stories such as using steel dampers, steel bracing, concrete jacketing, and other techniques (Kirac et al., 2011). Most of these techniques are either intrusive, expensive, or require high skill to install. In this research, a new technique that is simpler and more efficient will be investigated where the normal strength concrete (NSC) is replaced with UHPC at the conceptual or design phase. Where UHPC is expected to increase the stiffness and lateral strength of the columns for the irregular story. This newly proposed technique will be used to eliminate the soft and weak stories irregularities in the base story in sway-special reinforced concrete moment frames.

The study will quantify the effect of replacing NSC with UHPC on both stiffness and strength of the soft story and weak story and study the conditions under which such replacement will be sufficient to prevent the soft/weak story irregularity. Guidelines on using UHPC will be presented in this study.

1.3 Research Questions

It is important to mention that this solution is preventive in nature, and thus can only be used at the conceptual design phase of the building. It is intended to provide a viable alternative for eliminating the soft/weak story problem without sacrificing the architectural or functional requirements of the building. Therefore, the main focus of this research will be directed to answering two main categories of questions:

- To what extent can the replacement of NSC by UHPC in columns increase the stiffness and strength of the irregular story?
- How will the building response during earthquakes be affected by replacing NSC with UHPC?

1.4 Research Objectives

To come to conclusions regarding the previous research questions the research will be performed in accordance with the following objectives:

1.4.1 Research Overall Objective

The main objective of this study is to develop design guidelines for eliminating soft and weak story irregularities using UHPC instead of NSC in columns of soft or weak stories, particularly at the base level, while maintaining the architectural and functional aspects of the building.

Generally, using UHPC instead of NSC in the columns at the irregular story can have positive effects on the lateral stiffness of the soft story, lateral strength of the weak story, and the ductility of the irregular structure during earthquakes. Increasing the lateral stiffness and strength of the story can prevent the collapse of the structure during the earthquake and enhance the response of the building. The goal here is to propose a methodology for quantifying how successful this replacement is in eliminating a soft/weak irregularity.

1.4.2 Research Sub-objectives

To achieve the main objective mentioned above, the following sub-objectives will be achieved:

- Survey the common building codes for the design of irregular buildings, particularly for the soft and weak story irregularities.
- Quantify the increase in the lateral stiffness of the column when the UHPC material is used instead of NSC.
- Quantify the increase in the lateral strength of the column when UHPC material is used instead of NSC.
- Investigate the change in the cross-sectional property modifiers due to cracking when the UHPC material is used instead of NSC.

The previous objectives will result in establishing the response of the member (or cross-section) UHPCmaterial.

- Investigate, through a representative case study, the impact of using UHPC material instead of NSC in the columns of the soft and weak story on the overall stiffness, strength, and response of the building in the case study, and to check if the desired impact conforms with the predictions based on the cross-sectional response.

1.5 Research Scope and Limitations

The scope of this thesis is to provide a solution to soft/weak story problems at the design phase of the building. It is not intended as a retrofitting or remedial technique for existing buildings.

In particular, a sway special moment-resisting frame designed according to ACI 318-19 will be used as a representative earthquake resisting system. The position of the soft and weak is assumed at the base floor. The selected frames do not have any horizontal irregularities. Thus, the class of building in our mind is generally code-designed and possesses sufficient lateral resistance to earthquake loads except for the soft/weak story problems in them due to architectural restrictions. Thus, a building with many types of seismic irregularities or deficiencies is beyond the scope of this research.

1.6 Structure of Thesis

The thesis contains 5 chapters divided as follows:

Chapter 1-Introduction: Chapter 1 includes the research problem, research questions, research objectives, and research scope and limitations.

Chapter 2-Literature review: This chapter includes three main sections which are seismic behavior of irregular buildings, UHPC material, and UHPC members. The seismic behavior of irregular buildings section includes a description of the seismic design of the regular and irregular buildings with more details on the soft and weak stories according to common building codes. In addition, the section contains a detailed literature review of the seismic performance of buildings with vertical irregularities and weak/soft stories failure mechanisms. Moreover, the methods of improving seismic performance for the existing building and eliminating soft/weak stories at the design stage are also reviewed in this section. In the

UHPC material section, a brief review of UHPC material characteristics, development, mechanical properties, and design guidelines and standards will be presented. The UHPC members section includes a detailed description of the flexural rigidity, shear strength, and axial strength of members made of UHPC.

Chapter 3-Modeling: This chapter describes the model assumptions, material models, sections and frame details, and the programs used. In addition, the verification and validation of the models are presented.

Chapter 4-Parametric Study: In this chapter, sectional analysis is performed with carefully selected important parameters to investigate the stiffness and strength increase of the section due to using UHPC as compared to NSC material. Parameters used loads, and methods of analysis are discussed in this chapter.

Chapter 5-Case Study: 3D Frame Analysis: This chapter presents the overall response of a building after changing the column materials at the soft/weak story. The results will compare the results from the sectional analysis chapter.

Chapter 6 (Conclusions, recommendations, and future work): Chapter 6 includes the conclusions from the research with the results from chapters 4 and 5. Recommendations and future work are also presented.

Chapter Two

Literature Review

2. Literature Review

2.1 Overview

In this chapter, the literature related to this research will be studied. In the beginning, the seismic behavior of irregular buildings will be reviewed. Therefore, the seismic design of regular structures and the definition of building irregularities will be reviewed. Then the soft and weak story irregularities will be explained in depth. After that, common methods of improving the seismic performance of soft and weak stories will be presented.

The UHPC as a material will be discussed in detail including the definition, development, mechanical properties, and UHPC codes and design guidelines. Finally, the literature related to UHPC members includes the flexural moment capacity and one-way shear strength of the UHPC beam and column will be gathered. In addition, the previous studies for investigating the use of UHPC material in structural members will be discussed in this chapter.

2.2 Seismic Behavior of Irregular Buildings

In this section, all related literature to explain the seismic behavior of irregular buildings is gathered and discussed.

2.2.1 Seismic Design of Regular Structures and Seismic Design Objectives

When the earthquake shakes the building, the upper parts of the building resist the change of their original position relative to the base because of the inertia forces that develop in response to acceleration (Duggal, 2013).

Stiffness, strength, and ductility criteria are considered in the seismic design. Based on these three criteria, the design approaches are classified to (Murty et al., 2012):

- Strength-Based design (considering stiffness and strength): This approach is common in building codes and is classified as forced-based design and/or capacity design approaches. The building is designed to resist the stress resulting from the equivalent lateral load specified by the codes. The sequences of the plastic hinge formation in the members are not considered and the structural members are assumed to behave adequately in the non-linear range. The inelastic behavior of the building is incorporated as a single reduction factor "R" and the members are designed to the shear forces from the elastic analysis.

- Deformation-Based Design (considering stiffness, strength, and ductility): The building is designed for both stress resulting from linear structural analysis for the code lateral forces, and from equilibrium-compatible stress resultant from the collapse mechanism. This approach gives a better prediction of building performance compared to the strength design approach and requires more engineering experience.
- Energy-Based Design (considering stiffness, strength, ductility, and energy dissipation capacity): This approach is under research. The mechanical energy of the building is the sum of kinetic energy, elastic energy, energy dissipated through plastic deformations (hysteretic damping), and the equivalent viscous damping. These energies equal the input energy from the seismic action.

The objectives of the seismic design in the building design codes are to control the response of the building under different earthquake categories (Duggal, 2013, Armouti, 2008):

- At the minor and frequent earthquakes: prevent nonstructural damage.
- At moderate and less frequent earthquakes: prevent structural damage during the earthquake.
- At the major and rare earthquakes: prevent collapse during the earthquake.
- Maintain functionally of essential facilities during and after any earthquakes.

In the Deformation-Base Design approach, the performance objectives of the structure are related to two performance types which are structural and nonstructural level and they include immediate occupancy, life safety, or collapse prevention (structural stability). Figure E.1 in Appendix E displays the different states of the building when exposed to earthquake loads (Shehadah, 2017).

Different building codes allow the use of the equivalent lateral static force method ELF to design regular structures (UBC, 97, ASCE7, 2016, SI 413, 1995). The main assumptions for ELF are: first, the actual response distribution due to the earthquake is represented conservatively and reasonably by linearly varying lateral force. Secondly, the cyclic inelastic deformation demand is assumed to be uniform in all seismic resisting elements which allows using linear analysis with reduced modifications factors (Taranath, 2004, Valmundsson et al., 1997).

2.2.2 Building Irregularities in Building Codes

The structure is defined to be irregular when the limit defined by different codes concerning some irregularity is exceeded (Varadharajan et al., 2013). When irregularity exists, building codes provide additional requirements to predict the correct response of the structure. The requirements may include performing extra analysis and design consideration over the equivalent lateral procedure or prohibiting some irregularity types coincide with a high seismic zone (Taranath et al., 2009).

Different building codes classify building irregularities into two main categories: vertical and horizontal (plan) irregularities. The structural response and behavior for the vertically irregular structure will be different from regular structure and lead to different distribution of forces vertically from the distribution of the equivalent lateral force method (Taranath et al., 2009).

The performance of building with irregularity of mass, stiffness, and strength may differ from the regular buildings (Bhosale et al., 2017). Therefore, building codes provide criteria for checking irregularities in buildings and, in some cases of extreme irregularities, require a dynamic response spectrum or time history analysis instead of the equivalent lateral static force (ELF) analysis (Soni et al., 2006).

The effect of irregularities on estimating the seismic force was first considered in the UBC (1973) but without quantitative parameters. This remained a matter for the engineering judgment until 1988 (Taranath, 2004). The first publication of these quantifying defining irregularity limits started in 1988 in the UBC code and was based on the 1988 edition of the "Blue Book". These limits were used to make the code practical and can be converted to enforceable provisions (Taranath et al., 2009, Valmundsson et al., 1997). The seismic design codes provide criteria for the irregularity as qualitative or quantitative (Magliulo et al., 2002).

Briefly, vertical irregularities exist where the mass, stiffness, or strength are significantly different from adjacent stories or when there is asymmetrical geometry in the vertical axis. Horizontal irregularities exist when there are asymmetrical in plan shape, eccentricity between the mass center and the center of rigidity, non-uniform distribution of mass or vertical resisting elements, or non-uniform distribution of the stiffness in the plan (ASCE7, 2016, Taranath et al., 2009).

Tables D.1 and D.2 in Appendix D summarize the definitions of all horizontal and vertical irregularities. The required remedial measures according to ASCE7-16 are summarized in Table D.3 in Appendix D.

2.2.3 Soft Story and Weak Story Irregularity According to Building Codes

The definition of the soft and weak story irregularities is presented in Table D.2 in Appendix D according to ASCE 7-16 and the same UBC 97 definitions, but the extreme soft story and extreme weak story irregularities are defined only in ASCE7-16. The soft-story irregularity is defined to exist when the lateral stiffness of a story is less than 70% of the lateral stiffness for the story above or less than 80% of the average lateral stiffness of the three stories above and the weak story irregularity is defined to exist when the strength of a story is less than 80% of that in the story above.

ASCE7-16 and UBC 97 also require the same remedial measures for soft and weak stories irregularities. Also, the codes require to use of different analysis methods than equivalent lateral force (ELF) for soft and weak stories irregularities. Moreover, the codes do not permit design for extreme cases of weak and soft stories irregularity in some seismic design categories. In addition, the codes limit the story height to two-story or 9m height when the building has an extremely weak story irregularity in low SDC unless the extremely weak story is designed for a force equal to the over-strength factor (Ω_o) times the design force. It should be noted that UBC 97 and ASCE7-16 have the same provisions for the soft story and weak story irregularities.

The Israeli Standards SI 413 (1995) define the soft story, as the flexible story to exist if one condition of the following is satisfied:

a) The story stiffness is less than 70% of the stiffness of the story above or 80% of the average of the three stories above.
b) If the length of the concrete wall or masonry wall (15cm thickness or more) between columns in the story is less than half its length in the story above in at least one direction of its principal directions.

SI 413 (1995) defines a weak story to exist when the story has a shear capacity for lateral force less than 80% of the story above and an especially weak story when the ratio is less than 65%. SI 413 (1995) also requires for framed structures to be classified as regular, to have the ratio between the story shear capacity and the design shear force not vary by more than 20% from a story to another story. This requirement does not apply to the up most story in all structures.

SI 413(1995) requires using a dynamic analysis procedure when soft and weak stories exist. Also, SI 413 (1995) does not permit soft or weak stories for structures with high ductility levels. In addition, for the especially weak story irregularity SI 413 (1995), similar to UBC 97 and ASCE7-16, sets a limit on the story height of two-story or 9m unless the weak story and the story above are capable of resisting a seismic force = 0.75K times the design force, where K is the force reduction factor of a structure. Furthermore, SI 413(1995) requires to increase in the calculated design forces and moments for columns and beams in the weak story and for both the story above and the story below (if it exists) by a factor of 0.6K. Moreover, SI 413(1995) provides special requirements for column reinforcement details in the weak or soft story and both the story above and below (if it exists).

As noted in SI 413 (1995), the required remedial measures are not only for the weak and the soft story but also for the story above and the story below. These requirements for these stories are not considered in the ASCE7-16 and UBC 97 building codes.

2.2.4 Seismic Response of Building with Mass, Soft and Weak Story Irregularities

The seismic response of buildings with vertical irregularities has been the interest of many researchers, especially stiffness, strength, and mass irregularities. Different seismic design codes define these irregularities to exist when the ratio factor (stiffness, strength, and mass) between adjacent stories is more than a certain limit defined by the design code (Soni et al., 2006). Vertical irregularities can cause a concentration of the damage at the irregular story which leads to undesirable failure mechanisms (Magliulo et al., 2002).

Ruiz and Diederich (1989) evaluated the seismic performance of a building with the first story being a weak story. They found that the performance depends on the ratio of the lateral strength resistance (second-floor to first-floor) and the closeness of the dominant period of the excitation to the dominant response period. The ductility demand was increased when the P-delta effects were considered. The design for the weak first story should consider a large seismic coefficient to reduce the ductility demand and provide good reinforcement details at the end of the column in the weak story to increase its ability to resist this demand.

Valmundsson et al. (1997) studied the impact of mass, stiffness, and strength irregularities on the seismic response for 5, 10, and 20 story structures shear building types (strong beam weak column frame building). Equivalent lateral forces (ELF) with different assumptions were used and the results were compared with time history results. Reducing the stiffness only of the first story by 30% increased the first story drift by 20-40% and reducing the strength only of the first floor by 20% increased the ductility demand by 100-200%. Reducing the strength and stiffness proportionally by 30% for the first floor increased the ductility demand by 80-200%. Reducing strength has a larger impact than reducing stiffness. The mass irregularity was found to have a moderate increase in the seismic response and the base shear force was conservatively determined by the ELF as defined by the UBC code but the ductility demand was slightly increased.

Al-Ali et al. (1998) evaluated the seismic response of vertically irregular structures. A strong beam and weak column building frame model was used for 10 story building. Elastic and inelastic dynamic analyses were done. The effect of the combined strength and stiffness irregularities was found to be the largest. The strength irregularity alone was found to produce a larger effect than the stiffness irregularity alone and the smallest effect was found to be that of mass irregularity.

Magliulo et al. (2002) investigated the effect of mass irregularity. They concluded that mass irregularity, even the strong mass irregularity, had a negligible impact on the structure response. Seismic demand was more affected by the strength irregularity of the beams.

Das et al. (2003) studied the seismic response of structures with mass, strength, and stiffness irregularities. The masonry infill walls were considered in multi-stories frames that were designed as special moment-resisting frames according to UBC 97 and ACI 1999. The combination of the strength and stiffness irregularities had the largest impact and the mass irregularity had the least impact. Increasing the first story height from 10ft to15ft reduced the stiffness and strength by about 60% and 40%, respectively, which leads to an increase in the inelastic story drift ratio by about 60%.

Chintanapakdee et al. (2004) studied the seismic response of vertical irregularity similar to Al-Ali et al. (1998) but with the strong column weak beam model for 12 story frames. The impact of the combined strength and stiffness irregularity was also found to be the largest with about a 40% increase in the drift demand. The strength irregularity had a larger effect than the stiffness irregularity on the seismic demand with about a 25%, and 15% increase in the drift demand, respectively. The soft or weak story affected the seismic demand (drift) in the story and the neighboring stories. A large influence was found when the vertical irregularity existed in the lower stories.

Choi (2004) studied the vertical mass irregularity for high-rise steel moment-resisting frames. The effect of mass irregularity was higher on the top floors when compared to the bottom or the middle floors.

Soni et al. (2006) summarized the many studies on vertical irregularities. The effect of combined strength and stiffness irregularities had been the largest. The strength irregularity had more impact on the seismic response than the stiffness irregularity. The seismic behavior in the previous studies was influenced by the type of model (strong column-weak beams or strong beam-weak column) used in the study.

Aydin (2007) studied the building response under the equivalent lateral force defined by the Turkish seismic code and found it to be overestimating the building response when compared to the time history methods for the building with a mass irregularity. It is worth noting that, the building design codes of Italy, Romanian, and Turkey do not consider mass variation as an irregularity type.

Thuat (2011) studied the story strength demand which is needed to avoid the formation of plastic hinges in the columns on the irregular floor. Nonlinear dynamic time-history analysis was done using 29 strong earthquake records. Strength demand was found to vary with the characteristics and intensities of the earthquake ground motions even though when the response spectra were similar. Therefore, the seismic response demand of the irregular building could neither be evaluated based on the result of static analysis nor based on the use of a certain response spectrum.

Varadharajan et al. (2012) investigated the seismic response of structures having different types of vertical irregularities. The mass irregularity depends on the magnitude and the location of the irregularity. The vertical mass irregularity had a negligible impact compared to stiffness and strength irregularities. The different codes generally underestimate the fundamental period and overestimate the seismic demand for structures having vertical irregularity.

Sadashiva et al. (2012) focused on evaluating the effect of the realistic combination of strength and stiffness irregularities in shear-type buildings designed by the New Zealand seismic design standard. They concluded that the strength and stiffness of the members related and summarized the ratio of strength to stiffness for some lateral force-resisting systems. The greatest drift demand is found when the strength and stiffness are decreased by the same amount.

The forces were concentrated at the location where there was a stiffness reduction in the building. The seismic demand increased at these locations and the plastic hinges developed there. This concentration of forces leads to an increase in the risk on the building (Dya et al., 2015).

Pragalath D.C et al. (2016) studied the seismic performance of structures that have a weak story on the first floor and designed by using amplification factor MF defined by different design codes to estimate the design force in the irregular soft story and weak story. Designing the weak story with MF equal to 1 was more vulnerable than the bare frame and the fully infilled wall frame. They found that the Israeli code SI 413 considered the MF at the weak story and the adjacent floors with a range of 2.1 to 3 but other design codes considered this factor only for the weak story.

Rajeev et al. (2017) focused on studying the effect of vertical irregularities and the construction quality on the seismic fragility curves. They found that the soft story increases the local drift and this effect becomes higher when the soft story is located at the lower stories for all types of structures. The construction quality had more influence on the structural damage than the vertical irregularity.

Chandrahas et al. (2017) investigated the behavior of the soft story using pushover analysis. The largest effect on the frame displacement was found when the soft story is below the middle floor of the frame.

2.2.5 Soft/Weak Story Failure Mechanism

During the seismic action, the upper floors of the building with base soft or weak story move like a block or a semi-rigid body with a small relative displacement. Therefore the displacement concentrates in the base at the soft or weak story which leads to a large inelastic displacement and ductility demand as seen in Figure E.2 in Appendix E. The columns in the soft or weak story generally have less ductility capacity than the ductility demand which leads to the concentration of the plastic hinges in the soft or weak story columns which results in a poor distribution of plastic hinges and energy absorption in the building. The stability of the building (P-Δ effects) is also influenced by this because of the large displacement of the soft or weak story and gravity loads of the upper floors. All that leads to the collapse of the soft or weak story and the total collapse of the building despite that the upper floors may remain elastic. This failure is called a soft-story mechanism (Chandrahas et al., 2017, Mezzi et al., 2005, Guevara-Perez, 2012).

The Olive View Hospital building in California during the San Fernando earthquake in 1971 is a clear example of a weak story failure. The shear and masonry walls existed on the upper floors and do not extend to the base floors. The failure was observed in the column of the base floors with the large inelastic lateral deformation of more than 30 inches and brittle collapse of some columns as seen in Figure E.3 in Appendix E (Chopra, 2012, Moehle, 2015).

2.2.6 Improving the Seismic Performance for the Existing Building with Soft/Weak Story

Improving seismic performance is a concept used in retrofitting works. There are two strategies or techniques for improving seismic performance for structures (Mezzi et al., 2005, Sahoo et al., 2013, Shehadah, 2017):

1. Global or overall structure level modifications: In this strategy, the seismic demand is reduced and the energy dissipations are increased by using several techniques such as: adding new resisting elements (shear wall or bracing elements), using dampers (friction or viscoelastic dampers), and base isolations.
2. Local or member level modifications: In this strategy, the strength, stiffness, and ductility of some elements are increased by several techniques such as steel jacketing, concrete jacketing, FRP jacketing, etc.

Figure E.4 in Appendix E summarized the previous techniques in general not only for soft/weak story irregularity.

2.2.7 Eliminating Soft/Weak Story in the Design Stage

Sometimes, the architectural design may lead to inevitable soft/weak story irregularity and thus a solution becomes essential to maintain the architectural layout but eliminate the soft/weak story problem.

Preventing soft/weak story irregularity in the design stage can be done by increasing the stiffness and strength of the soft/weak story. This can be done by increasing the column's cross-sections at soft/weak story, adding new vertical resisting elements at soft/weak story only, such as shear walls or bracing elements. Also, the stiffness and strength between the soft/weak story and the upper story can be reduced by separating the masonry walls and the infill wall from the structural frames by gapes (Kirac et al., 2011).

In this study, a new technique will be presented to eliminate the soft/weak story irregularity. The basic idea is to replace the conventional material in the soft/weak story with new superior material to increase the stiffness and strength of the soft/weak story just enough to overcome the weak/soft story irregularity while maintaining architectural layout and dimensions. All effects resulting from this procedure will be investigated.

2.3 UHPC Material

In this section literature related to material definitions, development, material components, and mechanical properties are reviewed.

2.3.1 UHPC Definition

There is no precise definition for UHPC, but many standards and researchers define the UHPC as a cementitious material characterized by compressive strength exceeding 150 MPa. French Association for Civil Engineering (AFGC) defines the UHPC as concrete with a compressive strength between 150 to 250 MPa (Eide et al., 2012). The Federal Highway Administration (FHWA) adopted a definition set by Graybeal, 2014a for UHPC as: “a cementitious composite material composed of an optimized gradation of granular constituents, the ratio of a water-to-cementitious material less than 0.25, and a high percentage of discontinuous internal fiber reinforcement. The mechanical properties of UHPC include compressive strength greater than 21.7 ksi (150 MPa) and sustained post-cracking tensile strength greater than 0.72 ksi (5MPa). UHPC has a discontinuous pore structure that reduces liquid ingress, significantly enhancing durability compared to conventional concrete" (FHWA, 2018, FHWA, 2013). The Japanese recommendation for the design and construction of ultra-high-strength fiber reinforced concrete structures defines UHPC as a material exhibiting strain hardening under uniaxial tensile stress, with cracking stress of over 4 MPa and tensile strength of over 5 MPa at crack width of 0.5mm, respectively, together with high compressive strength in over 150 MPa (Solhmiraei, 2021).

2.3.2 UHPC Development, and Material Components

UHPC is a new class of cementitious material, that has excellent mechanical properties and durability compared to normal and high-strength concrete. Up to date, UHPC is being developed in the fields of construction and retrofitting to turn it into a regular and common technology.

Experimental studies showed that the concrete strength depends on the compaction of the concrete and the porosity (Caldwell, 2011). Results showed an enormous increase in the concrete compressive strength when the porosity is decreased by 0.2. Through 1970 several alternative methods to densify the composition and decrease the porosity were investigated (Caldwell, 2011). In addition, the absence of capillary pores and lower total porosity of UHPC compared to high strength concrete (HSC) and normal strength concrete (NSC) increase the UHPC resistance of chloride, carbonation, and freezing-thawing cycles is the highest (ChunPing et al., 2015).

The following four stages summarize the historical development of UHPC material (ChunPing et al., 2015, Caldwell, 2011, Azmee et al., 2018):

- Before the 1980s: The UHPC material was only produced in the lab under strict procedures such as vacuum mixing and high-temperature treatment. A compressive strength up to 510MPa was achieved under these conditions. But preparing for UHPC was still very difficult.
- In the 1980s: First, micro-defect-free cement (MDF) was invented. The principle of MDF is to prepare cement paste without defects with a special polymer and a low water-cement ratio. The compressive strength achieved by MDF could exceed 200MPa. The cost of raw materials and complicated preparation process obstructed the use of this material. Second,

the densified system containing homogeneously arranged ultrafine particles material (DSP) was prepared to reduce the defects by the particle parking theory. Silica fume was used to fill the voids and superplasticizers were used to reduce the water-cement ratio and increase the workability of UHPC with heat and temperature curing. The compressive strength of DSP could exceed 345 MPa. To improve the ductility of UHPC microfibers (steel or any synthetic) were added to the composite. Compact reinforced concrete (CRC) and slurry infiltrated fiber concrete (SIFCON) are examples of using steel fiber in the UHPC. But CRC and SIFCON have a problem with the workability due to the low effectiveness of superplasticizers. Therefore, its applications are limited.

- In the 1990s: To prepare a homogeneous and dense UHPC matrix coarse aggregate was eliminated and very fine powders such as cement, sand, quartz powder, and silica fume were used, and the granular packing of it was optimized. Also, steel fibers and superplasticizers were used. This composition is called Reactive Powder Concrete (RPC). The compressive strength of the RPC ranges between 200MPa to 800MPa. The development of the efficiency of superplasticizers makes the workability of UHPC excellent. The RPC was still limited in application due to the high cost of preparation due to the milling of quartz sand and heat curing.
- From the 2000s: The development of UHPC was achieved using mineral binder technology and the development of special superplasticizers which aimed at reducing the cost and improving the sustainability of UHPC. Fly ash (FA), slag, and silica fume (SF) are used to reduce the cement amount. Finally, UHPC was prepared without temperature curing. This engaged the use of UHPC and in many applications in many countries.

The main components of the popular UHPC matrix can be summarized as the following (Caldwell, 2011):

- Fine aggregates: To make the matrix homogeneous and denser.
- Silica fume: To fill the concrete void.
- Superplasticizers: To increase the concrete fluidity and decrease the cement/water ratio.
- Microfibers (steel or any synthon): To increase the ductility, tensile strength, flexural strength, and fire resistance (using polypropylene fibers). Also, to control the cracking pattern.
- Others: Cement and water with minimum cement water ratio.

Figure E.5 in Appendix E shows the typical composition of UHPC for a commercial product known as Ductal® and for class U-A type as FHWA.

Although steel fibers are commonly used in the UHPC matrix, there are many materials used for microfiber as seen in Figure E.6 in Appendix E (Eide et al., 2012). These microfibers are used in many shapes (straight, twisted, spiral…). The most important factors used to describe the fibers in the matrix are the volume fraction (percentage of fiber used) and the aspect or the slenderness ratio (the fiber length to diameter ratio). Also, the fiber shape, distribution, and orientation affect the performance of UHPC (Su et al., 2016).

Budelmann et al. (2010) studied the influence of fibers orientation on the flexural tensile strength and ductility of UHPC. To achieve the requirement of the orientation of the fibers screens were used for casting the UHPC. The results show that the maximum flexural tensile strength is when the fibers are parallel to the tension direction and it is minimum when the fibers are perpendicular to the tension direction, which even gives that less than the tension capacity of plain UHPC (Fehling et al., 2014). Figure E.7 in Appendix E displays the results.

The failure in fiber reinforcement concrete first starts with cracking in the material matrix then the stress is resisted by fibers. As tension is increased, two types of failure in fibers can occur: either fiber pull-out of the concrete or fibers break due to bridging effect as seen in Figure E.8 in Appendix E (ACI 544.4R-18, 2018).

In the last decade, UHPC material applications become widely spread and many companies started to produce it as a commercial market product. Some examples of commercial UHPC products are shown in Figure E.9 in Appendix E.

FHWA provided six types (classes) of UHPC products. UHPC class B (U-B) was adopted in this study with 2% steel fiber by volume which is recommended by Abu-Saffaqa's master thesis (2020), where he studied improving the behavior of sway-special exterior beam-column joint by using UHPC at the joint instead of NSC material. U-B has a high tensile strength and strain hardening compared to other FHWA classes as seen in Figure E.10 in Appendix E. The compositions of the material are shown in Table D.4 in Appendix D.

2.3.3 Mechanical Properties of UHPC

The mechanical properties of UHPC depend on the mix compositions, the way of preparation, and curing conditions. Moreover, the dispersion and orientation of the fiber reinforcement influence the mechanical properties (FHWA, 2013). UHPC does not have a unique mixture formulation which leads to varying in the mechanical properties of UHPC (ACI239-R-18, 2018). The main mechanical properties are as the following:

2.3.3.1 Compressive Strength

UHPC has high compressive strength compared to other concrete types, which exceeds 150 MPa as seen in Figure E.11 in Appendix E. The high compressive strength achieves up to 810 MPa at high pressure and heat treatment. Conventional cylinder and cube compression test methods are used for the determination of UHPC compressive strength with minor modifications to the test (FHWA, 2013).

Adding fibers to UHPC causes slight improvement to the compressive strength of UHPC but significantly increases the ductility (ChunPing et al., 2015, Eide et al., 2012). Figure E.12 in Appendix E shows the advantage of adding fibers to the UHPC mix on the compressive strength.

2.3.3.2 Tensile Strength and Flexural Strength

The tensile strength of UHPC is high compared to conventional concrete and it is usually in the range of 7 to 15MPa. There are many test methods for determining the tensile and flexural strengths of UHPC: flexural prisms, split cylinders, mortar briquettes, and direct tension tests of cylinders. The tensile strength depends on the amount, type, and orientation of the fibers. There are two types of behavior of tensile strength of UHPC: strain-softening when the maximum strength decreases after crack opening due to localize crack, and strain-hardening when the maximum strength increases after crack opening due to the bridging effect of fibers before it begins to pull out of the matrix (ChunPing et al., 2015, FHWA, 2013, Eide et al., 2012, Caldwell, 2011). AFGC, 2016a provides two tensile stress-strain models of UHPC for the thin and thick members. Where AFGC defines the member to be thin when the member thickness is less than three times the longest length of used fibers in the matrix.

FHWA, 2018 provided a typical tensile stress-strain curve with four phases for UHPC material as seen in Figure E.13 in Appendix E. In phase I the material responds elastically until the first crack appears. In phase II, multi-simultaneous cracks occur until a single discrete localized crack occurs. However, FHWA does not consider any material as UHPC class if phase II does not exist. Phase III is the strain hardening phase with individual localized cracks which become wider due to fibers bridging the cracks until the fibers pull out of the matrix. Phase IV is the strain-softening phase in which fibers pull out from the matrix and the material fails.

The tensile stress strain of UHPC class U-B from FHWA, 2018 resulted from the direct tensile test adopted in this research as seen in Figure E.14 in Appendix E.

2.3.3.3 Modulus of Elasticity and Poisson's Ratio

The modulus of elasticity of UHPC is higher than that of NSC. The modulus of elasticity for UHPC is in the range of 40 to 70GPa. This value depends on the UHPC compositions and curing conditions (ChunPing et al., 2015). Graybeal (2007) studied the compressive behavior of UHPC and concluded that the stress strain is approximately linear until 70% of its compressive strength. Moreover, Graybeal suggested a modification equation for the ACI 318 code equation to determine the modulus of elasticity of UHPC. Alsalman et al. (2017) studied the modulus of elasticity for UHPC and summarized several equations used to predict the modulus of elasticity in literature.

For the Poisson's ratio FHWA, 2013 gave a summary table for the value of Poisson's ratio as per previous researches as seen in Figure E.15 in Appendix E.

2.4 UHPC Members

In this section, the UHPC design codes and guidelines, and the response of the UHPC members are discussed.

2.4.1 UHPC Codes and Design Guidelines

The first comprehensive design guidelines for designing ultra-high-performance fiber-reinforced concrete UHPFRC was in France by the Association Française de Génie Civil (AFGC) Interim Recommendations of 2002. AFGC Interim Recommendations of 2002 contain three sections: the characterization section that provides definition and properties for UHPFRC, design and analysis section that provides guidelines for design UHPFRC based on the AFGC standard for pre-stressed concrete, and reinforced concrete codes, and the durability of UHPFRC section. After AFGC Interim Recommendations, AFGC national standards for UHPC were published in three parts: the French standard NF P18-470 (French-standard 2016a), which is a self-supporting document related to UHPFRC, the French standard NF P18-710 (French standard 2016b) which is integral with Eurocode 2 with specific rules for design concrete structures with UHPFRC, and the (NF P18-451) prepared to complete the standard for execution of concrete structures (Aboukifa et al., 2019, Caldwell, 2011, Azmee et al, 2018, Eide et al., 2012).

The draft of recommendations for the design and construction of ultra-high-strength fiber reinforced concrete structures published by the Japan Society of Civil Engineers (JSCE) in 2006 is also one of the earliest guidelines for the UHPC design. Such as the AFGC NF P18-710 standard, the draft was based on the JSCE standard specification for concrete standards. The draft provided values for design like stress-strain relationship and no minimum reinforcement is required for UHPC members (Aboukifa et al., 2019, Caldwell, 2011, Azmee et al., 2018).

In addition to France and Japan's design guidelines, there are several research programs and design recommendations such as the German recommendations (Azmee et al., 2018), the design guidelines for ductal pre-stressed concrete beams in Australia (FHWA, 2013), and others.

2.4.2 Flexural Moment Capacity of UHPC Member

The flexural moment capacity of NSC members is calculated based on applying principles of compatibility and internal equilibrium, with the following assumptions (Park and Paulay, 1975):

- The plane section remains plane before and after bending.
- The tensile strength of the concrete may be ignored if cracking has commenced at the extreme tension fiber.
- The stress-strain curves for concrete and steel are known.

The compressive strain of the NSC is 0.003 is usually used where there is not any visible cracking and/or spalling. The value for the compressive strain does not affect sensitively the flexural strength for beams but it does for the eccentrically loaded column. The main effect of compressive strain is on curvature (Park and Paulay, 1975). The spalling strain in flexural members for NSC is typically in the range of 0.003-0.006. The 0.003 limiting of the compressive strain is widely in many building codes such as ACI318-14, 2014 and NZS, 2006 310,1but other codes used a different value such as CAS, 2004 (0.0035). The compressive stress-strain of NSC concrete can be simplified from the parabolic curve to an equivalent rectangular block (Whitney's stress block) to simplify the calculation as seen in Figure E.16 in Appendix E.

But in the UHPC material, the tensile strength can not be neglected. In addition, the compressive strength is almost linear with some softening at the peak stress. In this section, the literature review of the flexural moment calculation methods for the UHPC sections is provided. Figure E.17 in Appendix E shows the typical bending constitutive relationships of the NSC beam compared with one of the proposed UHPC bending constitutive relationships at the ultimate limit state (ULS).

Association Française de Génie Civil AFGC (NF P18-710, 2016b) provides a method to calculate the flexural moment capacity based on a specified compressive and tensile stress-strain. AFGC provides two stress-strain in compression which are a parabolic curve for the nonlinear analysis purpose and a bilinear curve for the ultimate limit state design goal. For tensile stress-strain, testing is required to develop the curve or it can be primarily obtained from the key parameters provided by AFGC. The plane section before and after bending assumption is still assumed and the moment capacity is calculated based on the principles of equilibrium and strain compatibility.

Yang et al. (2012) provided an analytical method to predict the flexural moment capacity of beams that have a rebar reinforcement ratio of less than 0.02 using sectional analysis and compared the results with the experimental results from Yang et al. (2010). The analytical method divides the section into multiple layers along with the section height and relates it with the UHPC stress-strain to consider the nonlinearity of the UHPC material. Iterative calculations are performed until the equilibrium condition of the section is satisfied. The proposed numerical method predicted well the ultimate bending capacity of most UHPC test beams with small differences due to ignoring fiber orientations and segregation.

Chen et al. (2018) investigated the flexural strength of rebar reinforced UHPC beams that were subjected to pure bending and combined bending and shear. The shear stress to shear capacity is less than 1. In the beginning, they test four beams for each case with a different rebar ratio. Then the authors proposed a model to predict the ultimate flexural capacity of rebar reinforced UHPC beams by averaging the tensile stress of the section. The results from the proposed model are compared with the results of the test of this study and with published literature. The assumption of the plane section used in the flexural theory for the conventional concrete was also examined by the authors by placing strain gauges along with the depth of the tested beams and the results showed that this assumption is still valid for reinforced UHPC beams. The proposed method agrees well with the published literature tests with a mean value of ultimate moment from this method to the experimental 0.89. The ultimate moment capacity was found to be increased (1.28-1.75 times) when the shear stress is combined with the flexural compared with the ultimate moment capacity from pure bending in the beam. Also, the moment calculated without including the tensile strength of UHPC is in the range of 0.6 to 0.89 to the measured moment from the test.

Leutbecher et al., 2013 and Fehling et al., 2014 discussed a simple approach for calculating the bending moment of the UHPC section with/without axial force for combined reinforcement sections. The authors discussed the material model used in this method and the plane section remains plane is assumed with no crack width at the begging of the tensile zone. At the wide crack when the reinforcement rebar starts reaching the tensile strength, the hardening of the steel or the contribution of the tensile strength shall be ignored because the steel fibers pull out at wide crack width. The results of this method were compared with experimental results and showed a good agreement with an error of less than 6%.

Shafieifar et al. (2018) investigated the accuracy of the existing methods for calculating the flexural moment capacity for UHPC. An analytical method by finite element model was proposed and validated from experimental results for several small-scale beams to predict the flexural moment capacity of UHPC beams. Figure E.18 in Appendix E displays the stress distribution for the reinforcement UHPC beam with different methods. The proposed method was used for determining the flexural moment capacity for large-scale UHPC beams and the results were compared to those from ACI 544 and ACI 318 and FHWA. ACI and FHWA methods agreed well with the proposed analytical method with an error of less than 12%, but ACI 318 gives lower values for the moment capacity.

2.4.3 One-way Shear Capacity of UHPC Member

UHPC shear behavior is characterized by complex load transfer mechanisms because fibers gap the cracks and give additional strength and ductility. In the available literature, the factor that affects shear strength and ability of the codes is studied. Shear span to depth ratio, fiber content and orientation, and fiber shear strength are factors that affect the shear strength of UHPC members (ACI239, 2018). UHPC shear resistance of columns and frames is significantly enhanced by adding steel fiber to the mixture (Aboukifa et al., 2019).

Chao et al. (2016) tested two NSC beams designed special moment-resisting frame according to ACI318-14 despite that the longitudinal reinforcement ratio is 3% which is above the code limit for the beam of the special moment-resisting frame. In one of the beams, the material is replaced by UHPC at the plastic hinge region without including transverse reinforcement in this region. The beam with UHPC at the plastic hinge zone provided high shear strength and confinement capacity even though no transverse reinforcement was used compared to the NSC beam. The results show that the seismic requirement of ACI318 for confinement is relaxed if UHPC material is used.

Tong et al. (2020) investigated the shear capacity of UHPC squat shear wall with height to width ratio 1 under repeated low-cyclic loading. The author proposed formulas for calculating the shear capacity of the UHPC squat shear wall. The proposed formula considered the shear capacity from the sum of fiber resistance and horizontal steel reinforcement resistance and the formula agreed well with the test results.

Two tests at the University of Kassel are discussed here (Fehling et al., 2014). The first experiment investigated the beam shear capacity by four points bending test for two series of tests, each of which has four beams. The first testing series is rectangular beams with different flexural reinforcement rebar ratios and without fiber or shear reinforcement. In the second testing series, the beams sections are as in the first testing series but include only the fiber reinforcement. The second series has a higher load-carrying capacity with ductal behavior compared to the first series of beams. The second experiment is part of a German research program that investigated the shear capacity of fiber-reinforced beams with and without transverse reinforcement by three points bending test. The beams have an I section in a part of the beam length and a rectangular section in the rest length as seen in Figure E.19 in Appendix E. Many narrow shear cracks with close spacing were observed for the beams that have only fiber reinforcement, and the wide cracks were seen shortly before reaching the ultimate load. Beams with transverse reinforcement cracked upon reaching the ultimate load.

In 2004, a research program at Delft University of Technology investigated the shear capacity of three UHPC beams. The beams have an I section with different fiber content and without shear reinforcement. Three different crack patterns were found as seen in Figure E.20 in Appendix E depending on the fiber contain ratio. The fiber content has a significant effect on the shear behavior. The authors proposed to use the EN 1992-1-1 equation that uses the strut inclination method to calculate the shear capacity of beams having shear reinforcement, but with some modifications to consider the fiber reinforcement and absence of the shear reinforcement. The results from the tests agreed well with the proposed modified equation (Fehling et al., 2014). The proposed equation is as follows:

$$V_u = b_w h \cot \theta \sigma_{pf} \tag{1}$$

Where:

b_w: beam web width.
h: maximum depth of the cross-section.
θ: strut inclination angle and $1 \leq \cot\theta \leq 3$.
σ_{pf}: post-cracking tensile strength (a constant stress level is assumed) and was determined from the axial tensile tests.

Pourbaba et al. (2018) studied the shear strength of the beams by testing 19 UHPC beams with two types of UHPC mixes and 19 NSC beams. The studied parameters are the shear span to depth ratio (0.8, 1.2, and 2.8), longitudinal reinforcement ratio (2.2% to 7.8%), and the anchorage of the reinforcement. The results of the test showed that the shear capacity of UHPC beams was on average 3.5 times that of NSC beams and UHPC beams endured 2.5 times higher inelastic deflection than NSC beams. The longitudinal reinforcement ratio was found to have a limited effect on the shear capacity of the UHPC beams. The anchorage of the reinforcement was found very critical for the NSC beams where it suddenly failed if its anchorage is not found sufficient. However, this effect was found to be small for the UHPC beams. Finally, the authors of that work compared the test results to ACI318 and RILEM shear capacity calculation methods and indicated that the predicted values are more conservative compared to the experimental values with a ratio factor of more than 3.7.

Pourbaba et al. (2019) experimentally investigated the shear capacity of 19 UHPC beams. The tested beams include fiber reinforcement and no shear reinforcement. The experimental results were compared to the predicted shear strength computed as per ACI318, RILEM TC 162-TDF, Australian guidelines, and Iranian National Building Regulation. The ratio of experimental shear strength to predicted value is found for each code for each specimen. The results of the Australian guideline and RILEM TC 162-TDF gave smaller ratios of experimental to predicted shear strength (2.5 and 3.6 respectively), but the ACI318 and the National Building Regulation are more conservative and gave larger ratios of about 8 and 10 respectively because they ignored the effect of fiber reinforcement.

Lim et al. (2016) experimentally studied four simply supported UHPC beams to investigate the shear behavior of UHPC beams containing a steel fiber of 1.5% fraction by volume. One of the tested beams is without transverse reinforcement and the remaining beams are with shear reinforcement at different spacing (0.3d, 0.5d, and 0.75d) where d is the effective depth of the beam. The test results were compared with shear strength for the steel fiber-reinforced concrete predicted from the literature summarized in Figure E.21 in Appendix E. The test results show that the steel fiber substantially enhanced the shear resistance of the UHPC beam and the contribution of the steel fiber to the shear resistance increases when the distance of the stirrups increases. Shear reinforcement enhanced the ductility of the UHPC even though when the spacing of shear reinforcement exceeded the code spacing limitation. The shear reinforcement was found a small effect in increasing the shear strength. Where the transverse reinforcement is increased by about 55.6% compared to the design code requirements but the shear strength increased by about 2.6% only. The AFCG recommendation showed a relatively accurate prediction for the shear strength of the UHPC beams with or without including shear reinforcement compared to the existing method for steel fiber-reinforced concrete.

In our research, the AFCG (2016b) and Fehling et al (2014) will be used to calculate the shear capacity of the UHPC section because they agree well with the experimental results.

2.4.4 UHPC Columns

Hung et al. (2018) tested slender high-strength concrete columns under concentric loading to investigate the effect of using steel fibers on the slender high-strength concrete columns with 100MPa compressive concrete strength. The slender column failed despite the stirrups remaining elastic and without opening the stirrups hook. Using steel fiber in the slender high-strength concrete columns increased the crack control and enhanced the deformability by restraining concrete spalling and crushing and allowing multiple narrow cracks and no effect on the ductility.

El-Attar et al. (2015) tested 12 square ultra-high-strength RC columns under constant axial load combined with cyclic lateral load. The effect of the longitudinal reinforcement ratio, the steel fiber percentage, the concrete compressive strength, and the axial load level were studied. Test results are as follows: the column capacity, initial stiffness, and ductility are increased when the longitudinal reinforcement ratio or the steel fiber percentage are increased. The increase in the axial load level reduced the column capacity, initial stiffness, and ductility. Increasing the concrete compressive strength increased column capacity but decreased the initial stiffness and ductility.

Hung et al. (2021) experimentally investigated the compressive behavior of reinforced UHPC short columns. The parameters include coarse aggregate, transverse reinforcement, and fiber content. Twelve UHPC columns with large sections are to previous studies and with concrete cover as ACI318-19 per requirements are tested. The test results showed that adding steel fiber with a volume fraction of 0.75% by volume or more restrained the early damage of the column and improved the column axial capacity. Moreover, adding steel fiber with a volume fraction of 1.5% by volume allows removing half of the transverse reinforcement required by code to prevent premature buckling of steel reinforcing bars under axial loading.

Aboukifa et al. (2019) extensively studied the UHPC material with two parts of experimental work. First, the confinement behavior was investigated by testing specimens of unconfined and confined UHPC cylinders. Second, four large UHPC columns were tested under combined axial and cyclic loading to investigate the seismic response of the UHPC columns with conventional steel reinforcement grade 60 and high strength grade 100. In addition, an analytical model was used for the NSC column to compare the seismic response of the column. The results were as the following:

- Steel spiral confinement reinforcement improves the strength but the improvement is more significant for the ductility.
- For tested large columns the main failure of the columns was the tensile rupture of the longitudinal rebar without concrete spalling, core damage, reinforcement exposure, or

buckling as in a typical NSC column plastic hinge. Concrete damages were observed only at large drift without leading to any spalling or crushing for the concrete section.

- The initial stiffness of the tested column was found to be 0.6 to 0.7 times the modulus of elasticity multiplied by the moment inertial of the gross section area.
- The confinement was insignificantly activated in the UHPC column under combined axial and lateral cyclic loading.
- The strength of the UHPC column can be increased by about double the NSC columns without affecting the column ductility.
- Decreasing the transverse reinforcement to a half in the UHPC column had an insignificant effect on the lateral load capacity or the drift.

Joe et al. (2016), by an analytical study, showed that using UHPC in columns allowed reducing the column section by about 40% without affecting the flexural moment capacity and ductility compared to NSC under seismic loading.

Chao et al. (2016) investigated the seismic performance of full-scale moment frame columns and beams models with NSC and UHPC material tested under cyclic reversals load. Two square specimens column were tested with the same dimensions and reinforcement but in the plastic hinge zone, the NSC was replaced by the UHPC material for one of the specimens. The normal strength concrete column was designed according to ACI318-14. During the test, no visible crack was visible in the plastic hinge region cast by UHPC material. A column with UHPC material at the plastic hinge has minor damage at the drift of 2% which reduces the need for post-earthquake repair. Also, the high strength and ductility capacity compared with the column with NSC was achieved. The design of the column according to the ACI318-14 is relaxed as concluded from the test results. Figure E.22 in Appendix E showed the cracking in the tested columns at high drift.

Kimura et al. (2007) test ultra-high-strength RC columns under cyclic loading. 200 MPa concrete compressive strength including high-strength steel fibers was used. The test results show the use of high-strength steel fibers reduced the columns damage and increased the flexural strength of the RC column by about 1.47 without using high-strength steel fibers under varying axial loads up to drift of 3%.

2.5 Summary

The seismic behavior of irregular buildings was discussed in this chapter. The building irregularities according to the building codes are reviewed in general and in detail for the soft and weak story irregularities. Where many building codes define the soft story and weak story irregularities and require additional remedial measures for designing the soft and weak stories. In addition, several researchers studied the soft and weak stories and found that story drift demand is increased in the soft and weak stories which maybe lead to the total collapse of the buildings. Also, methods to improve the seismic performance of building with soft/weak stories are discussed.

UHPC material was reviewed at the material level and the member level in this chapter. Where UHPC is a new cementitious material with super properties (compressive strength, tensile strength, .. etc) that may be used to increase the column stiffness and strength in the soft and weak stories. Also, UHPC at the member level was discussed for estimating the flexural moment capacity, one-way shear capacity, and columns capacity.

Chapter Three

Modeling

3. Modeling

3.1 Overview

Numerical analyses with commercial software at two different analysis levels were performed in this research: sectional analysis and the 3D model frame analysis. SAP2000 program was used for the 3D frame model analysis, and XTRACT software was used for the sectional analysis. The material, geometry, boundary conditions, loading, assumptions, and analysis types are discussed in the following sections.

3.2 Materials Models

3.2.1 NSC model

Many stress-strain models for normal strength concrete (NSC) are available in the literature. Mander model (1988b) for the NSC was used. A concrete grade of B300 with a cylinder 28-day compressive strength of 24 MPa is chosen because it is commonly used in Palestine. Figure E.23 in Appendix E displays Mander unconfined concrete stress-strain curve. The stress-strain curves are obtained by the following equations:

For the curved portion $\varepsilon \leq 2{\varepsilon_c}'$:

$$f_c = \frac{f_{c'}}{r-1+x^r} \quad (2)$$

For the linear portion $2{\varepsilon_c}' \leq \varepsilon \leq \varepsilon_u$:

$$f_c = \left(\frac{2f_{c'}r}{r-1+2^r}\right)\left(\frac{\varepsilon_u-\varepsilon}{\varepsilon_u-2\varepsilon_{c'}}\right) \quad (3)$$

Where:

$$x = \frac{\varepsilon}{\varepsilon_{c'}} \quad (4)$$

$$r = \frac{E_c}{E_c - (\frac{f_c'}{\varepsilon_c'})} \tag{5}$$

E_c: concrete modulus of elasticity.

f_c': concrete compressive strength.

ε_c': concrete strain at f_c'.

ε: concrete strain.

ε_u: ultimate concrete strain capacity.

f_c: concrete stress.

The ACI318-19 equation for the normal weight concrete was used for calculating the modulus of elasticity of the concrete:

$$E_c = 4700\sqrt{f_c'}\ (in\ MPa) \tag{6}$$

Table 1 displays the NSC material properties used to create the unconfined concrete stress-strain curve as seen in Figure E.24 in Appendix E. This curve is used in the sectional analysis and the behavior of NSC in tension is neglected.

Table 1:

NSC material model parameters.

f_c' = 24 MPa	ε_c' = 0.002219	E_c = 23025.20 MPa	ε_u = 0.005

3.2.2 UHPC model

In this research, the UHPC material models and properties are adopted from FHWA for the class U-B with a 2 percent fiber ratio by volume. FHWA provided equations to produce the compressive stress-strain for nonlinear analysis purposes. Figure E.25 in Appendix E displays the stress-strain response of UHPC compared with the linear-elastic behavior.

$$f_c = \varepsilon_c E_c (1 - \alpha_1) \tag{7}$$

$$\alpha_1 = Ax^b \tag{8}$$

$$x = \frac{\varepsilon_c E_c}{f_c'} \tag{9}$$

Where:

$f_c{}'$: the compressive strength of UHPC.

f_c: the compressive stress of UHPC.

ε_c: the compressive strain of UHPC.

E_c: compressive elastic modulus of UHPC.

α_1: linearity deviation parameter.

A and b: the fit parameters are obtained from Figure E.26 in Appendix E.

Table 2 displays UHPC material properties used to create the concrete stress stain as seen in Figure E.27 in Appendix E.

Table 2:

UHPC model parameters.

f_c' = 159.76 MPa	E = 43200 MPa	ε_u = 0.0065	a = 0.106	b = 2.606

The result of the direct tensile test provided by FHWA for UHPC material class U-B was adopted in this research. Figure E.28 in Appendix E displays the adopted tensile stress-strain curve for UHPC type U-B with a 2% fiber ratio by volume.

3.2.3 Reinforcement steel model

The steel ASTM A615 grade 60 is commonly used in our locality. The elastic perfectly plastic model with 420MPa yield strength is assumed. The ultimate strain range depends on the manufacturing provenance and in this study, a value of 0.18 is used for the ultimate strain as recommended by Abu-Saffaqa (2020) in his MSc thesis.

3.3 Sectional Analysis

XTRACT v3.0.8 program is used in the sectional analysis. XTRACT is developed at the University of California at Berkeley as a research tool. The program divides the section into many small rectangular meshes with dimensions less than 20mm. XTRACT offers many analysis options for the nonlinear analysis including moment curvatures, axial force-moment interactions, and moment-moment interactions with graphical and tabular representations for the results (XTRACT, 2006).

The analytical methods used in the XTRACT can be summarized as follows: at the beginning, the material models, the fibers layout of the cross-section, and the applied axial force are defined. Displacement control methods are used in the moment-curvature analysis. The assumption of the plane section is assumed and the centroid of each individual fiber is known. Based on an assumed curvature, the strain is found for every fiber in the section. The stress of every fiber is recognized from the stress-strain relationships of the material models. The force at the centroid of each fiber is calculated by multiplying the fiber stress by the fiber area. Many iterations are done until the equilibrium is achieved within the defined tolerance. Figure E.29 in Appendix E shows strain distribution in the discretized cross-section and equations 11 to 13 are used to calculate the section forces and moments by XTRACT (Chadwell et al., 2004).

Under the conditions of static equilibrium:

$$P = \sum_i F_i \tag{10}$$

$$M_x = \sum_i -y_i F_i \tag{11}$$

$$M_y = \sum_i -x_i F_i \tag{12}$$

Where:

$$F_i = A_i \sigma_i \tag{13}$$

A_i: area of fiber i.

σ_i: the stress of fiber i.

P: applied axial load.

M_x: applied moment about X-axis.

M_y: applied moment about Y-axis.

The selected sections were analyzed assuming NSC material under various axial loads cases. After that, the NSC was replaced by the UHPC material. Figure E.30 in Appendix E displays an example of a load assigned to a section in XTRACT.

Figure E.31 in Appendix E displays an example of the M-K curve for the both NSC and UHPC section obtained by XTRACT software at different axial load levels.

3.4 Sectional Analysis Verification and Validation

Manual calculations are performed to verify EXTRACT by calculating the moment-curvature (M-K) for NSC and comparing the results to the EXTRACT results. To validate the UHPC beams, Yang et al.'s (2010) test results are used. The M-K experimental results for UHPC beams are compared to the XTRACT results.

3.4.1 Moment Curvature for NSC

The verification will be performed using the NSC beam displayed in Figure E.32 in Appendix E. Table 3.3 displays the used NSC beam section properties.

Table 3:

Used NSC beam section properties.

F_c'= 24 MPa	F_y = 420 MPa
E_c = 23025 MPa	E_s = 200 GPa
f_{cr} = 3.04 MPa	$\rho = A_s / bd$ = 0.00574
I_{cr} = 1.808*109 mm^4	$\rho' = A_s' / bd$ = 0.00574

The moment and curvature are calculated at three stages as follows:

- Before concrete cracking:

$$M_{cr} = \frac{f_{cr} * I_{cr}}{h/2} = \frac{3.04 * 1.808 * 10^9 * 10^{-6}}{400/2} = 27.49\ kN.m$$

$$\emptyset_{cr} = \frac{f_{cr}/E_c}{h/2} = \frac{3.04/23025 * 10^3}{400/2} = 0.66 * 10^{-3}\ 1/m$$

- At the first yield of the steel rebar at the tension side:

The compressive steel yielded when $\rho > \rho_{cy}$, where

$$\rho_{cy} = \frac{0.85 f_c{}' * d' * \beta 1}{d * f_y} * \frac{(600)}{(600 - f_y)} + \rho' = 0.0254 > \rho = 0.00574$$

Hence, compression steel does not yield. Assume tension-steel yields before concrete reaches peak strength as displayed in Figure E.33 in Appendix E.

$$C_c = 0.5 c f_c' b = 0.5 E_c \varepsilon_c b = 0.5 c E_c \left(\varepsilon_y \frac{c}{d - c}\right) b$$

$$C_c = 0.5c * 23025\left(0.0021\frac{c}{350-c}\right)350 * 10^{-3}$$

$$C_c = 7.253\frac{c^2}{350-c}$$

$$C_s = A_s'f_s' = A_s'\varepsilon_s'E_s = A_s'\left(\varepsilon_y\frac{c-d'}{d-c}\right)E_s$$

$$C_s = 3 * 201\left(0.0021\frac{c-50}{350-c}\right) * 200 * 10^3 * 10^{-3}$$

$$C_s = \frac{253.26c - 12663}{350-c}$$

$$T = A_s f_y = 3 * 201 * 420 * 10^{-3} = 253.26\ kN.$$

$$T = C_c + C_s$$

By solving the previous equation $c = 88.3\ mm.$

Check $f_c < f_c'$:

$$f_c = E_c\left(\varepsilon_y\frac{c}{d-c}\right) = 23025\left(0.0021\frac{88.3}{350-88.3}\right) = 16.31\ MPa\ (0.68f_c')$$

The moment is calculated as follows:

$$M_y = T\left(d - \frac{c}{3}\right) - C_s\left(d' - \frac{c}{3}\right)$$

$$C_s = \frac{253.26 * 88.3 - 12663}{350 - 88.3} = 37\ kN.$$

$$M_y = 253.26\left(350 - \frac{88.3}{3}\right) - 37\left(50 - \frac{88.3}{3}\right) = 880.42\ kN.m.$$

The curvature calculates as follows:

$$\emptyset_y = \frac{\varepsilon_y}{d-c} = \frac{0.0021}{350 - 88.3} * 10^{-3} = 8.02 * 10^{-3}\ 1/m$$

- At the ultimate strain of concrete at extreme compression fiber:

The compression steel does not yield since $\rho < \rho_{cy}$. Figure E.34 in Appendix E displays the section strain, stress, and forces at the ultimate strain of concrete at extreme compression fiber (0.003).

$$C_c = 0.85f_c'\beta_1 cb = 0.85 * 24 * 0.85 * c * 300 * 10^{-3} = 5.2c$$

$$C_s = A_s'f_s' = A_s'\varepsilon_s'E_s = A_s'\left(\varepsilon_c\frac{c-d'}{c}\right)E_s$$

$$C_s = 3*201\left(0.003\frac{c-50}{c}\right)*200*10^3*10^{-3}$$

$$C_s = \frac{361.8c-18090}{c}$$

$$T = C_c + C_s$$

By solving the previous equation $c = 49.4\ mm$.

The moment calculates as follows:

$$M_u = T\left(d-\frac{c\beta_1}{2}\right)$$

$$C_s = \frac{361.8*49.4-18090}{49.4} = 4.4\ kN\ (negelected).$$

$$M_u = 253.26\left(350-\frac{49.4*0.85}{2}\right)*10^{-3} = 83.3\ kN.m.$$

The curvature calculates as follows:

$$\emptyset_u = \frac{\varepsilon_{cu}}{c} = \frac{0.003}{49.4}*10^{-3} = 60.73*10^{-3}\ 1/m$$

The moment-curvature (M-K) curve obtained from XTRACT agrees well with the manual M-K curve as seen in Figure 2.

Figure 2:

M-K curves obtained from XTRACT compared to manual results.

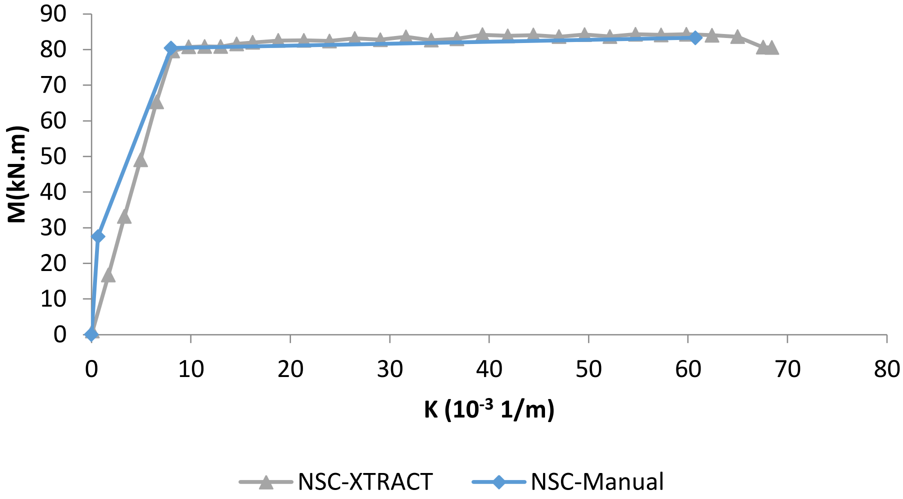

XTRACT considers only the compressive strength of the NSC therefore the cracking point is not shown for the XTRACT results as displayed in Figure 2.

3.4.2 Moment Curvature for UHPC

Yang et al., (2010) experimental results for the beams R12-2 and R13-2 are used to verify the M-K for the UHPC section. The yielding stress of the reinforcement rebar is 500 MPa for the tested beams. The UHPC material properties of the tested beams and the section properties are displayed in Figure E.35 and Figure E.36 in Appendix E.

Yang et al. (2012) proposed an analytical method to calculate the moment for the UHPC material sections based on the previous experiment. The suggested UHPC stress-strain relations proposed by Yang et al. (2012) for the experiment are displayed in Figure E.37 in Appendix E.

The XTRACT result agrees well with the experimental results as seen in the following figures:

Figure 3:

Comparison of moment-curvature curves for experimental results and XTRACT For beam R12-2.

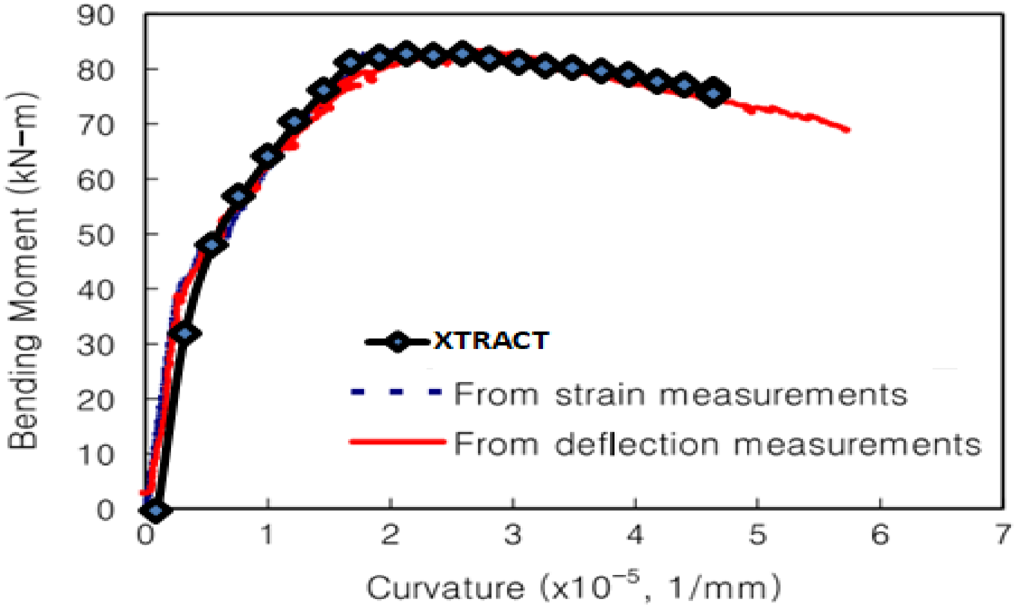

Figure 4:

Comparison of moment-curvature curves for experimental results and XTRACT For beam FR13-2.

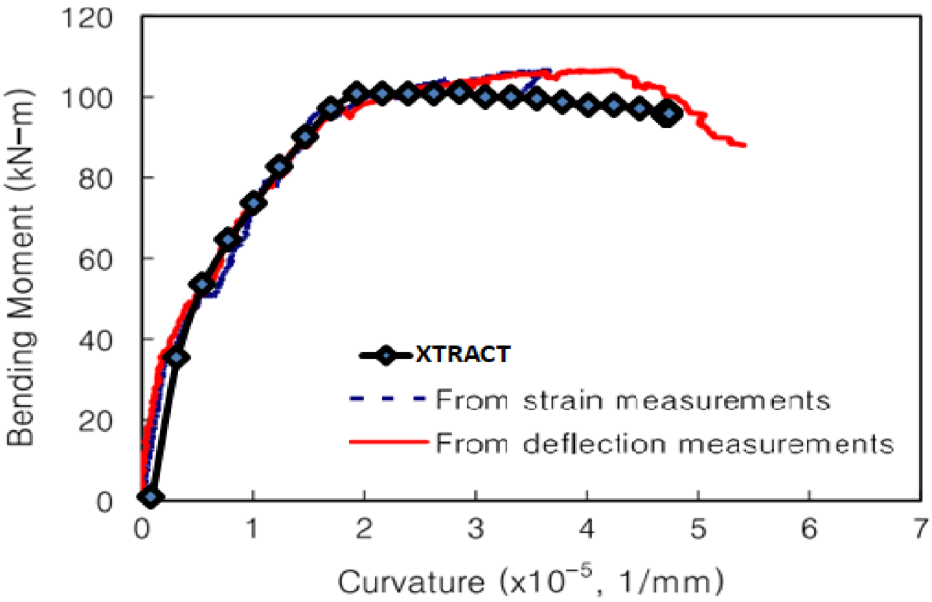

The results from the experiment match well with the XTRACT M-K curve results for both the NSC and UHPC materials. Thus, this is considered a validation of the XTRACT software and sectional analysis.

Chapter Four

Parametric Study

4. Parametric Study

4.1 Overview

A parametric study by a sectional analysis is done to investigate the strength and stiffness of the reinforced NSC and UHPC columns sections. The range of parameters and key factors affecting the strength and stiffness of the columns' cross-sections are explained in this chapter.

The analysis is performed by XTRACT software to obtain the moment-curvature of all sections. The results of all sections were used to develop equations for the strength and stiffness ratios of the two materials sections. The developed equations take into account the most significant parameters determined using multilinear regression analysis.

All key factors that affect the strength and stiffness of the columns are first gathered from the literature and the concepts of structural mechanics. The column cross-section size and longitudinal reinforcement affect the column strength. The slenderness effect of the column is not considered in this study. In calculating the stiffness, building codes (such as IBC) consider only the effect of axial load level on the effective rigidity of the columns. All these parameters are shown in the parameter matrix in Table 4 Based on the parameter matrix 216 rectangular columns were analyzed by XTRACT software to investigate the advantages of using UHPC instead of NSC in the soft/weak story columns.

Table 4:

Values of parameters used for various column sections.

Axial load level of NSC column	$N/f_c'A_g$	**0.2**	**0.4**	**0.6**	
Longitudinal reinforcement ratio	ρ_s	**0.01**	**0.02**	**0.03**	
Width of the column cross-section in mm	B	**300**	**400**	**500**	
Depth to width ratio of the colmn cross-section	H/B	**1**	**1.33**	**1.66**	**2**

4.2 Influence of Using UHPC Instead of NSC on The Columns Stiffness

The effect of using UHPC instead of NSC material on the lateral stiffness can be investigated by obtaining the effective flexural moment (EI_e) as described here. Then, the cracking modifiers usually used in the NSC columns analysis are checked to verify the validity of using it for the UHPC columns analysis

4.2.1 Effective Flexural Rigidity EI_e

Effective flexural rigidity is an important characteristic of the member that considers the cracking effect and internal force contribution of members of a frame. No unique definition of the EI_e has been given. In some approaches, the cracked state of the member is considered when computing the effective flexural rigidity. Others obtain effective flexural rigidity using the slope of the bilinear approximation of the moment curve diagram (Avşar et al., 2012). In addition, different building codes (such as IBC) provide modification factors to represent the cracking state of the member as the ratio of flexural rigidity of cracked cross-section to effective flexural rigidity of gross cross-section (EI_e / EI_g). These approaches neglect other deformations resulting from shear and/or bar slip and the effect of load reversal (such as seismic load). Also, the confinement effect is neglected where the yield point does not depend on it for members dominated by flexure (Park and Paulay, 1975).

The first and common equation for calculating the effective moment of inertia I_e by considering the cracking state at service load and is adopted by ACI318-19 was introduced by Branson (1965) (Mamaghani et al., 2021):

$$I_e = \left(\frac{M_{cr}}{M_{a0}}\right)^3 I_g + \left[1 - \left(\frac{M_{cr}}{M_a}\right)^3\right] I_{cr} \leq I_g \qquad (14)$$

Where: I_g is the gross moment of inertia, I_e = cracked moment of inertia, M_{a0} is the maximum service load moment, and M_{cr} is the cracking moment.

Priestly et al. (1996) proposed a method to calculate EI_e and is adopted by Caltrans (2010) to reflect the cracking state of the bride pier under seismic analysis (Avşar et al., 2012). Effective rigidity is defined as the slope of the first segment of the bilinear moment-curvature diagram. Figure E.38 in Appendix E shows a moment-curvature diagram and the EI_e calculate as:

$$\emptyset_y = \frac{m_y}{EI_e} \rightarrow Slope = EI_e = \frac{m_y}{\emptyset_y} \tag{15}$$

Where: m_y and $\emptyset_y$ represent the ideal yielding moment and curvature.

Two criteria are used to define the yielding point on the moment-curvature curve. For ductile sections, the yielding point is the point where the tensile reinforcement reaches the yielding strain. But for brittle sections, the yield point is defined for EI_e calculation as the point where the concrete extreme compressive fiber reaches the peak strength (Avşar et al., 2012). The concrete peak strength is usually at 0.002 strain (Avşar et al., 2012, Park and Paulay, 1975). Therefore, the EI_e is the slope between the origin and the point of first yielding as shown in Figure E.38 in Appendix E (Avşar et al., 2012).

Mamaghani et al. (2021) used the slope of moment-curvature to find the effective flexural stiffness EI_e of fiber-reinforced polymer reinforced concrete beams. Avşar et al. (2012) studied the cracking modifiers for ordinary reinforced concrete columns and beams and calculated EI_e from the slope of the moment-curvature diagrams.

Different parameters affect the EI_e for the member. The axial load level on the section is considered the main parameter that changes the EI_e and many building codes (such as IBC) give different cracking modifiers for columns depending on the axial load level. Figure E.39 in Appendix E displays the Caltrans (2010) chart for determining cracking modifiers for rectangular columns at the different axial levels. Also, It can be seen EI_e depends on the reinforcement ratio as seen in Figure E.39 in Appendix E.

4.2.2 The Effective Flexural Moment Rigidity Ratio

In this study, the effective flexural rigidity (EI_e) is defined to be the secant slope of the moment-curvature curve at the first yield point of the steel rebar or when the concrete reaches peak strength (at strain 0.002). EI_e is determined for all sections with NSC and UHPC materials. The ratio of the effective flexural rigidity of NSC to UHPC is defined as the *K* factor:

$$K = \frac{EI_{e,\ UHPC}}{EI_{e,\ NSC}} \tag{16}$$

K factor describes the increase in the flexural stiffness when the UHPC is used instead of the NSC in the column.

XTRACT software is used to obtain the moment-curvature curve and the effective flexural rigidity EI_e for both the NSC and UHPC columns sections. Then K factor is determined for all columns cross-section. The analysis results of the K factor are shown in Table A.1 in Appendix A. The analysis results of the K factor are plotted here to investigate the most significant parameters affecting the K factor. Finally, linear regression is performed to obtain the equation for the K factor with the most significant factors.

Figure A.1 in Appendix A shows that the K factor is linear inversely related to $N/f_c'A_g$. For most of the cases, different ρ_s values give almost the same K value for $N/f_c'A_g$ = 0.6. Moreover, the K factor is inversely related to ρ_s as seen in Figure A.2 in Appendix A.

Figure A.3 in Appendix A displays that the depth to width ratio of the column cross-section H/B has an insignificant effect on the K value. In addition, Figure A.4 in Appendix A shows that B has a small effect on K values. The results are shown in Figure A.3 and Figure A.4 are logical because the size effect is implicitly considered through the axial load level factor $N/f_c'A_g$.

Here only the axial load level $N/f_c'A_g$ and the reinforcement ratio ρ_s have a significant effect on the K factor with linear relation. But the B and H/B factors have smaller effects on the K factor.

The results above are used to fit an equation to predict the relation between the K factor and these parameters using linear regression analysis. K almost decreases linearly with ρ_s and $N/f_c'A_g$. The residual and line of fit for the regression analysis are shown in Appendix A. The following equation is created by linear regressions analysis with the goodness of fit R^2 = 0.79:

$$K = 2.43 - \frac{B}{5000} - 11.6\rho_s - \frac{(N/f_c'A_g)}{1.4} \tag{17}$$

The H/B factor is removed from the equation to simplify the equation because it has an insignificant effect on the K value.

To validate the proposed equation new different 72 sections are selected and the results are compared with predicted results from the proposed equation as seen in Table A.3 in and Figure A.5 in Appendix A displays the predicted and analyzed K factor.

4.2.3 The Validation for the Used Cracking Analysis Modifiers

The cracking analysis modifier for column section (α) is defined as the ratio of the effective flexural rigidity (EI_e) to the gross cross-sectional flexural rigidity (EI_g).

$$\alpha = \frac{EI_e}{EI_g} \tag{18}$$

α is calculated for all sections of the NSC and UHPC materials and the results are shown in Table A.1 in Appendix A. Also, the summary of α results is plotted here to investigate the changes in the cracking modifier.

Figure 5 shows $\alpha_{\_UHPC}/\alpha_{\_NSC}$ slightly decreases with increasing ρ_s and $N/f_c'A_g$. For $N/f_c'A_g$ = 0.6 the $\alpha_{\_UHPC}/\alpha_{\_NSC}$ ratios are less than unity at different $\rho_{s.}$ Therefore, the same NSC cracking modifiers can be conservatively used with UHPC material at high $N/f_c'A_g$ values. But the high $N/f_c'A_g$ values are not evident in our locality. At low, $N/f_c'A_g$ values the $\alpha_{\_UHPC}/\alpha_{\_NSC}$ ratios are in ranges about 0.95 to 1.25 depending on the ρ_s and $N/f_c'A_g$.

Figure 5.

α_{UHPC} / α_{NSC} VS $N/f_c'A_g$.

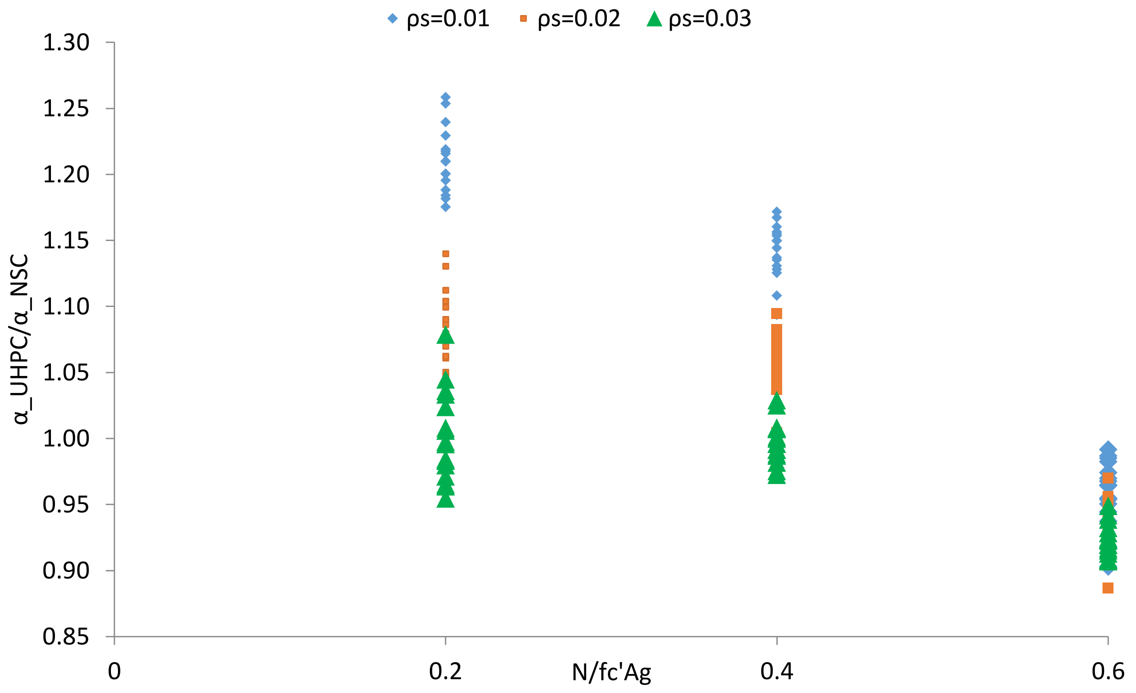

linear regression is used to fit an equation to predict $\alpha_{\_UHPC}/\alpha_{\_NSC}$ with the most significant parameters. The residual and line of fit for the regression analysis are shown in Appendix A.

The following equation is created by linear regressions analysis with the goodness of fit R^2 = 0.79:

$$\alpha_{UHPC}/\alpha_{NSC} = 1.36 - 6.5\rho_s - \frac{(N/f_c{}'A_g)}{2.5} \tag{19}$$

To validate the proposed equation new different 72 sections are selected and the results are compared with predicted results from the proposed equation as seen in Table A.4 and Figure A.6 in Appendix A displays the predicted and analyzed $\alpha_{UHPC}/\alpha_{NSC}$ factor.

Hence, the column analysis cracking modifiers before analysis should be adjusted by the $\alpha_{UHPC}/\alpha_{NSC}$ for UHPC column at low $N/f_c{}'A_g$ for the different ρ_s.

4.3 Influence of Using UHPC Instead of NSC on the Columns' Strength

The lateral strength of the columns at a given axial load can be found as either moment capacity or shear capacity. The moment capacity usually controls the strength of the column in the sway special moment-resisting frame. In the sectional analysis, the moment strength of the sections is obtained from XTRACT results for all sections with NSC and UHPC materials. The shear strength adequacy is computed using available methods in the literature for the UHPC.

4.3.1 Flexural Moment Capacity Ratio

To investigate the increase in the flexural strength of the cross-section when NSC is replaced by UHPC, the β factor is defined as the ratio of the maximum moment of the UHPC section over the NSC section at the same axial load level.

$$\beta = \frac{M_{UHPC}}{M_{NSC}} \tag{20}$$

XTRACT software is used to obtain the moment capacity for both the NSC and UHPC columns sections. Then β factor is determined for all columns cross-section. The analysis results of the β factor are shown in Table A.1 in Appendix A. The analysis results of the β factor are plotted here to investigate the most significant parameters affecting the β factor. Finally, linear regression is performed to obtain the equation for the β factor with the most significant factors.

Figure A.7 in Appendix A shows that the β factor linearly increases when the $N/f_c'A_g$ increases for different ρ_s values. Figure A.8 in Appendix A displays that the β factor linearly decreases with increasing ρ_s. Figure A.9 in Appendix A shows that *H/B* has an insignificant effect on β value. In addition, Figure A.10 in Appendix A shows that *B* has little effect on β value.

The β factor results are used to fit an equation to predict the relation between the β factor and these parameters using linear regression analysis. The residual and line of fit for the regression analysis are shown in Appendix A. The following equation is created from the linear regressions analysis with the goodness of fit $R^2 = 0.90$:

$$\beta = 2.19 - \frac{B}{1220} - 18.3\rho_s + 2(\frac{N}{f_c{}'A_g}) \tag{21}$$

The *H/B* factor is removed from the equation to simplify the equation because it has an insignificant effect on the β value.

To validate the proposed equation new 72 sections are selected and the results are compared with the predicted results from the proposed equation as seen in Table A.5 and Figure A.11 in Appendix A.

4.3.2 Check the Shear strength of the sections

The concrete shear strength of the sections is calculated and compared with UHPC shear strength without considering the shear strength of the transverse reinforcement in the comparison.

4.3.2.1 Concrete Shear Strength V_c

Concrete shear strength for NSC is determined using the ACI 318 detailed equations displayed in Figure 6 that consider the axial force effect. V_c is the max value determined from Figure 5 and V_c shall be less than $0.42\sqrt{f_c{}'}b_w d$. ACI 318-19 limits using concrete shear equations with the material strength as $\sqrt{f_c{}'} < 8.3\ MPa$.

All section shear reinforcement is designed as code provisions for the sway special moment-resisting frame. Hence $A_v > A_{v,min}$ and the two-equation in Figure 6 is used and the max V_c of the two equations is considered as the shear strength of the NSC section.

Figure 6:

Detailed Vc equations (ACI318, 2019).

Criteria	V_c		
$A_v \geq A_{v,min}$	Either of:	$\left[0.17\lambda\sqrt{f_c'} + \frac{N_u}{6A_g}\right]b_w d$	(a)
		$\left[0.66\lambda(\rho_w)^{1/3}\sqrt{f_c'} + \frac{N_u}{6A_g}\right]b_w d$	(b)
$A_v < A_{v,min}$	$\left[0.66\lambda_s\lambda(\rho_w)^{1/3}\sqrt{f_c'} + \frac{N_u}{6A_g}\right]b_w d$		(c)

Where:

A_v: area of shear reinforcement within spacing s, mm^2.

$A_{v,min}$: minimum area of shear reinforcement within spacing s, mm^2.

b_w: web width or diameter of circular section, mm.

d: distance from extreme compression fiber to centroid of longitudinal tension reinforcement, mm.

N_u: factored axial force normal to cross-section occurring simultaneously with V_u or T_u, to be taken as positive for compression and negative for tension, N. Also, $N_u/6A_g \leq 0.05f_c'$.

ρ_w: ratio of A_s to $b_w\,d$.

f_c': specified compressive strength of concrete, MPa.

4.3.2.2 UHPC Shear Strength

To estimate the shear strength of UHPC members two methods are used: French standard NF P18-710 (2016b) and Fehling et al. (2014) equation as a part of German research for creating codes for the UHPC.

- Fehling et al. (2014):

The proposed equation is as follows:

$$V_u = b_w h \cot\theta \sigma_{pf} \tag{1}$$

Where:

b_w: beam web width.
h: maximum depth of the cross-section.
θ: strut inclination angle and $1 \leq \cot\theta \leq 3$.
σ_{pf} : post-cracking tensile strength (a constant stress level is assumed) and was determined from the axial tensile tests.

- French standard NF P18-710 (2016b):

The shear strength $V_{Rd,total}$ for UHPC members is the minimum of V_{Rd} and $V_{Rd,max}$. Where, V_{Rd}: the superposition of shear strength provided by the cement matrix, steel fiber, and shear reinforcement. $V_{Rd,max}$: the limit force for the compressive strength of the concrete compression struts in the truss diagram (Eriksson, 2019).

$$V_{Rd} = V_{Rd,c} + V_{Rd,s} + V_{Rd,f} \tag{22}$$

$V_{Rd,c}$: the shear strength contribution of the cement matric of UHPC strength, and given by:

$$V_{Rd,c} = \frac{0.21}{\gamma_{cf}\gamma_E} k {f_{ck}}^{1/2} b_{w1} d \tag{23}$$

$$k = 1 + 3\frac{\sigma_{cp}}{f_{ck}} \tag{24}$$

$$\sigma_{cp} = \frac{N_{Ed}}{A_c}\left(\frac{N}{mm^2}\right) \tag{25}$$

$0 \leq \sigma_{cp} \leq 0.4 f_{ck}$

Where:

$\gamma_{cf}\gamma_E$: a safety factor is taken such that is equal to 1.5.
f_{ck}: the characteristic value of compressive strength (MPa).
b_{w1}: the smallest width of the cross-section in the tensile area (m).
d: the distance between the most compressed fiber and the longitudinal reinforcement.
N_{Ed}: the axial force in the cross-section, due to the external loads and N_{Ed} is positive for compression.
A_c: the cross-sectional area of the UHPC member.

$V_{Rd,s}$: the shear strength contribution of the shear reinforcement.

$$V_{Rd,s} = \frac{A_{sw}}{s} z f_y \cot\theta \tag{26}$$

Where:

s: spacing of the stirrups.

A_{sw}: the cross-sectional area of the shear reinforcement.

z: the lever arm of the internal forces for a member of constant height corresponding to the bending moment in the member considered and can estimate as z = 0.9 d.

θ: the inclination of the main compression stress on the longitudinal axis with a minimum value equal 30°.

$V_{Rd,f}$: the shear strength contribution of the fiber.

$$V_{Rd,f} = A_{fv}\sigma_{Rd,f} \cot\theta \tag{27}$$

$$\sigma_{Rd,f} = \begin{cases} \frac{1}{k\gamma_{cf}} \cdot \frac{1}{w^*} \int_0^{w^*} \sigma_f(w)\, dw \rightarrow for\ UHPC\ calss\ T1\ and\ T2 \\ \frac{1}{k\gamma_{cf}} \cdot \frac{1}{\varepsilon^* - \varepsilon_{el}} \int_{\varepsilon_{el}}^{\varepsilon^*} \sigma_f(\varepsilon)\, d\varepsilon \rightarrow\ for\ UHPC\ calss\ T3 \end{cases} \tag{28}$$

$$w^* = max(w_u = 0.3mm) \tag{29}$$

$$\varepsilon^* = max(\varepsilon_u, \varepsilon_{u,lim}) \tag{30}$$

Where:

A_{fv}: the projection in the cross-section of the inclined area on which the fiber act and is equal $A_{fv} = b_{w1}z$.

γ_{cf}: a safety factor is taken such that is equal to 1.3.

$\sigma_{Rd,f}$: the mean value of the post-cracking strength along the shear crack of inclination θ, and perpendicular to it.

$$V_{Rd,max} = 2.3 \frac{\alpha_{cc}}{\gamma_c} b_w z {f_{cu}}^{2/3} \left[\frac{V_{Rd,s}}{(1+cot^2\theta)} + V_{Rd,f} \tan\theta\right] \cdot \left[\frac{1}{V_{Rd,s}+V_{Rd,f}}\right] \tag{31}$$

The ratio of V_c of the UHPC to the V_c of the NSC is found in Table A.2 in Appendix A. Figure 7 displays the UHPC and NSC sectional shear strength of all studied columns sections without including the transverse shear strength.

Figure 7:

Vc for NSC VS UHPC

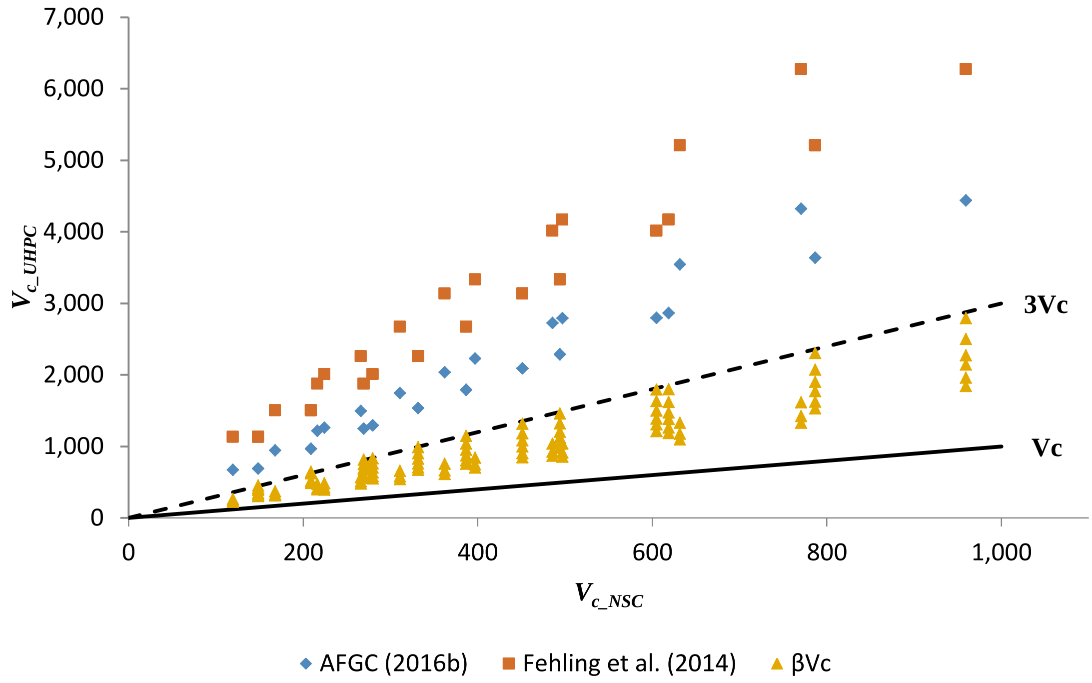

Figure 7 shows that the shear capacity of the UHPC column section is more than at least 3 times the V_c for NSC. The βV_c is less than the V_{c_UHPC} therefore, the moment capacity is controlled by column lateral strength.

4.4 Summary

A parametric study for the sectional analysis results is performed to obtain the effect of replacing the soft/weak story column material from NSC to UHPC. The results of the parametric study are summarized as the following:

1. Stiffness of the UHPC column:

The effect of replacing the NSC material with UHPC material on the column cross-sectional flexural rigidity can be computed using the ratio K, where :

$$K = \frac{EI_{e,\ UHPC}}{EI_{e,\ NSC}} = 2.43 - \frac{B}{5000} - 11.6\rho_s - \frac{(N/f_c{}'A_g)}{1.4}$$

Where:

$EI_{e,\ UHPC}$: effective flexural rigidity of UHPC column.

$EI_{e,\ NSC}$: effective flexural rigidity of NSC column.

B: column width in mm.

ρ_s: column Longitudinal reinforcement ratio.

$N/f_c{}'A_g$: column axial load level.

Therefore the UHPC column stiffness can be computed using the K factor and the stiffness of the NSC column is as follows:

UHPC column stiffness $=$ K * NSC column stiffness

2. Cracking analysis modifiers of the UHPC column:

The effect of replacing the NSC material with UHPC material on the cracking analysis modifiers can be computed using the ratio $\alpha_{UHPC}/\alpha_{NSC}$ where:

$$\alpha_{UHPC}/\alpha_{NSC} = 1.36 - 6.5\rho_s - \frac{(N/f_c{}'A_g)}{2.5}$$

Where:

$$\alpha = \frac{EI_e}{EI_g}$$

EI_e: effective flexural rigidity of column.

ρ_s: column Longitudinal reinforcement ratio.

$N/f_c{}'A_g$: column axial load level.

Therefore the cracking analysis modifiers of the UHPC column can be computed using the $\alpha_{UHPC}/\alpha_{NSC}$ and the cracking analysis modifiers of the NSC column are as follows:

UHPC column cracking analysis modifiers $=$ $\alpha_{UHPC}/\alpha_{NSC}$ * NSC column cracking analysis modifiers

3. Strength of the UHPC column:

The UHPC column strength is studied by investigating the flexural and shear capacities. The flexural strength is found to control the column strength since the shear capacity of the UHPC column is found satisfied.

The effect of replacing the NSC material with UHPC material on the column cross-sectional flexural strength can be computed using the ratio β, where :

$$\beta = \frac{M_{UHPC}}{M_{NSC}} = 2.19 - \frac{B}{1220} - 18.3\rho_s + 2(\frac{N}{f_c{}' A_g})$$

Where:

M_{UHPC}: maximum moment capacity of UHPC column.
M_{NSC}: maximum moment capacity of NSC column.
B: column width in mm.
ρ_s: column Longitudinal reinforcement ratio.
$N/f_c{}'A_g$: column axial load level.

Therefore the UHPC column strength can be computed using the β factor and the strength of the NSC column is as follows:

UHPC column strength $= \beta$ * NSC column strength

Chapter Five

Case Study: 3D Frame Analysis

5. Case Study: 3D Frame Analysis

5.1 Overview

In this chapter, a 3D special moment-resisting framed building is analyzed as a case study to investigate the overall behavior of the frame when NSC columns in the soft/weak story are replaced by UHPC. Also, the analysis results of the frame are compared to the proposed equations generated by the parametric study in chapter 4 for estimating the stiffness and strength of the UHPC columns.

The selected frame has a soft/weak story on the base floor which represents the worst case of this type of irregularity. Building with a first soft/weak story is seen in Palestine for many reasons such as the base floor level being higher or built without masonry and infill walls compared to the rest floors.

In the beginning, a frame with NSC material that has a soft/ weak story on the first floor is analyzed. After that, the columns material of the soft/weak story is replaced with UHPC material and analyzed. The analysis results for the two frames are compared and studied to investigate the enhancement of the building behavior when the UHPC material is used. Also, the increase in the seismic demand is checked to confirm that the increase in the seismic capacity of the frame will not change the seismic demand.

5.2 Modeling and Analysis

The 3D model analysis is usually used to realize the overall building response under lateral loading. Two models of the 3D frame will be used in this study with nonlinear static analysis (pushover) using SAP2000 version 22.

Models assumptions, geometry, hinges, cracking modifiers, loading, and model verification are displayed in this section

5.2.1 Lateral Resisting System

Palestine has regions with high seismic hazards that are required to be designed for the high seismic design category. In the high seismic design category, sway special moment-resisting frame or special reinforced concrete shear walls with about a 50 m height limit are only allowed as a lateral resisting system (ASCE7, 2016). The building is selected in the high seismic design category in Jericho. Therefore, the lateral resisting system was selected as a sway special moment-resisting frame.

5.2.2 Model Layout and Geometry

Two multistory frames with 6 stories were selected and the first floor was studied to be the soft /weak story. To create the soft/weak story the first floor is selected to be higher than the rest floors. Moreover, the selected building does not have any horizontal irregularity.

The frame was designed with NSC as per ACI318-19 and ASCE-16 instructions as seen in Appendix B. The final design frame layout and the dimensions are displayed in Table .

Table 5:

Frame layout and geometry.

Layout

4 bays with 4.5m bay length each dimension.
The first-floor height is 4.8 m (center to center).
The rest floor height is 3.5 m (center to center).

Slab

One-way solid slab 25cm thick.

Beam

Hoops spacing:
S_o = 80 mm.
S_1 = 150 mm.

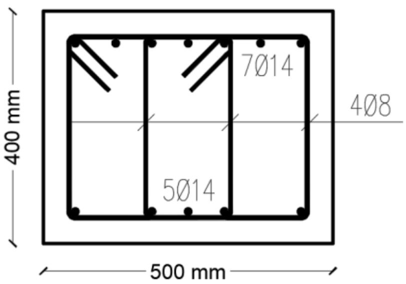

column

Hoops spacing:
S_o = 90 mm.
S_1 = 90 mm.

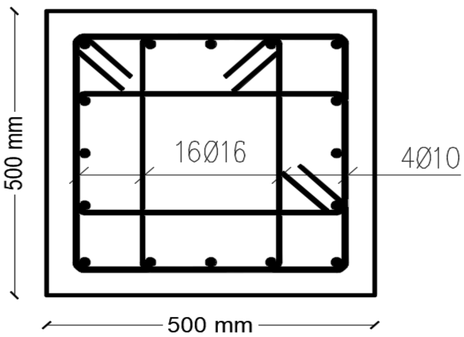

5.2.3 Base Fixity

Frame behavior is affected by the base restraint. Many methods are used to model the base flexibility as seen in Figure E.40 in Appendix E. Many building codes permit the model of the base as fixed support to determine the seismic loads (Moehle, 2015). The support of the frame is assumed fixed because the footing is usually linked with grade beams.

5.2.4 Hinge Definition

To consider the plastic behavior of the members the concentrated plasticity approach is adopted in this study by assigning plastic hinges at specified locations. SAP2000 provides three types of hinge properties: automatic hinge properties, user-defined hinges properties, and general hinge properties. Automatic hinges with ASCE41-13 criteria are used for NSC flexural beams hinges (M3) and combined flexural axial hinges are used (P-M2-M3) for NSC columns.

ASCE41-13 defines the force deformation relation parameters for NSC plastic hinges in tables for different members instead of curvature. Therefore the rotation is used to represent the inelastic behavior of the member at the plastic hinge zone without needing to calculate the plastic hinge length. The auto-hinge definition based on ASCE41-13 is verified next in this section. for each hinges type.

Figure E.41 in Appendix E shows the force deformation relation parameters for ASCE 41-13 hinge definition.

SAP2000 provides a fiber hinge option for creating a combined flexural axial hinge (P-M2-M3) generated from the section materials stress-strain curves (Computers & Structures, Inc. 2016). The fiber hinge method was used to simulate the UHPC column hinges only because it requires a lot of analysis time. Figure E.42 displays the analyzed cantilever column section. Figure E.43 in Appendix E displays the force deformation for the cantilever column section with (M3) auto hinge definition based on ASCE41-13 and with fiber hinge.

Ren et al. (2020) investigated the plastic hinge length of the UHPC columns under cycling load. The analysis is conducted using the finite element method that is calibrated with test results. Also, The applicability of the empirical method used for the NSC column for the UHPC column under is checked. The empirical method for the NSC column is found to underestimate the plastic hinge length when used for the UHPC column.

$$l_p = 0.272L_c + 0.00236f_y d_b - n \tag{32}$$

Where:

l_p: the plastic hinge of the UHPC column (m).

L_c: length of column (m).

f_y: yield strength of reinforcement rebar (MPa).

d_b: the reinforcement rebar diameter (m).

n: axial force ratio.

Table D.5 in Appendix D summarized the plastic hinge length of the UHPC columns. All hinges used in the models are summarized in the following table.

Table 6:

Summarized all hinges used in the models.

Element	**Member material**	**Hinge location**	**Hinge length/member length**	**Hinge type**
Column	UHPC	Each 0.25 of member length	As seen in Table D.5.	Fiber hinge
Column	NSC	Each member ends	Program calculated	ASCE41-13 (P-M2-M3) hinge
Beam	NSC	Each member ends	Program calculated	ACSE41-13 (M3) hinge

5.2.5 Cracking Modifiers

Degradation of stiffness and strength is considered in the models by using effective stiffness value as recommended by ASCE41-13. Effective stiffness is used to achieve the correct displacement of the analytical model when using ASCE41-13 hinges. ASCE41-13 provides a stiffness modifier for different structural elements. ACI318-19 table for effective stiffness modifier adopted in this study which is from the ASCE41-13 table. However, the stiffness values in the table do not apply to fiber hinge type (ACI318, 2019). Figure E.44 in Appendix E displays ACI318-19 effective stiffness values.

Linear interpolation is done to get the effective flexural stiffness values for the axial compression ratio falling between the limits provided as code recommendation. Table D.6 in Appendix D showed the modified flexural stiffness values of the columns interpolated according to the axial compression ratio related to the $A_g f_c'$.

5.2.6 Loading

Two types of loads are assigned to the model which are gravity loads and pushover lateral loads. Moreover, For design purposes, the frame is designed to resist earthquake load as per ASCE7-16.

The gravity loads include the dead load and live loads assigned to the slabs as the following: live load (LL) = 2.5 kN/m^2, dead load (DL) = 9 kN/m^2 (including slab self-weight), masonry wall load = 15KN/m. Also, the self-weight of columns is considered.

Pushover load starts after the nonlinear state of the dead load. Incremental lateral loads are assigned at each slab of the frame with vertical distribution selected as the design response spectrum force distribution. The applied pushover force is displacement-controlled with monitoring the last floor displacement as an indicative displacement.

5.2.7 Model Validation and Verification

SAP2000 is a widely spread and used software in the engineering community and is capable of predicting the linear and the nonlinear behavior of frame structures with acceptable accuracy. Model validation and verification are displayed here.

5.2.7.1 3D model Verification

The 3D model is verified for the elastic response. All model verification is presented in Appendix C.

5.2.7.2 SAP2000 Validation

The SAP2000 version 22 is validated for NSC and UHPC materials. The different hinge types used in the analysis are manually calculated and compared with the SAP2000 results for NSC.

For UHPC material with the used fiber hinge, the experimental test of Yang et al. (2010) is modeled by SAP2000 and the results are compared with the experimental results.

5.2.7.2.1 P-M3 hinge for NSC

The same cantilever column used in the checked by Shehadah (2017) is checked as seen in Figure E.45 in Appendix E. The column under combined axial and increment lateral load.

ASCE41-13 P-M3 hinge is determined as the following:

Conform section since hoops < d/3.

$V_p = (M_{n1} + M_{n2})/L_u$

Where: M_{n1} and M_{n2} are the nominal moments of the column, and L_u is the clear height of the column.

$\rightarrow V_p = \frac{253+0}{4} = 63.2\ kN.$

$$\frac{V}{b_w d\sqrt{f_c{}'}} = \frac{63.2 * 10^3}{400 * 360\sqrt{24}} = 0.09 \le 3$$

$$\rho = \frac{A_v}{b_w s} = \frac{2 * 78.5}{40 * 120} = 0.0033 \ge 0.002$$

$$\frac{s}{d} = \frac{120}{360} = 0.33 \le 0.5$$

$$\frac{p}{A_g f_c{}'} = \frac{1800 * 10^3}{400 * 400 * 24} = 0.47$$

$V_o = V_c + V_s = 306\ kN$

From Table 10.8 in ASCE41-13 and Figure E.41 in Appendix E the following values were obtained:

→a=0.016

$P_y = \frac{253}{4} = 63.2\ kN.$

$P_u = \frac{260}{4} = 65\ kN.$

$\Delta_y = \frac{P_y L^3}{3E_{cr} I_{cr}} = \frac{63.2*10^3*4000^3}{3*0.7*23025*400^4/12} = 39.21\ mm.$

$\Delta_u = \Delta_y + \Delta_p = 39.21 + 0.016 * 4000 = 103.21\ m.$

Figure E.46 in Appendix E displays the SAP2000 results for the column with the P-M3 hinge.

5.2.7.2.2 M3 hinge for NSC

The cross-section used in chapter 3 validation with the resultant M-∅ is used for validating the 3 m NSC cantilever column. The force and the column top displacement are calculated theoretically at two stages as the following:

- At the first yield of steel rebar:

- By virtual method:

$$P_y = \frac{M_y}{3} = \frac{80.4}{3} = 26.8\ kN.$$

$$\Delta_y = \frac{1}{3}\emptyset_y M_{virtual} L = \frac{1}{3} * 0.00802 * 3 * 3 = 24.06\ mm.$$

- By using analysis with cracking section (Caltrans (2010) method) :

$$C_p = C_y * \frac{M_p}{M_y} = 0.00802 * \frac{83.3}{80.4} = 0.00832$$

where $C_y = \emptyset_y$.

$$I_{cr} = \frac{M_p}{C_p E_c} = \frac{83.3 * 10^6}{0.00832 * 23025} * 10^3 = 0.4354 * 10^9\ mm^4.$$

$$\Delta_y = \frac{P_y L^3}{3 E_{cr} I_{cr}} = \frac{26.8 * 10^3 * 3000^3}{3 * 23025 * 0.4354 * 10^9} = 24.08\ mm.$$

- By approximate equation suggested by Pauley et al., 1992 :

$$\Delta_y = \frac{\emptyset_y L^2}{3} = \frac{0.00802 * 3^2}{3} = 24\ \text{mm}.$$

- At ultimate state:

$$P_u = \frac{M_u}{3} = \frac{83.3}{3} = 27.8\ kN.$$

- Using equations from literature for cantilever column (Pauly et al., 1992):

The plastic hinge length is calculated using the Paulay and Priestley (1992) equation is as the following:

$$l_p = 0.08L + 0.022 f_y d \qquad (33)$$

Where:

l_p: The plastic hinge length.

L: Member length.

f_y: Yielding strength of the longitudinal rebar.

d: Main longitudinal rebar diameter.

$l_p = 0.08 * 3 + 0.022 * 420 * 0.016 = 0.388$ m.

$\emptyset_p = (\emptyset_u - \emptyset_y) l_p = (0.063136 - 0.008) * 0.388 = 0.0207\ rad.$

$\Delta_p = \emptyset_p (l - 0.5 l_p) = 0.0207 * (3 - 0.5 * 0.388) = 0.05807\ m.$

$\Delta_u = \Delta_y + \Delta_p = 24 + 58 = 82\ mm.$

- ASCE41-13 methods:

Figure E.41 in Appendix E displays the hinge definition by ASCE41-13.

$$\frac{\rho - \rho'}{\rho_{ce}} \leq 0 \rightarrow \rho - \rho' = 0$$

$M_y = 80.4\ kN.$

$V_y = \frac{M_y}{L} = \frac{80.4}{3} = 26.8\ kN.$

$V_c = 0.17\sqrt{f_c{}'} b_w d = 0.17 * \sqrt{24} * 300 * 350 * 10^{-3} = 85.7\ kN.$

$V_y < V_c$

$$\frac{V}{b_w d \sqrt{fc'}} = \frac{26.8 * 10^3}{300 * 350\sqrt{24}} = 0.05 \leq 3$$

From Table 10.7 from ASCE41-13 for not confined (NC) and $\frac{\rho - \rho\prime}{\rho_{blance}} = 0$:

$a = 0.02$, $b = 0.03$ and c=0.2.

$\Delta_u = \Delta_y + \Delta_p = 24 + 0.02 * 3000 = 84\ m.$

The column is modeled in SAP2000. The hinge is defined as an auto hinge defined as ASCE41-13 and the cracking section is used. The P-Δ curve results from the SAP2000 and the manual calculation are displayed in Figure E.47 in Appendix E.

5.2.7.2.3 Fiber hinge for UHPC column

Yang et al. (2010) tested the FR12-2 beam is modeled by SAP2000 and the results are compared to the experimental results. UHPC material definition and beam section property is detailed in chapter 3. The test beam's geometry is shown in Figure E.48 in Appendix E. The fiber hinge is used and assigned at each 0.1/member length.

The M-∅ curve for beam FR12-2 is compared with the SAP2000 curve obtained from the section designer section definition. The comparison of moment-curvature curves for experimental results and SAP2000 For beam FR12-2 is shown in Figure E.49 in Appendix E.

The moment and displacement at the medial of the beam are calculated as the following:

$$P = 2 * M/1.13$$

$$P_p = 2 * \frac{85}{1.13} = 150.4\ kN$$

$$\Delta_p = \frac{317.55 * 10^6 P}{EI_e}$$

From experimental results $EI_e = 4.44 * 1012$ mm^4.

$$\Delta_p = \frac{317.55*10^6*150.4*10^3}{4.44*10^{12}} = 10.76\ mm$$

Test results are:

P_p = 147.4 kN, Δ_p= 14.54 mm.

The SAP2000 force results from Figure E.50 in Appendix E are:

P_p = 147.6 kN, Δ_p= 14.5 mm.

As seen SAP 2000 agrees well with the experimental results.

5.3 Frame with Soft/Weak Story Irregularity

The NSC frame has a soft/weak story on the base floor. The stiffness and strength irregularities result because the first floor is higher than the rest floors. In this section, the existence of the soft/weak story irregularity is checked. ASCE7-16 definitions for soft and weak story irregularity are used in this research. Also, the behavior of the soft/weak story is presented.

5.3.1 The Existence of Soft Story Irregularity

In this subsection, the common methods for the estimated story lateral stiffness are discussed. Then the story lateral stiffness is calculated and verified. Finally, the existence of soft story irregularity is checked.

5.3.1.1 Lateral Translational Stiffness of Story

Lateral translational stiffness is the maximum resistance for the relative lateral displacement and is usually estimated at the initial state even though it is decreasing with increasing story damage (Murty et al., 2012). The lateral stiffness of the story is the sum of all resisting structural members resisting the relative lateral displacement. Different methods are found in the literature for estimating the story stiffness. These methods can be grouped by two approaches which are: direct stiffness summation for all individual structural resisting elements of the story or using linear elastic analysis.

1. Story Stiffness by the direct stiffness summation

In this approach, the story stiffness is the sum of the stiffness of the structural elements that resist the lateral load. The sum of stiffness includes the contribution from:

1. Flexural deformation:

The lateral stiffness against flexural deformation is as follows (Priestley et al., 1996):

$$K = \alpha_0 \frac{EI_e}{{H_e}^3} \tag{34}$$

Where: E is the modulus of elasticity, I_e is the effective moment of inertia of the cross-sections, H_e is the effective column height and α_0 is boundary conditions coefficients. Figure E.51 in Appendix E displays the stiffness of columns with different boundary conditions and α values. The stiffness of the columns is in a range from $3EI_e / h^3$ to $12EI_e / h^3$ depending on the boundary conditions of the column. To estimate α factor the following equation is proposed by Heidebrecht et al. (1973) is used (Caterino et al., 2013):

$$\alpha_0 = 12\left[1 + \frac{2I_{e,c}}{H_e(\frac{I_{e,b1}}{L_{b,1}} + \frac{I_{e,b2}}{L_{b,2}})}\right]^{-1} \tag{35}$$

Where: $I_{e,b}$ and $I_{e,c}$ is the effective moment of inertia for the beam and the column respectively. L_b is the beam span length and H_e is the clear height of the column.

2. Shear deformation:

The lateral stiffness against shear deformation is as follows (Priestley et al., 1996):

$$K = \frac{H_e}{A_{ve}G} \tag{36}$$

Where: A_{ve} is the effective shear area and the shear modulus. The shear deformation of the column is significant when the flexural moment to shear force ratio is less than three times of column depth when the column height is no longer significant from column depth (Priestley et al., 1996).

3. Axial deformation:

The lateral stiffness against axial deformation due to axial stiffness in the bracing elements is as follows (Papia et al., 2003):

$$K = \frac{\frac{E_{br}\,A}{L_S} cos^2\,\theta}{1 + \frac{E_{br}\,A}{L_S E}\left[\frac{h_{c/c}}{A_c} sin^2\,\theta + \frac{L_b}{A_b} cos^2\,\theta\right]} \tag{37}$$

Where: L_s is the length of the bracing element, θ is the angle of the bracing element, and E_{br} , E is the modulus of elasticity of the bracing element and the frame respectively. A, A_c and A_b, is the cross-section area of the bracing element, column, and beam respectively. $h_{c/c}$ is the column center to center height and L_b is the beam length.

2. Story Stiffness from linear elastic analysis

Vijayanarayanan et al. (2017) summarized seven methods from literature used to estimate the story lateral stiffness of the multi-story frame. Two methods of using linear elastic analysis are explained here.

- Single story stiffness:

Stiffness is estimated for the individual story as the lateral force at the story top produces the translation displacement when the story bottom is retrained against lateral translation motion only. This procedure is cumbersome and time-consuming and requires repetition for each story. Figure E.52 in Appendix E displays the idea of the method.

In this method, the stiffness of the story is calculated by:

$$K = \frac{F_i}{\Delta_i} \tag{38}$$

Where: F_i and Δ_i is the lateral force and the produced displacement at i story.

- Lateral force-deformation method

This method does not require additional analysis from the designer and the results from analysis for earthquake design are used to estimate the story stiffness. The stiffness of the story is calculated as the ratio of the story shear force to story relative internal displacement. This method saves considerable time and effort but the story stiffness varies by the distribution of the lateral design forces over the height of the building. Figure E.53 in Appendix E displays the method.

$$K = \frac{F_i}{(\Delta_i - \Delta_{i-1})} \tag{39}$$

Where: F_i and $(\Delta_i - \Delta_{i-1})$ is the lateral design force and the produced displacement at i story.

5.3.1.2 Story Stiffness Verification

The stiffness of the stories is calculated and compared with SAP2000 results. Tables D.7 through D.10 in Appendix D display the calculations.

The stiffness is estimated manually using the direct stiffness summation method. The cracking analysis modifiers are calculated as discussed previously depending on the axial load to $A_g f_c'$ ratio for the columns.

To determine the story stiffness by SAP2000 the joints at the bottom is restrained for displacement in the load direction and a known lateral load is applied at the joints at the top for the considered story and these procedures are repeated for all story. The manual calculations and the sum of the two stories' stiffness are used for comparison with SAP2000 results.

The SAP2000 results agree well with the manual calculations. There is a difference between the results of SAP2000 and the manual values because the beams have rotated due to the stiffness difference of columns on the ground floor. The max difference was found on the 1st floor due to the base fixation condition.

5.3.1.3 Soft story check

According to ASCE7-16, the soft story exists when the story lateral stiffness to the above stiffness is less than 70% or less than 80% of the average stiffness of the three stories above. Moreover, the soft story is considered an extremely soft story when the lateral stiffness of the story to the story above is less than 60% or less than 80% of the average stiffness of the three stories above. Table 7 displays the soft story check as per the ASCE7-16 definition.

Table 7:

Soft story irregularity check.

Story	Stiffness (kN/m)	K_1/K_2	$K_1/(K_4+K_3+K_2)_{avg}$
1st floor	108,743	59.5%	65.3%
2nd floor	182,669	110.4%	119.0%
3rd floor	165,534	109.2%	114.9%
4th floor	151,650	105.8%	
5th floor	143,344	104.5%	
6th floor	137,236		

Where: K1, K2, K3, and K4 are the stiffness of the first, second, third, and fourth floors respectively. As seen in Table 5.3 the frame has extreme soft story irregularity on the first floor.

5.3.2 The Existence of Weak Story Irregularity

In this subsection, the methods for the estimated story lateral strength are discussed. Then the story lateral strength is calculated and verified. Finally, the existence of weak story irregularity is checked.

5.3.2.1 Story Lateral Strength

The story's lateral strength is the maximum internal strength resisted by the story under increased displacement loading. Two methods are used to calculate the story's lateral strength by using nonlinear static analysis (pushover) or by summation of all structural resisting members of the story (column, wall, and bracing elements).

1. Estimating story lateral strength by pushover analysis

To determine the lateral strength of all stories of the building sequentially, a story is restrained to lateral displacement and incremental load with displacement control is applied at the considered direction and the maximum lateral force considers the story's lateral strength. This procedure is repeated for all stories (Murty et al., 2012). Figure E.54 in Appendix E displays the idea of the method.

Some researchers compared the strength with building code drift limitations and considered the force corresponding to the maximum story drift code limit as the story lateral strength (Das et al., 2003).

2. Estimating story lateral strength by direct strength summation

The lateral strength of the story in this method is calculated as the sum of all strengths of all resisting structural members that share the story strength (Shea et al, 1999). Structural resisting members usually are columns, walls, and bracing elements. The strength of the resisting members when subjected to lateral load can be controlled by flexural moment strength, axial strength, or shear strength (ASCE41, 2013, Rai, 2005).

For column or wall, the geometry and reinforcement control the failure type, therefore moment strength and shear strength capacities shall be calculated. The member lateral strength is considered the least value obtained from the moment strength or shear strength.

The column or wall lateral strength from flexural moment capacity is obtained by calculating the shear force resulting from the moment capacity associated with the axial force at the ends of the column or wall. The moment is determined considering the material's nonlinearity properties. For example, some codes (such as ACI318-19) suggest using $1.25f_y$ for steel yielding stress when calculating the probable flexural moment instead of f_y used for the nominal flexural moment. Figure E.55 in Appendix E displays the column internal forces and moment diagrams used in this method.

The lateral strength of the column or wall from flexural strength is calculated as the following:

$$V = (M_a + M_b)/L_u \tag{40}$$

Column or wall lateral strength from shear strength is the sum of the shear strength of concrete and shear reinforcement. Different codes (such as ACI318-19) provide methods to determine section shear strength as the sum of V_c and V_s.

$$V = V_c + V_s \tag{41}$$

Where: V_c is the concrete shear strength and V_s is the shear reinforcement strength.

Thus, lateral flexural capacity for the frame element is as the following:

$$V_e = (M_a + M_b)/L_u \leq \emptyset V_n \tag{42}$$

Where: M_a and M_b is the probable moment calculated at the designed axial force P_u from factored gravity load with $\phi = 1$ and $f_u = 1.25 f_y$. L_u is the clear height of the column (ACI318, 2019).

In some references, the sum of the moment columns capacities compared with the sum of beams' flexural moment capacity at the joint and the lower value of them is considered for calculating the column strength (Manohar et al., 2015, Shea et al., 1999).

5.3.2.2 Story Strength Verification

The lateral strength of the stories is manually calculated and compared with SAP2000 results.

The lateral strength of the story is manually calculated by the direct strength summation of columns. Table D.11 in Appendix D displays the manual story lateral strength calculations.

Nonlinear static analysis (pushover) is used to calculate the story strength which the strength is the maximum force can the story resist. To calculate the story strength all bottom column joints are restrained and the lateral increment loads are assigned to the top column joints. The plasticity of the column is considered by the concreted hinge as detailed previous 3 at the end of the columns.

The probable moment-plastic rotation curves for the interior columns in the first story resulting from SAP2000 analysis are displayed in the following Figure E.56 in Appendix E.

Table D.12 in Appendix D displays the comparison between manual calculation and SAP2000 for the first and second stories column's probable moment.

SAP2000 hinge moment agrees with the manual calculated probable moment with some differences of the exterior and corner columns probable moment at the 2^{nd} story.

P-Δ curves for the first and the second stories by SAP2000 pushover analysis are displayed in Figure E.57 and Figure E.58 in Appendix E.

Table D.13 in Appendix D displays the first and second stories' lateral strength from SAP2000 results and manual calculation. As seen in Table D.13 in Appendix D SAP2000 agreed well with the manual calculation for the lateral strength of the first and second floors.

The P-delta effect on first lateral story strength is investigated by SAP2000 pushover analysis. Figure E.59 in Appendix E displays the P-Δ curve for the first story by SAP2000 pushover analysis with and without considering the P-delta effect.

At the ASCE7-16 drift limit of 0.02 of the story height, the P-delta effect reduced the first lateral story strength by about 85%. Thus, the P-delta effect will be considered in frame pushover analysis.

5.3.2.3 Weak story check

According to ASCE7-16, the weak story exists when the story's lateral strength to the story above is less than 80%. Moreover, the weak story is considered an extremely weak story when the lateral strength of the story to the story above is less than 65%. Table 8 displays the weak story check as per the ASCE7-16 definition.

Table 8:

The check of the existence of the weak story irregularity on the first floor.

Story	Story strength (kN)	Strength ratio
1^{st} floor	5,750	75.3%
2^{nd} floor	7,640	

The frame has weak story irregularity on the first story, where the story strength ratio of the second floor to the first floor is less than 80% as is seen in Table 5.4.

5.3.3 Frame Behavior with Soft / Weak Story

Figure E.60 in Appendix E displays the story's lateral displacement of the frame floors under a lateral pushover load by SAP2000 nonlinear static analysis. As seen the lateral displacement is concentrated at the extremely soft story and weak story (1st floor).

Figure 8 displays the plastic hinge distributed on the beams at different stories on the frame since the frame is not prohibited according to ASCE7-16 for the extremely soft and weak story at the seismic design category D. The plastic hinges on the top and bottom columns are generated on all the first story columns. Hence, the hinges at the soft/weak story columns have high rotation leading to overall failure of the frame.

Figure 8:

Plastic hinges distribution for the formed building with the soft/weak story irregularities

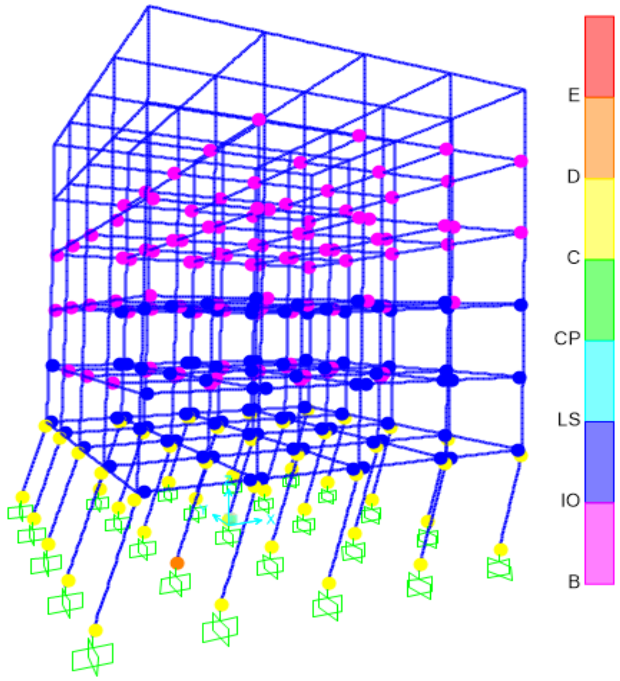

Figure E.61 in Appendix E displays the P-Δ curve for the irregular frame with the soft/weak story by SAP2000 pushover analysis.

5.4 Frame with UHPC Column in The Soft/Weak Story Irregularity

The columns material in the soft/weak story (1st story) is replaced with UHPC material. In the beginning, the increase in the stiffness and strength of the first story is determined when the column material is changed depending on the proposed questions obtained from the parametric study in chapter 4. Then the existence of the soft/weak story irregularity on the first floor is checked for the frame. In addition, The change in earthquake design force values and vertical distribution is checked when the columns' material changes. Then, the overall behavior of the frame is investigated.

5.4.1 Stiffness Increasing of the 1st Story

The increase in the stiffness of the 1st story is estimated by using the equation for K proposed in chapter 4. The 1st story stiffness is estimated as the 1st story stiffness with NSC multiplied by K. Where K is the ratio of the UHPC column stiffness to the NSC column stiffness and is calculated as the following:

$$K = 2.43 - \frac{B}{5000} - 11.6\rho_s - \frac{(N/f_c{}'A_g)}{1.4} \tag{43}$$

K calculation for 1st story columns is displayed in Table D.14 in Appendix D.

To simplify calculation used the average value for all columns:

$$K = \frac{1.94*9+2.01*12+2.05*4}{25} = 1.99.$$

➔ 1st story stiffness with UHPC columns = 1.99*108,743 = 216,399 kN.

The cracking analysis modifiers are adjusted by $\alpha_{UHPC}/\alpha_{NSC}$ in the SAP2000 model for the UHPC column as seen in Table D.15 in Appendix D, where $\alpha_{UHPC}/\alpha_{NSC}$ as the following:

$$\alpha_{UHPC}/\alpha_{NSC} = 1.36 - 6.5\rho_s - \frac{(N/f_c{}'A_g)}{2.5}$$

By SAP2000 1st story stiffness with UHPC columns = 218,373 kN/m. There are small differences between the story stiffness value by predicted equation and SAP2000 analysis.

Table D.16 in Appendix D displays the 1st story lateral stiffness by SAP2000 results vs the predicted value depending K on the 1st story with the UHPC columns.

5.4.2 Lateral Strength Increase of the 1st Story

The increase in the lateral strength of the 1st story is estimated by using the equation for β proposed in chapter 4. The 1st story lateral strength with UHPC is estimated as the 1st story lateral strength with NSC multiplied by β. Where β is the ratio of the UHPC column to the NSC column strength and is calculated as the following:

$$\beta = 2.19 - \frac{B}{1220} - 18.3\rho_s + 2(\frac{N}{f_c{}'A_g})$$

Table D.17 in Appendix D displays the β calculation for 1st story columns. To simplify calculation used the average value for all columns:

$$\beta = \frac{2.20*9+2.02*12+1.90*4}{25} = 2.06.$$

➔ 1st story stiffness = 2.06*5750 = 11,500 kN.

Nonlinear static (pushover) is used to calculate the story strength by SAP2000. The pushover load is applied only to the top of the 1st story to obtain the 1st story lateral strength. Figure E.62 in Appendix E displays the P-Δ curve for the first story with UHPC columns by using SAP2000 pushover analysis.

The predicted 1st story lateral strength by using β is compared with SAP2000 pushover results. Table D.18 in Appendix D displays the 1st story lateral strength by SAP2000 results vs the predicted value depending β on the 1st story with the UHPC column.

5.4.3 The Soft/Weak Story Check

The soft and weak stories irregularities are checked for the first floor after the columns material is replaced with UHPC. Table 9 and Table 10 display the check.

Table 9:

Soft story irregularity check.

Story	Stiffness (kN/m)	K_1/K_2	$K_1/(K_4+K_3+K_2)_{avg}$
1st floor	218,373	97.5%	106.9%
2nd floor	182,669	110.4%	119.0%
3rd floor	165,534	109.2%	114.9%
4th floor	151,650	105.8%	
5th floor	143,344	104.5%	
6th floor	137,236		

As seen in Table 5.5 the frame does not have a soft story irregularity.

Table 10:

The check of the existence of the weak story irregularity on the first floor.

Story	Story strength (kN)	Strength ratio
1st floor	10,000	130.9%
2nd floor	7,640	

As seen in Table 5.6 the frame does not have a weak story irregularity.

5.4.4 Earthquake Design Force Check

The change in the design base shear is checked to investigate whether the increase in the seismic capacity increases the seismic demand. The fundamental period T of the frame decreased when the columns material is replaced with UHPC on the first story form $T = 1.68\ sec$ sec to $T = 1.58\ sec$. However, the fundamental period of the frame with UHPC in the first story is great than the ASCE7-16 code limit for the period $C_u T_a = 1.07 sec$. Therefore, the design base shear does not change.

In addition, the vertical distribution of the design force obtained from the response spectrum method is checked. Figure E.63 in Appendix E displays the response spectrum force vertical distribution for the frame with NSC and for the frame with UHPC columns material in the first story.

As seen in Figure E.62 the vertical distribution of the force is the same for both two frames.

5.4.5 The Behavior of the Frame with UHPC Columns Material

The story lateral displacement for the regular and modified frame is achieved. As seen from Figure 9 the story displacement is distributed on all floors at the frame height and did not concentrate on only the soft/weak story when UHPC material is used in the columns.

Figure 9:

Storie's lateral displacement under lateral pushover load resulting from SAP2000 nonlinear static analysis.

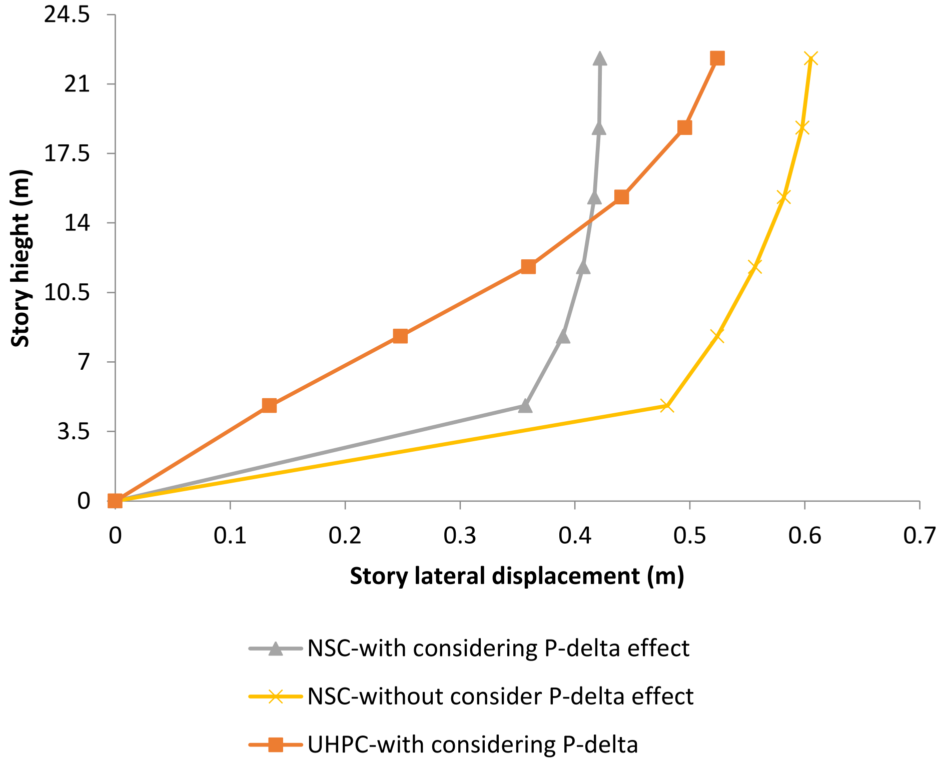

Figure E.64 in Appendix E displays the P-Δ curve for the frame with NSC on the soft/weak story columns and with UHPC columns on the soft/weak story from SAP2000 pushover analysis.

Figure 10 displays the plastic hinge distributed on the frame with UHPC columns on the soft/weak story from the pushover analysis by SAP2000.

Figure 10:

Plastic hinges distribution for the formed building with UHPC columns on the soft/weak story irregularities.

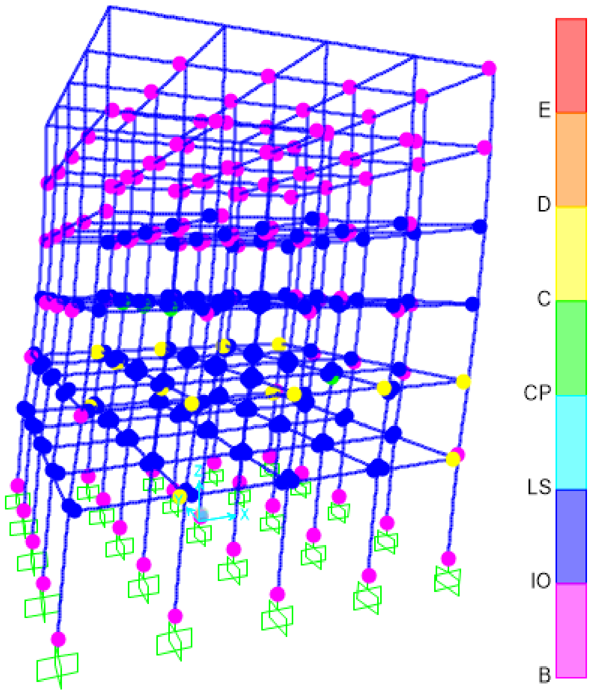

Figure E.65 in Appendix E displays the ATC-40 capacity spectrum from SAP2000 analysis for: a) the frame with NSC on the soft/weak story columns. b) the frame with UHPC on the soft/weak story columns.

Chapter Six

Conclusions, Recommendations, And Future Work

6. Conclusions, Recommendations, And Future Work

6.1 Summary

In this research, UHPC material is used in the columns of the soft/weak story to eliminate the soft/weak story irregularity. A parametric study using sectional analysis by XTRACT software is performed. The parametric study results are used to investigate the effectiveness of using UHPC in the soft/weak story columns. Regression analysis is performed to propose equations to predict the stiffness and strength of the columns when the UHPC material is used. Finally, a 3D sway special moment-resisting framed building is nonlinear static (pushover) analyzed to investigate the overall behavior of the frame. SAP2000 program is used in the pushover analysis for the irregular frame with NSC and UHPC material in the columns of the soft/weak story. The frame analysis results are compared with the parametric study results to confirm the predicted impact.

6.2 Conclusions

Based on the study and results obtained in the thesis, the following conclusions can be drawn:

1. The replacement of NSC with UHPC is an effective tool for solving soft/weak story irregularities while maintaining the architectural requirements at the design stage.
2. The effect of replacing the NSC material with UHPC material on the column cross-sectional flexural rigidity can be computed using the ratio K.
3. The effect of replacing the NSC material with UHPC material on the column cross-sectional flexural strength can be computed using the ratio β.
4. The effect of replacing the NSC material with UHPC material on the cracking analysis modifiers can be computed using the ratio $\alpha_{UHPC}/\alpha_{NSC}$.
5. The increase in the shear capacity of the soft/weak story due to the use of UHPC instead of NSC is greater than the increase in the moment capacity. Thus, the moment capacity would still control the lateral strength of the column in the soft/weak story irregularity.
6. Based on the case study of the 3D frame building the following conclusions are obtained:

a. The maximum inter-story displacement and drift are found in the first story where the soft/weak story has existed for irregular frame with NSC in the soft/weak story columns. But the inter-story displacement or drift is distributed along with the building height when UHPC material is used in the soft/weak story columns.
b. The plastic hinge is distributed effectively when the UHPC is used in the soft/weak story columns. In spite that the plastic hinges are concentrated at the soft/weak story column for the frame with NSC columns in soft/weak story.
c. The prediction of the story lateral stiffness and strength using the results obtained from the parametric study is reasonable.

6.3 Future work and Recommendations

While this research is examined the ability to use UHPC material to eliminate the soft and weak stories irregularities in the first floor of the sway special moment-resisting frame. Further researches are required to generalize the results. The followings are the recommendations for further research in this area:

1. This researches deal with sway special moment-resisting frame. However, there are other concrete lateral resisting systems such as dual systems that can behave differently. Thus, extended behavior is needed to investigate the behaviors of other concrete lateral revisiting systems.
2. The study is concerned with the soft and weak story's irregularities. But there are many vertical and horizontal irregularities that may be solved when the UHPC material is used such as torsional irregularity.
3. This study deals with using UHPC material for the irregular building at the design stage and it can be extended for the retrofitting of the existing building.

List of Abbreviations

A_i:	area of fiber i.
A_v:	area of shear reinforcement.
$A_{v,min}$:	minimum area of shear reinforcement within spacing s, mm^2.
A_c:	the cross-sectional area of the UHPC member.
A_{sw}:	the cross-sectional area of the shear reinforcement.
A_{fv}:	the projection in the cross-section of the inclined area on which the fiber act and is equal $A_{fv} = b_w z$.
A_{ve} :	the effective shear area and the shear modulus
A:	the cross-section area of the bracing element.
A_c:	the cross-section area of the column.
A_b:	the cross-section area of the beam.
b_w:	web width or diameter of circular section.
b_{w1}:	the smallest width of the cross-section in the tensile area.
b_c:	the core dimension perpendicular to the tie legs.
C_d:	the deflection amplification factor.
C_t:	a coefficient equal to 0.0466 for the frame.
C_u:	coefficient for the upper limit on the calculated period.
C_s:	the seismic response coefficient.
d:	distance from extreme compression fiber to centroid of longitudinal tension reinforcement.
d:	reinforcement rebar diameter.
d_b:	the diameter of reinforcement bare.
E_c:	concrete modulus of elasticity.
E_{br} :	the modulus of elasticity of the bracing element.
E:	seismic load effect.
E_v:	effect of horizontal seismic forces.
E_h:	vertical seismic effect.
f_c':	concrete compressive strength.
f_c:	concrete stress.
f_{ck}:	the characteristic value of compressive strength.
f_y:	yield strength of reinforcement rebar (MPa).
F_i:	the lateral design force at i story.
F_a and F_v:	site coefficients and is given from ASCE7-16 tables.
g:	the gravitational acceleration.
h:	maximum depth of the cross-section.
h_w:	the member height.
$h_{c/c}$:	the column center to center height.
h_n:	the structural height.
h_{sx}:	story height below level x.
H_e:	is effective column height.
HSC:	high strength concrete.
I_g:	the gross moment of inertia.
I_e :	the effective moment of inertia of the cross-sections.
k_f:	concrete strength factor.

k_n:	confinement effectiveness factor.
K:	factor describes the increase in the flexural stiffness when the UHPC is used instead of the NSC in the column.
L_b:	the beam length.
L_c:	length of column.
L_u:	the clear height of the column.
l_p:	the plastic hinge length.
l_w:	the member length.
L_s :	the length of the bracing element.
l_d:	development length of longitudinal bars.
m_y:	the ideal yielding moment.
M_x:	applied moment about X-axis.
M_y:	applied moment about Y-axis.
M_{a0} :	is the maximum service load moment.
M_{cr} :	is the cracking moment.
M_a and M_b:	the probable moment calculated at the designed axial force P_u from factored gravity load with $\phi = 1$ and $f_u = 1.25f_y$.
M_{nc}:	the nominal strength of the columns framing into the joint.
M_{nb}:	the nominal strength of the beams framing into the joint.
n:	axial force ratio.
n_1:	the number of longitudinal bars or bundles around the perimeter of a column core with rectilinear hoops that are laterally supported by the corner of hoops or by seismic hooks.
NSC:	normal strength concrete.
N_u:	factored axial force normal to cross-section occurring simultaneously with V_u or T_u.
N_{Ed}:	the axial force in the cross-section, due to the external loads.
P:	applied axial load.
P_x:	service total vertical design load at and above level x.
R:	the reponse modification coefficient.
s:	spacing of the stirrups.
S_s:	the spectral response acceleration parameter at short periods.
S_1:	the spectral response acceleration parameter at 1 s.
S_{Ds}:	the design spectral response acceleration parameter at short periods.
S_{D1}:	the design spectral response acceleration parameter at a period of 1 s.
T_a:	the approximation fundamental period.
T:	fundamental period determined by analysis.
ρ:	the redundancy factor.
$V_{Rd,c}$:	the shear strength contribution of the cement matric of UHPC.
$V_{Rd,s}$:	the shear strength contribution of the shear reinforcement.
$V_{Rd,f}$:	the shear strength contribution of the fiber.
V_c:	the concrete shear strength.
V_x:	seismic shear force acting between levels x and x-1.
w:	the effective mass weight.
w_i :	the story weight at the story level i.
x:	a coefficient equal to 0.9 for the frame.

z:	the lever arm of the internal forces for a member of constant height corresponding to the bending moment in the member.
α_1:	linearity deviation parameter.
α:	the ratio of effective flexural rigidity.
α_0 :	boundary conditions coefficients.
β_0:	is the ratio of shear demand to shear capacity for the story between levels a and x-1.
β:	factor is defined as the ratio of the maximum moment of the UHPC section over the NSC section at the same axial load level.
$\gamma_{cf}\gamma_E$:	a safety factor.
γ_{cf}:	a safety factor.
δ_i :	the lateral displacement at i story t.
δ_x and δ_{x-1}:	the inelastic story displacement at level x and $x-1$ respectively at the center of mass.
Δ_i:	the produced displacement at i story.
$(\Delta_i - \Delta_{i-1})$:	the lateral drift at i story.
Δ :	is the design inter-story drift.
$\Delta_{inelastic}$:	design story drift occurring simultaneously with V_x.
$\varepsilon_c{}'$:	concrete strain at $f_c{}'$.
ε:	concrete strain.
ε_u:	ultimate concrete strain capacity.
θ:	strut inclination angle or the angle of the bracing element.
λ:	factor for lightweight or normal weight concrete.
ρ_w:	ratio of A_s to $b_w d$.
$\emptyset_y$:	the ideal yielding curvature.
σ_{pf} :	post-cracking tensile strength.
σ_i:	the stress of fiber i.
$\sigma_{Rd,f}$:	the mean value of the post-cracking strength along the shear crack of inclination θ, and perpendicular to it.
ψ_t:	casting location in tension factor.
ψ_e:	reinforcement coating factor.
ψ_g:	grade of reinforcement factor.
Ω_o:	the over-strength factor.

References

[1] Aboukifa, M., Moustafa, M. A., Itani, A. M., & Naeimi, N. (2019). Durable UHPC Columns with High-Strength Steel (No. ABC-UTC-2013-C3-UNR02-Final). Accelerated Bridge Construction University Transportation Center (ABC-UTC).

[2] ACI 239R-18. (2018). Ultra-High-Performance Concrete: An Emerging Technology Report", ISBN:978-1-64195-034-3, *American Concrete Institute*, Farmington Hills, MI, October 2018.

[3] ACI Committee. (2019). Building code requirements for structural concrete (ACI 318-19) and commentary. In *American Concrete Institute*.

[4] ACI. 544.4 R-18. (2018). Guide to Design with Fiber-Reinforced Concrete".

[5] AFNOR (Association Française de Normalisation). (2016). National addition to Eurocode 2—Design of concrete structures: Specific rules for ultra-high performance fibre-reinforced concrete (UHPFRC).

[6] Al-Ali, A. A. (1999). Effects of vertical irregularities on seismic behavior of building structures. Stanford University.

[7] Aliasghar-Mamaghani, M., & Khaloo, A. (2021). Effective flexural stiffness of beams reinforced with FRP bars in reinforced concrete moment frames. Journal of Composites for Construction, 25(1), 04020083.

[8] Alnajajra, H. (2017). Enhancing Earthquake Resistance of Local Structures by Reducing Superimposed Dead Load. An-Najah National University, MSc thesis.

[9] Alsalman, A., Dang, C. N., Prinz, G. S., & Hale, W. M. (2017). Evaluation of modulus of elasticity of ultra-high performance concrete. Construction and Building Materials, 153, 918-928.

[10] American Society of Civil Engineers. (2017, June). Minimum design loads and associated criteria for buildings and other structures. American Society of Civil Engineers.

[11] Armouti, N. (2008). Earthquake Engineering: Theory and Implementation with the 2006 International Building Code. McGraw-Hill Education.

[12] Avşar, Ö. Z. G. Ü. R., Bayhan, B. E. Y. H. A. N., & Yakut, A. (2014). Effective flexural rigidities for ordinary reinforced concrete columns and beams. *The Structural Design of Tall and Special Buildings*, *23*(6), 463-482.

[13] Aydin, K. (2007). Evaluation of Turkish seismic code for mass irregular buildings.

[14] Azmee, N. M., & Shafiq, N. (2018). Ultra-high performance concrete: From fundamental to applications. *Case Studies in Construction Materials*, *9*, e00197.

[15] Bhosale, A. S., Davis, R., & Sarkar, P. (2017). Vertical irregularity of buildings: regularity index versus seismic risk. *ASCE-ASME Journal of Risk and Uncertainty in Engineering Systems, Part A: Civil Engineering*, *3*(3), 04017001.

[16] Caldwell, T. (2011). Plastic Hinge Behavior of Reinforced Concrete and Ultra High Performance Concrete Beam-Columns under Severe and Short Duration Dynamic Loads (Doctoral dissertation, University of Florida).

[17] Caltrans, S. D. C. (2010). Caltrans seismic design criteria version 1.6. *California Department of Transportation, Sacramento*.

[18] Chadwell, C. B., & Imbsen, R. A. (2004). XTRACT: A tool for axial force-ultimate curvature interactions. In *Structures 2004: Building on the past, securing the future* (pp. 1-9).

[19] Chandrahas, B. L., & Raju, P. P. (2017). Behaviour of Soft Storey RC Framed Building Under Seismic Loading. International Journal of Civil Engineering and Technology (IJCIET), 8(4), 265-277.

[20] Chao, S. H., Kaka, V., Palacios, G., Kim, J., Choi, Y. J., Aghdasi, P., ... & Schultz, A. (2016, July). Seismic behavior of ultra-high-performance fiber-reinforced concrete moment frame members. In International Interactive Symposium on Ultra-High Performance Concrete (Vol. 1, No. 1). Iowa State University Digital Press.

[21] Chen, S., Zhang, R., Jia, L. J., & Wang, J. Y. (2018). Flexural behaviour of rebar-reinforced ultra-high-performance concrete beams. Magazine of Concrete Research, 70(19), 997-1015.

[22] Chintanapakdee, C., & Chopra, A. K. (2004). Seismic response of vertically irregular frames: response history and modal pushover analyses. *Journal of Structural Engineering*, *130*(8), 1177-1185.

[23] Choi, B. J. (2004). Hysteretic energy response of steel moment- resisting frames with vertical mass irregularities. The Structural Design of Tall and Special Buildings, 13(2), 123-144.

[24] Chopra, A. K. (2012). Dynamics of structures. theory and applications to *Earthquake Engineering*.

[25] Code, U. B. (1997). UBC-97. In Structural engineering design provisions. International conference of building officials, Whittier, California.

[26] Das, S., & Nau, J. M. (2003). Seismic design aspects of vertically irregular reinforced concrete buildings. *Earthquake Spectra*, *19*(3), 455-477.

[27] Duggal, S. K. (2007). Earthquake resistant design of structures. New Delhi: Oxford university press.

[28] Dya, A. F. C., & Oretaa, A. W. C. (2015). Seismic vulnerability assessment of soft story irregular buildings using pushover analysis. *Procedia Engineering*, *125*, 925-932.

[29] Eide, M. B., & Hisdal, J. M. (2012). Ultra High Performance Fibre Reinforced Concrete (UHPFRC)–State of the art: FA 2 Competitive constructions: SP 2.2 Ductile high strength concrete.

[30] EL-Attar, M. M., El-Karmoty, H. Z., & EL-Moneim, A. A. (2016). The behavior of ultra-high-strength reinforced concrete columns under axial and cyclic lateral loads. *HBRC journal*, *12*(3), 284-295.

[31] Fehling, E., Schmidt, M., Walraven, J., Leutbecher, T., Frohlich, S., & Ultra-High Performance Concrete, U. H. P. C. (2014). Fundamentals, Design, Examples. *Ernst & Sohn, Berlin, Germany*.

[32] Graybeal, B. A. (2007). Compressive behavior of ultra-high-performance fiber-reinforced concrete. *ACI materials journal*, *104*(2), 146.

[33] Gu, C., Ye, G., & Sun, W. (2015). Ultrahigh performance concrete-properties, applications and perspectives. Science China Technological Sciences, 58(4), 587-599.

[34] Guevara, L. T., & Garcia, L. E. (2005). The captive-and short-column effects. Earthquake Spectra, 21(1), 141-160.

[35] Guevara-Perez, L. T. (2012). Soft story and weak story in earthquake resistant design: A multidisciplinary approach. 15WCEE. Lisboa. Retrieved from https://www. iitk. ac. in/nicee/wcee/article/WCEE2012_0183. pdf.

[36] Haber, Z. B., De la Varga, I., Graybeal, B. A., Nakashoji, B., & El-Helou, R. (2018). *Properties and behavior of UHPC-class materials* (No. FHWA-HRT-18-036). United States. Federal Highway Administration. Office of Infrastructure Research and Development.

[37] Hung, C. C., & Hu, F. Y. (2018). Behavior of high-strength concrete slender columns strengthened with steel fibers under concentric axial loading. *Construction and Building Materials*, *175*, 422-433.

[38] Hung, C. C., & Yen, C. H. (2021). Compressive behavior and strength model of reinforced UHPC short columns. *Journal of Building Engineering*, *35*, 102103.

[39] International Code Council. (2015). *2015 IBC: International Building Code*. ICC, International Code Council, Incorporated.

[40] Joe, C. D., & Moustafa, M. (2016, July). Cost and ecological feasibility of using UHPC in bridge piers. In *International Interactive Symposium on Ultra-High Performance Concrete* (Vol. 1, No. 1). Iowa State University Digital Press.

[41] Kimura, H., Ishikawa, Y., Kambayashi, A., & Takatsu, H. (2007). Seismic behavior of 200 MPa ultra-high-strength steel-fiber reinforced concrete columns under varying axial load. *Journal of advanced concrete technology*, *5*(2), 193-200.

[42] Kirac, N., Dogan, M., & Ozbasaran, H. (2011). Failure of weak-storey during earthquakes. Engineering Failure Analysis, 18(2), 572-581.

[43] Kirac, Nevzat, Mizam Dogan, and Hakan Ozbasaran. "Failure of weak-storey during earthquakes." *Engineering Failure Analysis* 18.2 (2011): 572-581.

[44] Leutbecher, T., & Fehling, E. (2013). A simple design approach for UHPFRC in bending. In RILEM-fib-AFGC Int. Symp. Ultra-High Perform. Fibre-Reinf. Concr (pp. 509-518).

[45] Lim, W. Y., & Hong, S. G. (2016). Shear tests for ultra-high performance fiber reinforced concrete (UHPFRC) beams with shear reinforcement. *International Journal of Concrete Structures and Materials*, *10*(2), 177-188.

[46] Madhekar, S., & Manohar, S. (2015). Seismic design of RC buildings: Theory and practice.

[47] Magliulo, G. E. N. N. A. R. O., Ramasco, R. O. B. E. R. T. O., & Realfonzo, R. O. B. E. R. T. O. (2002, September). A critical review of seismic code provisions for vertically irregular frames. In Proceedings of the third European workshop on the seismic behavior of irregular and complex structures, Florence.

[48] Mander, J. B., Priestley, M. J., & Park, R. (1988). Theoretical stress-strain model for confined concrete. *Journal of structural engineering*, *114*(8), 1804-1826.

[49] Mezzi, M., & Parducci, A. (2005, August). Preservation of existing soft-first-story configurations by improving the seismic performance. In *3rd Int. Spec. Conf on The Conceptual Approach to Structural Design*.

[50] Moehle, J. (2015). Seismic design of reinforced concrete buildings. McGraw-Hill Education.

[51] Murty, C. V. R., Goswami, R., Vijayanarayanan, A. R., & Mehta, V. V. (2012). Some concepts in earthquake behaviour of buildings. Gujarat State Disaster Management Authority, Government of Gujarat.

[52] No, E., & STANDARD, I. (1994). Design provisions for earthquake resistance of structures.

[53] Papia, M., Cavaleri, L., & Fossetti, M. (2003). Infilled frames: developments in the evaluation of the stiffening effect of infills. *Structural engineering and mechanics*, *16*(6), 675-693.

[54] Park, R., & Paulay, T. (1975). Reinforced Concrete Structures, John Wiley & Sons. NY, USA.

[55] Paulay, T., & Priestley, M. N. (1992). Seismic design of reinforced concrete and masonry buildings.

[56] Pekelnicky, R., Engineers, S. D., Chris Poland, S. E., & Engineers, N. D. (2012). ASCE 41-13: Seismic evaluation and retrofit rehabilitation of existing buildings. *Proceedings of the SEAOC*.

[57] Pourbaba, M., & Joghataie, A. (2019). Determining shear capacity of ultra-high performance concrete beams by experiments and comparison with codes. *Scientia Iranica*, *26*(1), 273-282.

[58] Pourbaba, M., Joghataie, A., & Mirmiran, A. (2018). Shear behavior of ultra-high performance concrete. *Construction and Building Materials*, *183*, 554-564.

[59] Pragalath, D. H., Avadhoot, B., Robin, D. P., & Pradip, S. (2016). Multiplication factor for open ground storey buildings–a reliability based evaluation. *Earthquake Engineering and Engineering Vibration*, *15*(2), 283-295.

[60] Priestley, M. N., Seible, F., & Calvi, G. M. (1996). *Seismic design and retrofit of bridges*. John Wiley & Sons.

[61] Rai, D. C. (2005). Review of documents on seismic evaluation of existing buildings. *Department of Civil Engineering, Indian Institute of Technology Kanpur India.*

[62] Rajeev, P., & Tesfamariam, S. (2017). Effects of vertical irregularities and construction quality in seismic fragilities for reinforced concrete buildings. *International Journal of Earthquake and Impact Engineering*, *2*(1), 1-31.

[63] Ren, L., Fang, B., Wang, K., & Yuan, F. (2020). Numerical Investigation on Plastic Hinge Length of Ultra-high Performance Concrete Column under Cyclic Load. Journal of Earthquake Engineering, 1-19.

[64] Ruiz, S. E., & Diederich, R. (1989). The Mexico earthquake of September 19, 1985—the seismic performance of buildings with weak first storey. *Earthquake Spectra*, *5*(1), 89-102.

[65] Russell, H. G., Graybeal, B. A., & Russell, H. G. (2013). *Ultra-high performance concrete: A state-of-the-art report for the bridge community* (No. FHWA-HRT-13-060). United States. Federal Highway Administration. Office of Infrastructure Research and Development.

[66] Sadashiva, V. K., MacRae, G. A., & Deam, B. L. (2012). Seismic response of structures with coupled vertical stiffness–strength irregularities. Earthquake engineering & structural dynamics, 41(1), 119-138.

[67] Sahoo, D. R., & Rai, D. C. (2013). Design and evaluation of seismic strengthening techniques for reinforced concrete frames with soft ground story. *Engineering structures*, *56*, 1933-1944.

[68] SAP 2000. (2000). CSI analysis reference manual for SAP2000®, ETABS®, SAFE® and cSiBridge®.

[69] SASPARM Project, (2014). "Support Action for Strengthening Palestine capabilities for seismic Risk Mitigation ", Report done by SASPARM project, "Seismic Risk Mitigation in Palestine", Urban Planning and Disaster Risk Reduction Center at An Najah National University.

[70] Shafieifar, M., Farzad, M., & Azizinamini, A. (2018). A comparison of existing analytical methods to predict the flexural capacity of Ultra High Performance Concrete (UHPC) beams. *Construction and Building Materials*, *172*, 10-18.

[71] Shea. G, Albany. Structural Engineers Association of California SEAC. (1999). Seismic Design Manual. Volume I. Code Application Examples

[72] Shehadah, A. (2017) Seismic Assessment and Rehabilitation of Existing Buildings Using Nonlinear Static Procedures (NSPs) -Pushover Procedures. An-Najah National University, MSc thesis.

[73] Solhmirzaei, R. (2021). Response of Ultra High Performance Fiber Reinforced Concrete Beams under Flexure and Shear. Michigan State University.

[74] Soni, D. P., & Mistry, B. B. (2006). Qualitative review of seismic response of vertically irregular building frames. ISET Journal of Earthquake Technology, Technical Note, 43(4), 121-132.

[75] Su, Y., Li, J., Wu, C., Wu, P., & Li, Z. X. (2016). Effects of steel fibres on dynamic strength of UHPC. *Construction and Building Materials*, *114*, 708-718..

[76] Taerwe, L., & Matthys, S. (2013). Fib model code for concrete structures 2010.

[77] Taranath, B. S. (2004). Wind and earthquake resistant buildings: Structural analysis and design. CRC press.

[78] Taranath, B. S. (2009). Reinforced concrete design of tall buildings. CRC press.

[79] Tong, X., Fang, Z., Luo, X., & Gong, L. (2020). Study on shear capacity of ultra-high performance concrete squat shear walls. *Case Studies in Construction Materials*, *12*, e00314.

[80] Valmundsson, E. V., & Nau, J. M. (1997). Seismic response of building frames with vertical structural irregularities. *Journal of Structural Engineering*, *123*(1), 30-41.

[81] Van Thuat, D. (2013). Story strength demands of irregular frame buildings under strong earthquakes. *The Structural Design of Tall and Special Buildings*, *22*(9), 687-699.

[82] Varadharajan, S., Sehgal, V. K., & Saini, B. (2012). Review of different structural irregularities in buildings. *Journal of structural engineering*, *39*(5), 393-418.

[83] Varadharajan, S., Sehgal, V. K., & Saini, B. (2012). Review of different structural irregularities in buildings. *Journal of structural engineering*, *39*(5), 393-418.

[84] Varadharajan, S., Sehgal, V. K., & Saini, B. (2013). Seismic response of multistory reinforced concrete frame with vertical setback irregularities. *The structural design of tall and special buildings*, *Wiley publications*, *DOI*, *10*.

[85] Verde, R. V. (1991). Explanation for the numerous upper floor collapses during the 1985 Mexico City earthquake. *Earthquake engineering & structural dynamics*, *20*(3), 223-241.

[86] Vijayanarayanan, A. R., Goswami, R., & Murty, C. V. R. ESTIMATION OF STOREY STIFFNESS IN MULTI-STOREY BUILDINGS.

[87] Walraven, J. (2013). fib Model Code for Concrete Structures 2010: mastering challenges and encountering new ones. *Structural Concrete*, *14*(1), 3-9.

[88] XTRACT version 3.0.5. (2006). Release notes.

[89] Yang, I. H., Joh, C., & Kim, B. S. (2010). Structural behavior of ultra high performance concrete beams subjected to bending. *Engineering structures*, *32*(11), 3478-3487.

[90] Yang, I. H., Joh, C., & Kim, B. S. (2012). Flexural response predictions for ultra-high-performance fibre-reinforced concrete beams. *Magazine of Concrete Research*, *64*(2), 113-127.

Appendices

Appendix A: Sectional Analysis Results

1. Sectional analysis results

Table A. 1:

Sectional analysis results.

B	H/B	ρ_s	$N/f_c'A_g$	$EI_{g,\ UHPC}$ (N.m2)	$EI_{e,\ UHPC}$ (N.m^2)	α_{UHPC}	$EI_{e,\ NSC}$ (N.m^2)	K ($EI_{e,UHPC}/EI_{e,\ NSC}$)	α_{NSC}	$\alpha_{UHPC}/\alpha_{NSC}$	$M_{u,UHPC}$ (kN.m)	$M_{u,NSC}$ (kN.m)	β
300	1	0.01	0.2	2.77E+07	1.07E+07	0.39	4.77E+06	2.24	0.31	1.26	181.7	82.5	2.20
300	1	0.01	0.4	2.77E+07	1.22E+07	0.44	6.27E+06	1.95	0.40	1.09	229.5	97.8	2.35
300	1	0.01	0.6	2.77E+07	1.34E+07	0.48	8.33E+06	1.61	0.54	0.90	275.2	91	3.02
300	1	0.02	0.2	2.77E+07	1.22E+07	0.44	6.01E+06	2.03	0.39	1.14	219.5	110.1	1.99
300	1	0.02	0.4	2.77E+07	1.36E+07	0.49	7.32E+06	1.86	0.47	1.04	267.1	122.9	2.17
300	1	0.02	0.6	2.77E+07	1.47E+07	0.53	9.08E+06	1.62	0.58	0.91	311.7	111.4	2.80
300	1	0.03	0.2	2.77E+07	1.38E+07	0.50	7.18E+06	1.92	0.46	1.08	257.4	137.6	1.87
300	1	0.03	0.4	2.77E+07	1.50E+07	0.54	8.43E+06	1.78	0.54	1.00	303.9	148.3	2.05
300	1	0.03	0.6	2.77E+07	1.60E+07	0.58	9.89E+06	1.62	0.64	0.91	347.9	132.4	2.63
300	1.33	0.01	0.2	6.51E+07	2.66E+07	0.41	1.19E+07	2.24	0.33	1.25	323.9	147.7	2.19
300	1.33	0.01	0.4	6.51E+07	3.04E+07	0.47	1.51E+07	2.01	0.41	1.13	409	175.7	2.33
300	1.33	0.01	0.6	6.51E+07	3.35E+07	0.51	1.99E+07	1.68	0.54	0.94	485.4	161.3	3.01
300	1.33	0.02	0.2	6.51E+07	3.06E+07	0.47	1.52E+07	2.01	0.42	1.13	394.9	202	1.95
300	1.33	0.02	0.4	6.51E+07	3.41E+07	0.52	1.78E+07	1.91	0.49	1.07	477.3	193.5	2.47
300	1.33	0.02	0.6	6.51E+07	3.69E+07	0.57	2.19E+07	1.68	0.60	0.94	554.6	180.3	3.08
300	1.33	0.03	0.2	6.51E+07	3.39E+07	0.52	1.82E+07	1.86	0.50	1.04	464.1	249.3	1.86
300	1.33	0.03	0.4	6.51E+07	3.70E+07	0.57	2.06E+07	1.80	0.56	1.01	544.41	230.3	2.36
300	1.33	0.03	0.6	6.51E+07	3.95E+07	0.61	2.41E+07	1.64	0.66	0.92	619.2	209.2	2.96
300	1.66	0.01	0.2	1.27E+08	5.34E+07	0.42	2.42E+07	2.21	0.34	1.24	505.8	231	2.19
300	1.66	0.01	0.4	1.27E+08	6.11E+07	0.482	2.98E+07	2.05	0.42	1.15	636.4	254.6	2.50

300	1.66	0.01	0.6	1.27E+08	6.74E+07	0.532	3.92E+07	1.72	0.55	0.96	764	253	3.02
300	1.66	0.02	0.2	1.27E+08	6.14E+07	0.485	3.10E+07	1.98	0.44	1.11	615.1	317.1	1.94
300	1.66	0.02	0.4	1.27E+08	6.83E+07	0.539	3.54E+07	1.93	0.50	1.08	744.4	343	2.17
300	1.66	0.02	0.6	1.27E+08	7.40E+07	0.584	4.35E+07	1.70	0.61	0.95	870.1	311.7	2.79
300	1.66	0.03	0.2	1.27E+08	6.90E+07	0.545	3.74E+07	1.84	0.53	1.04	726.3	396.6	1.83
300	1.66	0.03	0.4	1.27E+08	7.53E+07	0.594	4.12E+07	1.83	0.58	1.02	851.1	411.8	2.07
300	1.66	0.03	0.6	1.27E+08	8.06E+07	0.636	4.80E+07	1.68	0.68	0.94	972.4	376.3	2.58
300	2	0.01	0.2	2.22E+08	9.60E+07	0.433	4.45E+07	2.16	0.36	1.21	735.8	346.3	2.12
300	2	0.01	0.4	2.22E+08	1.10E+08	0.497	5.35E+07	2.06	0.43	1.16	929	405	2.29
300	2	0.01	0.6	2.22E+08	1.21E+08	0.546	7.00E+07	1.73	0.56	0.97	1112	373.4	2.98
300	2	0.02	0.2	2.22E+08	1.11E+08	0.501	5.77E+07	1.92	0.46	1.08	901.1	472.6	1.91
300	2	0.02	0.4	2.22E+08	1.23E+08	0.555	6.47E+07	1.90	0.52	1.07	1089	511.5	2.13
300	2	0.02	0.6	2.22E+08	1.34E+08	0.605	7.87E+07	1.70	0.63	0.96	1267	465.9	2.72
300	2	0.03	0.2	2.22E+08	1.25E+08	0.564	7.03E+07	1.78	0.57	1.00	1064	595.4	1.79
300	2	0.03	0.4	2.22E+08	1.37E+08	0.618	7.63E+07	1.80	0.61	1.01	1247	618.2	2.02
300	2	0.03	0.6	2.22E+08	1.46E+08	0.659	8.79E+07	1.66	0.71	0.93	1421	569.2	2.50
400	1	0.01	0.2	8.75E+07	3.61E+07	0.412	1.66E+07	2.17	0.34	1.22	434.2	202	2.15
400	1	0.01	0.4	8.75E+07	4.13E+07	0.472	2.06E+07	2.00	0.42	1.13	547.9	242.4	2.26
400	1	0.01	0.6	8.75E+07	4.54E+07	0.519	2.72E+07	1.67	0.55	0.94	655.5	220.6	2.97
400	1	0.02	0.2	8.75E+07	4.19E+07	0.479	2.14E+07	1.96	0.44	1.10	529.2	279.7	1.89
400	1	0.02	0.4	8.75E+07	4.65E+07	0.531	2.48E+07	1.88	0.50	1.05	640.5	308.4	2.08
400	1	0.02	0.6	8.75E+07	5.03E+07	0.575	3.03E+07	1.66	0.62	0.93	746	274.9	2.71
400	1	0.03	0.2	8.75E+07	4.74E+07	0.542	2.60E+07	1.82	0.53	1.02	623.3	357.6	1.74
400	1	0.03	0.4	8.75E+07	5.16E+07	0.59	2.91E+07	1.77	0.59	1.00	731.6	374.1	1.96
400	1	0.03	0.6	8.75E+07	5.50E+07	0.628	3.37E+07	1.63	0.69	0.92	834.7	332.5	2.51
400	1.33	0.01	0.2	2.06E+08	8.85E+07	0.43	4.14E+07	2.14	0.36	1.20	771.6	365.5	2.11
400	1.33	0.01	0.4	2.06E+08	1.01E+08	0.491	4.99E+07	2.02	0.43	1.14	971.5	431.3	2.25
400	1.33	0.01	0.6	2.06E+08	1.11E+08	0.539	6.53E+07	1.70	0.57	0.95	1166	394.9	2.95
400	1.33	0.02	0.2	2.06E+08	1.03E+08	0.5	5.40E+07	1.91	0.47	1.07	942.7	504.8	1.87
400	1.33	0.02	0.4	2.06E+08	1.14E+08	0.554	6.08E+07	1.88	0.53	1.05	1140	549.7	2.07
400	1.33	0.02	0.6	2.06E+08	1.23E+08	0.597	7.37E+07	1.67	0.64	0.94	1330	496.3	2.68
400	1.33	0.03	0.2	2.06E+08	1.16E+08	0.563	6.61E+07	1.75	0.57	0.98	1111	638.6	1.74
400	1.33	0.03	0.4	2.06E+08	1.27E+08	0.617	7.19E+07	1.77	0.62	0.99	1306	668.1	1.95
400	1.33	0.03	0.6	2.06E+08	1.35E+08	0.656	8.27E+07	1.63	0.72	0.92	1492	606.5	2.46

400	1.66	0.01	0.2	4.00E+08	1.76E+08	0.44	8.27E+07	2.13	0.37	1.20	1207	571.5	2.11
400	1.66	0.01	0.4	4.00E+08	2.01E+08	0.502	9.81E+07	2.05	0.44	1.15	1523	671.8	2.27
400	1.66	0.01	0.6	4.00E+08	2.22E+08	0.555	1.28E+08	1.73	0.57	0.97	1820	617.9	2.95
400	1.66	0.02	0.2	4.00E+08	2.04E+08	0.51	1.08E+08	1.89	0.48	1.06	1480	789.8	1.87
400	1.66	0.02	0.4	4.00E+08	2.27E+08	0.567	1.20E+08	1.89	0.53	1.06	1793	856.5	2.09
400	1.66	0.02	0.6	4.00E+08	2.46E+08	0.614	1.45E+08	1.70	0.65	0.95	2081	779.5	2.67
400	1.66	0.03	0.2	4.00E+08	2.32E+08	0.58	1.33E+08	1.74	0.59	0.98	1756	997.7	1.76
400	1.66	0.03	0.4	4.00E+08	2.52E+08	0.629	1.43E+08	1.76	0.64	0.99	2056	1041	1.98
400	1.66	0.03	0.6	4.00E+08	2.70E+08	0.674	1.64E+08	1.65	0.73	0.92	2338	961.6	2.43
400	2	0.01	0.2	7.00E+08	3.10E+08	0.443	1.45E+08	2.14	0.37	1.20	1752	822.1	2.13
400	2	0.01	0.4	7.00E+08	3.56E+08	0.508	1.71E+08	2.08	0.44	1.17	2207	964.6	2.29
400	2	0.01	0.6	7.00E+08	3.92E+08	0.56	2.23E+08	1.76	0.57	0.99	2642	892.2	2.96
400	2	0.02	0.2	7.00E+08	3.58E+08	0.511	1.89E+08	1.89	0.48	1.06	2147	1127	1.91
400	2	0.02	0.4	7.00E+08	3.99E+08	0.57	2.23E+08	1.79	0.57	1.00	2593	1204	2.15
400	2	0.02	0.6	7.00E+08	4.33E+08	0.618	2.74E+08	1.58	0.70	0.89	3021	1119	2.70
400	2	0.03	0.2	7.00E+08	4.05E+08	0.578	2.31E+08	1.75	0.59	0.98	2539	1425	1.78
400	2	0.03	0.4	7.00E+08	4.42E+08	0.631	2.46E+08	1.80	0.63	1.01	2971	1483	2.00
400	2	0.03	0.6	7.00E+08	4.73E+08	0.676	2.83E+08	1.67	0.72	0.94	3387	1370	2.47
500	1	0.01	0.2	2.14E+08	9.18E+07	0.43	4.34E+07	2.12	0.36	1.19	850	408.4	2.08
500	1	0.01	0.4	2.14E+08	1.05E+08	0.491	5.22E+07	2.01	0.44	1.13	1073	486.5	2.21
500	1	0.01	0.6	2.14E+08	1.16E+08	0.543	6.82E+07	1.70	0.57	0.95	1288	442.1	2.91
500	1	0.02	0.2	2.14E+08	1.07E+08	0.501	5.72E+07	1.87	0.48	1.05	1037	569.9	1.82
500	1	0.02	0.4	2.14E+08	1.19E+08	0.557	6.43E+07	1.85	0.54	1.04	1256	627.7	2.00
500	1	0.02	0.6	2.14E+08	1.29E+08	0.604	7.77E+07	1.66	0.65	0.93	1471	561.8	2.62
500	1	0.03	0.2	2.14E+08	1.22E+08	0.571	7.05E+07	1.73	0.59	0.97	1225	727	1.69
500	1	0.03	0.4	2.14E+08	1.33E+08	0.622	7.67E+07	1.73	0.64	0.97	1442	768.9	1.88
500	1	0.03	0.6	2.14E+08	1.42E+08	0.665	8.78E+07	1.62	0.73	0.91	1652	689.4	2.40
500	1.33	0.01	0.2	5.03E+08	2.23E+08	0.444	1.06E+08	2.10	0.38	1.18	1517	727.2	2.09
500	1.33	0.01	0.4	5.03E+08	2.55E+08	0.507	1.25E+08	2.04	0.44	1.14	1912	858.2	2.23
500	1.33	0.01	0.6	5.03E+08	2.81E+08	0.559	1.63E+08	1.72	0.58	0.97	2284	786.2	2.91
500	1.33	0.02	0.2	5.03E+08	2.61E+08	0.519	1.40E+08	1.86	0.50	1.05	1862	1015	1.83
500	1.33	0.02	0.4	5.03E+08	2.89E+08	0.575	1.55E+08	1.86	0.55	1.05	2253	1106	2.04
500	1.33	0.02	0.6	5.03E+08	3.13E+08	0.623	1.86E+08	1.68	0.66	0.94	2620	1002	2.61
500	1.33	0.03	0.2	5.03E+08	2.97E+08	0.591	1.73E+08	1.72	0.61	0.96	2213	1292	1.71

500	1.33	0.03	0.4	5.03E+08	3.23E+08	0.643	1.86E+08	1.74	0.66	0.98	2591	1354	1.91
500	1.33	0.03	0.6	5.03E+08	3.45E+08	0.686	2.12E+08	1.63	0.75	0.91	2949	1240	2.38
500	1.66	0.01	0.2	9.77E+08	4.39E+08	0.449	2.08E+08	2.11	0.38	1.18	2364	1126	2.10
500	1.66	0.01	0.4	9.77E+08	5.02E+08	0.514	2.43E+08	2.07	0.44	1.16	2979	1324	2.25
500	1.66	0.01	0.6	9.77E+08	5.53E+08	0.566	3.16E+08	1.75	0.58	0.98	3566	1219	2.93
500	1.66	0.02	0.2	9.77E+08	5.11E+08	0.523	2.74E+08	1.86	0.50	1.05	2904	1563	1.86
500	1.66	0.02	0.4	9.77E+08	5.68E+08	0.581	3.00E+08	1.89	0.55	1.06	3501	1698	2.06
500	1.66	0.02	0.6	9.77E+08	6.15E+08	0.629	3.62E+08	1.70	0.66	0.95	4080	1550	2.63
500	1.66	0.03	0.2	9.77E+08	5.80E+08	0.593	3.37E+08	1.72	0.61	0.97	3441	1983	1.74
500	1.66	0.03	0.4	9.77E+08	6.32E+08	0.647	3.58E+08	1.77	0.65	0.99	4026	2073	1.94
500	1.66	0.03	0.6	9.77E+08	6.75E+08	0.691	4.10E+08	1.65	0.75	0.92	4587	1900	2.41
500	2	0.01	0.2	1.71E+09	7.81E+08	0.457	3.73E+08	2.09	0.39	1.18	3446	1648	2.09
500	2	0.01	0.4	1.71E+09	8.93E+08	0.522	4.33E+08	2.06	0.45	1.16	4331	1940	2.23
500	2	0.01	0.6	1.71E+09	9.84E+08	0.576	5.61E+08	1.75	0.58	0.99	5188	1785	2.91
500	2	0.02	0.2	1.71E+09	9.12E+08	0.534	4.94E+08	1.85	0.51	1.04	4244	2302	1.84
500	2	0.02	0.4	1.71E+09	1.01E+09	0.591	5.38E+08	1.88	0.56	1.05	5108	2501	2.04
500	2	0.02	0.6	1.71E+09	1.10E+09	0.644	6.48E+08	1.70	0.68	0.95	5945	2282	2.61
500	2	0.03	0.2	1.71E+09	1.04E+09	0.608	6.11E+08	1.70	0.64	0.95	5031	2925	1.72
500	2	0.03	0.4	1.71E+09	1.13E+09	0.661	6.46E+08	1.75	0.67	0.98	5883	3063	1.92
500	2	0.03	0.6	1.71E+09	1.21E+09	0.708	7.36E+08	1.64	0.77	0.92	6678	2823	2.37
350	1	0.01	0.2	5.13E+07	2.05E+07	0.4	9.37E+06	2.19	0.33	1.23	288.4	133.4	2.16
350	1	0.01	0.4	5.13E+07	2.35E+07	0.458	1.19E+07	1.97	0.41	1.11	361.7	146.9	2.46
350	1	0.01	0.6	5.13E+07	2.58E+07	0.503	1.58E+07	1.63	0.55	0.92	431	137.8	3.13
350	1	0.02	0.2	5.13E+07	2.38E+07	0.464	1.21E+07	1.97	0.42	1.10	351.6	183	1.92
350	1	0.02	0.4	5.13E+07	2.64E+07	0.515	1.43E+07	1.85	0.50	1.04	423.5	177.8	2.38
350	1	0.02	0.6	5.13E+07	2.85E+07	0.556	1.75E+07	1.63	0.61	0.91	489.3	164.8	2.97
350	1	0.03	0.2	5.13E+07	2.69E+07	0.524	1.46E+07	1.84	0.51	1.03	414.7	230.9	1.80
350	1	0.03	0.4	5.13E+07	2.92E+07	0.569	1.66E+07	1.76	0.58	0.99	483.6	208.9	2.31
350	1	0.03	0.6	5.13E+07	3.12E+07	0.608	1.93E+07	1.62	0.67	0.91	549.1	192.6	2.85
350	1.33	0.01	0.2	1.21E+08	5.07E+07	0.42	2.34E+07	2.17	0.35	1.22	516.2	239.4	2.16
350	1.33	0.01	0.4	1.21E+08	5.80E+07	0.481	2.87E+07	2.02	0.42	1.14	650.4	264	2.46
350	1.33	0.01	0.6	1.21E+08	6.39E+07	0.529	3.77E+07	1.69	0.56	0.95	779.2	246.6	3.16
350	1.33	0.02	0.2	1.21E+08	5.86E+07	0.486	3.03E+07	1.93	0.45	1.09	629.5	334	1.88
350	1.33	0.02	0.4	1.21E+08	6.51E+07	0.539	3.46E+07	1.88	0.51	1.06	762.2	322.4	2.36

350	1.33	0.02	0.6	1.21E+08	7.05E+07	0.584	4.22E+07	1.67	0.62	0.94	887.2	297.6	2.98
350	1.33	0.03	0.2	1.21E+08	6.62E+07	0.548	3.69E+07	1.79	0.54	1.01	742	417.4	1.78
350	1.33	0.03	0.4	1.21E+08	7.21E+07	0.597	4.06E+07	1.78	0.60	1.00	871.3	381.6	2.28
350	1.33	0.03	0.6	1.21E+08	7.70E+07	0.638	4.70E+07	1.64	0.69	0.92	993.4	370.1	2.68
350	1.66	0.01	0.2	2.35E+08	1.01E+08	0.43	4.68E+07	2.16	0.36	1.21	803.8	372.4	2.16
350	1.66	0.01	0.4	2.35E+08	1.16E+08	0.494	5.64E+07	2.06	0.43	1.15	1014	413.2	2.45
350	1.66	0.01	0.6	2.35E+08	1.27E+08	0.541	7.39E+07	1.72	0.56	0.96	1216	385.6	3.15
350	1.66	0.02	0.2	2.35E+08	1.16E+08	0.494	6.06E+07	1.91	0.46	1.07	981.8	515.5	1.90
350	1.66	0.02	0.4	2.35E+08	1.30E+08	0.554	6.81E+07	1.91	0.52	1.07	1189	506.3	2.35
350	1.66	0.02	0.6	2.35E+08	1.41E+08	0.601	8.29E+07	1.70	0.63	0.95	1385	466.7	2.97
350	1.66	0.03	0.2	2.35E+08	1.31E+08	0.558	7.38E+07	1.78	0.56	1.00	1159	645.2	1.80
350	1.66	0.03	0.4	2.35E+08	1.43E+08	0.609	8.01E+07	1.79	0.61	1.00	1361	614.1	2.22
350	1.66	0.03	0.6	2.35E+08	1.53E+08	0.652	9.25E+07	1.65	0.70	0.93	1552	550.4	2.82
350	2	0.01	0.2	4.10E+08	1.78E+08	0.434	8.21E+07	2.17	0.36	1.22	1168	536.9	2.18
350	2	0.01	0.4	4.10E+08	2.04E+08	0.497	9.77E+07	2.09	0.42	1.17	1472	593.6	2.48
350	2	0.01	0.6	4.10E+08	2.26E+08	0.551	1.28E+08	1.77	0.56	0.99	1762	555.2	3.17
350	2	0.02	0.2	4.10E+08	2.04E+08	0.497	1.05E+08	1.94	0.46	1.09	1426	736.1	1.94
350	2	0.02	0.4	4.10E+08	2.28E+08	0.556	1.17E+08	1.95	0.51	1.09	1719	721.9	2.38
350	2	0.02	0.6	4.10E+08	2.47E+08	0.602	1.43E+08	1.73	0.62	0.97	2004	668.3	3.00
350	2	0.03	0.2	4.10E+08	2.30E+08	0.56	1.28E+08	1.80	0.56	1.01	1678	921.1	1.82
350	2	0.03	0.4	4.10E+08	2.51E+08	0.612	1.37E+08	1.83	0.59	1.03	1963	853.1	2.30
350	2	0.03	0.6	4.10E+08	2.69E+08	0.655	1.59E+08	1.69	0.69	0.95	2240	784.5	2.86

Table A. 2:

Sectional analysis calculations for the shear capacity.

B	*H/B*	ρ_s	$N/f_c'A_g$	NSC				UHPC					
								AFGC				Fehling et al. (2014)	
				$V_{c,a}$ (kN)	$V_{c,b}$ (kN)	$V_{c,simplified}$ (kN)	$V_{c,max}$ (kN)	$V_{rd,c}$ (kN)	$V_{rd,f}$ (kN)	V_c+V_f (kN)	V_{c_UHPC}/V_{c_NSC}	V_c+V_f (kN)	$V_{\_UHPC}/V_{\_NSC}$
300	1	0.01	0.2	120	110	61	120	212	458	670	5.6	1129	9.4
300	1	0.01	0.4	149	139	61	149	229	458	688	4.6	1129	7.6
300	1	0.01	0.6	149	139	61	149	229	458	688	4.6	1129	7.6
300	1	0.02	0.2	120	123	61	120	212	458	670	5.6	1129	9.4
300	1	0.02	0.4	149	152	61	149	229	458	688	4.6	1129	7.6
300	1	0.02	0.6	149	152	61	149	229	458	688	4.6	1129	7.6
300	1	0.03	0.2	120	132	61	120	212	458	670	5.6	1129	9.4
300	1	0.03	0.4	149	161	61	149	229	458	688	4.6	1129	7.6
300	1	0.03	0.6	149	161	61	149	229	458	688	4.6	1129	7.6
300	1.33	0.01	0.2	168	154	86	168	298	645	942	5.6	1501	8.9
300	1.33	0.01	0.4	209	195	86	209	322	645	967	4.6	1501	7.2
300	1.33	0.01	0.6	209	195	86	209	322	645	967	4.6	1501	7.2
300	1.33	0.02	0.2	168	173	86	168	298	645	942	5.6	1501	8.9
300	1.33	0.02	0.4	209	214	86	209	322	645	967	4.6	1501	7.2
300	1.33	0.02	0.6	209	214	86	209	322	645	967	4.6	1501	7.2
300	1.33	0.03	0.2	168	186	86	168	298	645	942	5.6	1501	8.9
300	1.33	0.03	0.4	209	227	86	209	322	645	967	4.6	1501	7.2
300	1.33	0.03	0.6	209	227	86	209	322	645	967	4.6	1501	7.2
300	1.66	0.01	0.2	217	198	110	217	384	831	1214	5.6	1873	8.7
300	1.66	0.01	0.4	270	251	110	270	415	831	1246	4.6	1873	7.0
300	1.66	0.01	0.6	270	251	110	270	415	831	1246	4.6	1873	7.0
300	1.66	0.02	0.2	217	222	110	217	384	831	1214	5.6	1873	8.7
300	1.66	0.02	0.4	270	275	110	270	415	831	1246	4.6	1873	7.0
300	1.66	0.02	0.6	270	275	110	270	415	831	1246	4.6	1873	7.0
300	1.66	0.03	0.2	217	239	110	217	384	831	1214	5.6	1873	8.7
300	1.66	0.03	0.4	270	292	110	270	415	831	1246	4.6	1873	7.0

300	1.66	0.03	0.6	270	292	110	270	415	831	1246	4.6	1873	7.0
300	2	0.01	0.2	266	244	136	266	472	1022	1494	5.6	2257	8.5
300	2	0.01	0.4	332	310	136	332	511	1022	1533	4.6	2257	6.8
300	2	0.01	0.6	332	310	136	332	511	1022	1533	4.6	2257	6.8
300	2	0.02	0.2	266	274	136	266	472	1022	1494	5.6	2257	8.5
300	2	0.02	0.4	332	339	136	332	511	1022	1533	4.6	2257	6.8
300	2	0.02	0.6	332	339	136	332	511	1022	1533	4.6	2257	6.8
300	2	0.03	0.2	266	295	136	266	472	1022	1494	5.6	2257	8.5
300	2	0.03	0.4	332	360	136	332	511	1022	1533	4.6	2257	6.8
300	2	0.03	0.6	332	360	136	332	511	1022	1533	4.6	2257	6.8
400	1	0.01	0.2	225	206	115	225	398	862	1260	5.6	2006	8.9
400	1	0.01	0.4	280	261	115	280	431	862	1293	4.6	2006	7.2
400	1	0.01	0.6	280	261	115	280	431	862	1293	4.6	2006	7.2
400	1	0.02	0.2	225	231	115	225	398	862	1260	5.6	2006	8.9
400	1	0.02	0.4	280	286	115	280	431	862	1293	4.6	2006	7.2
400	1	0.02	0.6	280	286	115	280	431	862	1293	4.6	2006	7.2
400	1	0.03	0.2	225	248	115	225	398	862	1260	5.6	2006	8.9
400	1	0.03	0.4	280	303	115	280	431	862	1293	4.6	2006	7.2
400	1	0.03	0.6	280	303	115	280	431	862	1293	4.6	2006	7.2
400	1.33	0.01	0.2	311	285	159	311	551	1193	1743	5.6	2669	8.6
400	1.33	0.01	0.4	387	361	159	387	596	1193	1789	4.6	2669	6.9
400	1.33	0.01	0.6	387	361	159	387	596	1193	1789	4.6	2669	6.9
400	1.33	0.02	0.2	311	319	159	311	551	1193	1743	5.6	2669	8.6
400	1.33	0.02	0.4	387	396	159	387	596	1193	1789	4.6	2669	6.9
400	1.33	0.02	0.6	387	396	159	387	596	1193	1789	4.6	2669	6.9
400	1.33	0.03	0.2	311	344	159	311	551	1193	1743	5.6	2669	8.6
400	1.33	0.03	0.4	387	420	159	387	596	1193	1789	4.6	2669	6.9
400	1.33	0.03	0.6	387	420	159	387	596	1193	1789	4.6	2669	6.9
400	1.66	0.01	0.2	397	364	203	397	704	1523	2227	5.6	3331	8.4
400	1.66	0.01	0.4	494	461	203	494	762	1523	2285	4.6	3331	6.7
400	1.66	0.01	0.6	494	461	203	494	762	1523	2285	4.6	3331	6.7
400	1.66	0.02	0.2	397	408	203	397	704	1523	2227	5.6	3331	8.4
400	1.66	0.02	0.4	494	505	203	494	762	1523	2285	4.6	3331	6.7
400	1.66	0.02	0.6	494	505	203	494	762	1523	2285	4.6	3331	6.7

400	1.66	0.03	0.2	397	439	203	397	704	1523	2227	5.6	3331	8.4
400	1.66	0.03	0.4	494	536	203	494	762	1523	2285	4.6	3331	6.7
400	1.66	0.03	0.6	494	536	203	494	762	1523	2285	4.6	3331	6.7
400	2	0.01	0.2	486	445	248	486	861	1864	2725	5.6	4013	8.3
400	2	0.01	0.4	605	564	248	605	932	1864	2796	4.6	4013	6.6
400	2	0.01	0.6	605	564	248	605	932	1864	2796	4.6	4013	6.6
400	2	0.02	0.2	486	499	248	486	861	1864	2725	5.6	4013	8.3
400	2	0.02	0.4	605	618	248	605	932	1864	2796	4.6	4013	6.6
400	2	0.02	0.6	605	618	248	605	932	1864	2796	4.6	4013	6.6
400	2	0.03	0.2	486	537	248	486	861	1864	2725	5.6	4013	8.3
400	2	0.03	0.4	605	656	248	605	932	1864	2796	4.6	4013	6.6
400	2	0.03	0.6	605	656	248	605	932	1864	2796	4.6	4013	6.6
500	1	0.01	0.2	362	332	185	362	642	1390	2033	5.6	3135	8.6
500	1	0.01	0.4	451	421	185	451	695	1390	2086	4.6	3135	6.9
500	1	0.01	0.6	451	421	185	451	695	1390	2086	4.6	3135	6.9
500	1	0.02	0.2	362	372	185	362	642	1390	2033	5.6	3135	8.6
500	1	0.02	0.4	451	461	185	451	695	1390	2086	4.6	3135	6.9
500	1	0.02	0.6	451	461	185	451	695	1390	2086	4.6	3135	6.9
500	1	0.03	0.2	362	401	185	362	642	1390	2033	5.6	3135	8.6
500	1	0.03	0.4	451	489	185	451	695	1390	2086	4.6	3135	6.9
500	1	0.03	0.6	451	489	185	451	695	1390	2086	4.6	3135	6.9
500	1.33	0.01	0.2	497	456	254	497	881	1907	2788	5.6	4170	8.4
500	1.33	0.01	0.4	619	578	254	619	954	1907	2861	4.6	4170	6.7
500	1.33	0.01	0.6	619	578	254	619	954	1907	2861	4.6	4170	6.7
500	1.33	0.02	0.2	497	511	254	497	881	1907	2788	5.6	4170	8.4
500	1.33	0.02	0.4	619	633	254	619	954	1907	2861	4.6	4170	6.7
500	1.33	0.02	0.6	619	633	254	619	954	1907	2861	4.6	4170	6.7
500	1.33	0.03	0.2	497	550	254	497	881	1907	2788	5.6	4170	8.4
500	1.33	0.03	0.4	619	671	254	619	954	1907	2861	4.6	4170	6.7
500	1.33	0.03	0.6	619	671	254	619	954	1907	2861	4.6	4170	6.7
500	1.66	0.01	0.2	632	579	322	632	1120	2424	3544	5.6	5204	8.2
500	1.66	0.01	0.4	787	734	322	787	1212	2424	3636	4.6	5204	6.6
500	1.66	0.01	0.6	787	734	322	787	1212	2424	3636	4.6	5204	6.6
500	1.66	0.02	0.2	632	649	322	632	1120	2424	3544	5.6	5204	8.2

500	1.66	0.02	0.4	787	804	322	787	1212	2424	3636	4.6	5204	6.6
500	1.66	0.02	0.6	787	804	322	787	1212	2424	3636	4.6	5204	6.6
500	1.66	0.03	0.2	632	698	322	632	1120	2424	3544	5.6	5204	8.2
500	1.66	0.03	0.4	787	853	322	787	1212	2424	3636	4.6	5204	6.6
500	1.66	0.03	0.6	787	853	322	787	1212	2424	3636	4.6	5204	6.6
500	2	0.01	0.2	771	706	393	771	1366	2956	4322	5.6	6270	8.1
500	2	0.01	0.4	959	895	393	959	1479	2956	4435	4.6	6270	6.5
500	2	0.01	0.6	959	895	393	959	1479	2956	4435	4.6	6270	6.5
500	2	0.02	0.2	771	792	393	771	1366	2956	4322	5.6	6270	8.1
500	2	0.02	0.4	959	981	393	959	1479	2956	4435	4.6	6270	6.5
500	2	0.02	0.6	959	981	393	959	1479	2956	4435	4.6	6270	6.5
500	2	0.03	0.2	771	852	393	771	1366	2956	4322	5.6	6270	8.1
500	2	0.03	0.4	959	1041	393	959	1479	2956	4435	4.6	6270	6.5
500	2	0.03	0.6	959	1041	393	959	1479	2956	4435	4.6	6270	6.5

Table A. 3:

K factor results for the new different 72 sections compared to the results predicted from the proposed equation.

B	***H/B***	ρ_s	$N/f_c'A_g$	***K***	**Proposed Equation**	**Error %**
350	1	0.01	0.2	2.19	2.10	-3.99
350	1	0.01	0.4	1.97	1.96	-0.84
350	1	0.01	0.6	1.63	1.82	11.18
350	1	0.02	0.2	1.97	1.99	0.93
350	1	0.02	0.4	1.85	1.84	-0.21
350	1	0.02	0.6	1.63	1.70	4.35
350	1	0.03	0.2	1.84	1.87	1.45
350	1	0.03	0.4	1.76	1.73	-1.86
350	1	0.03	0.6	1.62	1.58	-2.05
350	1.33	0.01	0.2	2.17	2.10	-3.02
350	1.33	0.01	0.4	2.02	1.96	-3.1
350	1.33	0.01	0.6	1.69	1.82	7.11
350	1.33	0.02	0.2	1.93	1.99	2.64
350	1.33	0.02	0.4	1.88	1.84	-2.08
350	1.33	0.02	0.6	1.67	1.70	1.72
350	1.33	0.03	0.2	1.79	1.87	4.19
350	1.33	0.03	0.4	1.78	1.73	-2.79
350	1.33	0.03	0.6	1.64	1.58	-3.35
350	1.66	0.01	0.2	2.16	2.10	-2.64
350	1.66	0.01	0.4	2.06	1.96	-4.79
350	1.66	0.01	0.6	1.72	1.82	5.64
350	1.66	0.02	0.2	1.91	1.99	3.71
350	1.66	0.02	0.4	1.91	1.84	-3.49
350	1.66	0.02	0.6	1.70	1.70	-0.08
350	1.66	0.03	0.2	1.78	1.87	5.3
350	1.66	0.03	0.4	1.79	1.73	-3.3
350	1.66	0.03	0.6	1.65	1.58	-4.27
350	2	0.01	0.2	2.17	2.10	-3.09
350	2	0.01	0.4	2.09	1.96	-6.21
350	2	0.01	0.6	1.77	1.82	2.82
350	2	0.02	0.2	1.94	1.99	2.18
350	2	0.02	0.4	1.95	1.84	-5.46
350	2	0.02	0.6	1.73	1.70	-1.61
350	2	0.03	0.2	1.80	1.87	4.02
350	2	0.03	0.4	1.83	1.73	-5.78
350	2	0.03	0.6	1.69	1.58	-6.41

Table A. 4:

$\alpha_{UHPC}/\alpha_{NSC}$ factor results for the new different 72 sections compared to the results predicted from the proposed equation.

B	***H/B***	ρ_s	***N/f$_c$'A$_g$***	$\alpha_{UHPC}/\alpha_{NSC}$	**Proposed Equation**	**Error %**
350	1	0.01	0.2	2.19	1.18	-4.03%
350	1	0.01	0.4	1.97	1.10	-0.74%
350	1	0.01	0.6	1.63	1.02	11.28%
350	1	0.02	0.2	1.97	1.12	0.98%
350	1	0.02	0.4	1.85	1.04	-0.19%
350	1	0.02	0.6	1.63	0.96	4.39%
350	1	0.03	0.2	1.84	1.05	1.61%
350	1	0.03	0.4	1.76	0.97	-1.72%
350	1	0.03	0.6	1.62	0.89	-1.88%
350	1.33	0.01	0.2	2.17	1.18	-2.95%
350	1.33	0.01	0.4	2.02	1.10	-3.11%
350	1.33	0.01	0.6	1.69	1.02	7.31%
350	1.33	0.02	0.2	1.93	1.12	2.62%
350	1.33	0.02	0.4	1.88	1.04	-1.92%
350	1.33	0.02	0.6	1.67	0.96	1.87%
350	1.33	0.03	0.2	1.79	1.05	4.37%
350	1.33	0.03	0.4	1.78	0.97	-2.62%
350	1.33	0.03	0.6	1.64	0.89	-3.21%
350	1.66	0.01	0.2	2.16	1.18	-2.49%
350	1.66	0.01	0.4	2.06	1.10	-4.65%
350	1.66	0.01	0.6	1.72	1.02	5.79%
350	1.66	0.02	0.2	1.91	1.12	3.85%
350	1.66	0.02	0.4	1.91	1.04	-3.40%
350	1.66	0.02	0.6	1.70	0.96	0.02%
350	1.66	0.03	0.2	1.78	1.05	5.44%
350	1.66	0.03	0.4	1.79	0.97	-3.13%
350	1.66	0.03	0.6	1.65	0.89	-4.13%
350	2	0.01	0.2	2.17	1.18	-3.09%
350	2	0.01	0.4	2.09	1.10	-6.12%
350	2	0.01	0.6	1.77	1.02	2.87%
350	2	0.02	0.2	1.94	1.12	2.27%
350	2	0.02	0.4	1.95	1.04	-5.45%
350	2	0.02	0.6	1.73	0.96	-1.52%
350	2	0.03	0.2	1.80	1.05	4.19%
350	2	0.03	0.4	1.83	0.97	-5.73%
350	2	0.03	0.6	1.69	0.89	-6.21%

Table A. 5:

β factor results for the new 72 sections compared to the predicted results from the proposed equation.

B	H/B	ρ_s	$N/f_c'A_g$	β	Proposed Equation	Error %
350	1	0.01	0.2	2.16	2.12	-1.9%
350	1	0.01	0.4	2.46	2.52	2.4%
350	1	0.01	0.6	3.13	2.92	-6.6%
350	1	0.02	0.2	1.92	1.94	0.8%
350	1	0.02	0.4	2.38	2.34	-1.9%
350	1	0.02	0.6	2.97	2.74	-7.8%
350	1	0.03	0.2	1.80	1.75	-2.3%
350	1	0.03	0.4	2.31	2.15	-6.9%
350	1	0.03	0.6	2.85	2.55	-10.4%
350	1.33	0.01	0.2	2.16	2.12	-1.7%
350	1.33	0.01	0.4	2.46	2.52	2.3%
350	1.33	0.01	0.6	3.16	2.92	-7.6%
350	1.33	0.02	0.2	1.88	1.94	2.8%
350	1.33	0.02	0.4	2.36	2.34	-1.1%
350	1.33	0.02	0.6	2.98	2.74	-8.2%
350	1.33	0.03	0.2	1.78	1.75	-1.3%
350	1.33	0.03	0.4	2.28	2.15	-5.7%
350	1.33	0.03	0.6	2.68	2.55	-4.8%
350	1.66	0.01	0.2	2.16	2.12	-1.8%
350	1.66	0.01	0.4	2.45	2.52	2.7%
350	1.66	0.01	0.6	3.15	2.92	-7.4%
350	1.66	0.02	0.2	1.90	1.94	1.7%
350	1.66	0.02	0.4	2.35	2.34	-0.5%
350	1.66	0.02	0.6	2.97	2.74	-7.8%
350	1.66	0.03	0.2	1.80	1.75	-2.4%
350	1.66	0.03	0.4	2.22	2.15	-2.8%
350	1.66	0.03	0.6	2.82	2.55	-9.4%
350	2	0.01	0.2	2.18	2.12	-2.5%
350	2	0.01	0.4	2.48	2.52	1.6%
350	2	0.01	0.6	3.17	2.92	-8.0%
350	2	0.02	0.2	1.94	1.94	0.0%
350	2	0.02	0.4	2.38	2.34	-1.9%
350	2	0.02	0.6	3.00	2.74	-8.7%
350	2	0.03	0.2	1.82	1.75	-3.7%
350	2	0.03	0.4	2.30	2.15	-6.4%
350	2	0.03	0.6	2.86	2.55	-10.5%

Figure A. 1:

Effect of N/f_c'A_g on K factor.

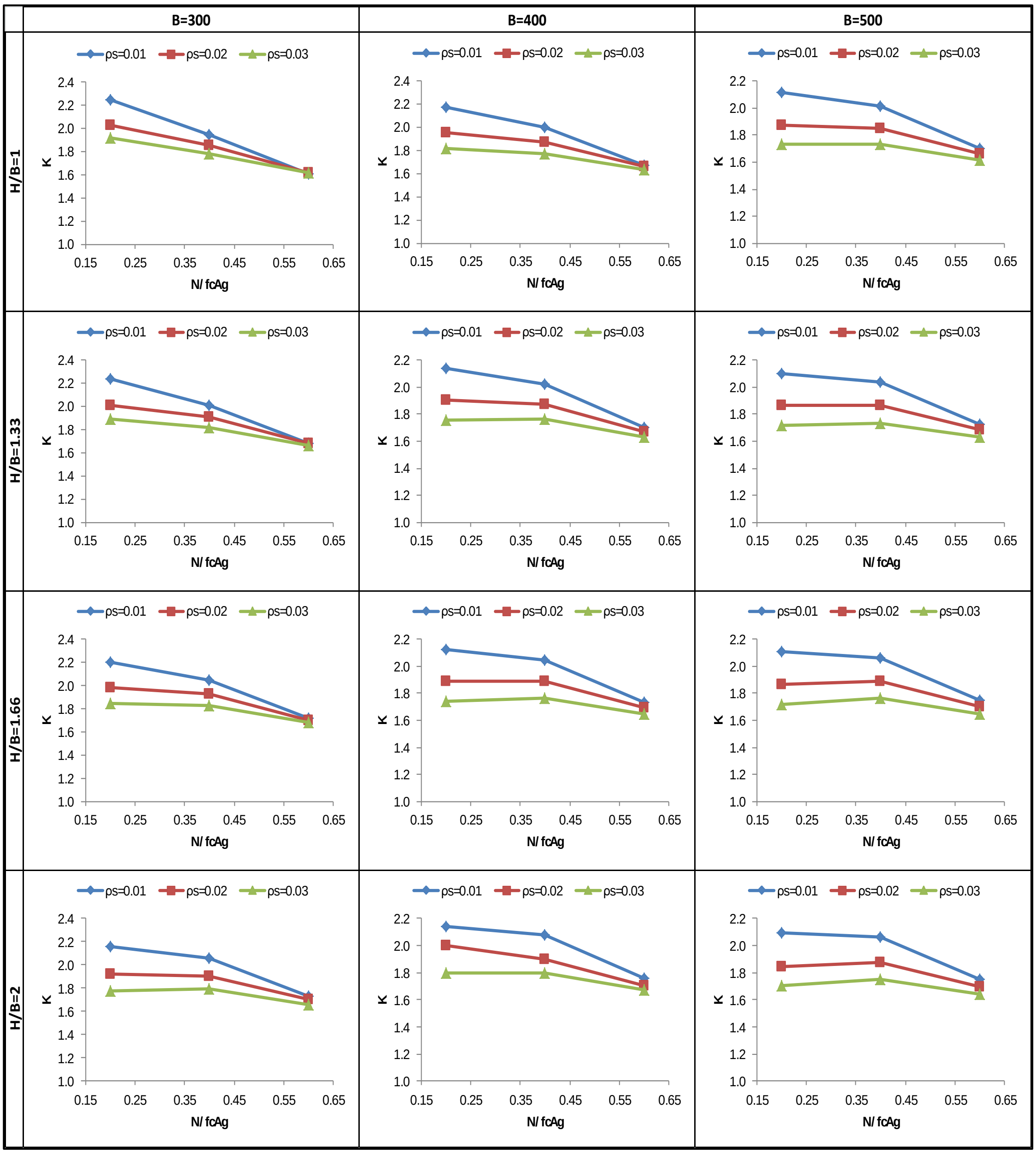

Figure A. 2:

Effect of ρ_s on K factor.

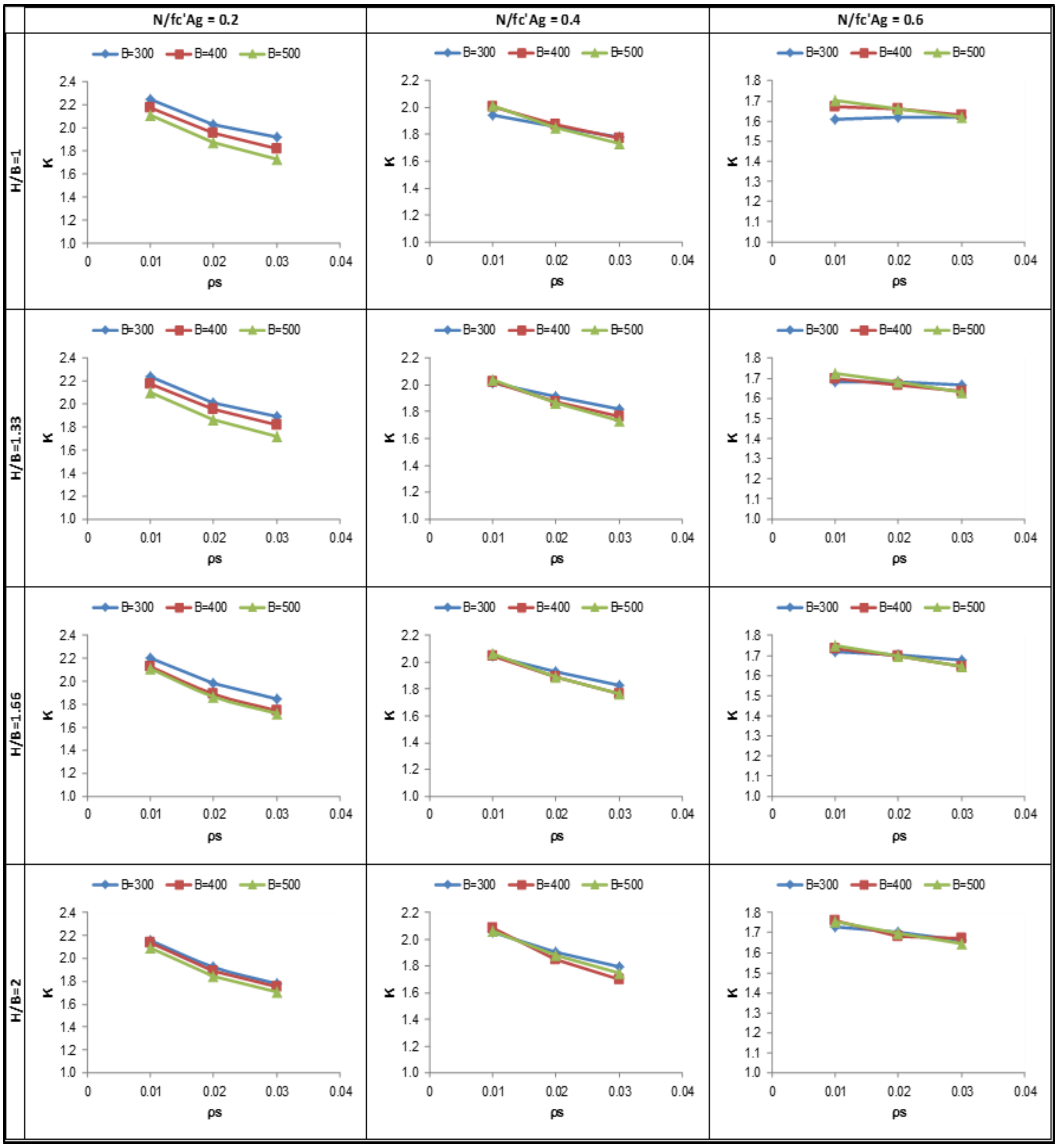

Figure A. 3:

Effect of H/B on K factor.

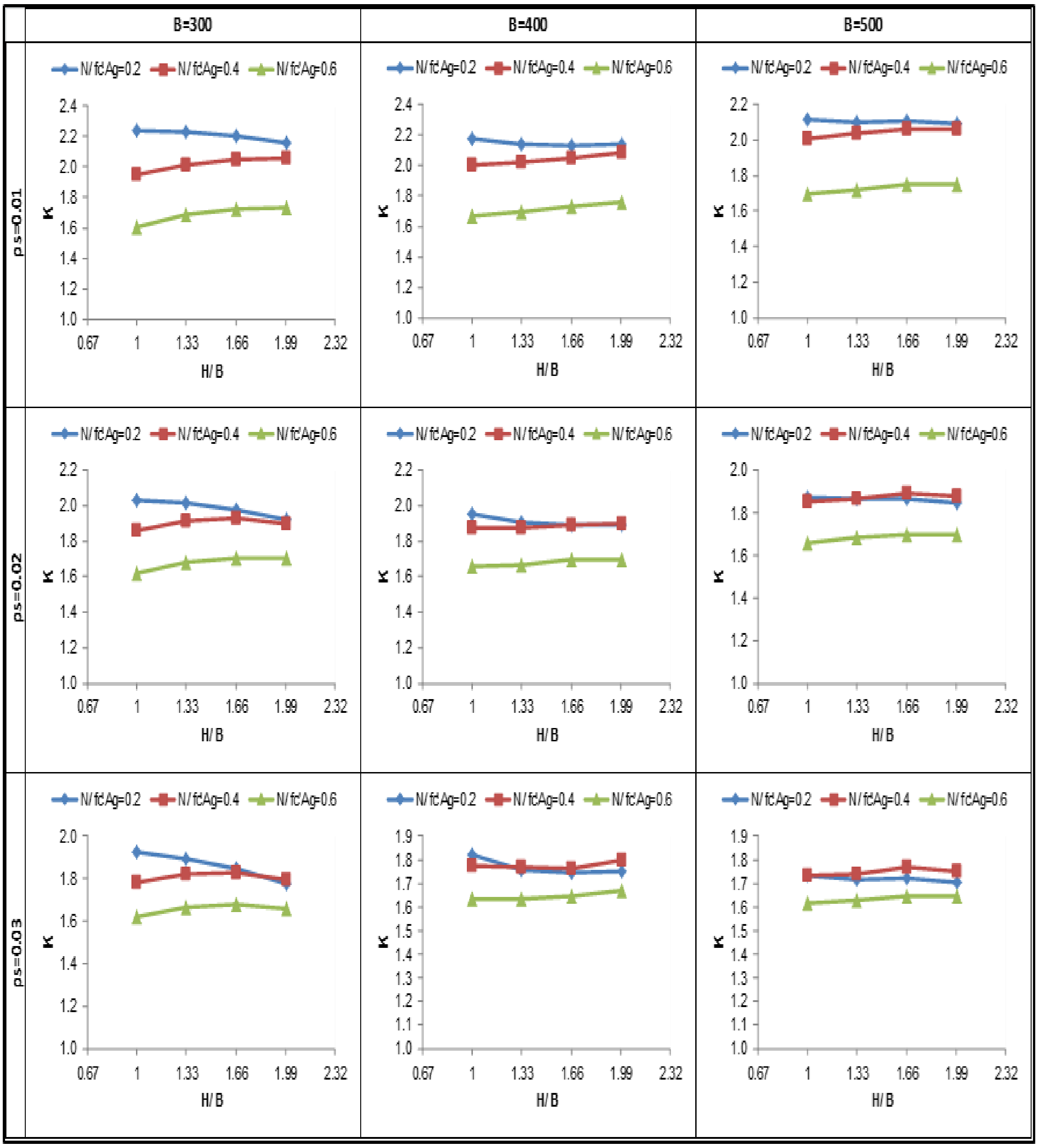

Figure A. 4:

Effect of B on K factor.

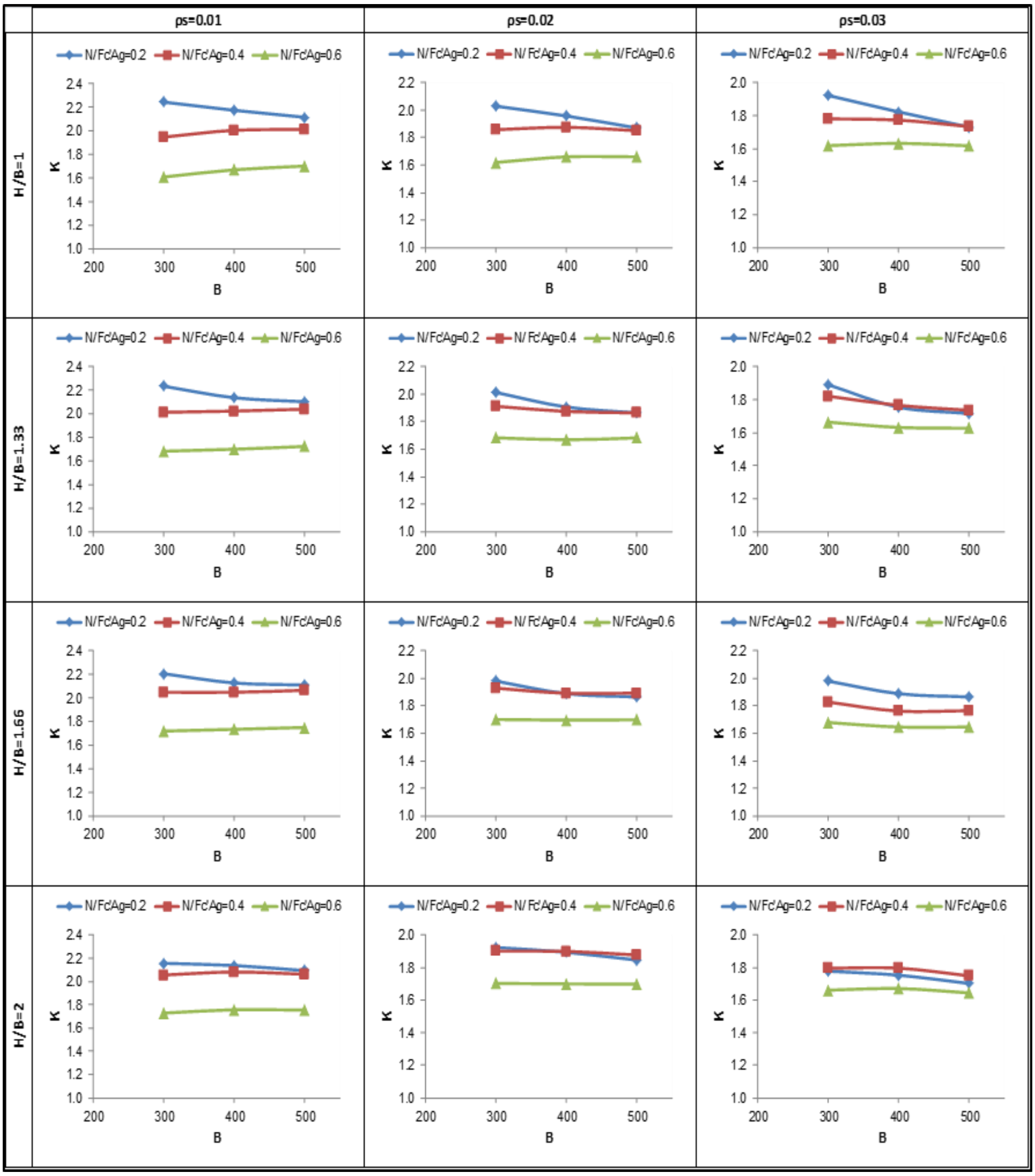

Figure A. 5:

Predicted and analyzed K factor.

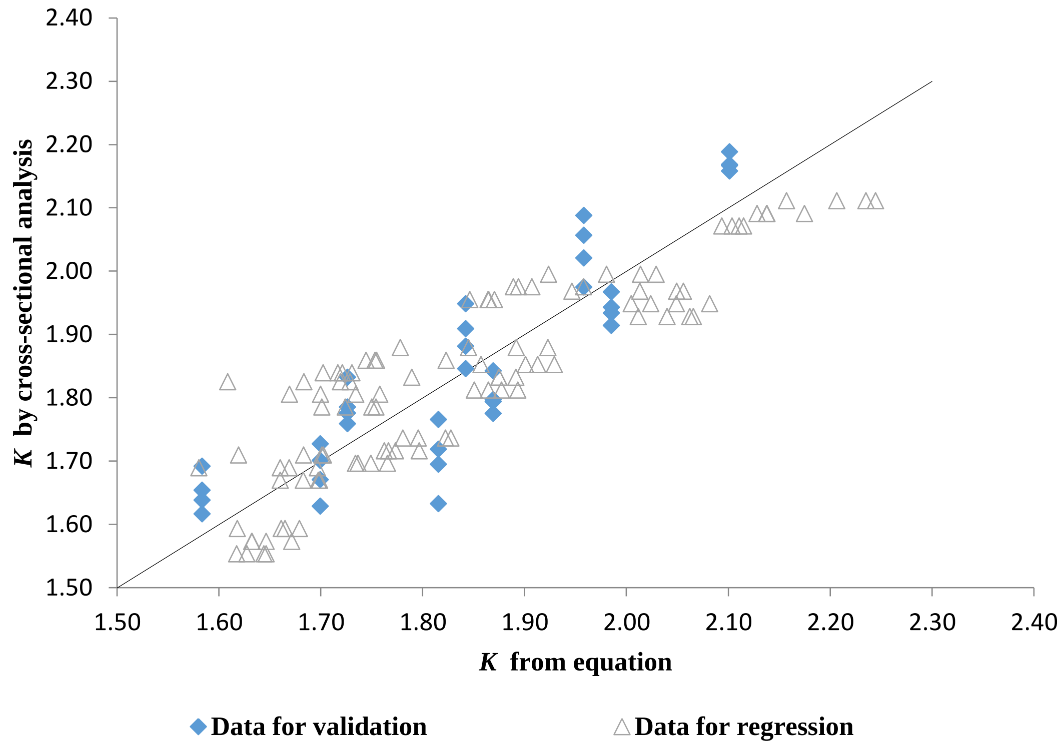

Figure A. 6:

Predicted and analyzed $\alpha_{UHPC}/\alpha_{NSC}$ factor.

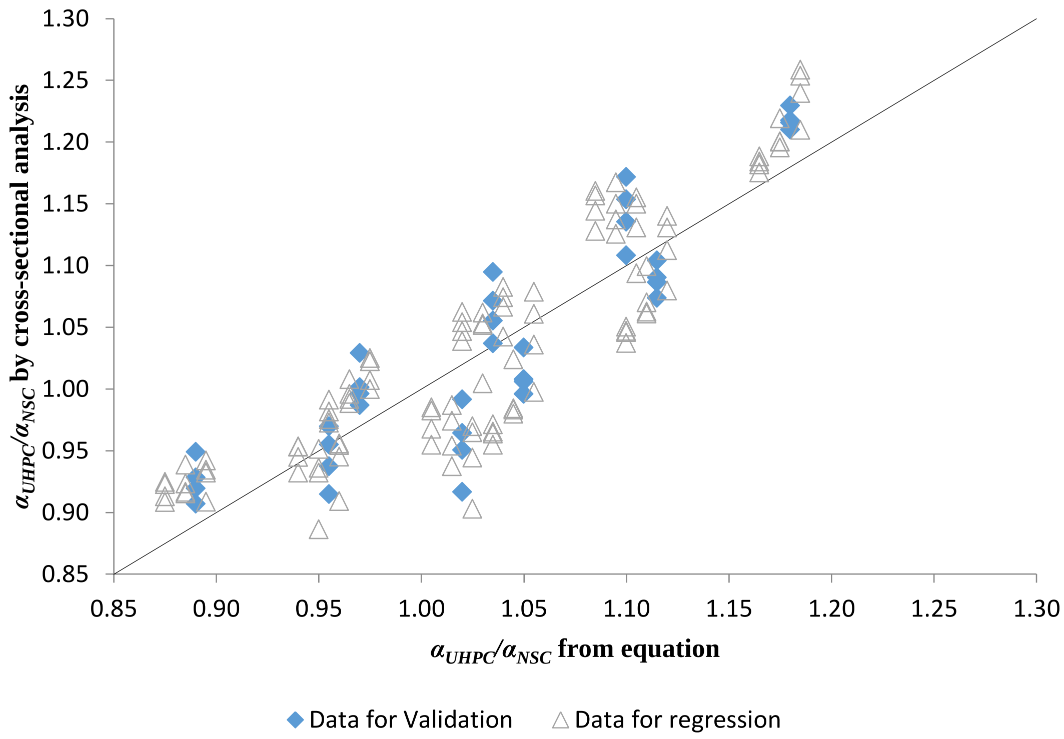

Figure A. 7:

Effect of $N/fc'A_g$ on β factor.

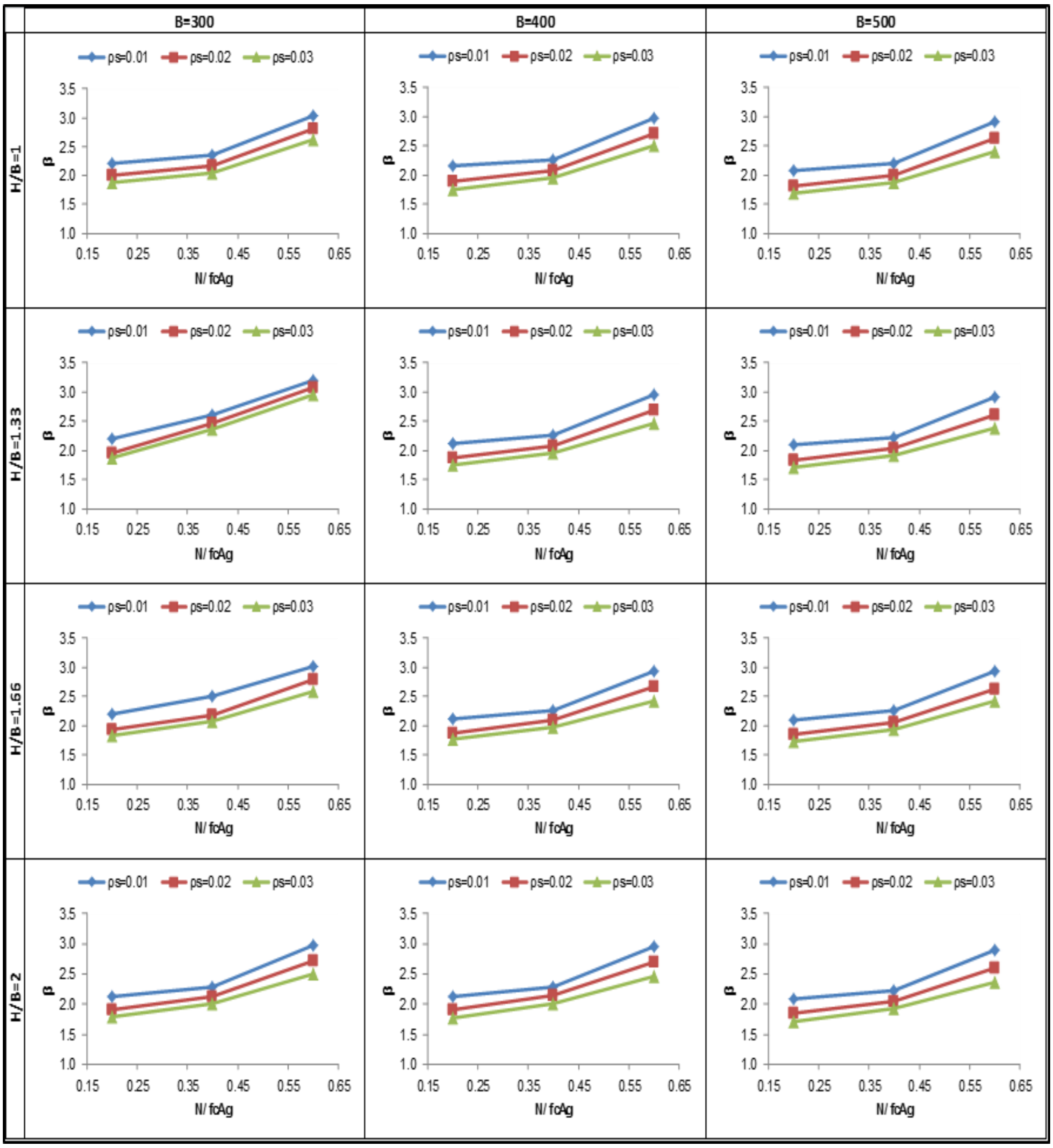

Figure A. 8:

Effect of ρ_s on β factor.

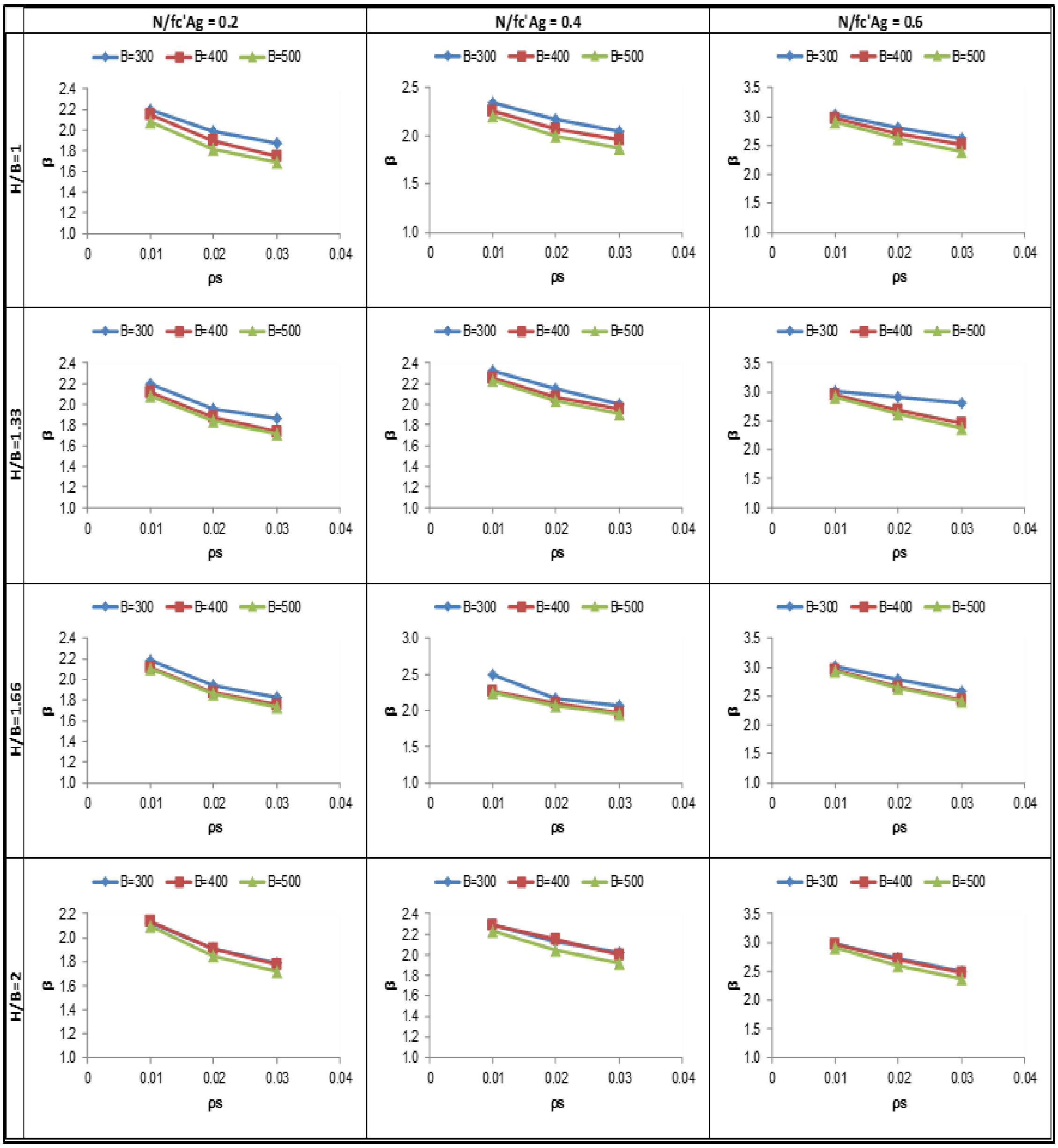

Figure A. 9:

Effect of H/B on β factor.

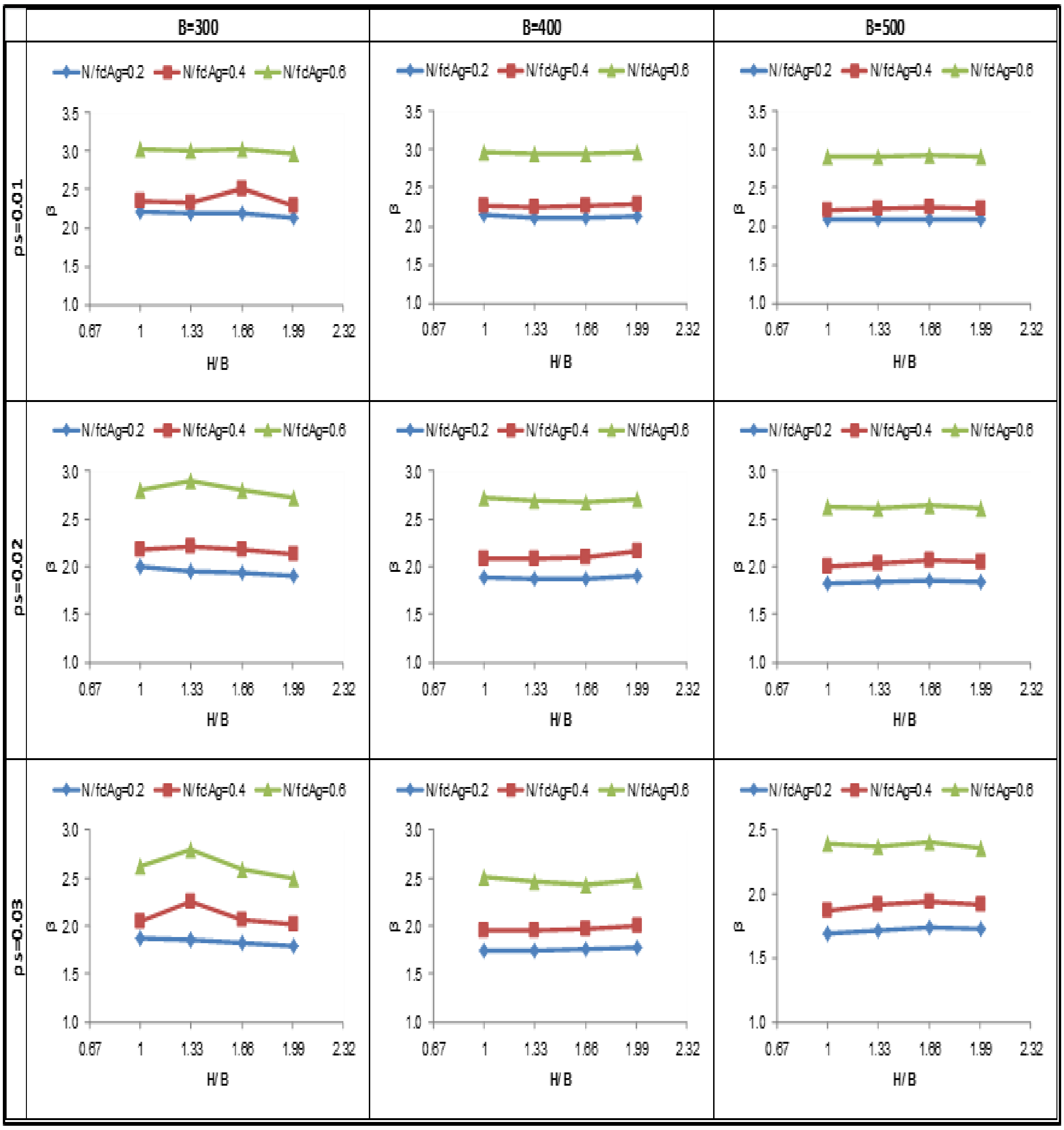

Figure A. 10:

Effect of B on β factor.

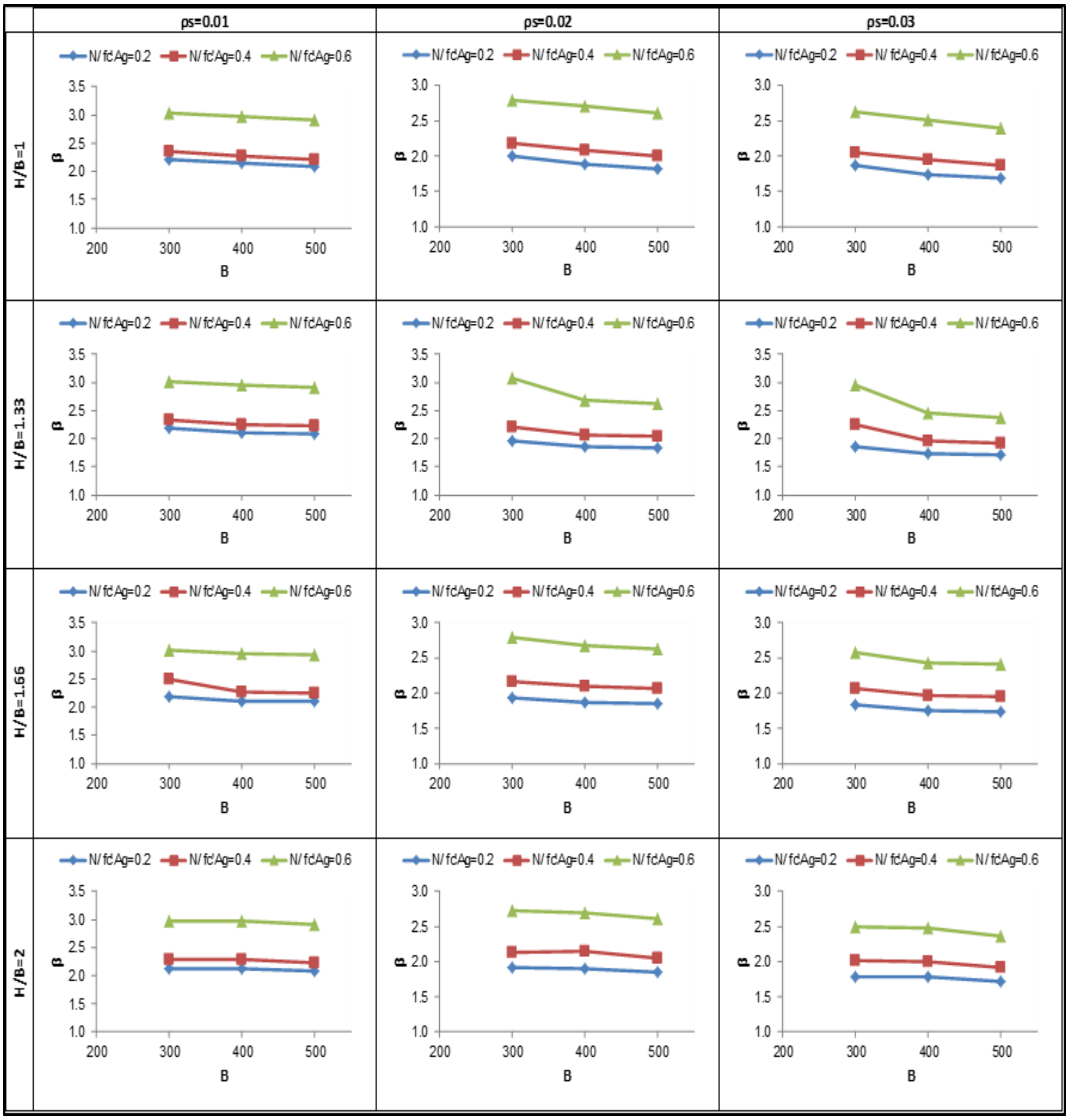

Figure A. 11:

Predicted and analyzed β factor.

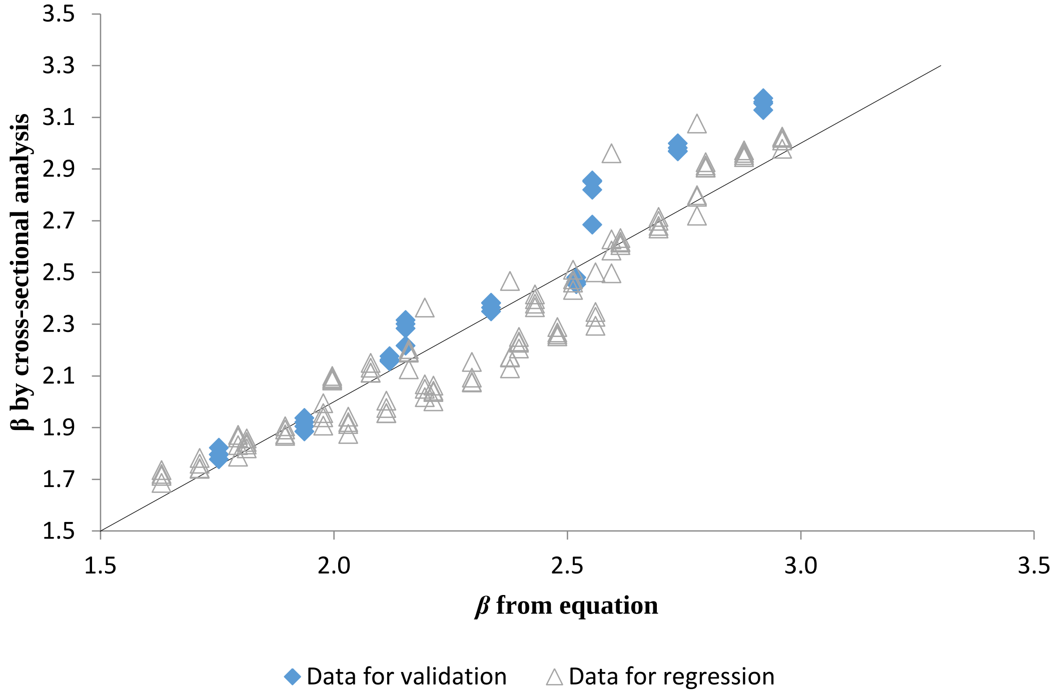

1. **The residual and line fit plots of the regression analysis for the studied factors.**

- *K* factor:

Figure A. 12:

Residual plots of the K factor.

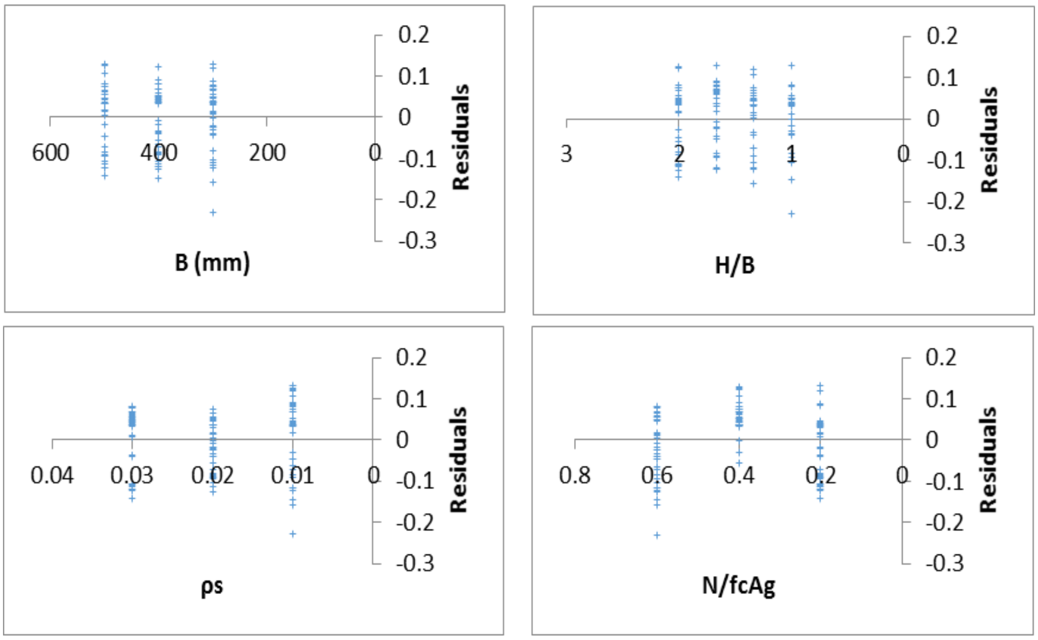

Figure A. 13:

Line fit plots of K factor.

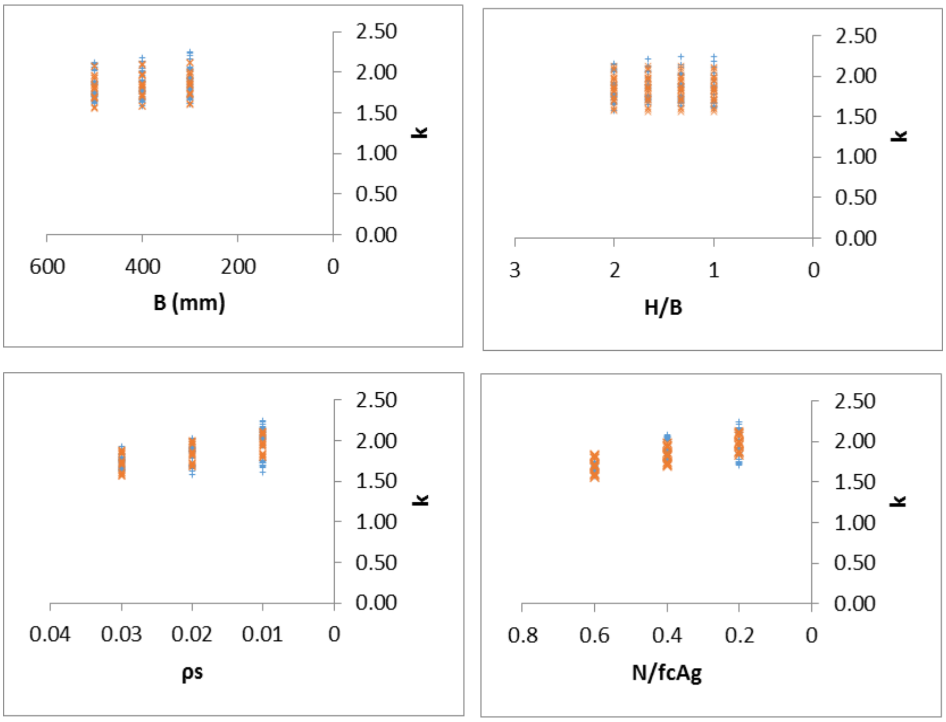

- *β* factor:

Figure A. 14:

Residual plots of β factor.

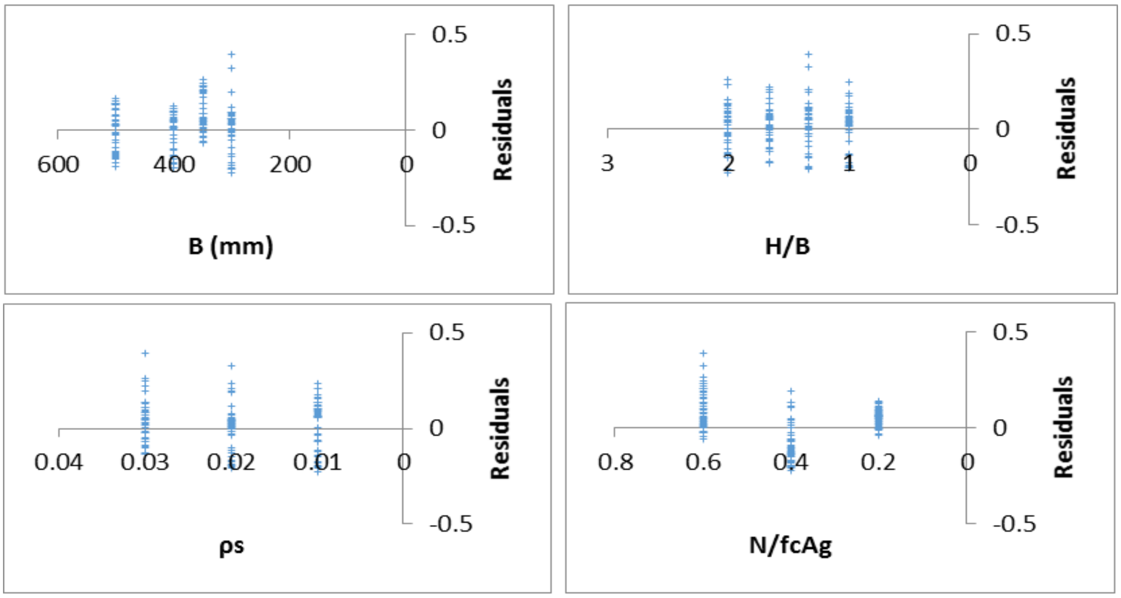

Figure A. 15:

Line fit plots of β factor.

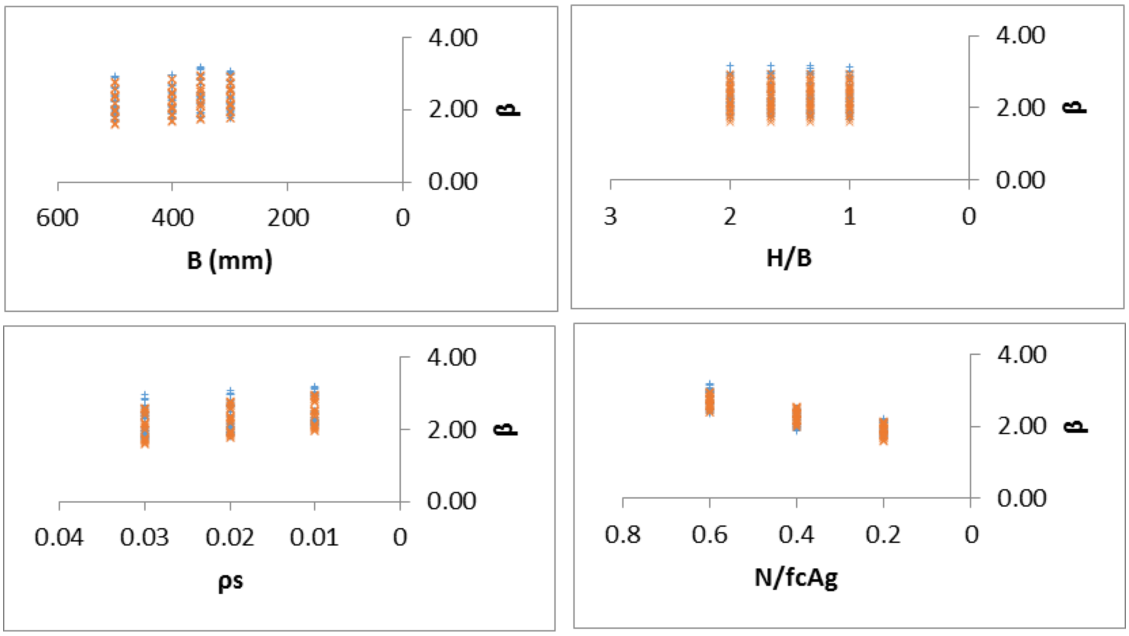

- $\alpha_{UHPC}/\alpha_{NSC}$:

Figure A. 16:

Residual plots of $\alpha_{UHPC}/\alpha_{NSC}$ factor.

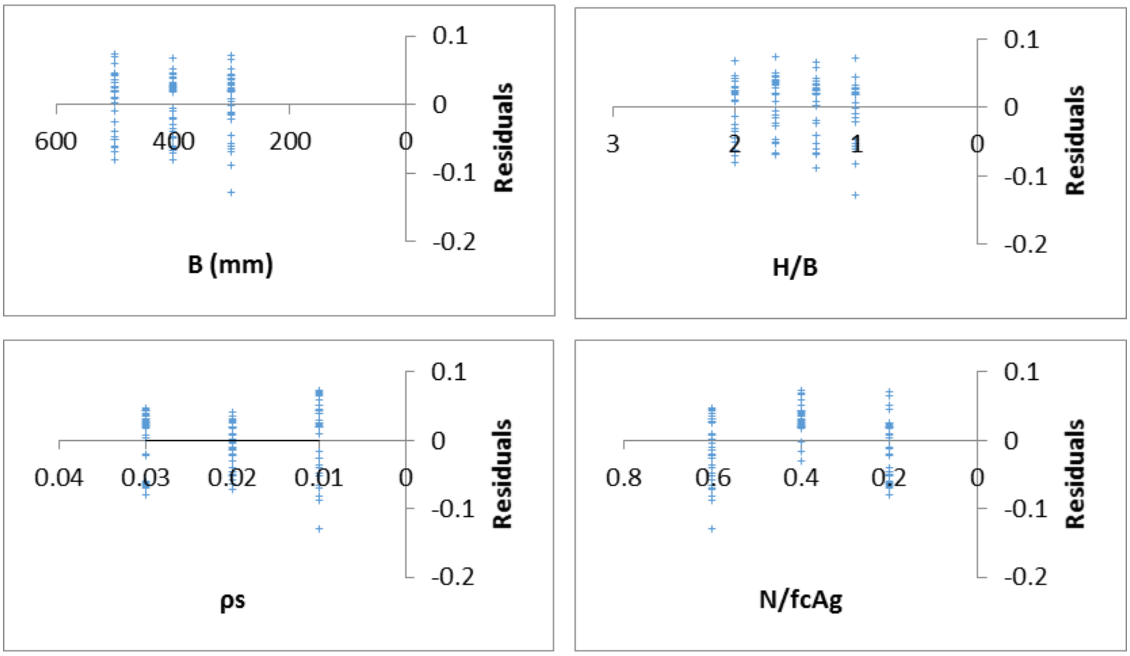

- plots of $\alpha_{UHPC}/\alpha_{NSC}$ factor.

Figure A. 17:

Line fit

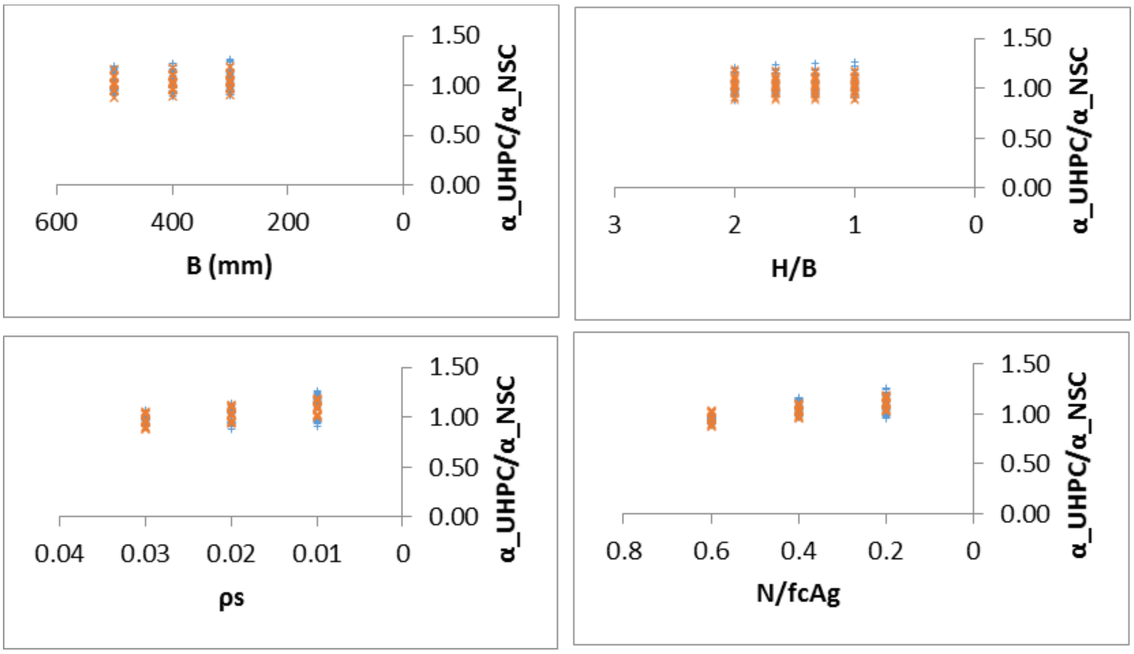

Appendix B: Design Steps of the 3D Frame

In this appendix, the loads applied in the frame are calculated and the frame is designed to resist earthquake and gravity loads. Also, the ACI318-19 requirement for the sway special moment-resisting frame is performed.

1. Loads

1.1. Earthquake Load

The building is selected at high seismic design category D in Jericho city. The zone factor Z = 0.30, the soil profile is S_B, and the important factor I_e = 1. The earthquake force is calculated according to ASCE7-16 instructions.

$$S_s = 2.5Z = 2.5 * 0.3g = 0.75g \tag{44}$$
$$S_1 = 1.25Z = 1.25 * 0.3g = 0.37g \tag{45}$$
$$S_{Ds} = F_aS_s = 0.9 * 0.75g = 0.675g \tag{46}$$
$$S_{D1} = F_vS_s = 0.8 * 0.375g = 0.3g \tag{47}$$

Where: S_s and S_1 are the spectral response acceleration parameters at short periods and a period of 1 s respectively. S_{Ds} and S_{D1} are the design spectral response acceleration parameter at short periods and a period of 1 s respectively. F_a and F_v are site coefficients and is given from ASCE7-16 tables.

The seismic force-resisting system is selected as sway special moment-resisting frame which is not limited to using at seismic design category D with the following parameters:

R = 8, C_d = 5.5, Ω_o = 3

Where:

R: the reponse modification coefficient.

C_d: the deflection amplification factor.

Ω_o: the over-strength factor.

- Fundamental period:

The fundamental period is determined as follows:

$$T_a = C_t h_n^x \tag{48}$$

Where:

T_a: the approximation fundamental period.

h_n: the structural height.

C_t: a coefficient equal to 0.0466 for the frame.

x: a coefficient equal to 0.9 for the frame.

$h_n = 22.3$ m

$T_a = 0.0466 * 22.3^{0.9}$=0.762 sec.

$$\mathrm{T} \leq \mathrm{C_u T_a} \tag{49}$$

Where:

T: fundamental period determined by analysis.

C_u: coefficient for the upper limit on the calculated period.

$\mathrm{C_u T_a} = 1.4 * 0.762 = 1.07\mathrm{sec}$

- **Base shear force:**

The design base shear force is calculated as the following:

$$\mathrm{V} = \mathrm{C_s w} \tag{50}$$

Where:

C_s: the seismic response coefficient.

w: the effective mass weight.

$$\mathrm{C_{s,min}} \leq \mathrm{C_s} = \frac{\mathrm{S_{DS}}}{\mathrm{R/I_e}} \leq \mathrm{C_{s,max}}$$

$$\mathrm{C_s} = \frac{0.675}{8/1} = 0.084$$

$$\mathrm{C_{s,min}} = 0.044\mathrm{S_{DS}I_e} \leq 0.01 \tag{51}$$

$\mathrm{C_{s,min}} = 0.044 * 0.675 * 1 = 0.03 \leq 0.01$

$\mathrm{C_{s,max}} = \dfrac{\mathrm{S_{D1}}}{\mathrm{T(R/I_e)}}$

$\mathrm{C_{s,max}} = \frac{0.3}{1.07(8/1)} = 0.035 \rightarrow \mathrm{C_s} = 0.035$ (52)

$\mathrm{w} = 28{,}264$ kN.

$\mathrm{V} = 0.035 * 28{,}264 = 990$ kN

- **Design load combination:**

The frame shall design to the strength design combination including seismic load effect.

$E = \rho[E_v + E_h]$ (53)

Where:

E: seismic load effect.

ρ: redundancy factor equal 1 for the studied.

E_v: effect of horizontal seismic forces. For the orthogonal combination procedure, 30% of the horizontal seismic forces in are taken the perpendicular direction to the direction design.

E_h: vertical seismic effect applied in the vertically downward direction and is equal to $0.2S_{ds}D$.

$E_h = EQ_x + 0.3EQ_y$ (54)

$E_v = 0.2S_{ds}D$ (55)

$E = 1 * \left[0.2S_{ds}D + EQ_x + 0.3EQ_y\right]$

The strength design combination is:

$U1 = 1.4D$ (56)

$$U2 = 1.2D + 1.6L \tag{57}$$

$$U3 = 1.2D + E + L \tag{58}$$

$$= 1.135D + EQ_x + 0.3EQ_y + L$$

$$U4 = 0.9D - E_v + E_h \tag{59}$$

$$= 0.765D + EQ_x + 0.3EQ_y$$

- **The number of modes:**

The selected number of modes shall be given a modal participation ratio of more than 90%.

By SAP2000 modal analysis the modal participation ratio = 99.99% > 90%.

- **Scaling response spectrum forces:**

The equivalent lateral force method is not permitted for the selected frame with seismic design category D. Therefore the modal response spectrum analysis method is used and scaled to be as the equivalent lateral force value.

- **Drift check:**

The stories drift under the earthquake is checked to be less than the ASCE7-16 code limit.

Drift limit = $0.02H_x$. Where H_x is the story height.

→0.02*4.8 = 0.096 m for first floor and 0.02*3.5 = 0.07 m for the rest floor.

The story drift is calculated as:

$$\Delta = \delta_x - \delta_{x-1} \tag{60}$$

Where: Δ is the design inter-story drift. δ_x and δ_{x-1} are the inelastic story displacement at level x and $x-1$ respectively at the center of mass.

The inelastic displacement for the story is calculated by the following equation:

$$\delta_{\text{inelastic}} = \frac{C_d \delta_{\text{elastic}}}{I_e} \quad (61)$$

Table B.1 displays the drift check calculations.

Table B. 1:

Story drift check calculations.

Level	$\delta_{elastic}$ (m)	$\delta_{inelastic}$ (m)	Δ (m)	Δ_{limit} (m)
6th	0.03849	0.211695	0.012375	0.07
5th	0.03624	0.19932	0.022825	0.07
4th	0.03209	0.176495	0.032945	0.07
3rd	0.0261	0.14355	0.03883	0.07
2nd	0.01904	0.10472	0.044825	0.07
1st	0.01089	0.059895	0.059895	0.096

- **P-delta effects:**

The p-delta effects are negligible when the stability index θ is less than 0.1. The θ is given as the following:

$$\theta = \frac{P_x \Delta_{\text{inelastic}} I_e}{V_x h_{sx} C_d} \leq \theta_{\text{max}} \quad (62)$$

$$\theta_{\text{max}} = \frac{0.5}{\beta C_d} \leq 0.25 \quad (63)$$

Where:

P_x: service total vertical design load at and above level x.

$\Delta_{inelastic}$: design story drift occurring simultaneously with V_x.

V_x: seismic shear force acting between levels x and x-1.

h_{sx}: story height below level x.

C_d: deflection amplification factor.

β_0: is the ratio of shear demand to shear capacity for the story between levels a and x-1. This ratio is permitted to be conservatively taken as 1.

$$\theta_{max} = \frac{0.5}{1 * 5.5} = 0.09 \leq 0.25$$

Table B. 2:

Stability analysis of model.

Level	P_{DL} (kN)	P_{LL} (kN)	P_x (kN)	$\delta_{elastic}$ (m)	$\delta_{inelastic}$ (m)	Δ (m)	V_x (kN)	h_{sx} (m)	θ
6th floor	4014	810	4824	0.03849	0.211695	0.012375	338	3.5	0.009175
5th floor	5348	810	6158	0.03624	0.19932	0.022825	578	3.5	0.012633
4th floor	5348	810	6158	0.03209	0.176495	0.032945	719	3.5	0.014658
3rd floor	5348	810	6158	0.0261	0.14355	0.03883	836	3.5	0.014858
2nd floor	5348	810	6158	0.01904	0.10472	0.044825	959	3.5	0.014952
1st floor	4014	810	4824	0.01089	0.059895	0.059895	1054	4.8	0.010384

1.2. Gravity Loads

The frame is designed with the following gravity loads:

- Live load (LL) = 2.5 kN/m^2.
- Superimposed dead load including slab weight = 9 kN/m^2.
- Masonry wall = 15 kN/m
- Columns and beams self-weight.

2. Design for forces

The frame is designed to resist the previous loads. All preliminary geometry and reinforcement of all structural elements are determined as the following:

2.1 Slab design

The solid slab type is selected with a thickness of 25cm which satisfies the ACI318-19 minimum thickness and is commonly used in our locality. The slab is designed to resist all assigned loads.

2.2 Beams design

- **Geometry**

The beam depth h is selected 40 cm which is satisfy the ACI318-19 minimum thickness 4.5/18.5 = 0.24 < h = 40 cm. The width of the beam is selected 50 cm then is checked.

- **Load combination**

The following combination gives the maximum forces:

$$1.135D + L + EQ_x + 0.3EQ_y \tag{59}$$

- **Flexural design**

The analysis is performed by SAP2000 for the beam. The longitudinal reinforcement is:

Figure B. 1:

The required longitudinal reinforcement (cm^2) of the beam analyzed by SAP2000.

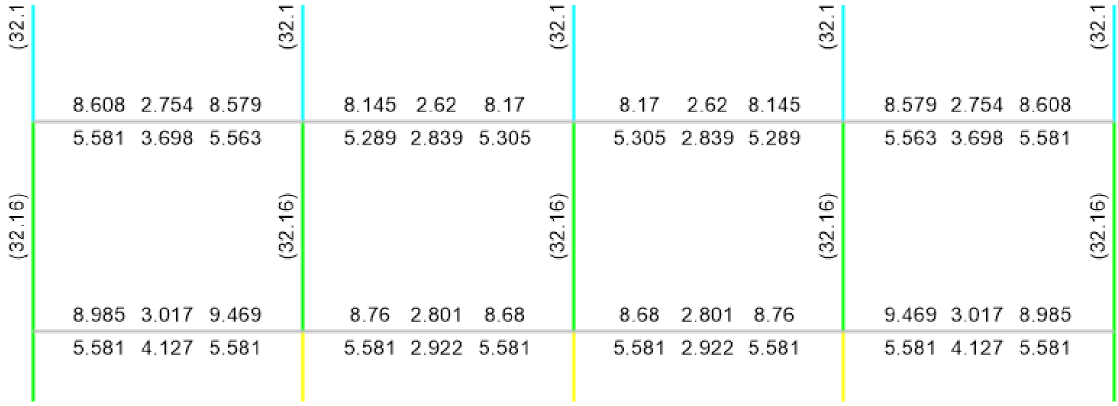

use:

$A_{s,top} = $ 9.4 cm^2 use 7ø14 (10.78 cm^2) →$\rho = 0.0063$

$A_{s,bot} = $ 5.6 cm^2 use 5ø14 (7.7cm^2) →$\rho = 0.0045$

- **Shear design**

The beam shear force analyzed by SAP2000 is V_u=120 kN.

$$d = 400 - 40 - 10 - \frac{14}{2} = 343 \text{ mm}$$

$$V_c = 0.17\sqrt{f_c{}'}b_w d$$

$$V_c = 0.17\sqrt{24} * 500 * 343 * 10^{-3} = 143 \text{ kN}$$

$$V_s = \frac{V_u}{\emptyset} - V_c = \frac{120}{0.75} - 143 = 17 \text{ kN.}$$

$$A_{v,min} = \frac{1}{16}\sqrt{f_c{}'}\frac{b_w s}{f_y} \geq \frac{1}{3}\frac{b_w s}{f_y}$$

$$\frac{A_{v,min}}{s} = \frac{1}{16}\sqrt{24}\frac{500}{420} = 0.0364 \geq \frac{1}{3} * \frac{500}{420} = 0.0396$$

$\rightarrow A_{v,min} = 0.0396 \text{ cm}^2/\text{cm}$

2.3 Column design

SAP2000 is used to analyze and design the columns. The following table displays the columns' internal forces.

Table B. 3:

The columns' internal forces.

Level	Column location	P_u (kN)	M_3 (kN.m)	M_2 (kN.m)	V_u (kN)
	Interior	2080	134	40	47
1st floor	Exterior	1710	119	33	46
	Corner	1203	101	39	36
	Interior	1727	84	25	47
2nd floor	Exterior	1390	95	20	53
	Corner	973	77	51	43
	Interior	343	28	8	15
6th floor	Exterior	186	83	8	42
	Corner	111	30	46	30

By using SAP2000 to obtain the interaction diagram and check the nominal capacity. 50*50cm column with assuming ρ = 1.286% is adequate.

3. Additional requirements for sway special moment-resisting frame

After selection of the preliminary geometry and reinforcement of all structural elements from design for force, chapter 18 in ACI318-19 requirements for designing the special are archived as the following:

3.1. Beam

- **Dimension limits**

▪ Clear span length ≥ 4d.

→ clear span length 4.5m ≥ 4*0.343=1.372m→ Satisfied.

▪ Width ≥ minimum of 0.3H or 250mm.

→ Width =50cm ≥ min(0.3*40=12cm or 25cm)→ Satisfied.

- Projection of the beam width beyond the width of the supporting column on each side shall not exceed the lesser of least column dimension or 0.75 maximum column dimension.

→(beam width – column width) / 2 = 0 cm < min (50 cm or 0.75*50) = 37.5 cm. →Satisfied.

- **Longitudinal reinforcement**

At least are two continuous bars at both top and bottom faces.

ρ_{min} = max ($\frac{0.25\sqrt{f_c'}}{f_y}, \frac{1.4}{f_y}$) ≤ ρ ≤ 0.025

→$\rho_{min} = max\left(\frac{0.25\sqrt{24}}{420}, \frac{1.4}{420}\right)$ = max (0.003,0.0033)

→$\rho = A_s/(b_w\ d)$.

$A_{s,top} =\ 9.34\ cm^2\ use$ 7ø14 (10.78 cm^2)

→$\rho_{min} < \rho = 0.0063 < 0.025 \ldots .ok$

$A_{s,bot} =\ 5.6\ cm^2\ use$ 5ø14 (7.7cm^2)

→$\rho_{min} < \rho = 0.0045 < 0.025 \ldots .ok$

- Positive moment strength at joint face ≥ 0.5 negative moment strength at joint face.

Nominal moment of beams at the joint face:

$$M_n = A_s f_y \left(d - \frac{a}{2}\right)$$

$$a = \frac{A_s f_y}{0.85 f_c' b}$$

For the negative nominal moment :

$$a = \frac{1078 * 420}{0.85 * 24 * 500} = 44.39\ mm$$

$$M_n = 1078 * 420 \left(343 - \frac{44.39}{2}\right) * 10^{-6} = 145.2\ kN.m.$$

For the positive nominal moment :

$$a = \frac{770 * 420}{0.85 * 24 * 500} = 31.7mm$$

$$M_n = 770 * 420 \left(343 - \frac{31.7}{2}\right) * 10^{-6} = 105.8\ kN.m.$$

Positive M_n=105.8 kN.m > 0.5*negative M_n=145.2 =72.6 kN.m.

→ Satisfied

- Positive and negative moment strength at any section along the member length ≥ 0.25 maximum positive or negative moment strength provided at the face of either joint.

Positive M_n or negative M_n at any section along with the member length ≥ 0.25 max (positive M_n or negative M_n):

(105.8 or 145.2) kN.m ≥ 0.25*max (105.8 or 145.2) = 0.25*145.2 = 36.3 kN.m ……ok

- Lap splice shall location shall have transverse reinforcement with spacing less than *d*/4 or 100 mm and the lap splice shall not be used in the following locations the location:

1. Within joint.
2. Within a distance 2*d* from the joint face. →2*43.3 = 86.6 cm.
3. Within a distance 2*d* from the critical sections results from lateral displacement beyond the elastic behavior.

- **Transverse reinforcement:**

ACI318-19 considers two zones in the transverse reinforcement which are the zone where the hoops are required and where the hoops are not required.

- The location where the hoops are required Zone:

- The length of the location where the hoops are required is determined as the following:

1. Length ≤ $2d$ from the face of the supporting column toward mid-span. →2*43.3 = 86.6 cm.
2. Length ≤ $2d$ from both sides of the critical sections results from lateral displacement beyond the elastic behavior.

- At the location where the hoops are required the following requirements shall apply:

1. Spacing of transversely supported flexural reinforcing bars ≤350mm.

Clear space between longitudinal bare is:

$$(500 - 2 * (40 + 8) - 7 * 14)/6 = 51mm$$

$$\rightarrow 51 * 2 + 2 * 14 = 130\ mm < 350\ mm.$$

2. The longitudinal bar shall have lateral support every corner and alternate longitudinal bars by ties with an angle less than 135 degrees. Clear spacing of all supported longitudinal bar ≤ 150mm.

$$\rightarrow 51 * 2 + 14 = 116\ mm < 150\ mm$$

Figure B.2 displays the section detail of the beam of the frame.

Figure B. 2:

The beam of the frame section details.

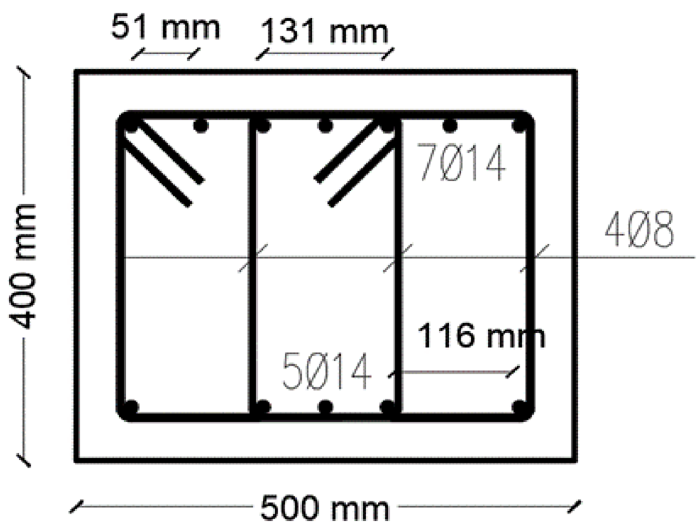

- The first hoop location ≤ 50 mm from the joint face.
- The spacing (s_o) of the hoops shall be the lesser of the following:

1. $s \le d/4$. → $d/4 = 343/4 = 85.8$ mm.
2. $s \le 150$ mm.
3. $6d_b$, where d_b is the minimum bar diameter of the longitudinal reinforcement. → $6d_b = 6*14 = 84$ mm.

→84 mm control select $s_o = 80$ mm.

- Neglect V_c if both following conditions occur:

1. Shear forced-induced by the earthquake (V_E) ≥ $0.5V_e$. Where V_E is the shear force due to earthquake effect only (Armouti, 2008) and V_e is defined in the next point.
2. The factored axial compressive force P_u including earthquake effects is less than $A_g f_c'/20$.

The V_c is neglected here to simplify the analysis and P_u is less than $A_g f_c'/20$.

- $\emptyset V_n \ge V_e$, Where V_e is the design shear force for load combinations including earthquake effects. V_e is calculated as displayed in the following figure.

Figure B. 3:

Design shear force for beams (ACI318, 2019).

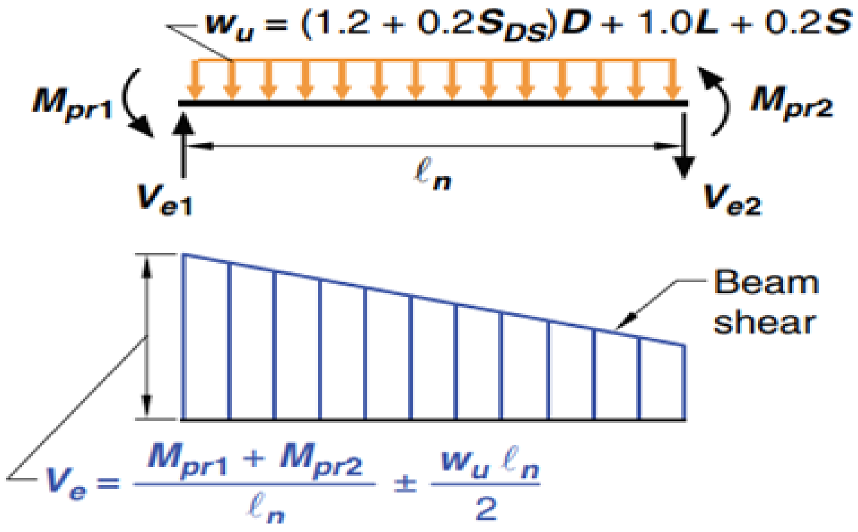

Where M_{pr1} and M_{pr2} are probable flexural strength of members, determined using the properties of the member at joint faces assuming tensile stress in the longitudinal bars of at least $1.25f_y$ and a strength reduction factor $\emptyset$ of 1.0. L_n is the clear length of the beam.

Firstly determine probable moments:

$f_s = 1.25f_y = 1.25 * 420 = 525\ MPa, \phi = 1.00, d = 190\ mm$

$l_n = 4.5 - (0.25 + 0.25) = 4m$

$W_u = 1.335D + L = 1.335 * (4.5 * 9 + 0.15 * 0.5 * 25) + 2.5$

$= 67.8\ kN/m$

$M_{pr} = A_s f_s \left(d - \frac{a}{2}\right)$

$a = \frac{A_s f_s}{0.85 f_c{}' b}$

For the negative probable moment :

$a = \frac{1078 * 525}{0.85 * 24 * 500} = 55.48\ mm$

$M_{pr1} = 1078 * 525 \left(343 - \frac{55.48}{2}\right) * 10^{-6} = 178.4\ kN.m.$

For the positive probable moment :

$a = \frac{770 * 525}{0.85 * 24 * 500} = 39.63\ mm$

$M_{pr2} = 770 * 525 \left(343 - \frac{39.63}{2}\right) * 10^{-6} = 130.6\ kN.m.$

$$V_e = \frac{M_{pr1} + M_{pr2}}{l_n} \pm \frac{W_u l_n}{2} \qquad (64)$$

$V_e = \frac{178.4 + 130.6}{4} \pm \frac{67.8 * 4}{2} = 77.25 \pm 135.6\ kN.$

$\rightarrow V_e = 212.8\ kN.$

V_c = 0 kN , s_o = 80 mm

$$V_s = \frac{V_u}{\emptyset} - V_c = \frac{212.8}{0.75} - 0 = 284\ kN.$$

$$V_s = \frac{A_v f_y d}{s}$$

$$\rightarrow \frac{A_v}{s} = \frac{V_s}{f_y d} = \frac{284 * 10^3}{420 * 343} * 10^{-1} = 0.197\ cm^2/cm$$

$$A_v = 0.197 * s = 0.197 * 8 = 1.576\ cm^2.$$

Select 4leg∅8 with A_v=2.01cm^2.

Figure B. 4:

Final section details for the beam of the frame.

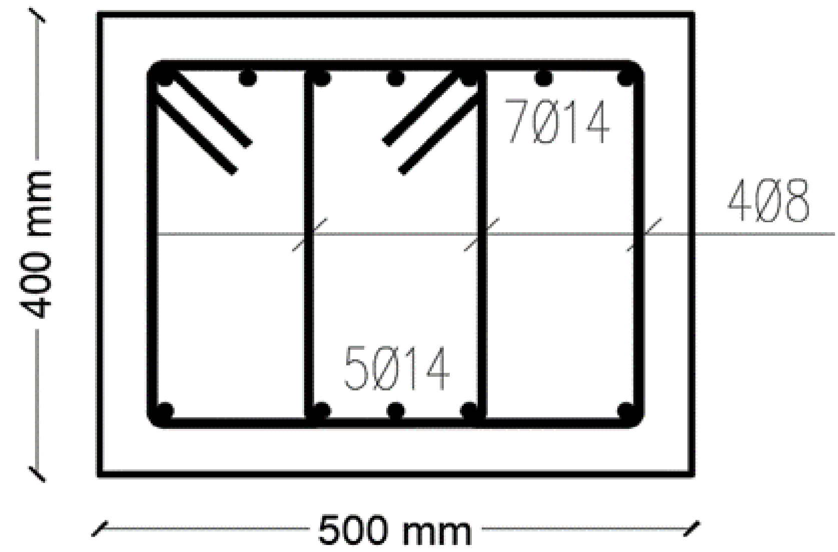

- The location where the hoops are not required Zone:

  - The location where the hoops are not required, seismic stirrups spacing shall be ≤ d/2. → 343/2 = 171.5 mm select s_1 = 150mm.

The design beam of the frame layout is seen in the following figures:

Figure B. 5:

Design beam of the frame layout.

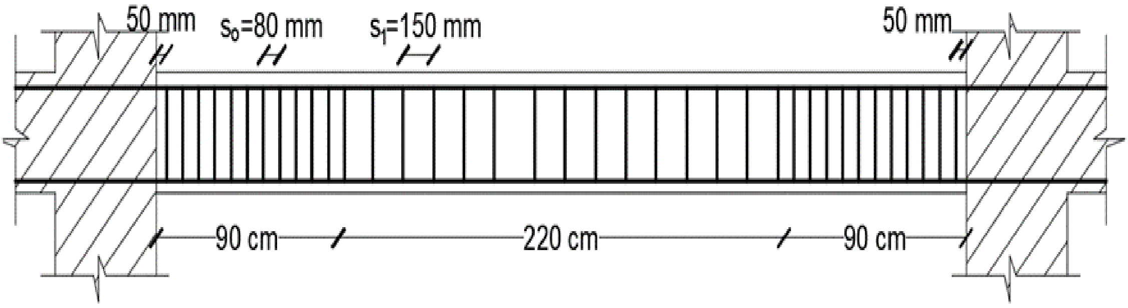

3.2. Column

- **Dimension limits**

▪ The shortest cross-sectional dimension ≥ 300 mm.

The shortest cross-sectional dimension =5 00 mm ≥ 300mm

→ Satisfied.

▪ The shortest cross-sectional dimension to the perpendicular dimension ratio ≥ 0.4.

→ The shortest cross-sectional dimension to the perpendicular dimension ratio 500/500 = 1 ≥ 0.4→ Satisfied.

- **Flexural strength**

▪ The following condition shall be satisfied:

$$\sum M_{nc} \geq (6/5) \sum M_{nb}$$

Where:

M_{nc}: the nominal strength of the columns framing into the joint.

M_{nb}: the nominal strength of the beams framing into the joint.

Figure B.6 display the nominal moment of the column and beam at the joint for the two considered directions and the axial load combinations considered for determining the nominal moment of columns including earthquake effect

Figure B. 6:

a) Nominal moment of the column and beam at the joint for the two considered directions. b) Axial load combinations are considered for determining the nominal moment of columns including earthquake effect (Moehle, 2015).

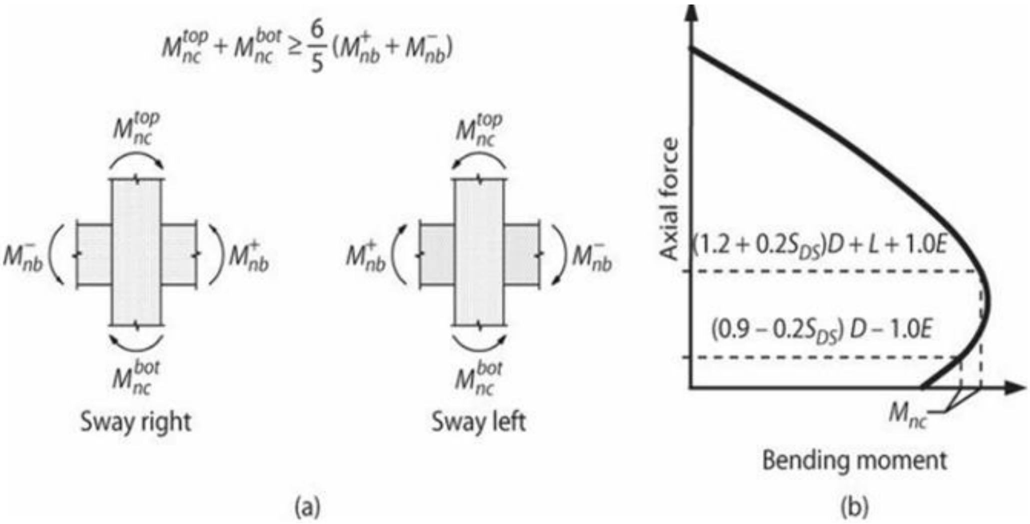

Nominal moment of beams at the joint face:

$M_{n,b1} = 145.2\ kN.m.$

$M_{n,b2} = 105.8\ kN.m.$

$\sum M_{n,b} = M_{n,b1} + M_{n,b2} = 145.2 + 105.8 = 251\ kN.$

The nominal moment of columns at the joint face is shown in Table B.4.

Table B. 4:

The nominal moment of columns at the joint face.

Joint Level		Column location	P_u (kN)	$M_{n,c}$ (kN.m)	$\sum M_{n,c}$ (kN.m)	$\sum M_{n,c} / \sum M_{n,c}$
1st floor	Bottom of joint	Interior	2080	490	970	3.86
	Top of joint		1727	480		
	Bottom of joint	Exterior	1710	480	940	3.74
	Top of joint		1390	460		
	Bottom of joint	Corner	1203	442	862	3.43
	Top of joint		1203	420		
6th floor	Bottom of joint	Interior	343	332	332	1.32
		Exterior	186	306	306	1.22
		Corner	111	300	300	1.2

- **Longitudinal reinforcement**

▪ 0.01 ≤ ρ ≤ 0.06

→ρ = 16*201 / (500*500) = 0.012861

▪ Lap splice shall be at the mid-height of column and design as tension lap splice and enclosed with transverse reinforcement.

▪ Longitudinal reinforcement shall be selected as $1.25\, l_d \leq L_u/2$ →max $l_d = 3.1/(2 * 1.25) = 1.24\, m$.

Where:

l_d: development length of longitudinal bars.

L_u: clear height of the column.

The development length is calculated as the following:

$$l_d = \left(\frac{f_y \psi_t \psi_e \psi_g}{2.1 \lambda \sqrt{f_c{}'}}\right) d_b \qquad (65)$$

Where:

f_y: reinforcement yield strength.

ψ_t: casting location in tension factor and is equal to 1 for the column.

ψ_e: reinforcement coating factor and is equal to 1 for uncoating reinforcement.

ψ_g: grade of reinforcement factor and is equal to 1 for grade 420.

λ: factor for lightweight or normal weight concrete and is equal to 1 for the normal weight concrete.

$f_c{}'$: concrete compressive strength.

d_b: the diameter of reinforcement bare.

$$l_d = \left(\frac{420*1*1}{2.1*1\sqrt{24}}\right)1.6 = 65.3\ cm \leq 1.24\ m.$$

$$Tension\ lap\ splice\ length = 1.3 l_d = 1.3 * 65.3 = 84.9\ cm$$

$\rightarrow select\ 90cm.$

- **Transverse reinforcement**

▪ The location where the hoops are required Zone:

○ The least length of the location where the hoops (l_o) required is the greatest of determined as the following:

1. Depth of the column. →500mm
2. Clear height of the column L_u / 6.

→4400 / 6 = 733.3 mm for the first floor.

→3100 / 6 = 517 mm for rest column.

3. 450mm.

→Select l_o = 750 mm.

○ At the location where the rectilinear hoops are required the following requirements shall apply:

1. Diameter of transverse bare Ø10 for Longitudinal bars ≤ Ø32.
2. The longitudinal bar shall have lateral support every corner and alternate longitudinal bars by ties with an angle less than 135 degrees. Clear spacing of all supported longitudinal bar ≤ 150 mm.
3. $h_x \leq 350$ mm. Where h_x is the largest value of x_i displayed in Figure B.7.

Figure B. 7:

Example of transverse reinforcement in columns (ACI318, 2019).

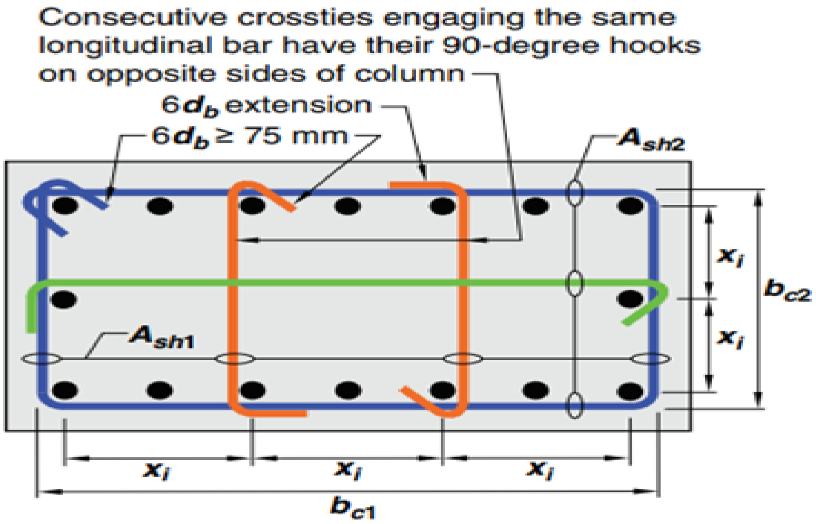

4. If P_u > 0.3$A_g f_c$' every longitudinal bar shall be supported by crossties with seismic hook and $h_x \leq$ 200 mm.

$$0.3A_g f_c' = 0.3 * 500 * 500 * 24 * 10^{-3} = 1800\ kN.$$

The column axial forces at the 1st floor are:

For interior columns P_u = 2060 kN > 0.3$A_g f_c$' =1800 kN.

For exterior columns P_u = 1727KN < 0.3$A_g f_c$' =1800 kN.

For corner columns P_u = 1203KN < 0.3$A_g f_c$' =1800 kN.

→ only the interior columns at the first floor satisfied the condation.

Figure B.8 displays The final section detail of the columns of the frame.

$x_1 = (500 - 40 * 2 - 10 * 2)/4 = 100\ mm$

$x_2 = 2 * (500 - 40 * 2 - 10 * 2)/4 = 200 mm$

$\rightarrow h_x = 192 < 200\ mm.$

Figure B. 8:

The section detail of the frame columns.

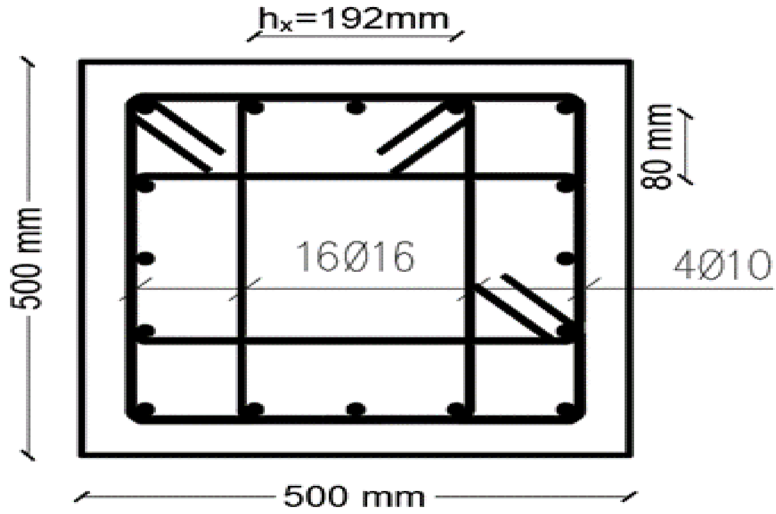

- Spacing of transverse S_o reinforcement at l_o is the least of:

1. Minimum column dimension / 4. → $500/4 = 125mm$.
2. $6d_b$, where d_b is the minimum bar diameter of the longitudinal reinforcement. →$6d_b = 6 * 16 = 96\ mm$.
3. $100 + \frac{350-hx}{3} \leq 150mm$.

$$\rightarrow 100 + \frac{(350-192)}{3} = 152.7\ mm \rightarrow 150mm.$$

→Select $S_o = 90mm < 96\ mm$.

- The amount of transverse reinforcement shall be more than the values in the following table.

Table B. 5:

Transverse reinforcement for the columns of special moment frames (ACI318, 2019).

Transverse reinforcement	Conditions	Applicable expressions	
A_{sh}/sb_c for rectilinear hoop	$P_u \le 0.3A_g f_c'$ and $f_c' \le 70$ MPa	Greater of (a) and (b)	$0.3\left(\frac{A_g}{A_{ch}}-1\right)\frac{f_c'}{f_{yt}}$ (a) $0.09\frac{f_c'}{f_{yt}}$ (b) $0.2k_f k_n \frac{P_u}{f_{yt}A_{ch}}$ (c)
	$P_u > 0.3A_g f_c'$ or $f_c' > 70$ MPa	Greatest of (a), (b), and (c)	
ρ_s for spiral or circular hoop	$P_u \le 0.3A_g f_c'$ and $f_c' \le 70$ MPa	Greater of (d) and (e)	$0.45\left(\frac{A_g}{A_{ch}}-1\right)\frac{f_c'}{f_{yt}}$ (d) $0.12\frac{f_c'}{f_{yt}}$ (e) $0.35k_f \frac{P_u}{f_{yt}A_{ch}}$ (f)
	$P_u > 0.3A_g f_c'$ or $f_c' > 70$ MPa	Greatest of (d), (e), and (f)	

Where:

b_c: is the core dimension perpendicular to the tie legs as seen in the previous figure.

k_f: concrete strength factor.

k_n: confinement effectiveness factor.

n_1: is the number of longitudinal bars or bundles around the perimeter of a column core with rectilinear hoops that are laterally supported by the corner of hoops or by seismic hooks.

$$k_f = \frac{f_c'}{175} + 0.6 \ge 1 = \frac{24}{175} + 0.6 = 0.74 \rightarrow \ k_f = 1$$

$$k_n = \frac{n_1}{n_1 - 2} = \frac{12}{12 - 2} = 1.2$$

where n_1 is the number of longitudinal bars that are laterally supported by seismic hoops. → $n_1 = 12$.

b_{c1} and b_{c2} display in Figure B.7.

→ $b_{c1} = b_{c2} = 500 - 40 * 2 = 420\ mm.$

$A_{ch} = b_{c1} * b_{c2} = 420 * 420 = 176400\, mm^2$

$a) \frac{A_{sh}}{sb_c} = 0.3\left(\frac{A_g}{A_{ch}} - 1\right)\frac{f_c'}{f_y} = 0.3\left(\frac{500*500}{176400} - 1\right)\frac{24}{420} = 0.0072$

$b) \frac{A_{sh}}{sb_c} = 0.09\frac{f_c'}{f_y} = 0.09\frac{24}{420} = 0.0051$

$c) \frac{A_{sh}}{sb_c} = 0.2k_f k_n \frac{P_u}{f_y A_{ch}} = 0.2 * 1 * 1.2\frac{2060}{420 * 176400} = 0.0067$

→$\frac{A_{sh}}{sb_c} = 0.0072 \rightarrow A_{sh} = 0.0072 * 90 * 420 = 272.2mm^2$.

4leg$\emptyset 10$→$A_{ch} = 4 * 78.5 = 314\, mm^2$…Ok.

- The location beyond l_o:

- Spacing of transverse S reinforcement is the least of:

1. 150 mm.
2. $6d_b$, where d_b is the minimum bar diameter of the longitudinal reinforcement. →$6d_b$ $6 * 16 = 96\, mm$.

- **Shear strength**

- Neglect V_c if both following conditions occur:

1. Shear forced-induced by the earthquake (V_E) ≥ 0.5V_e within l_o. Where V_E is the shear force due to earthquake effect only (Armouti, 2008) and V_e is defined in the next point. → V_E = 47 kN
2. The factored axial compressive force P_u including earthquake effects is less than A_g f_c'/20.

The V_c is neglected here to simplify the analysis.

- $\emptyset V_n \geq V_e$, Where V_e is the design shear force for load combinations including earthquake effects. V_e is calculated as displayed in the following figure.

Figure B. 9:

Design shear force for the columns (ACI318, 2019).

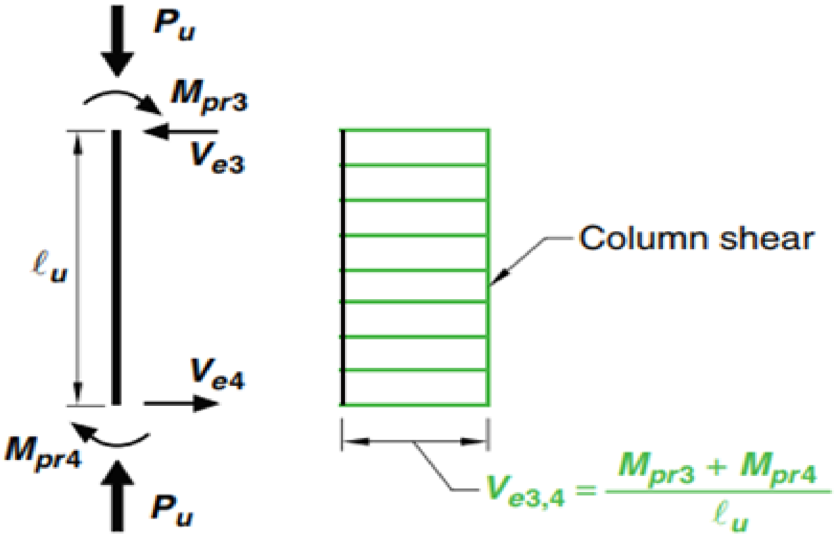

Where: M_{pr1} and M_{pr2} are the probable flexural strength of members, determined using the properties of the member at joint faces assuming tensile stress in the longitudinal bars of at least $1.25f_y$ and a strength reduction factor $\emptyset$ of 1.0. l_u is the clear height of the column.

Table B.6 displays the column probable moments and V_e at different stories level.

Table B. 6:

The column probable moments and Ve at different stories level.

Joint Level	Column location	P_u (kN)	$M_{pr,c}$ (kN.m)	l_u (m)	V_e (kN)
	Interior	2080	512		233
1st floor	Exterior	1710	508	4.4	231
	Corner	1203	482		219
	Interior	1727	509		291
2nd floor	Exterior	1390	493	3.5	282
	Corner	973	462		264
	Interior	343	384		219
6th floor	Exterior	186	368	3.5	210
	Corner	111	355		63

$$V_c = \ 0\ kN\ , s_o\ = 90\ mm$$

$$V_s = \frac{V_e}{\emptyset} - V_c = \frac{291}{0.75} - 0 = 388\ k\text{N}.$$

$$V_s = \frac{A_v f_y d}{s}$$

$$\rightarrow \frac{A_v}{s} = \frac{V_s}{f_y d} = \frac{388 * 10^3}{420 * (500 - 58)} * 10^{-1} = 0.209\ cm^2/cm$$

$A_v = 0.209 * s_o = 0.209 * 9 = 1.88\ cm^2$.

Select 4legØ10 with $A_v = 3.14\ cm^2$.

Figure B. 10:

Final section details of the column for the frame.

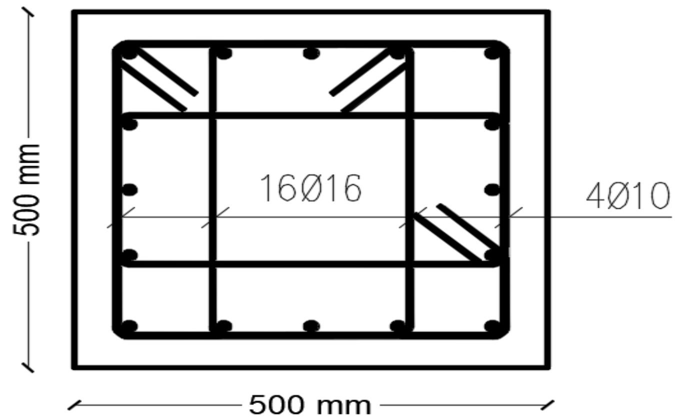

Figure B. 11:

Design column of the frame layout.

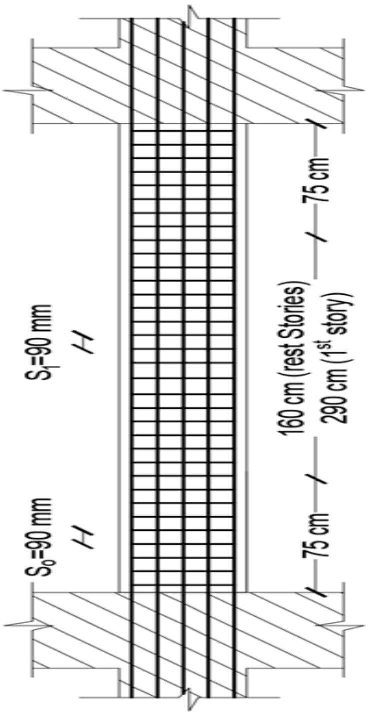

Column beam Joints:

The effective area of the joint A_j is seen in the following figure.

Figure B. 12:

Effective area of the joint (ACI318, 2019).

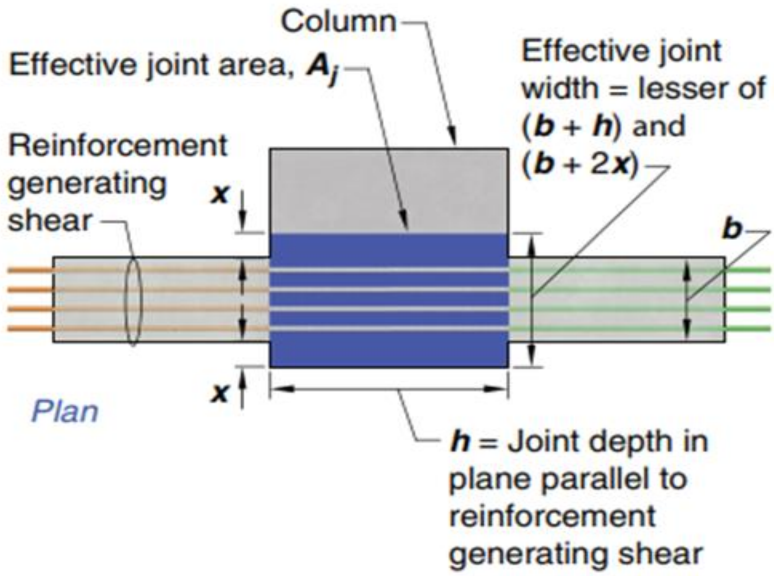

Where: *h:* the joint depth and is equal to the column depth parallel to the beam. Effective joint width is the beam width when the beam is wider than the column width.

When the column width is wider than the beam width the effective width of the joint is calculated as in Figure B.12.

h = 500 mm, effective joint width(beam width) = 500mm

→A_j =500*500 = 250000 mm^2.

h at least shall be the greatest value of :

1. $20d_b$, where d_b is the longitudinal reinforcement bar diameter of the beam→20*14 = 280 mm.
2. h / 2, where h is the depth of the beam. →250 / 2 =125 mm.

$\emptyset V_n \geq V_u$.

Where V_u is calculated from forces at the joint resulting from the probable moment from the columns and beams at the joint as seen in Figure B.13 with $\emptyset = 0.85$.

Figure B. 13:

Joint forces resulting from the probable moment from the columns and beams (Armouti, 2008).

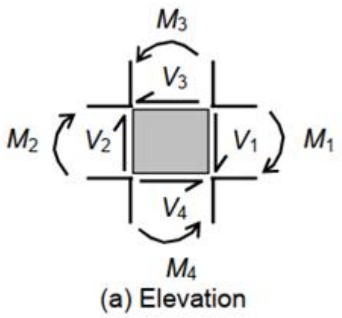

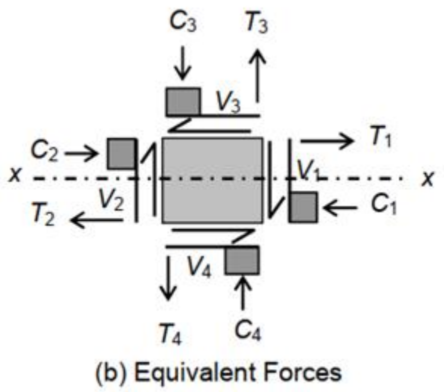

$$V_n = 1.7\sqrt{f_c'}A_j = 1.7 * \sqrt{24} * 250000 * 10^{-3} = 2082KN$$

Column shear consistent with M_{pr} beam

$$= \sum M_{pr,b}/L_u = (178.4 + 130.6)/3.1 = 99.7\ kN.$$

Compression and tension beams forces with f_s = 1.25f_y:

$$T_1\ or\ C_1 = 1078 * 525 * 10^{-3} = 566\ kN$$

$$T_2\ or\ C_2 = 770 * 525 * 10^{-3} = 404\ kN$$

$\rightarrow V_u = 99.7 - 566 - 404 = -870.3\ kN$

$\rightarrow \emptyset V_n = 0.85 * 2082 = 1770 \geq V_u = 870.3\ kN.$

Appendix C: 3D Model Verification

To verify the model elastically the following calculated and compared with the SAP2000 results:

1. Compatibility:

This can be achieved by checking the frame deformations to confirm all member models are correctly and connected well. Compatibility is achieved as seen in Figure C.1.

Figure C. 1:

The deformed shape of the 3D model frame from gravity load on SAP2000.

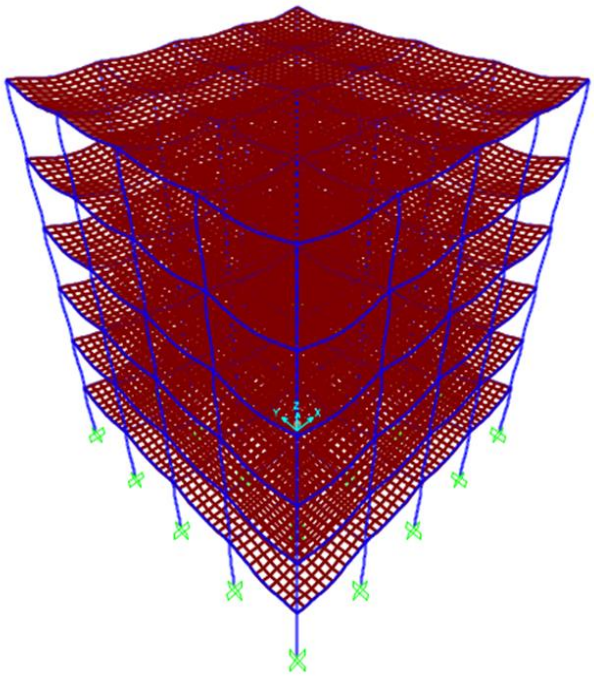

2. Equilibrium:

This can be checked by calculating manually the gravity loads and compared with the SAP2000 results. The following tables display the manual calculation

Table C. 1:

Geometry of the beams and columns in the model.

Member	Width (m)	Depth (m)	Height c/c (m)
Column (1st story)	0.5	0.5	4.8
Column (rest stories)	0.5	0.5	3.5
Beam	0.5	0.4	4.5

Table C. 2:

Gravity loads manually calculation for the model.

Slab	DL = 9 kN/m2 LL = 2.5 kN/m2	No. floor 6 Floor area =324m2	DL = 9*6*324 = 17,496 kN LL = 2.5*6*324 = 4,860 kN
Column	Self-weight	50*50cm section 3.5-0.4 = 3.1 m clear height No. column at one story =25	DL = 0.52*3.1*25*25*6 = 2906 kN
Beam	Self-weight of drop beam	50*40 cm section. The total length of the beam = 167.5 m.	DL = 0.15*0.5*180*25*6 = 2025 kN.
Masonry wall	DL = 15KN/m	No. story with wall = 5 Perimeter length of building = 72m.	DL = 15*72*5 = 5,400KN
Sum	DL = 27,827 kN		LL = 4,860 kN

Table C. 3:

Gravity loads manual calculation compared vs SAP2000 results.

Load	Manually (kN)	SAP2000 (kN)	Error
DL	27,827	28,264	1.57%
LL	4,860	4,860	0.00%

As seen from Table C.3 the equilibrium is achieved.

3. Stress-strain relationship:

This can be checked by calculating manually the moment and deformation and comparing with the SAP2000 results. This check is done in chapter 5 for the NSC hinge verifications.

4. Elastic period of the structure:

The period of the frame at the direction of analysis is calculated manually by the Rayleigh-Ritz method using SAP2000 to determine the lateral displacement.

$$T = 2\pi\sqrt{\frac{\sum_{i=1}^{n} w_i \delta_i^2}{g\sum_{i=1}^{n} F_i \delta_i}} \tag{66}$$

Where F_i and δ_i are the assigned lateral loads and the associated lateral displacement respectively. w_i is the story weight at the story level i. g is the gravitational acceleration.

Table C.4 displays the manual calculation for the model Stories weights.

Table C. 4:

Manual calculation for the model Stories weights.

Story	Calculation Detail	Total weight (kN)
1st floor	Slab = 324*9 = 2,916 kN Beam = 0.15*0.5*180*25 = 338 kN. 0.5Column =0.5*25*0.5^2*4.4*25 = 344 kN Masonry = 15*72 = 1,080 kN	4,678
2nd floor	Slab = 324*9 = 2,916 kN Beam = 0.15*0.5*180*25 = 338 kN. Column = 25*0.5^2*3.1*25 = 484 kN Masonry = 15*72 = 1,080 kN	4,818
3rd floor	Same as above	4,818
4th floor	Same as above	4,818
5th floor	Same as above	4,818
6th floor	Slab = 324*9 = 2,916 kN Beam = 0.15*0.5*180*25 = 338 kN. 0.5Column = 0.5*25*0.52*3.1*25 = 242 kN	3,496
	Sum	27,344

Table C.5 displays the manual calculation of the elastic period of the model.

Table C. 5:

Manual calculation for the model period.

Story	W_i (kN)	F_i (kN)	δ_i (m)	δ_i^2	$F_i\,\delta_i$	$W_i\,\delta_i^2$
1st floor	4,678	3240	0.19994	0.039976	647.8056	187.007745
2nd floor	4,818	3240	0.33599	0.11288928	1088.608	543.900552
3rd floor	4,818	3240	0.44835	0.20101772	1452.654	968.503387
4th floor	4,818	3240	0.53781	0.2892396	1742.504	1393.55637
5th floor	4,818	3240	0.60059	0.36070835	1945.912	1737.89282
6th floor	3,496	3240	0.63432	0.40236186	2055.197	1406.65707
		Sum			8,933	6,238

$\rightarrow T = 2\pi\sqrt{\frac{\sum_{i=1}^{n} w_i\delta_i^2}{g\sum_{i=1}^{n} F_i\delta_i}} = 2\pi\sqrt{\frac{6238}{9.81*8933}}$ = 1.675sec.

by SAP2000 $T = 1.621\ sec$ → Error = 3.3%....ok

Appendix D: Tables

Table D. 1:

Definitions of the horizontal irregularities as per ASCE7-16.

Irregularity Type	Definition as ASCE7-16	Graphic Interpretation
	Horizontal Irregularities	
1a. Torsional irregularity	"Torsional irregularity is defined to exist where the maximum story drift, computed including accidental torsion with Ax = 1.0, at one end of the structure transverse to an axis is more than 1.2 times the average of the story drifts at the two ends of the structure. Torsional irregularity requirements in the reference sections apply only to structures in which the diaphragms are rigid or semi-rigid."	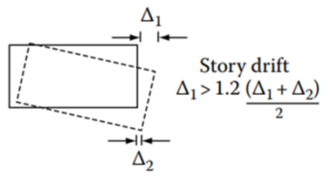
1b. Extreme torsion irregularity	Ditto above but the ratio is 1.4	
2. Reentrant corner irregularity	"Reentrant corner irregularity is defined to exist where both plan projections of the structure beyond a reentrant corner are greater than 15% of the plan dimension of the structure in the given direction."	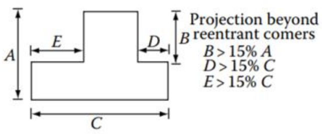
3. Diaphragm Discontinuity irregularity	"Diaphragm discontinuity irregularity is defined to exist where there is a diaphragm with an abrupt discontinuity or variation in stiffness, including one that has a cutout or open area greater than 50% of the gross enclosed diaphragm area, or a change in effective diaphragm stiffness of more than 50% from one story to the next."	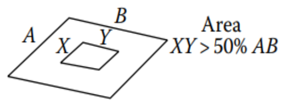
4. Out-of-plane offsets irregularity	"Out-of-plane offset irregularity is defined to exist where there is a discontinuity in a lateral force-resistance path, such as an out-of-plane offset of at least one of the vertical elements."	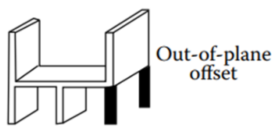
5. Nonparallel systems irregularity	"Nonparallel system irregularity is defined to exist where vertical lateral force-resisting elements are not parallel to the major orthogonal axes of the seismic force-resisting system."	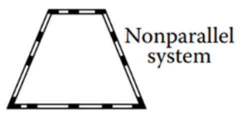

Table D. 2:

Definitions of the vertical irregularities as per ASCE7-16.

Vertical Irregularities		
1a. Stiffness irregularity (soft-story)	"Stiffness–soft story irregularity is defined to exist where there is a story in which the lateral stiffness is less than 70% of that in the story above or less than 80% of the average stiffness of the three stories above."	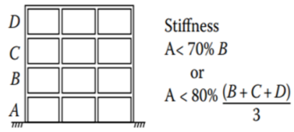
1b. Stiffness irregularity (extreme soft story)	Ditto above but the percentages are 60% and 70% respectively.	
2. Weight (mass) irregularity	"Weight (mass) irregularity is defined to exist where the effective mass of any story is more than 150% of the effective mass of an adjacent story. A roof that is lighter than the floor below need not be considered."	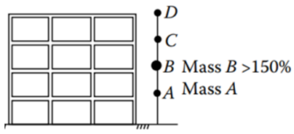
3. Vertical geometric irregularity	"Vertical geometric irregularity is defined to exist where the horizontal dimension of the seismic force-resisting system in any story is more than 130% of that in an adjacent story."	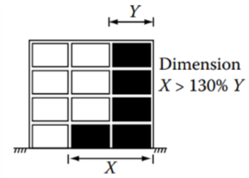
4. In-plane discontinuity in vertical lateral force–resisting systems	"In-plane discontinuity in vertical lateral force-resisting element irregularity is defined to exist where there is an in-plane offset of a vertical seismic force-resisting element resulting in overturning demands on supporting structural elements."	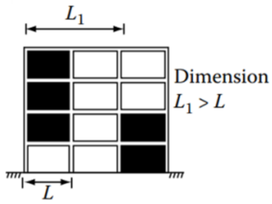
5a. Discontinuity in lateral Strength (weak story)	"Discontinuity in lateral strength–weak story irregularity is defined to exist where the story lateral strength is less than 80% of that in the story above. The story lateral strength is the total lateral strength of all seismic-resisting elements sharing the story shear for the direction under consideration."	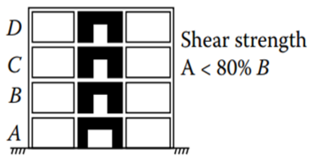
5b. Discontinuity in lateral strength (extreme weak story).	Ditto above but the percentage is 65%.	

Table D. 3:

Remedial measures for horizontal and vertical irregularities.

ASCE 7-16 section	Remedial Measure	Irregularity Type		Seismic Design Category Application
		Horizontal Irregularities	Vertical Irregularities	
12.3.3.4	25% increase of the connection and collector design force calculated by static method unless over-strength factor used in design combinations.	Torsional irregularity, Reentrant corner irregularity, Diaphragm discontinuity irregularity, and Out-of-plane offset irregularity.	In-plane discontinuity in vertical lateral force–resisting systems	D through F
		Extreme torsional irregularity		D
12.8.4.3	Amplification of the torsional moment by A_x factor, $1 \leq A_x = (\frac{\delta_{max}}{1.2\delta_{avg}})^2 \leq 3$	Torsional irregularity.		C through F
		Extreme torsional irregularity.		C and D
12.7.3	Perform 3D dynamic analysis with cracked section properties and consider P-Δ effects.	Torsional irregularity, Out-of-plane offsets irregularity, and Nonparallel systems irregularity.		B through F
		Extreme torsional irregularity		B through D
12.12.1	The story drift shall not exceed the drift limit.	Torsional irregularity		C through F
		Extreme torsional irregularity.		C and D
Table 12.6.1	Use model analysis or more rigorous procedure	Torsional irregularity, Reentrant corner irregularity, Diaphragm discontinuity irregularity, and Nonparallel systems irregularity.	Stiffness irregularity (soft story), Stiffness irregularity (extreme soft story), Weight (mass) irregularity, Vertical geometric irregularity, In-plane discontinuity in vertical lateral force-resisting systems, discontinuity in lateral strength (weak story), and Discontinuity in lateral strength (extreme weak story).	D through F
		Extreme torsional irregularity		D

12.3.3.1	Not permitted in design	Extreme torsional irregularity	Stiffness irregularity (extreme soft story)	E and F
			Discontinuity in lateral strength (weak story).	E and F
			Discontinuity in lateral strength (extreme weak story)	D through F
12.3.3.3	Design the structural elements that support discontinuous walls or frames for the maximum axial load form combinations include the over-strength factor	Out-of-plane offsets irregularity	In-plane discontinuity in vertical lateral force–resisting systems	B through F
12.5.3	Use 100x + 30y, for ELF and modal analysis or use simultaneous application of load for linear or nonlinear response history procedure	Nonparallel systems irregularity		C through F
12.3.3.2	Maximum height limit 30 ft (9m) or two stories, unless the weak story is capable of resisting a seismic force = Ω_o times the design force		Discontinuity in lateral strength (extreme weak story)	B and C

Table D. 4:

The compositions of UHPC for class U-B (FHWA, 2018).

Material	Kg/m^3	Percentage By Weight
Pre-Blended, Pre-Bagged Powder	2,086	84.0
Liquid Admixtures	28	1.1
Short, Steel Fibers	52	2.1
Long, Steel Fibers	106	4.3
Water	210	8.5

Table D. 5:

Summarized the plastic hinge length of the UHPC columns.

Story	n	Ren et al. (2020) (m)
Interior column	0.33	0.991
Exterior column	0.24	1.08
Corner column	0.18	1.14

Table D. 6:

Modified flexural stiffness of the NSC columns.

Interior column					
Story	**Axial force (kN)**	**Axial force/$A_g f_c'$**	**Modifier**	**EI_e (N.m^2)**	**No. column**
1st floor	1977	0.33	0.53	6.36E+07	9
2nd floor	1644	0.27	0.47	5.64E+07	9
3rd floor	1313	0.22	0.42	5.04E+07	9
4th floor	984	0.16	0.36	4.32E+07	9
5th floor	657	0.11	0.31	3.72E+07	9
6th floor	332	0.06	0.3	3.60E+07	9
Exterior column					
Story	**Axial force (kN)**	**Axial force/$A_g f_c'$**	**Modifier**	**EI_e (N.m^2)**	**No. column**
1st floor	1444	0.24	0.44	5.28E+07	12
2nd floor	1167	0.19	0.39	4.68E+07	12
3rd floor	922	0.15	0.35	4.20E+07	12
4th floor	674	0.11	0.31	3.72E+07	12
5th floor	423	0.07	0.3	3.60E+07	12
6th floor	169	0.03	0.3	3.60E+07	12
Corner column					
Story	**Axial force (kN)**	**Axial force/$A_g f_c'$**	**Modifier**	**EI_e (N.m^2)**	**No. column**
1st floor	1060	0.18	0.38	4.56E+07	4
2nd floor	920	0.15	0.35	4.20E+07	4
3rd floor	737	0.12	0.32	3.84E+07	4
4th floor	542	0.09	0.3	3.60E+07	4
5th floor	340	0.06	0.3	3.60E+07	4
6th floor	132	0.02	0.3	3.60E+07	4

Table D. 7:

Manual calculation for the stiffness of the column at all stories.

Story	H_e (m)	$L_{b,1}$ (m)	$L_{b,2}$ (m)	$I_{e,b1}$ (m^3)	$I_{e,b2}$ (m^3)	I_{ec} (m^3)	α_0	EI_e (N.m2)	No. column	K (kN/m)
Interior column										
1st floor	4.4	2.25	2.25	9.33E-04	9.33E-4	2.76E-3	5.03	6.36E+7	9	33,790
2nd floor	3.1	2.25	2.25	9.33E-04	9.33E-4	2.45E-3	4.5	5.64E+7	9	76,120
3rd floor	3.1	2.25	2.25	9.33E-04	9.33E-4	2.19E-3	4.8	5.04E+7	9	72,890
4th floor	3.1	2.25	2.25	9.33E-04	9.33E-4	1.88E-3	5.2	4.32E+7	9	68,346
5th floor	3.1	2.25	2.25	9.33E-04	9.33E-4	1.61E-3	5.7	3.72E+7	9	63,851
6th floor	3.1	2.25	2.25	9.33E-04	9.33E-4	1.56E-3	5.8	3.60E+7	9	62,859
Exterior column										
1st floor	3.1	2.25	2.25	9.33E-04	9.33E-4	2.29E-3	5.58	5.28E+7	12	41,496
2nd floor	3.1	2.25	2.25	9.33E-04	9.33E-4	2.03E-3	5.0	4.68E+7	12	94,293
3rd floor	3.1	2.25	2.25	9.33E-04	9.33E-4	1.82E-3	5.3	4.20E+7	12	90,005
4th floor	3.1	2.25	2.25	9.33E-04	9.33E-4	1.61E-3	5.7	3.72E+7	12	85,135
5th floor	3.1	2.25	2.25	9.33E-04	9.33E-4	1.56E-3	5.8	3.60E+7	12	83,812
6th floor	3.1	2.25	2.25	9.33E-04	9.33E-4	1.56E-3	5.8	3.60E+7	12	83,812
Corner column										
1st floor	3.1	2.25	2.25	9.33E-4	0	1.98E-3	4.0	4.56E+7	4	8,599
2nd floor	3.1	2.25	2.25	9.33E-4	0	1.82E-3	3.4	4.20E+7	4	19,273
3rd floor	3.1	2.25	2.25	9.33E-4	0	1.67E-3	3.6	3.84E+7	4	18,772
4th floor	3.1	2.25	2.25	9.33E-4	0	1.56E-3	3.8	3.60E+7	4	18,400
5th floor	3.1	2.25	2.25	9.33E-4	0	1.56E-3	3.8	3.60E+7	4	18,400
6th floor	3.1	2.25	2.25	9.33E-4	0	1.56E-3	3.8	3.60E+7	4	18,400

Table D. 8:

Manual calculation for the stories stiffness.

Story	Interior column	Exterior column (kN/m)	Corner Column (kN/m)	Total story stiffness (kN/m)
1st floor	33,790	41,496	8,599	83,885
2nd floor	76,120	94,293	19,273	189,686
3rd floor	72,890	90,005	18,772	181,667
4th floor	68,346	85,135	18,400	171,881
5th floor	63,851	83,812	18,400	166,063
6th floor	62,859	83,812	18,400	165,071

Table D. 9:

SAP2000 results for the stories stiffness.

Story	Load (kN)	Displacement (m)	Stiffness (kN/m)
1st floor	32400	0.29795	108,743
2nd floor	32400	0.17737	182,669
3rd floor	32400	0.19573	165,534
4th floor	32400	0.21365	151,650
5th floor	32400	0.22603	143,344
6th floor	32400	0.23609	137,236

Table D. 10:

SAP2000 results vs manual calculation for the stories stiffness.

Story	SAP2000 (kN/m)	Manually (kN/m)	Error
1st floor	108,743	83,885	29.6%
2nd floor	182,669	189,686	3.7%
1st floor+2nd floor	291,412	273,571	6.5%
3rd floor	165,534	181,667	8.9%
4th floor	151,650	171,881	11.8%
3rd floor+4th floor	317,184	353,548	10.3%
5th floor	143,344	166,063	13.7%
6th floor	137,236	165,071	16.9%
5th floor+6th floor	280,580	331,134	15.3%

Table D. 11:

Manual story lateral strength calculations.

Story	Column location	P_u (kN)	M_a and M_b (kN.m)	l_u (m)	$(M_a + M_b)/L_u$ (kN)	$\emptyset V_n$ (kN)	V_e (kN)	No. column	Column Strength (kN)	Story Strength (kN)
1st story	Interior	2080	512	4.4	233	634	233	9	2,097	5,745
	Exterior	1710	508		231	634	231	12	2,772	
	Corner	1203	482		219	634	210	4	876	
2nd story	Interior	1727	509	3.5	291	634	291	9	2,619	7,059
	Exterior	1390	493		282	634	282	12	3,384	
	Corner	973	462		264	634	275	4	1,056	

Table D. 12:

Comparison between manual calculation and SAP2000 for the first and second stories columns probable moment.

Story	Column location	Manually (kN.m)	SAP2000 (kN/m)	Error
1st story	Interior	512	515	0.6%
	Exterior	508	487	4.3%
	Corner	482	474	2.5%
2nd story	Interior	509	520	2.1%
	Exterior	493	461	6.9%
	Corner	462	414	10.4%

Table D. 13:

SAP2000 results vs manual calculation for the first and second floors' lateral strength.

Story	SAP2000 (kN/m)	Manually (kN/m)	Error
1st floor	5,750	5,745	0.1%
2nd floor	7,640	7,059	8.23%

Table D. 14:

K calculation for 1st story columns.

Story	Column location	B (mm)	ρ_s	$N/f_c{}'A_g$	K
	Interior	500	0.01286	0.33	1.94
1st story	Exterior	500	0.01286	0.24	2.01
	Corner	500	0.01286	0.18	2.05

Table D. 15:

UHPC column adjusted cracking analysis modifiers are by $\alpha_{UHPC}/\alpha_{NSC}$ in the SAP2000 model.

Story	Column location	No. Column	ρ_s	$N/f_c{}'A_g$	Modifier	$\frac{\alpha_{UHPC}}{\alpha_{NSC}}$	$\frac{\alpha_{UHPC}}{\alpha_{NSC}}$ * Modifier
	Interior	9	0.01286	0.33	0.53	1.14	0.60
1st story	Exterior	12	0.01286	0.24	0.44	1.18	0.52
	Corner	4	0.01286	0.18	0.38	1.20	0.46

Table D. 16:

1st story lateral stiffness by SAP2000 results vs the predicted value depending K on the of the 1st story with the UHPC column.

SAP2000 (kN/m)	Depending on K (kN/m)	Error
218,373	216,399	0.9 %

Table D. 17:

β calculation for 1st story columns.

Story	Column location	No. Column	B (mm)	ρ_s	$N/f_c{}'A_g$	β
	Interior	9	500	0.01286	0.33	2.20
1st story	Exterior	12	500	0.01286	0.24	2.02
	Corner	4	500	0.01286	0.18	1.90

Table D. 18:

1st story lateral strength by SAP2000 results vs the predicted value depending β on the of the 1st story with the UHPC column.

SAP2000 (kN)	Depending on β (kN)	Error
11,095	11,500	3.6 %

Appendix E: Figures

Figure E. 1:

Building Capacity Curve (ATC-40, 1996, Shehadah, 2017).

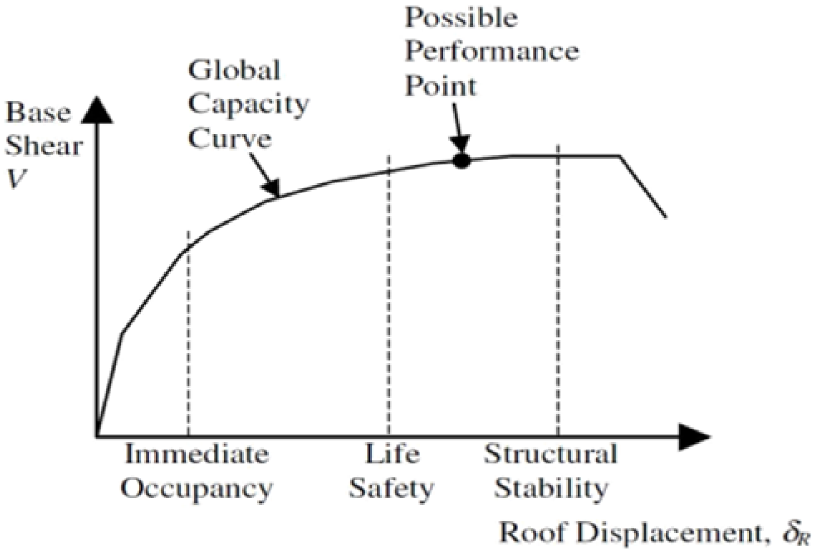

Figure E. 2:

Distribution of total displacement generated by an earthquake in (a) a regular building, and (b) a building with soft story irregularity (Guevara-Perez, 2012).

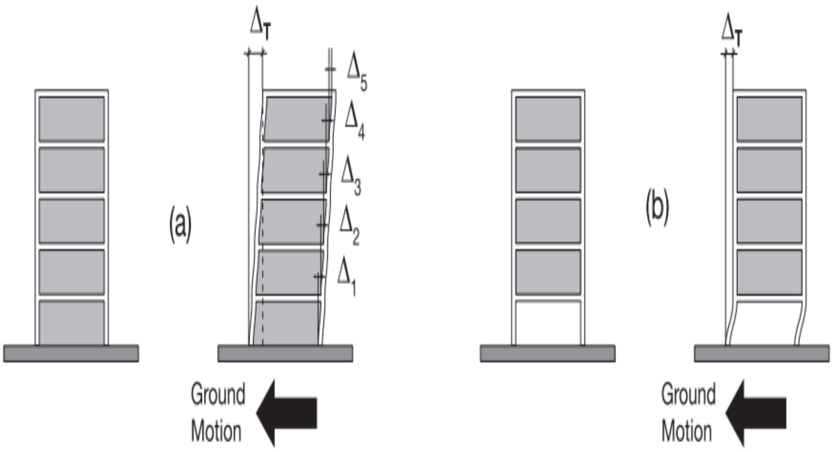

Figure E. 3:

Olive View Hospital building Failure: (A and B) Large inelastic deformation in the column at the base, and (c) The brittle collapse of some columns at the base floor (Chopra, 2012).

(A)

(B)

(C)

Figure E. 4:

Strategies of retrofitting techniques and their divisions (Shehadah, 2017).

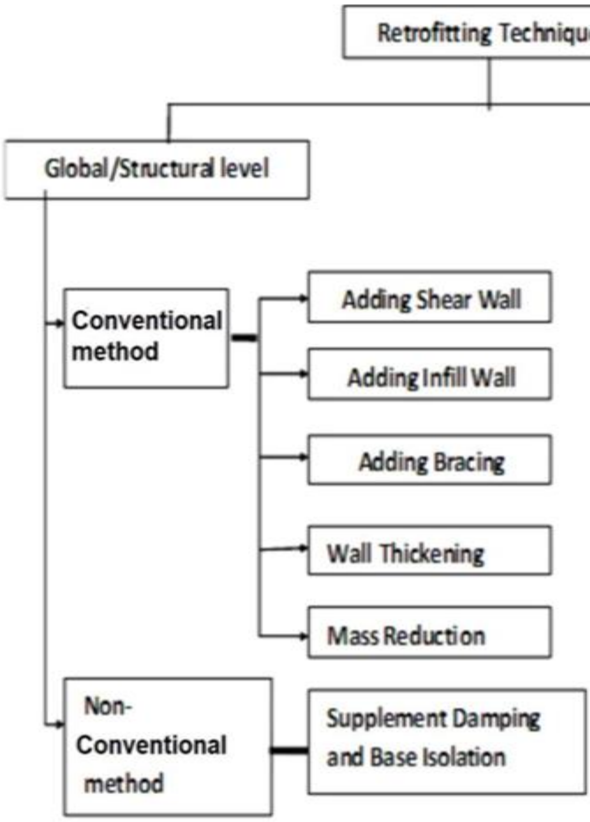

Figure E. 5:

Typical compositions of UHPC for Ductal® and class U-A (FHWA, 2013, FHWA, 2018).

Ductal®			Class U-A		
Material	Kg/m³	Percentage By Weight	Material	Kg/m³	Percentage By Weight
Portland Cement	712	28.5	Cement	788	31.5
Fine Sand	1,020	40.8	Silica Sand	764	30.5
Silica Fume	231	9.3	Ground Quartz	218	8.7
Ground Quartz	211	8.4	Silica Fume	307	12.3
Accelerator	30	1.2	Superplasticizer	14	0.5
Steel Fibers	156	6.2	Water	165	6.6
Water	184	4.4	Steel Fibers	247	9.9
Water-Reducing Admixture	30.7	1.2			

Figure E. 6:

Properties of microfiber used in UHPC matrix for different materials (From fib, Eide et al., 2012).

type of fibre	unit weight [kg/dm³]	tensile strength [MPa]	modulus of elasticity [GPa]	strain at fracture [‰]	alkali resis-tance [-]	max. tempera-ture [°C]	diameter [μm]
steel	7.8	500-2600	200	5-35	high	1000	100-500
alkali-resistant glass	2.6	2000-4000	75	20-35	med./low	800	12-20
carbon	1.75-1.91	2000-4000	200-450	4-15	high	3000	15
polypro-pylene	0.98	450-700	7.5-12	60-90	high	150	50
polyvinyl alcohol	1.3	800-900	26-30	50-75	high	240	13-300
polyester	1.4	800-1100	10-19	8-20	med.	240	10-50
aramide	1.42	700-3600	70-130	21-40	med.	600	12

Figure E. 7:

How fiber orientation influences flexural tensile strength and ductility (Budelmann et al., 2010, Fehling et al., 2014).

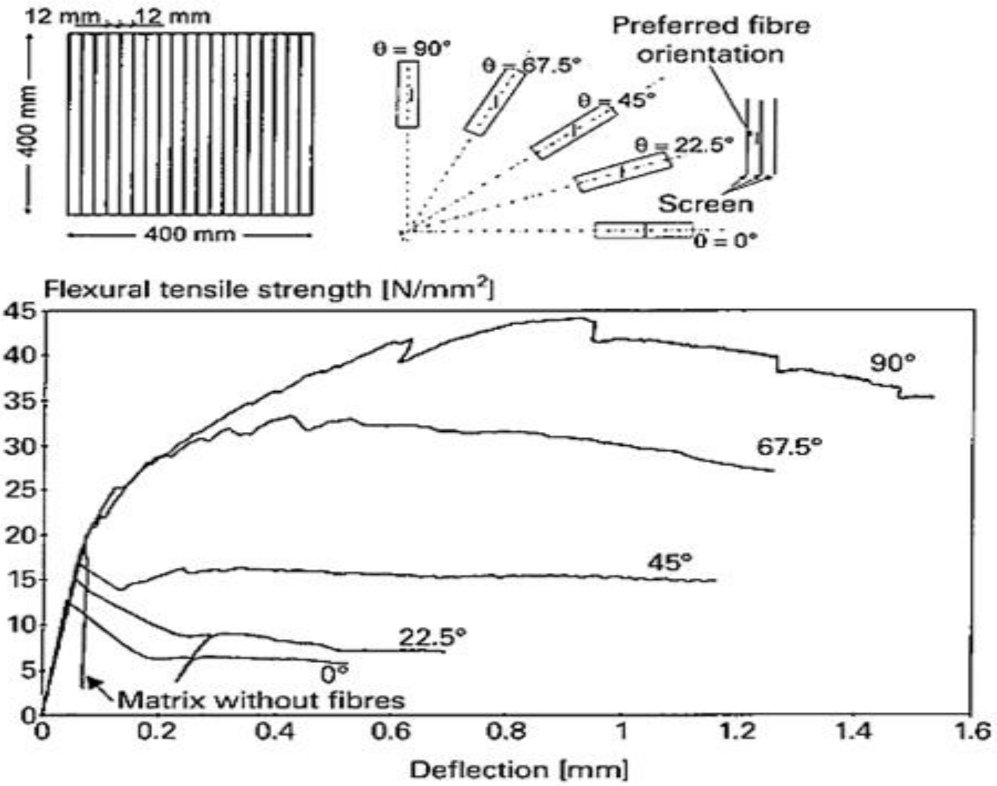

Figure E. 8:

Schematics of the mechanism in which fiber reinforcement works (ACI 544.4R-18, 2018).

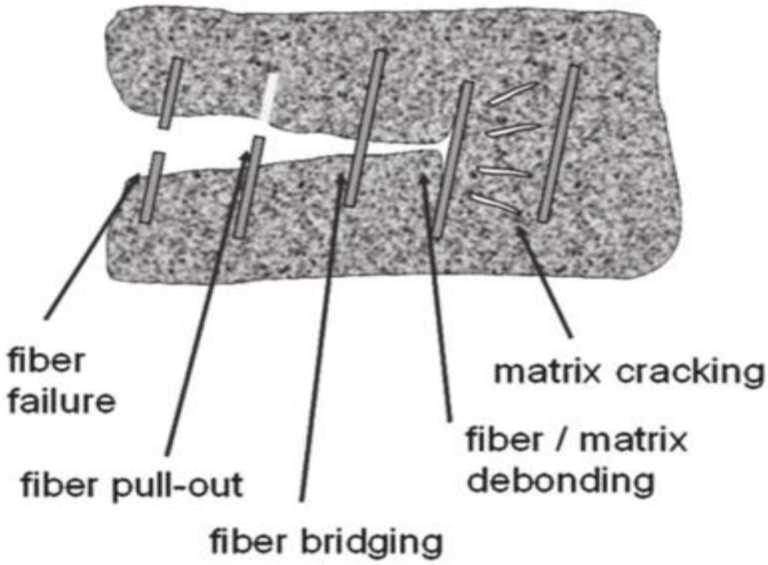

Figure E. 9:

Compositions and properties of UHPC for some commercial products (Eide et al., 2012).

	Ductal®		BSI®		CRC®		$\text{CEMTEC}_{\text{multiscale}}$®		BCV®	
	Type	kg/m^3	Type	kg/m^3	Type	kg/m^3	Type	kg/m^3	Type	kg/m^3
Cement	Portl.	746	-	1114			CEM I 52.5	1050		↑
Silica fume	-	242	-	169	Binder	930	-	275		2115
Quartz flour	-	224	-	-			-	-		premix
Sand (mm)	0,1-0,6	1066	0-6	1072	0-5	1325	<0,5	730	2-3	⊥
Water	W/C	0,19	W/C	0,19	W/B	0,16	W/C	0,181	W/C	0,25
Admixture	Chryso	9	SIKA	40	-	-	Chryso	35	-	21.5
Fiber	13/0.2	161	20/0.3	234	12/0.4	150-300	10/0.2	470	$20_{2/3}13_{1/3}$	156
SlumpFlow(mm)		700		640		-		-		750
$f_{ct,28}$ (MPa)		8		8.8		-		-		8
$f_{cm,7}$ (Mpa)	20°	101	20°	165		-	20°	-	20°	98
$f_{cm,28}$ (Mpa)	20°/90°	124/198	20°	199	20°/90°	150/400	20°	168	20°/90°	130-150

Figure E. 10:

Comparison between the Tensile Behaviors for UHPC Classes with 2% Volumetric Fracture of Fiber (FHWA, 208).

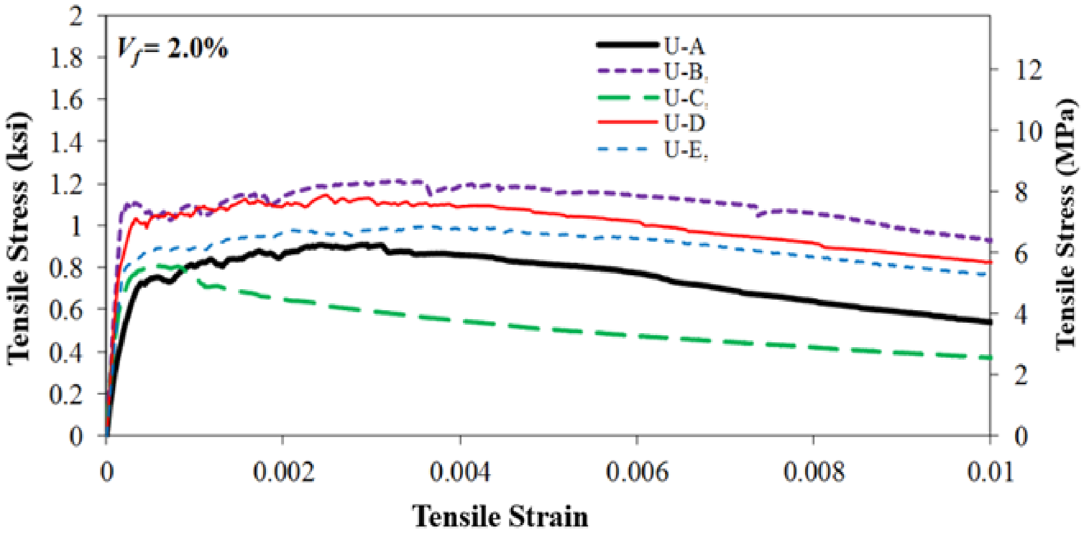

Figure E. 11:

Stress-strain for UHPC vs NSC (Caldwell, 2011).

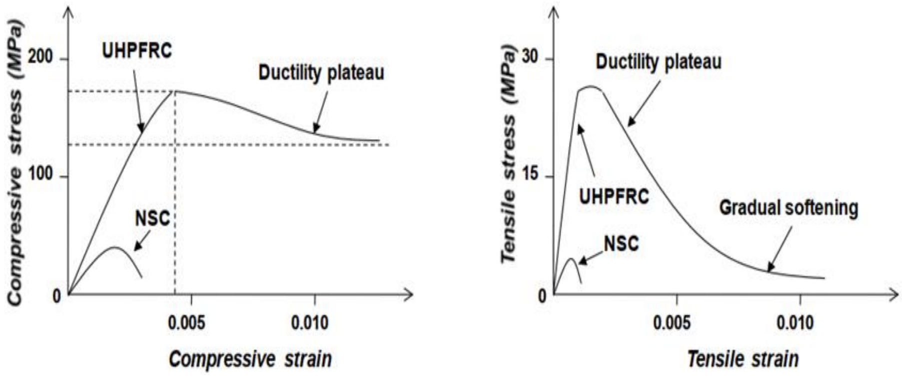

Figure E. 12:

Compressive stress-strain diagram of UHPC with fibers (Eide et al.,2012, ChunPing et al., 2015).

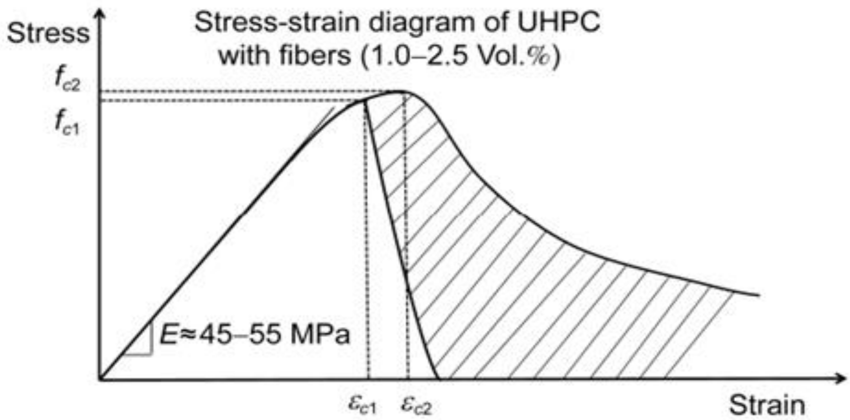

Figure E. 13:

Idealized uniaxial tensile response of UHPC (FHWA, 2013).

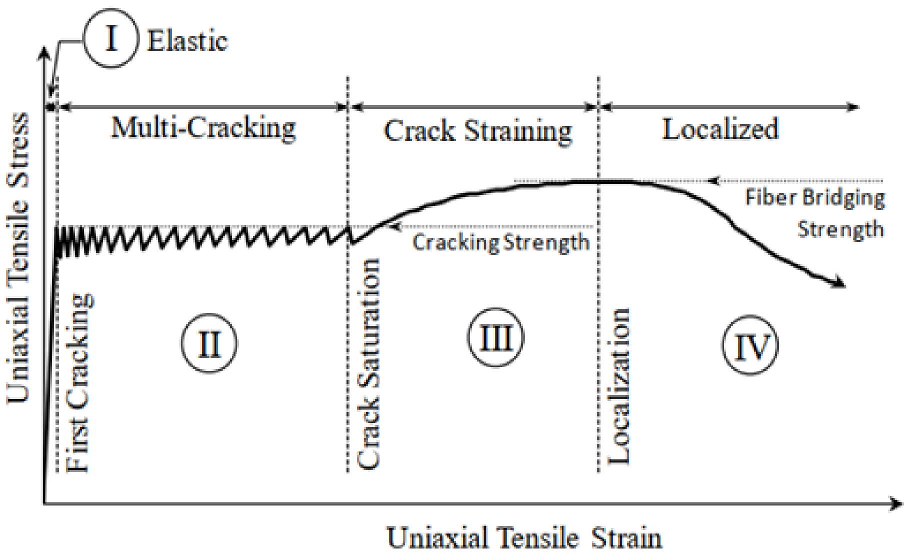

Figure E. 14:

Tensile stress-strain of U-B with 2 percent fiber volume (FHWA, 2018).

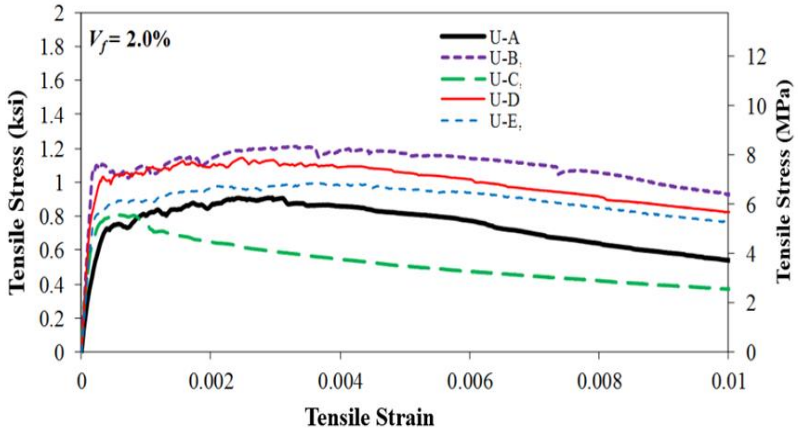

Figure E. 15:

Values of Poisson's ratio (FHWA, 2013).

Poisson's Ratio	Reference (First Author)
0.2	Simon
0.16	Joh
0.21	Ahlborn
0.19	Bonneau
0.18	Graybeal
0.18	Ozyildirim

Figure E. 16:

Flexural strength of singly reinforced concrete section (Park and Paulay, 1975).

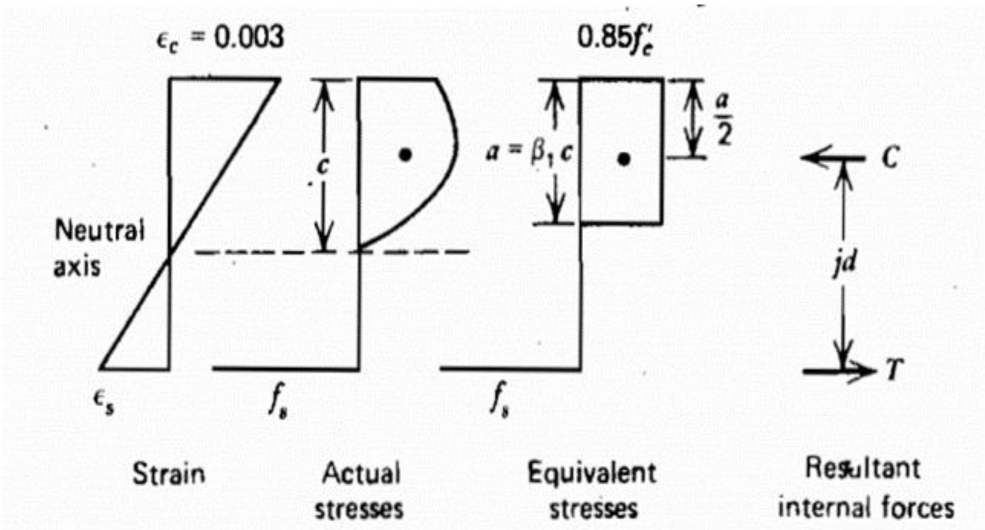

Figure E. 17:

Bending constitutive relationships at ULS for (a) reinforced UHPC, and (b) reinforced NSC (ACI 239R-18, 2018).

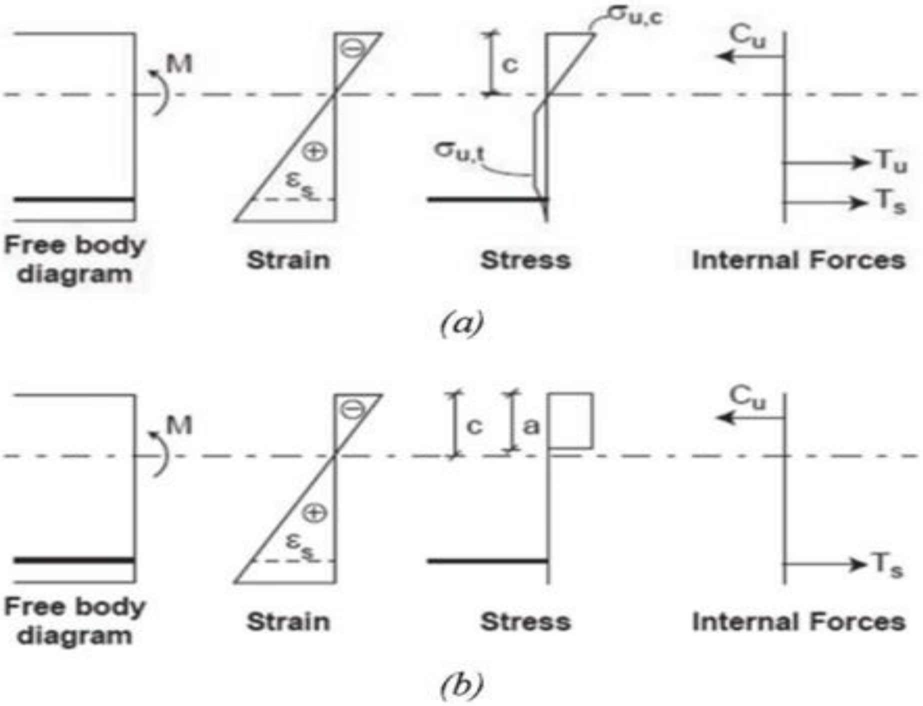

Figure E. 18:

The stress distribution for the reinforcement UHPC beam with different methods (Shafieifar et al., 2018).

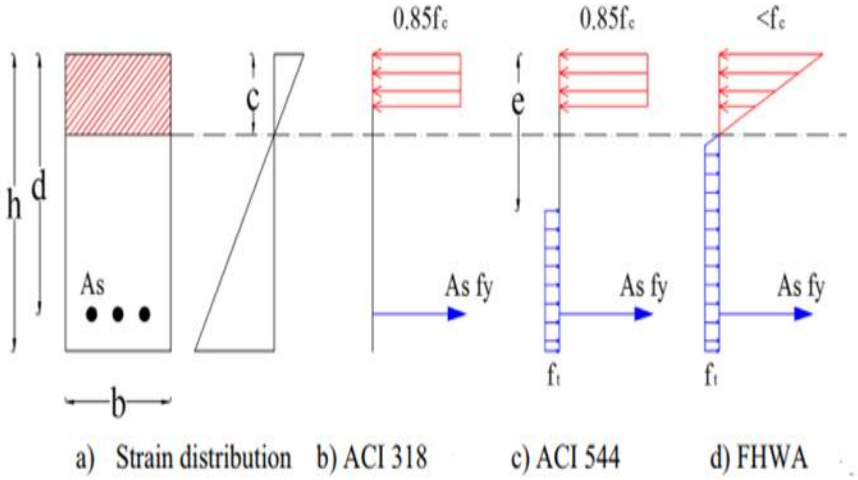

Figure E. 19:

The geometry of the tested beam (Fehling et al., 2014).

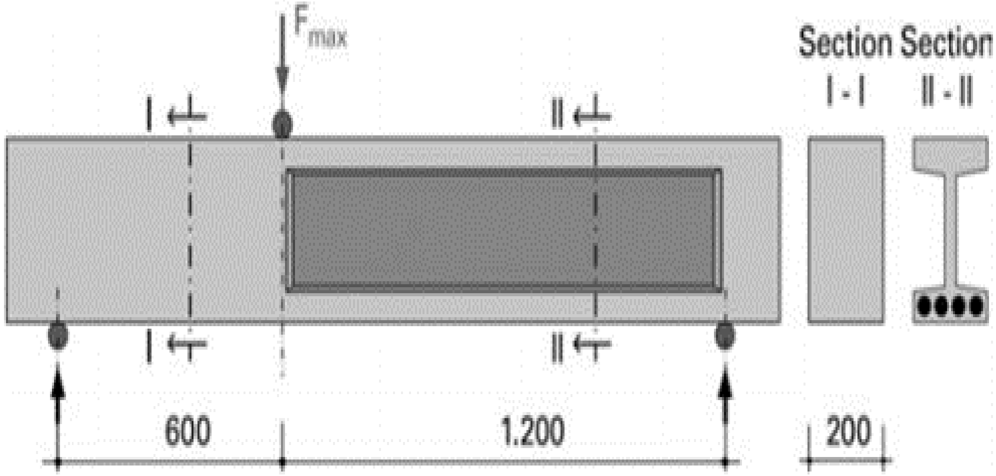

Figure E. 20:

Crack patterns of UHPC beams with (from top to bottom) 0, 0.8, and 1.6% by volume fiber reinforcement (Fehling et al., 2014).

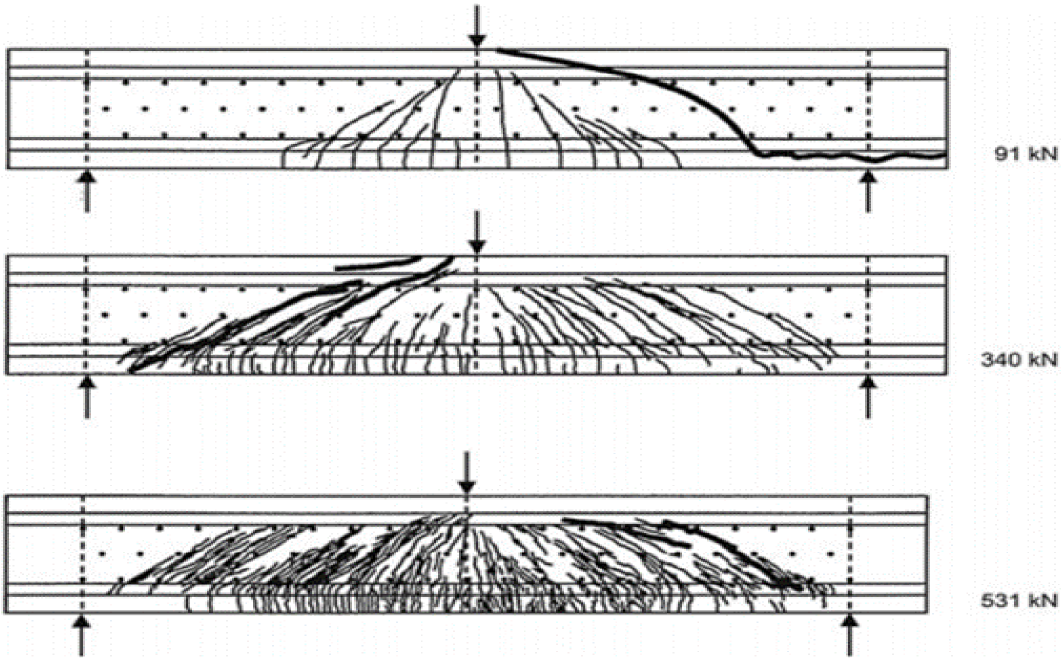

Figure E. 21:

Existing shear strength models for steel fiber-reinforced concrete (Lim et al., 2016).

Authors	Shear strength models
Sharma (1986)	$v_u = kf_t'(d/a)^{0.25}$ where $k = 2/3$; a/d is the shear span-to-depth ratio; $f_t' = 0.17\sqrt{f_{cf}}$, if the tensile strength is unknown, and f_{cf} is the concrete cylinder compressive strength
Narayanan et al. (1987)	$v_u = e\left[0.24f_{spfc} + 80\rho\frac{d}{a}\right] + v_b$ where f_{spfc} is the computed split-cylinder strength of fiber concrete (= $f_{cuf}/(20 - \sqrt{F}) + 0.7 + 1.0\sqrt{F}$); ρ is the longitudinal reinforcement ratio; F is the fiber factor (=$(L_f/D_f)V_fd_f$; e is the arch action factor, 1.0 for $a/d > 2.8$ and $2.8d/a$ for $a/d \leq 2.8$; f_{cuf} is the cube strength of fiber concrete; V_f is the fiber volume fraction; d_f is a bond factor, 0.5 for round fibers, 0.75 for crimped fibers, and 1.0 for indented fibers; v_b is equal to the equations of $0.41\tau F$, and τ is the average fiber matrix interfacial bond stress, taken as 4.15 MPa
Ashour et al. (1992)	For $a/d \geq 2.5$ $v_u = \left(2.11\sqrt[3]{f_{cf}} + 7F\right)\left(\rho\frac{d}{a}\right)^{1/3}$
Kwak et al. (2002)	$v_u = 3.7ef_{spfc}^{2/3}\left(\rho\frac{d}{a}\right)^{1/3} + 0.8v_b$ where e is the arch action factor, 1 for $a/d > 3.4$, and $3.4d/a$ for $a/d \leq 3.4$

Figure E. 22:

Comparison of damages of RC (left) and UHPC (right) column at 5.25% drift (Chao et al., 2016).

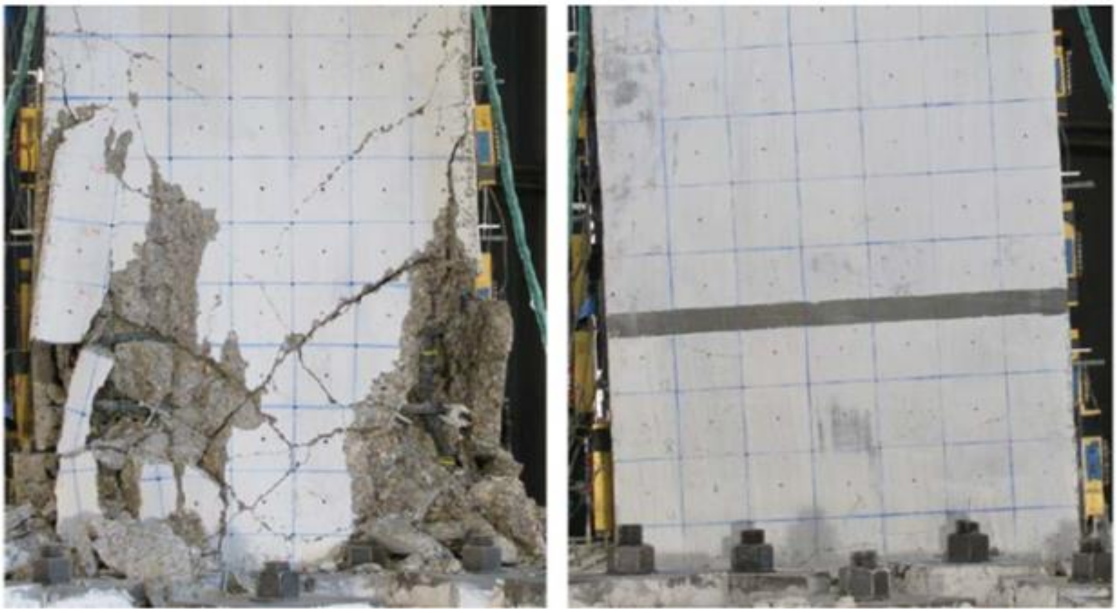

Figure E. 23:

Mander unconfined concrete stress-strain curve (Mander, 1988b).

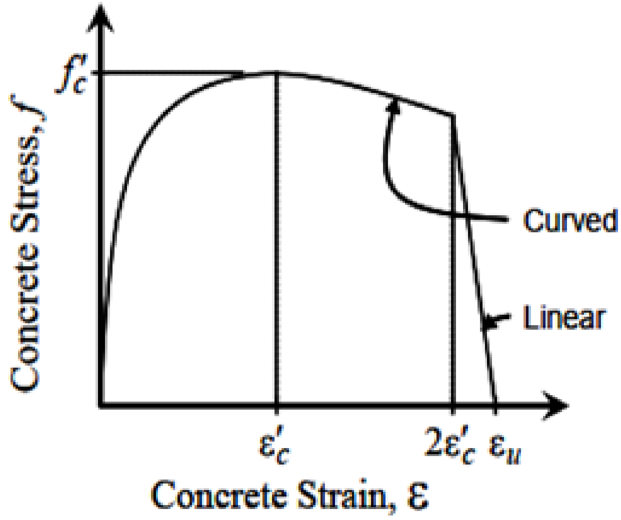

Figure E. 24:

Adopted Mander unconfined concrete stress-strain curve.

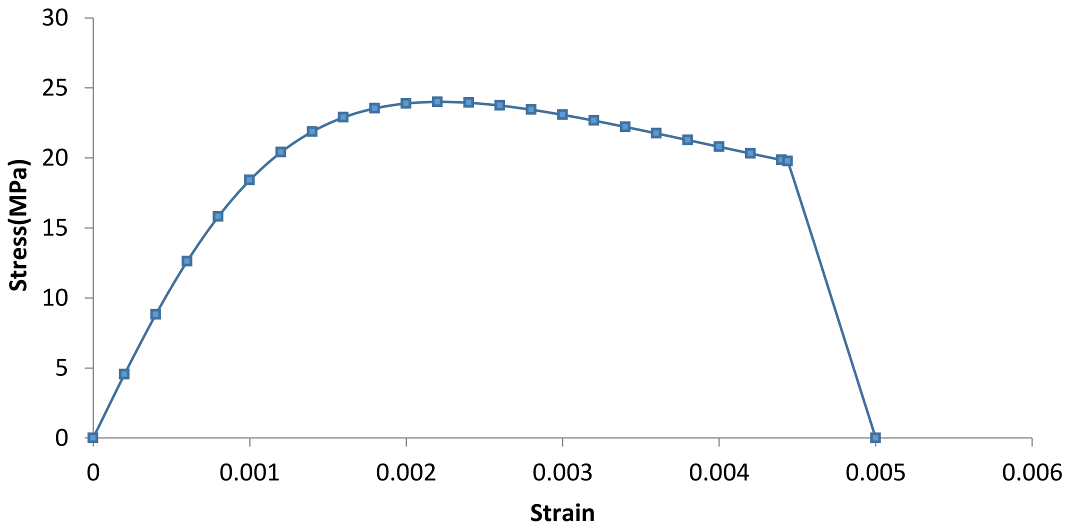

Figure E. 25:

Stress-strain response of UHPC compared with the linear-elastic behavior (FHWA, 2018).

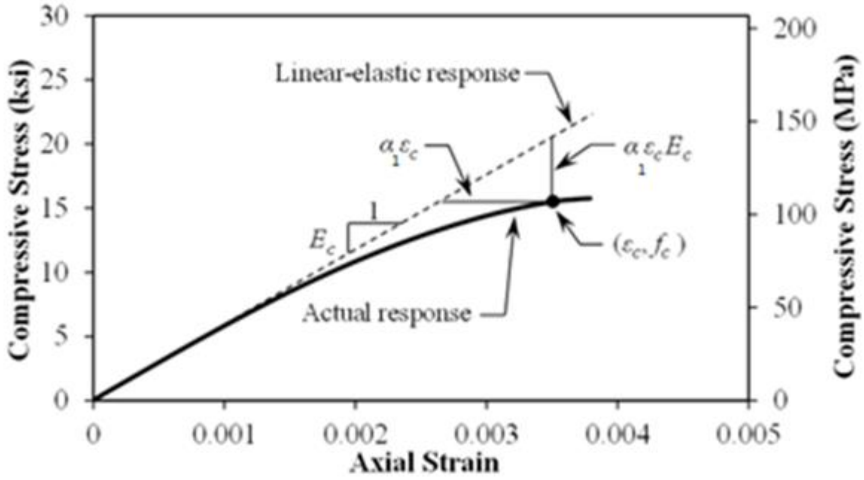

Figure E. 26:

Best-fit curve parameters from linearity analysis (FHWA, 2018).

Material	Fit Parameters	
	A	*b*
U-A	0.106	2.683
U-B	0.106	2.606
U-C	0.095	2.792
U-D	0.108	3.168
U-E	0.115	2.764
Average	0.106	2.754

Figure E. 27:

Adopted compressive stress-strain curve for UHPC.

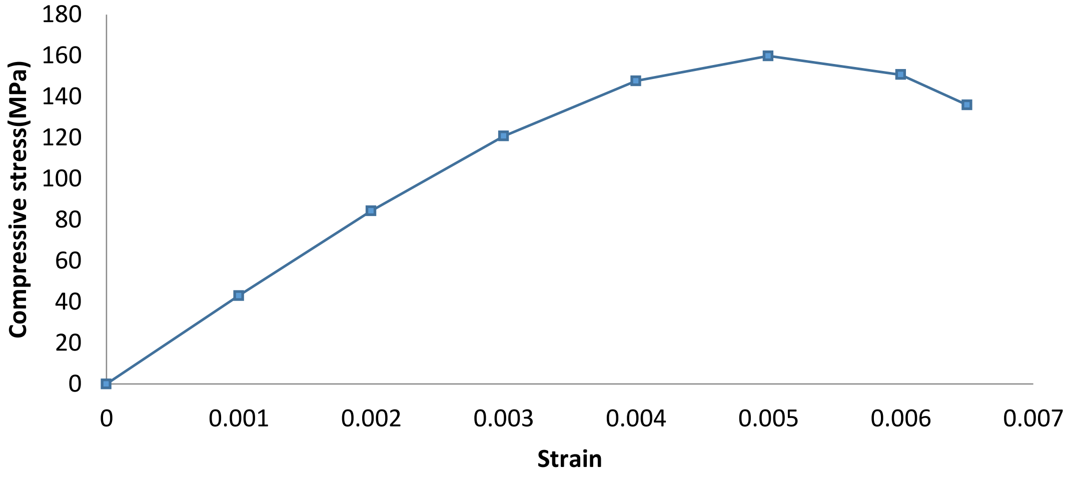

Figure E. 28:

The adopted tensile stress-strain curve for UHPC type U-B with a 2% fiber ratio by volume.

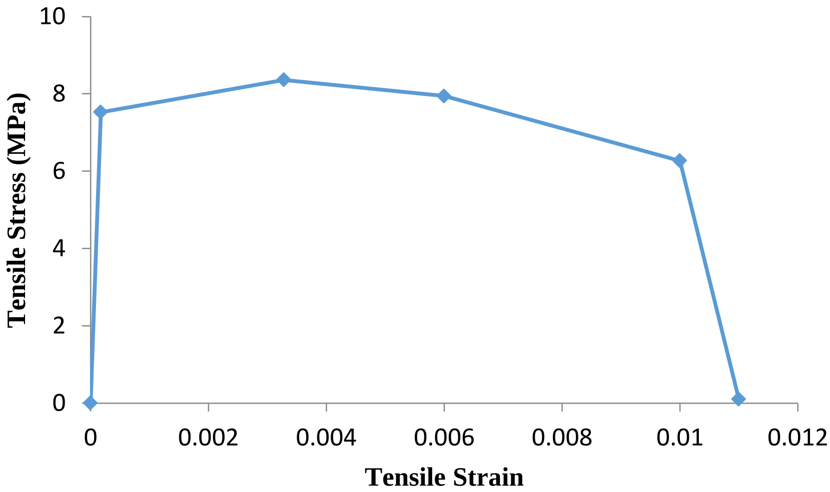

Figure E. 29:

Strain distribution in the discretized cross-section (Chadwell et al., 2004).

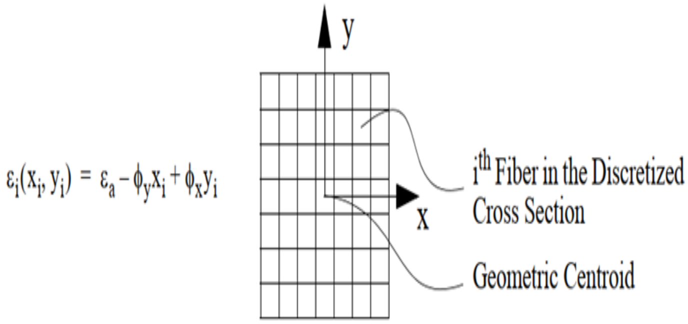

Figure E. 30:

An example of load assigned to a section in XTRACT.

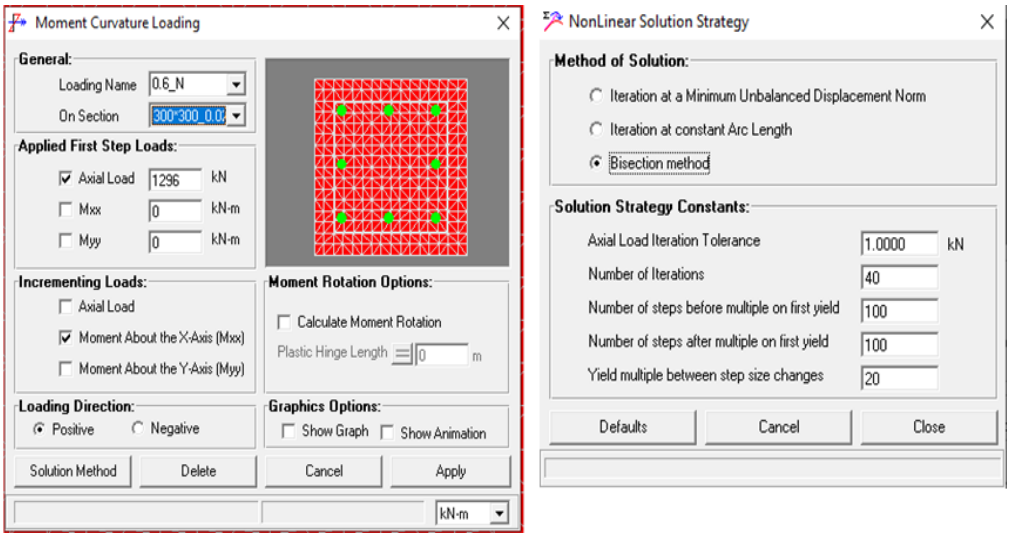

Figure E. 31:

An example of the M-K curve for the both NSC and UHPC section obtained by XTRACT software at different axial load levels of the NSC column.

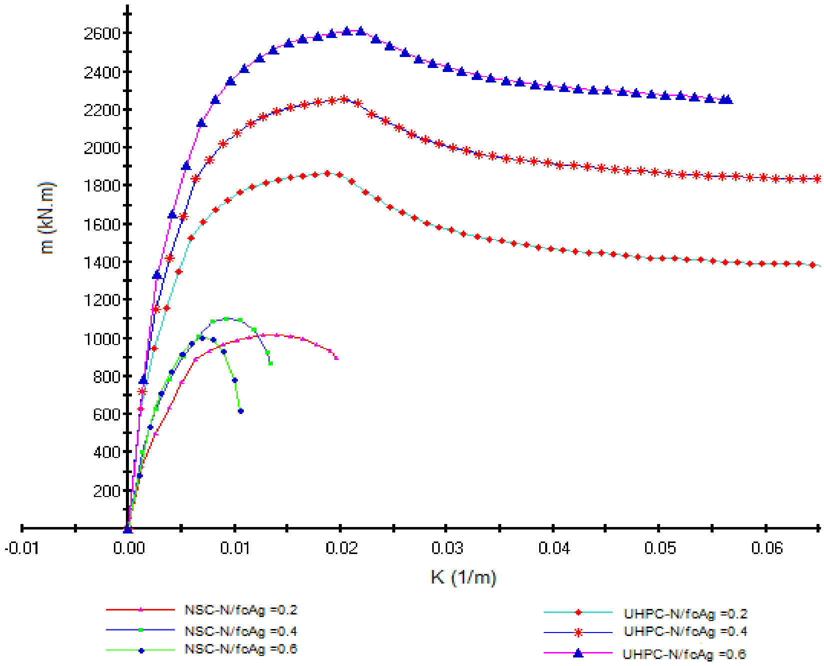

Figure E. 32:

The NSC beam section used for M-K verification.

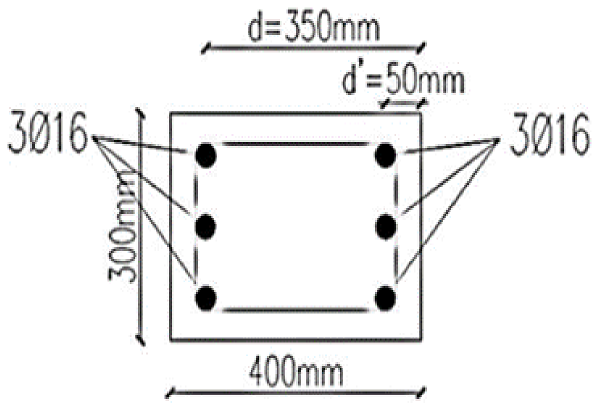

Figure E. 33:

Section strain, stress, and forces at the first yield of steel at the tension side.

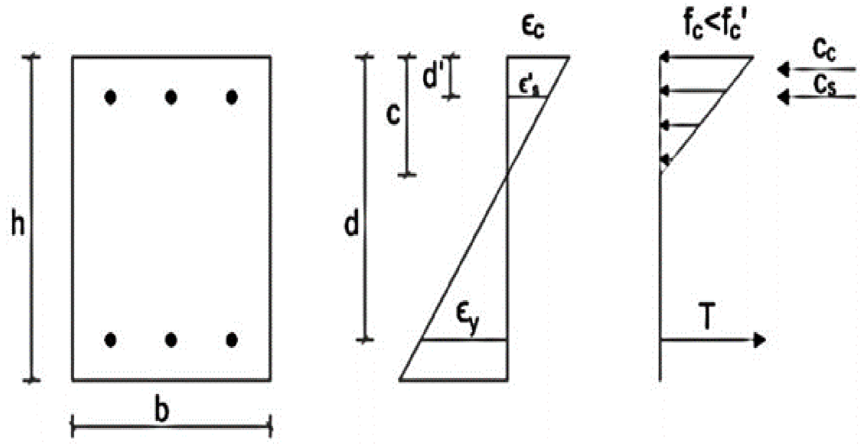

Figure E. 34:

Section strain, stress, and forces at the ultimate strain of concrete at extreme compression fiber (0.003).

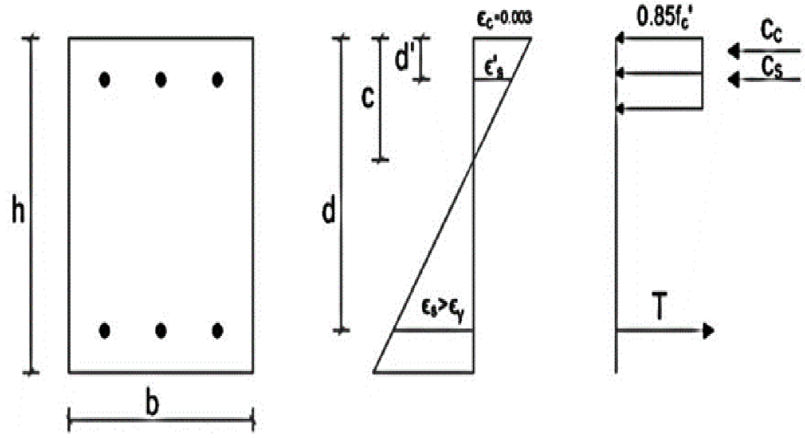

Figure E. 35:

The UHPC material properties of the tested beams (Yang et al., 2010).

Material properties	Batch 1	Batch 2	Batch 3	Batch 4
Compressive strength: MPa	190·9	192·2	196·1	196·7
Tensile strength resulting from inverse analysis: MPa	11·4	11·2	10·8	13·0
Elastic modulus: MPa	46418	46680	45530	46818

Figure E. 36:

The section properties of the tested beams (Yang et al., 2010).

Specimen	R12-1, 2	R13-1, 2
Cross section	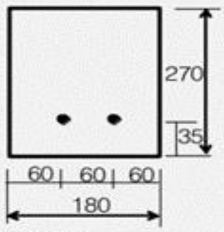	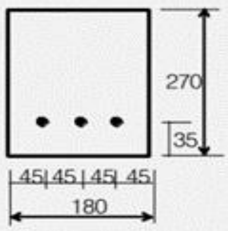
Rebar	2-D13 1 layer	3-D13 1 layer
Rebar area (mm^2)	253.4	380.1
Rebar ratio	0.0060	0.0090
Batch number	1	2

Figure E. 37:

Suggested stress-strain of UHPC for Yang et al. test: a)compressive and b) Tensile for batch 2 (Yang et al., 2012).

(a) (b)

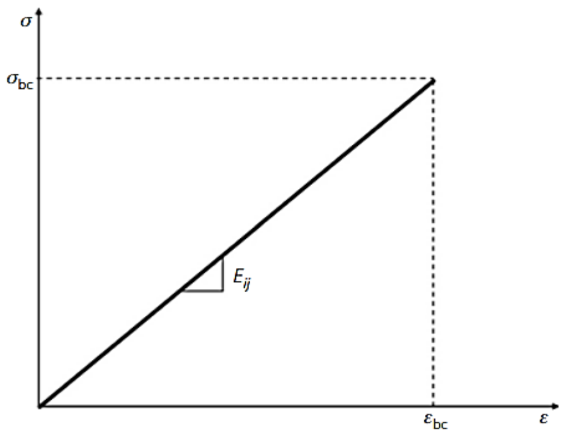

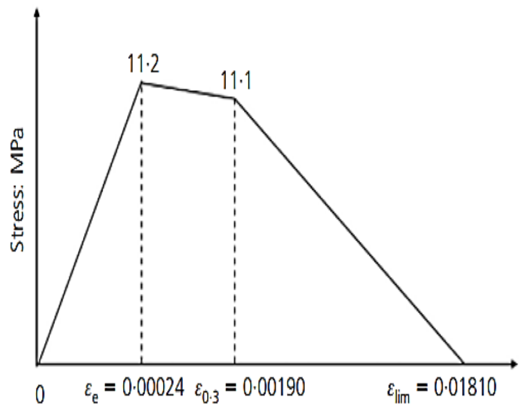

Figure E. 38:

Moment curvature curve (Avşar et al., 2012, Caltrans, 2010).

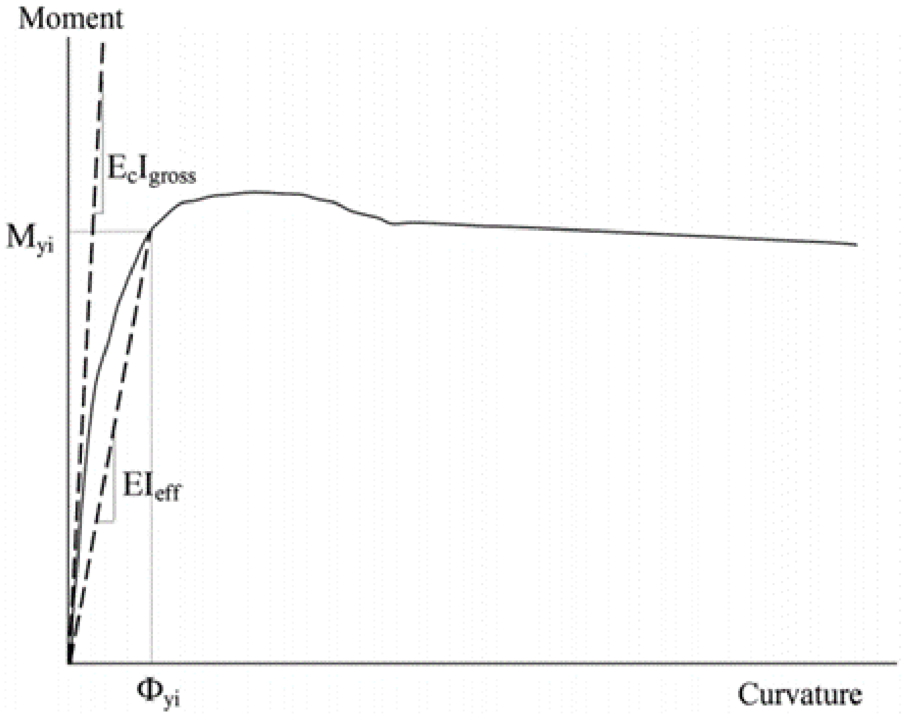

Figure E. 39:

Caltrans chart for determining cracking modifier for rectangular columns at different axial levels (Caltrans, 2010).

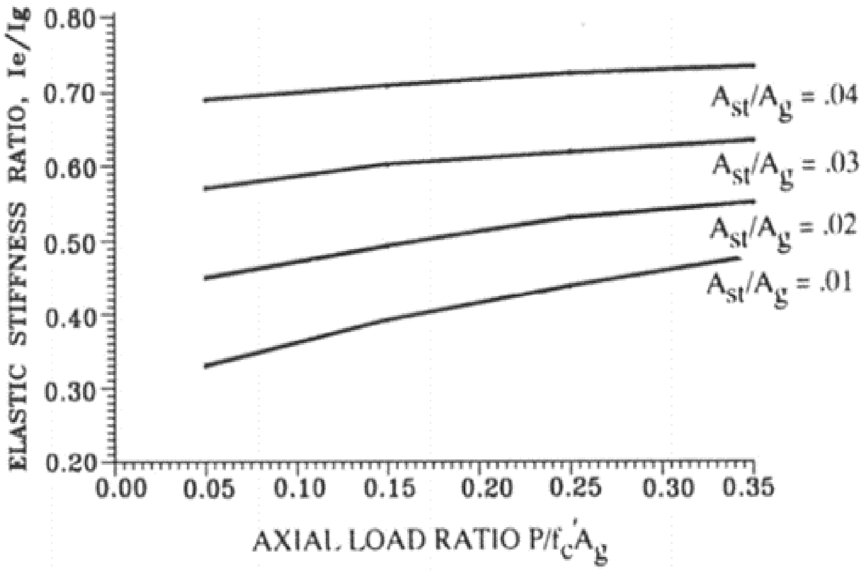

Figure E. 40:

Column base restraint conditions (Moehle, 2015).

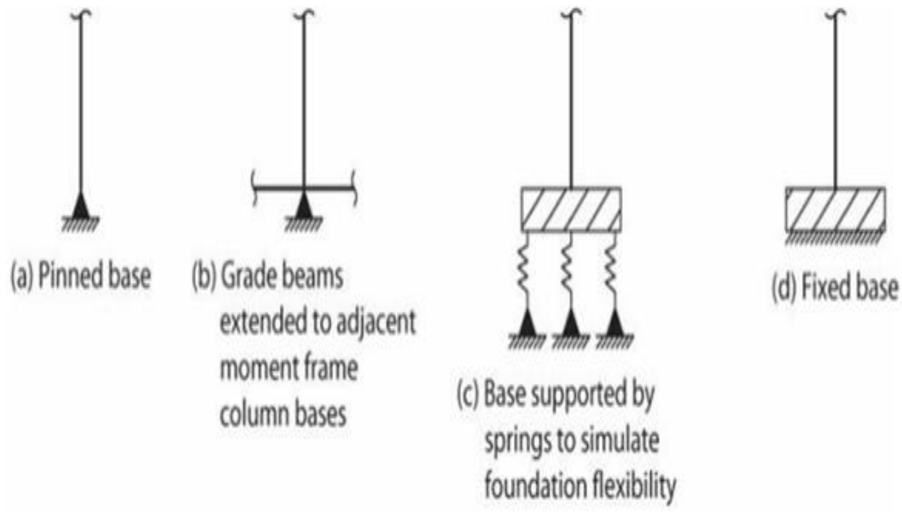

Figure E. 41:

Generalized force-deformation relation for concrete elements or components (ASCE41, 2013).

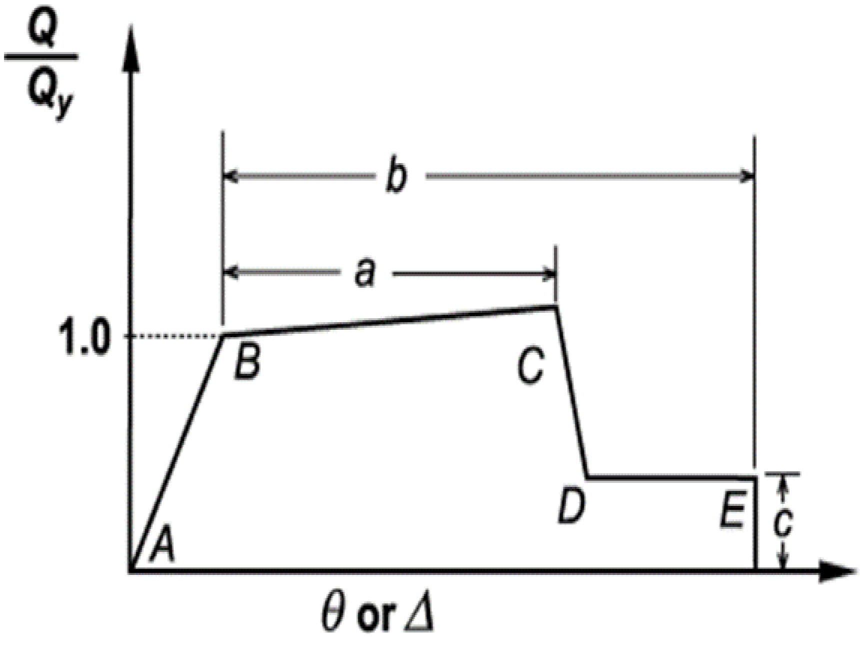

Figure E. 42:

The analyzed cantilever column section.

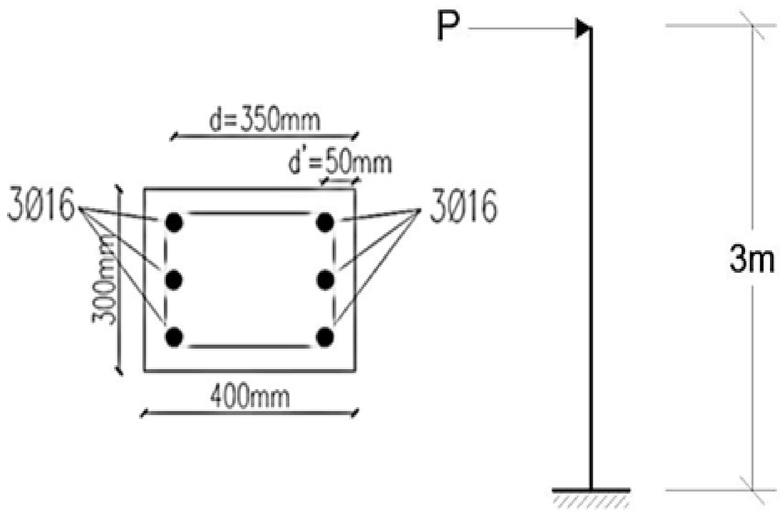

Figure E. 43:

the force deformation for the same cantilever column section with (M3) auto hinge definition based on ASCE41-13 and with fiber hinge.

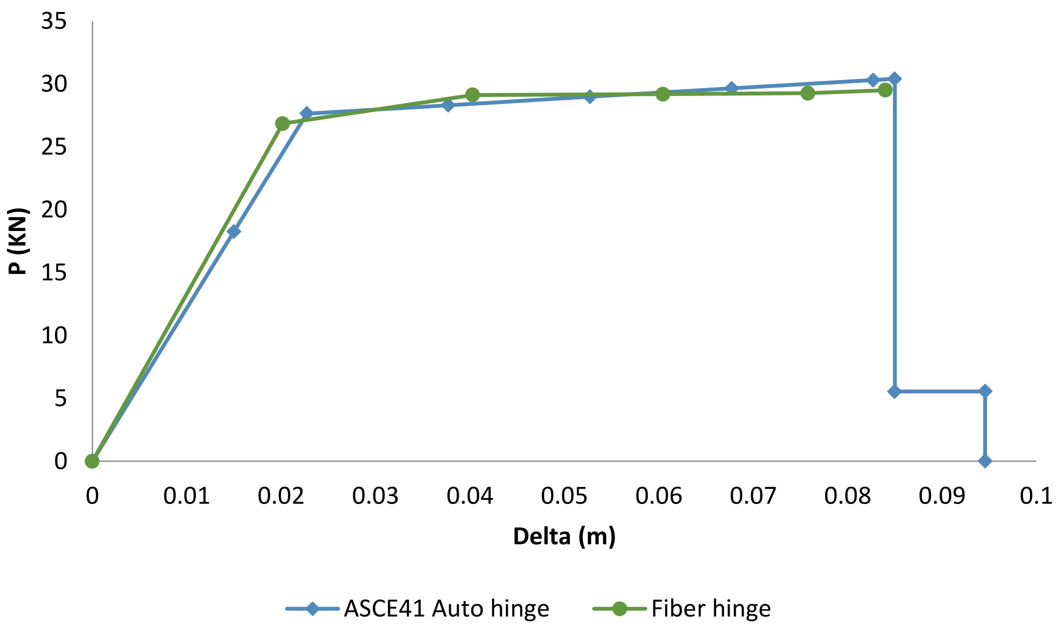

Figure E. 44:

ACI318-19 effective stiffness values (ACI318, 2019).

Component		Axial	Flexural	Shear
Beams	nonprestressed	$1.0E_cA_g$	$0.3E_cI_g$	$0.4E_cA_g$
	prestressed	$1.0E_cA_g$	$1.0E_cI_g$	$0.4E_cA_g$
Columns with compression caused by design gravity loads[2]	$\geq 0.5A_gf_c'$	$1.0E_cA_g$	$0.7E_cI_g$	$0.4E_cA_g$
	$\leq 0.1A_gf_c'$ or with tension	$1.0E_cA_g$ (compression) $1.0E_sA_{st}$ (tension)	$0.3E_cI_g$	$0.4E_cA_g$
Structural walls[3]	in-plane	$1.0E_cA_g$	$0.35E_cI_g$	$0.2E_cA_g$
	out-of-plane	$1.0E_cA_g$	$0.25E_cI_g$	$0.4E_cA_g$
Diaphragms (in-plane only)[4]	nonprestressed	$0.25E_cA_g$	$0.25E_cI_g$	$0.25E_cA_g$
	prestressed	$0.5E_cA_g$	$0.5E_cI_g$	$0.4E_cA_g$
Coupling beams	with or without diagonal reinforcement	$1.0E_cA_g$	$0.07\left(\frac{\ell_n}{h}\right)E_cI_g$ $\leq 0.3E_cI_g$	$0.4E_cA_g$
Mat foundations	in-plane	$0.5E_cA_g$	$0.5E_cI_g$	$0.4E_cA_g$
	out-of-plane[5]		$0.5E_cI_g$	

Figure E. 45:

Cantilever column model for checking auto concrete P-M3 hinge in SAP2000 (Shehadah, 2017).

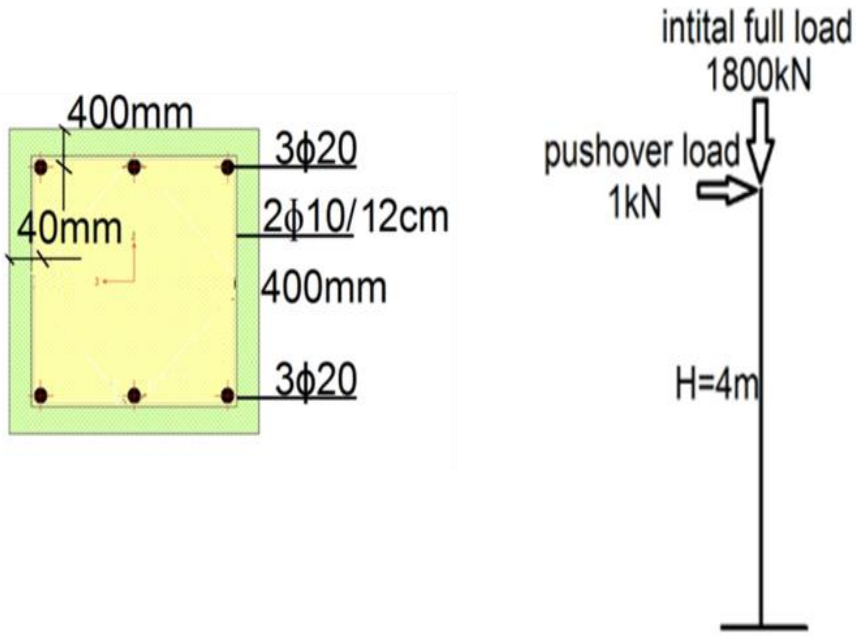

Figure E. 46:

Generalized force-deformation relation for the column with P-M3 hinge obtained by SAP2000 analysis.

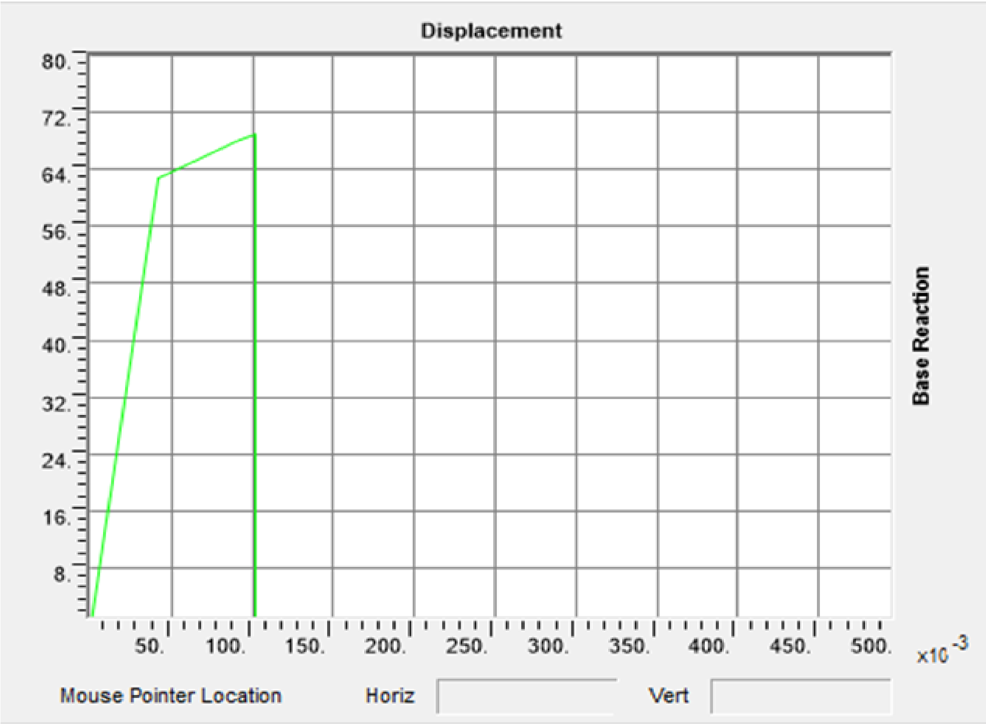

Figure E. 47:

The P-Δ curve results from the SAP2000 and the manual calculation.

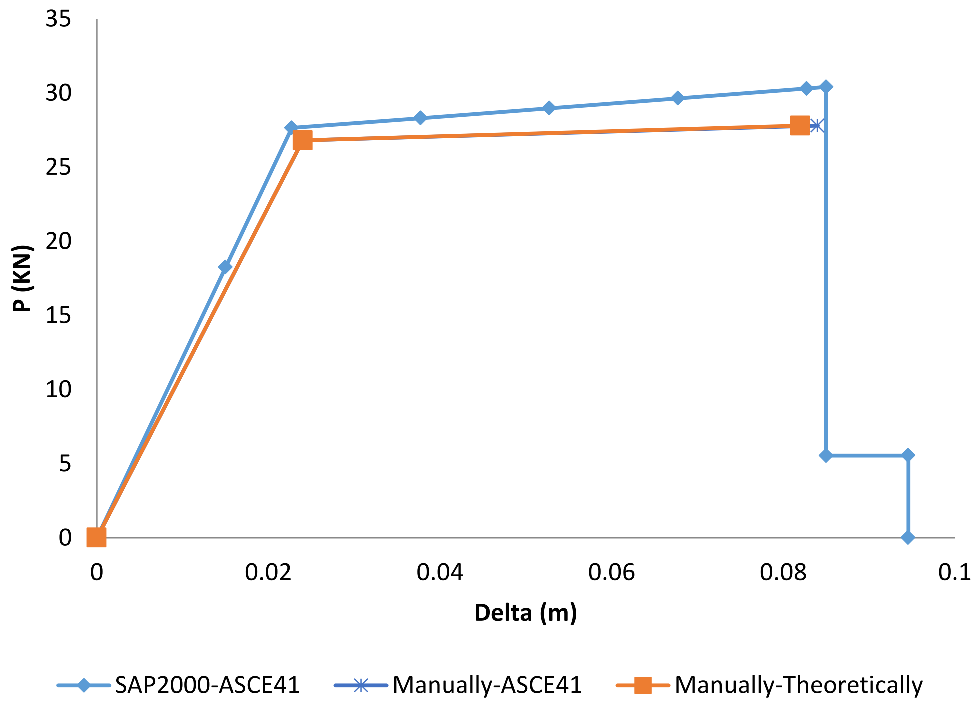

Figure E. 48:

Tested beams geometry (Yang et al., 2010).

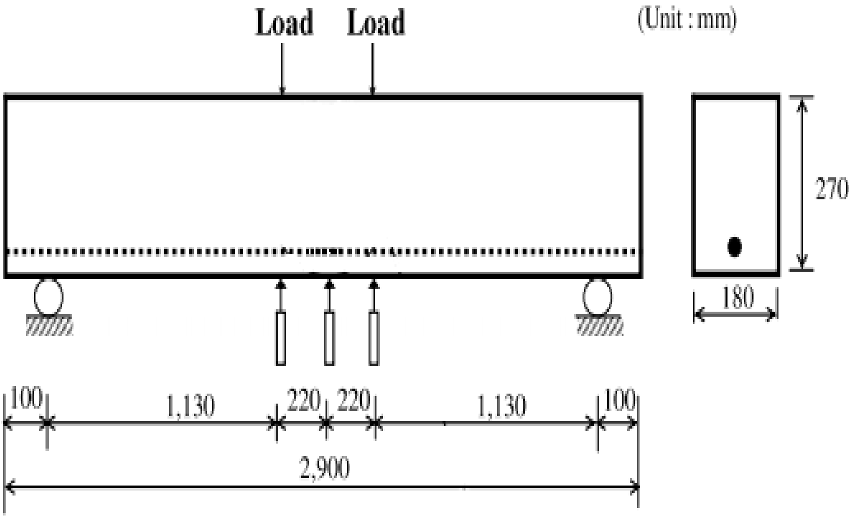

Figure E. 49:

Comparison of moment-curvature curves for experimental results and SAP2000 For beam FR12−2.

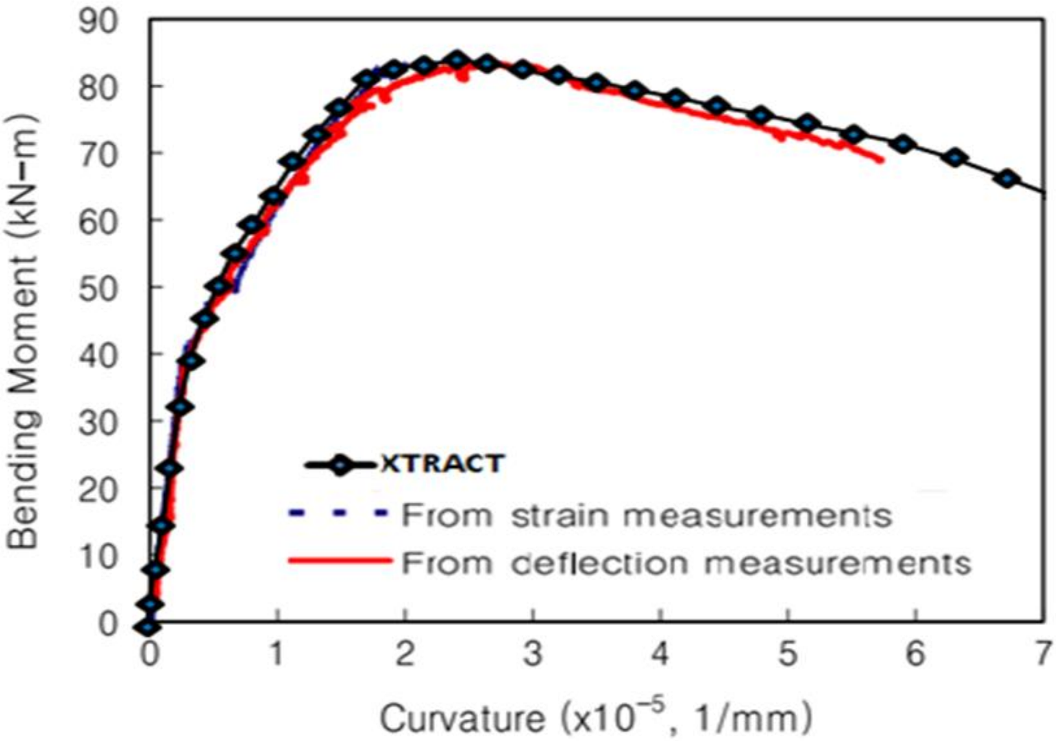

Figure E. 50:

Beam FR12-2 pushover curve analyzed by SAP2000.

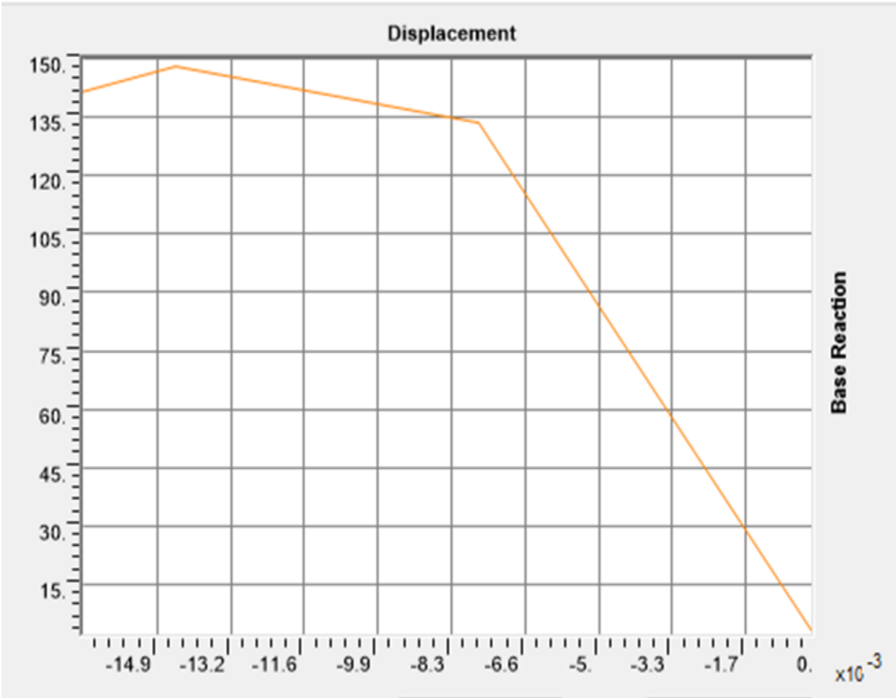

Figure E. 51:

The stiffness of column with different boundary conditions and α values (Priestley et al., 1996).

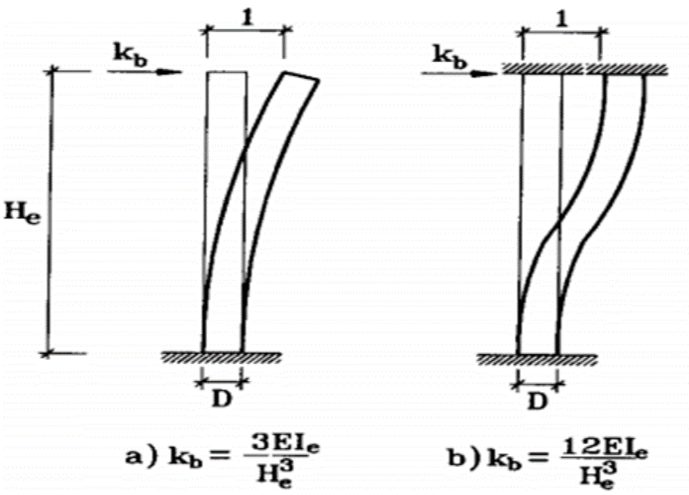

Figure E. 52:

Single story method to estimate the story stiffness (Vijayanarayanan et al., 2017).

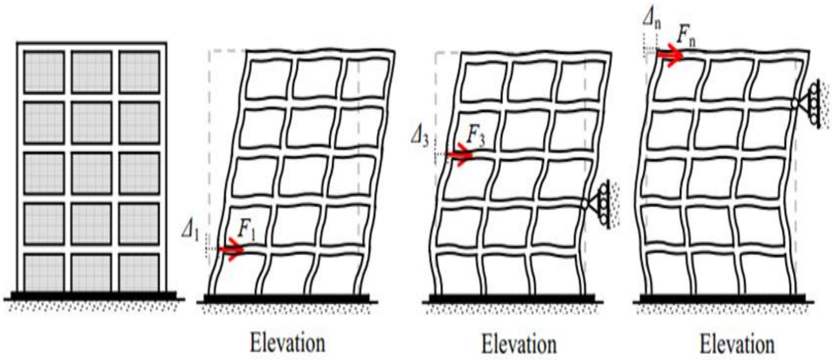

Figure E. 53:

Lateral force-deformation method to estimate the story stiffness (Vijayanarayanan et al., 2017).

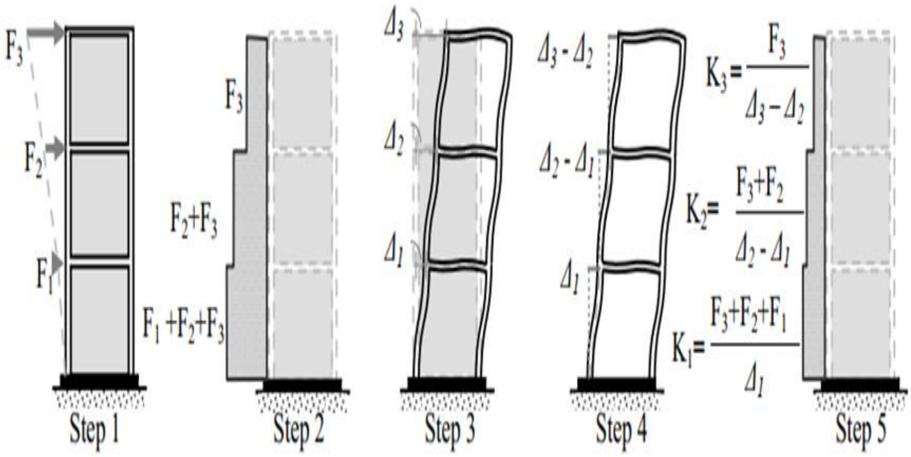

Figure E. 54:

Method to estimate the lateral strength for the individual story by pushover analysis (Murty et al., 2012).

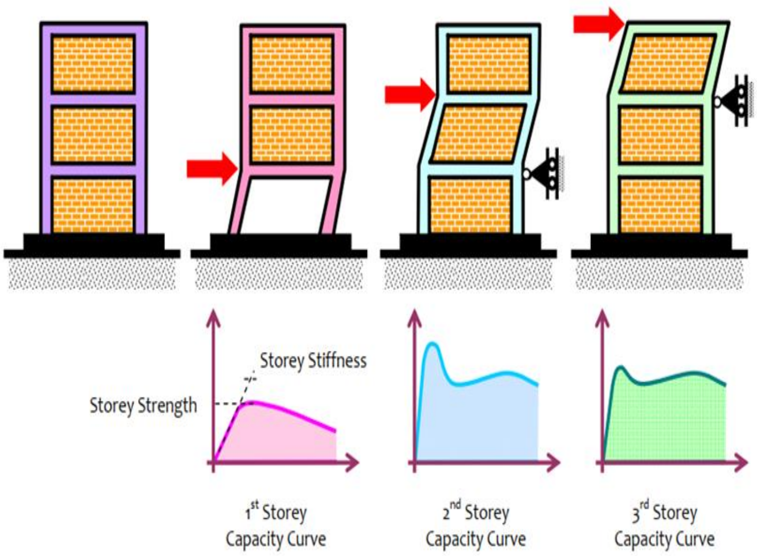

Figure E. 55:

The column internal forces and moment diagrams used in this method(Guevara et al., 2005).

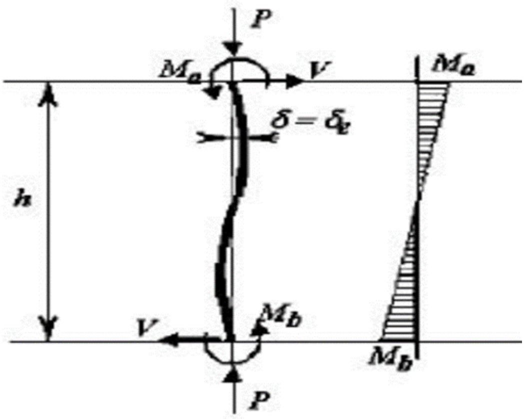

Figure E. 56:

The probable moment- plastic rotation of the interior columns from SAP2000.

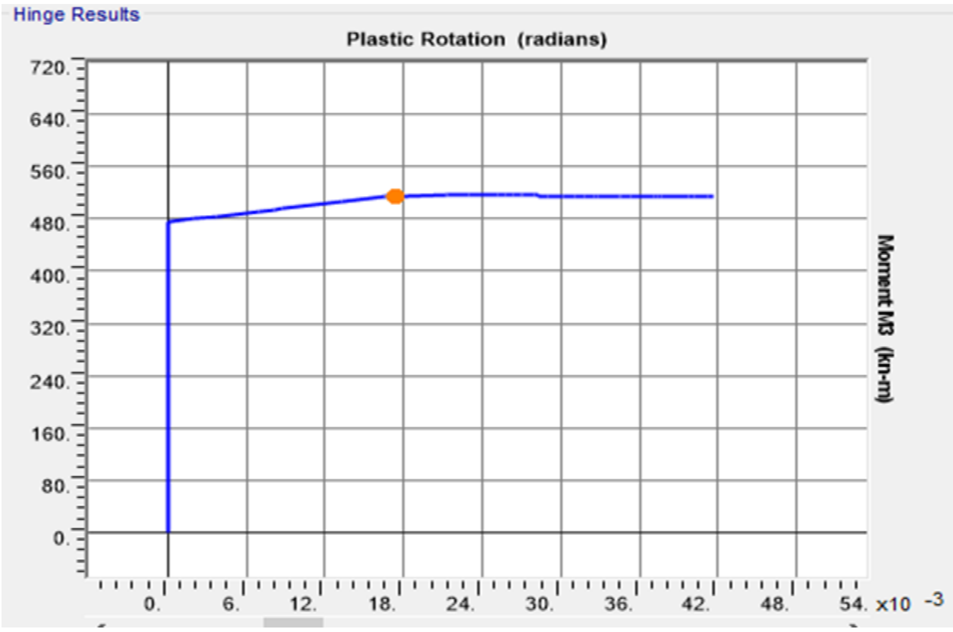

Figure E. 57:

P-Δ curve for the first story by SAP2000 pushover analysis.

Figure E. 58:

P-Δ curve for the second story by SAP2000 pushover analysis.

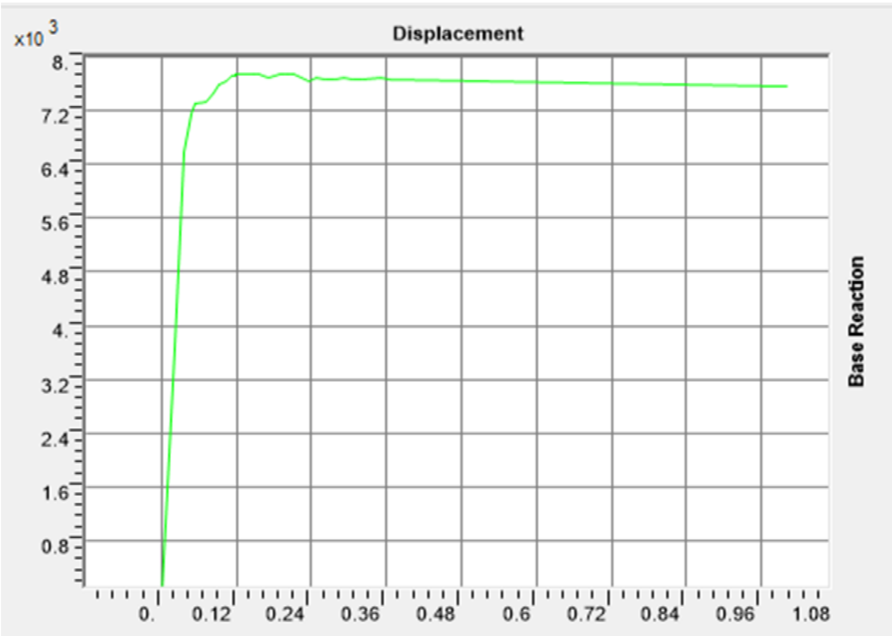

Figure E. 59:

P-Δ curve for the first story by SAP2000 pushover analysis with and without considering the P-delta effect.

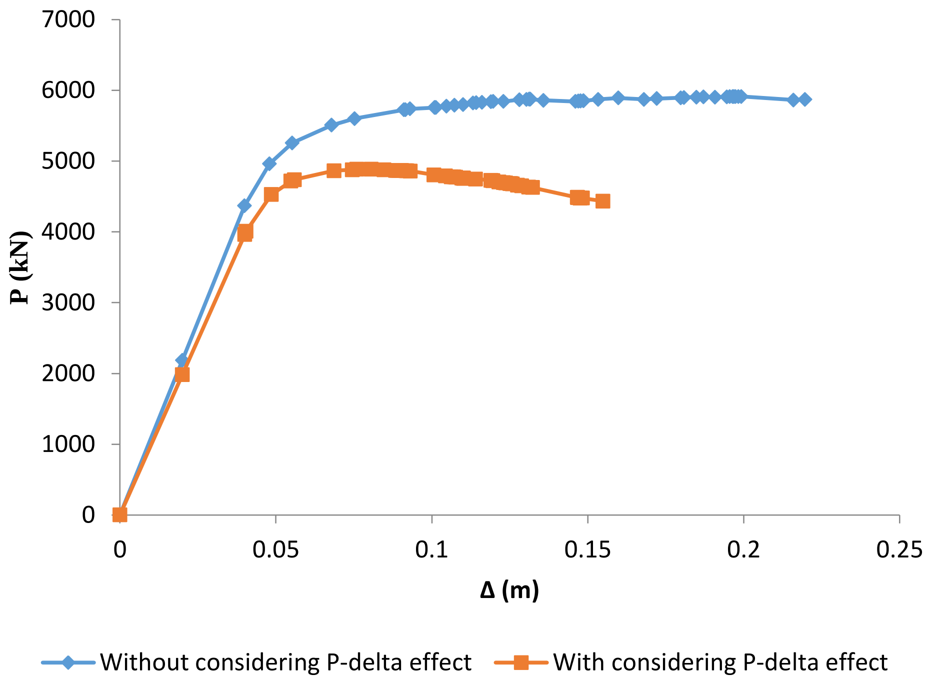

Figure E. 60:

The story's lateral displacement of the frame floors under a lateral pushover load by SAP2000 nonlinear static analysis.

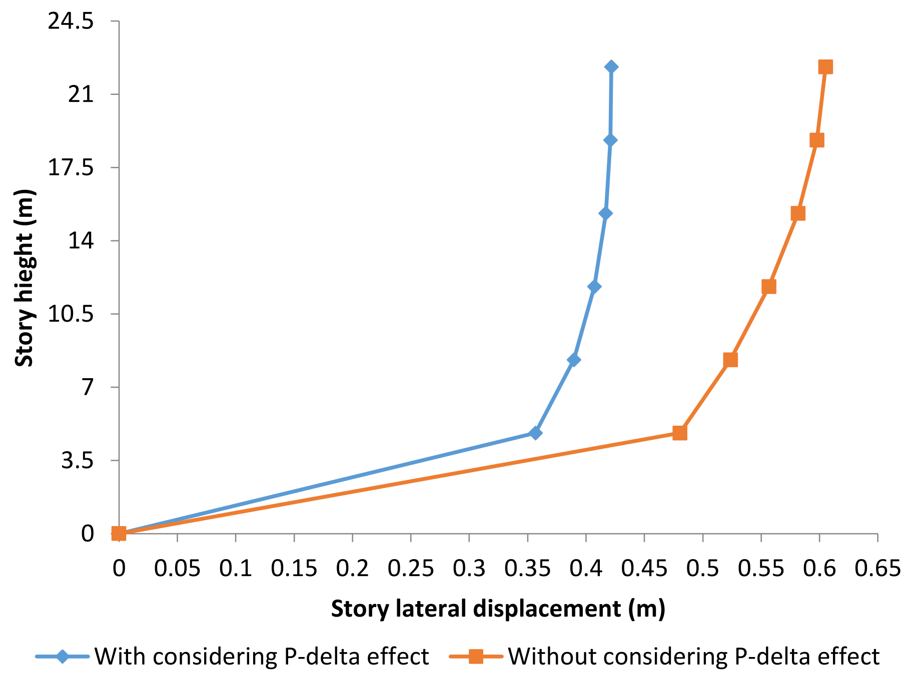

Figure E. 61:

P-Δ curve for the irregular frame with soft/weak story by SAP2000 pushover analysis.

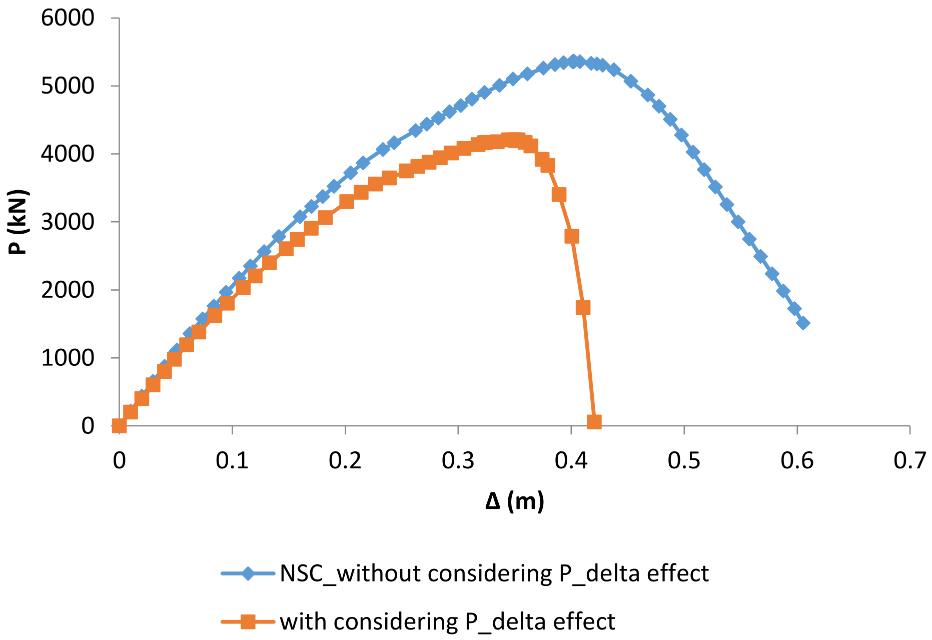

Figure E. 62:

P-Δ curve for the first story with UHPC columns from the pushover analysis SAP2000.

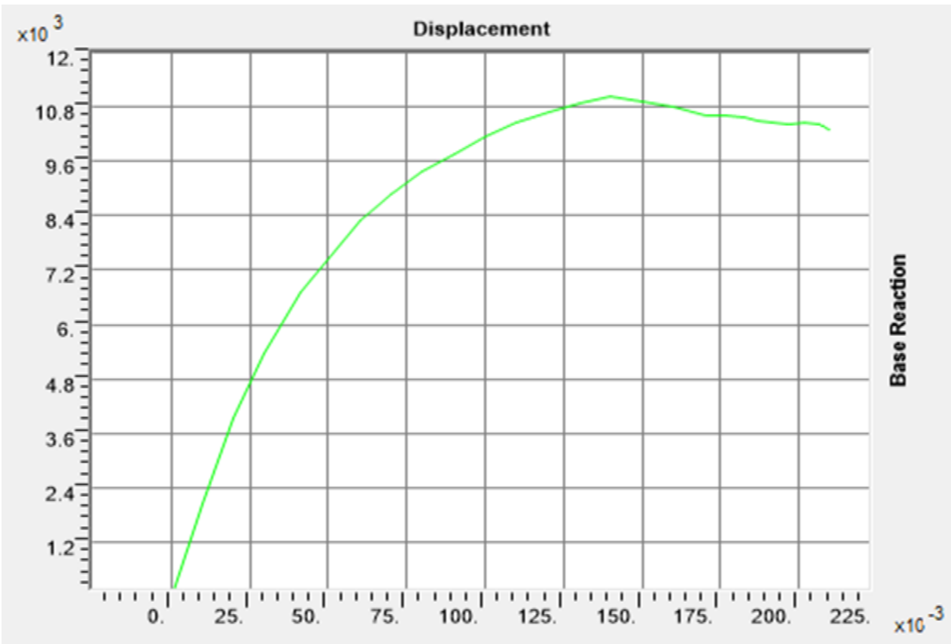

Figure E. 63:

The response spectrum force vertical distribution for the frame with NSC and for the frame with UHPC columns material in the first story.

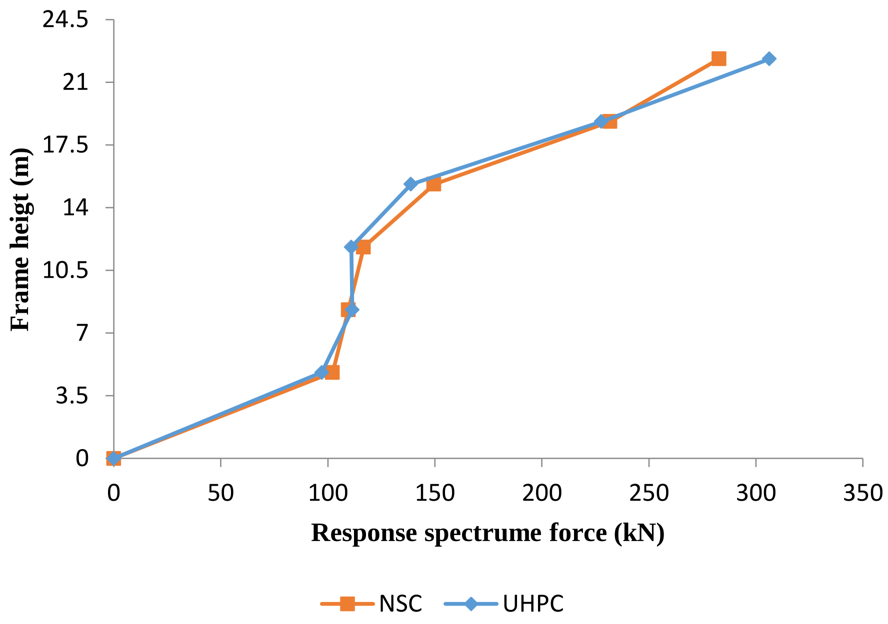

Figure E. 64:

P-Δ curve for the frame with NSC on the soft/weak story columns and with UHPC columns on the soft/weak story from SAP2000 pushover analysis.

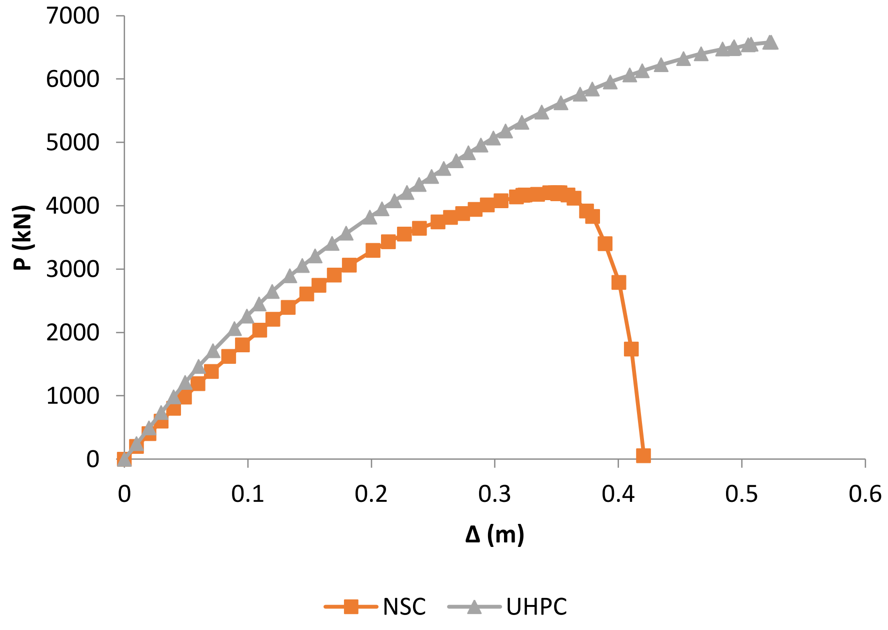

Figure E. 65:

ATC-40 capacity spectrum from SAP2000 analysis for: a) the frame with NSC on the soft/weak story columns. b) the frame with UHPC on the soft/weak story columns.

(a)

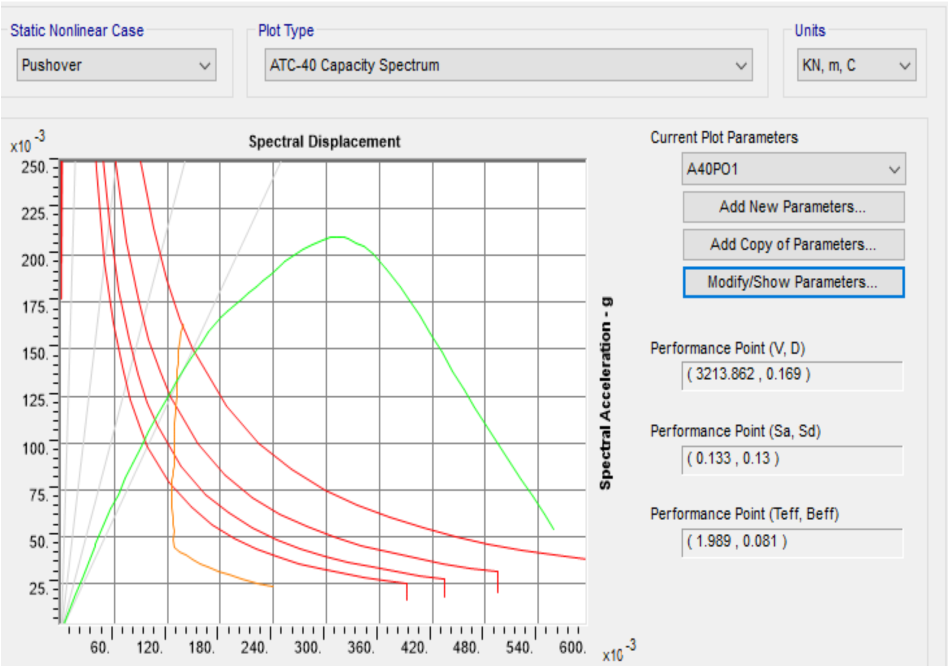

(b)

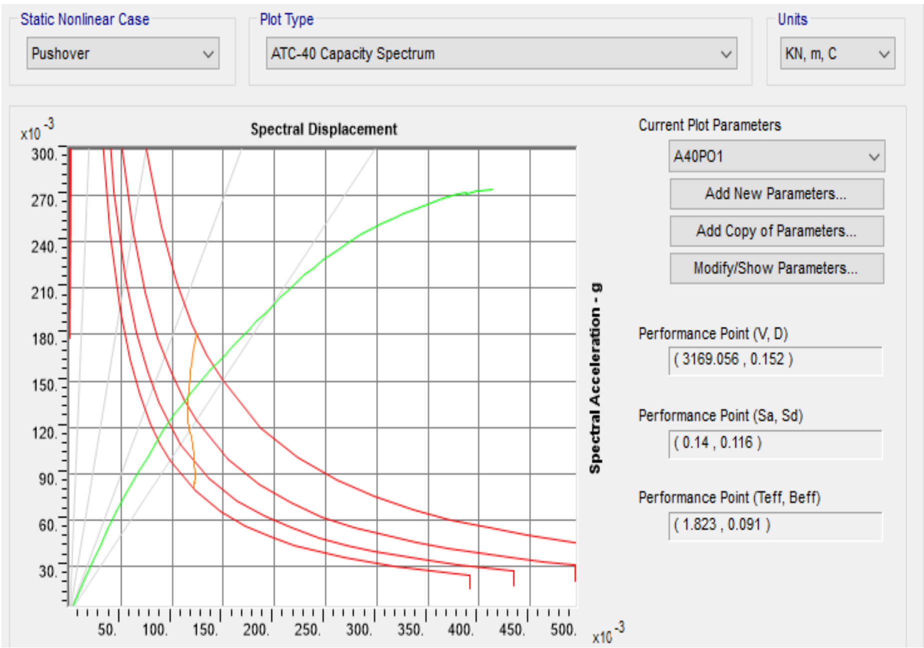

جامعة النجاح الوطنية

كلية الدراسات العليا

إستخدام الخرسانة الفائقة الأداء لمنع تشكل الطابق الرخو والطابق الضعيف في المباني ذات الأطر العزمية الخاصة

إعداد

علي محمد شراونة

إشراف

د. محمود دويكات

د. منذر دويكات

قدمت هذه الرسالة استكمالا لمتطلبات الحصول علي درجه الماجستير في هندسة الانشاءات، من كلية الدراسات العليا، في جامعة النجاح الوطنية، نابلس– فلسطين.

2022م

إستخدام الخرسانة الفائقة الأداء لمنع تشكل الطابق الرخو والطابق الضعيف في المباني ذات الأطر العزمية الخاصة

إعداد

علي محمد شراونة

إشراف

د. محمود دويكات

د. منذر دويكات

الملخص

المباني متعددة الطوابق منتشرة في فلسطين، وغالباً يتم بنائها بطابق ارضي مفتوح أو إرتفاعه أعلى من باقي الطوابق لأغراض تجارية، لذلك فان الطابق الرخو أو الضعيف قد يتشكل في الطابق الارضي، هذا البحث يهدف للتخلص من الطابق الرخو والضعيف في مرحلة التصميم بدون التأثير على المتطلبات المعمارية من خلال تغيير مادة الأعمدة من خرسانة عادية (NSC) إلى خرسانة فائقة الأداء (UHPC) في الطابق الرخو أو الضعيف.

لقياس مدى تأثير إستبدال المادة من الخرسانة العادية (NSC) إلى خرسانة فائقة الأداء (UHPC) على خصائص مقاطع الأعمدة، تم إنجاز دراسة بارامترية من خلال عمل تحليل مقطعي، بشكل عام 216 مقطع من أعمدة (NSC) و (UHPC) تم تحليلها تحت المتغيرات التالية : نسبة القوة المحورية، نسبة التسليح الطولي، عرض المقطع، نسبة العمق إلى العرض للمقطع.

تم دراسةّ فعالية إستخدام (UHPC) على صلابة الأعمدة (stiffness) حيث أن التغير في صلابة المرونة (flexural rigidity) تم تمثيلها من خلال صلابة المرونة الفعالة (EI_e) لأعمدة

(UHPC) نسبةً إلى أعمدة (NSC)، بالإضافة إلى ذلك تم التحقق من صحة إستخدام معاملات أعمدة (NSC) لتحليل المقاطع المتشققة لأعمدة (UHPC).

فعالية إستخدام (UHPC) غلى قوة الأعمدة (strength) تم قياسها بإستخدام نسبة العزوم أعمدة (UHPC) بالنسبة لأعمدة (NSC) تحت عدد من المتغيرات، بعد ذلك تم التحقق من قدرة الأعمدة على القص و وجد أن القوة الجانبية لأعمدة (UHPC) ما زالت محكومة بقوة العزوم.

علاوة على ذلك تم عمل تحليل إنحدار لنتائج الدراسة البارامترية من أجل عمل معادلات تتوقع الزيادة في صلابة (stiffness) وقوة الأعمدة (strength).

في النهاية، مبنى مكون من إطارات عزمية فراغية أستخدمت كحالة دراسية للتأكد من نتائج تحليل المقطع والتحقق من سلوك الإطار الكلي قبل وبعد إضافة (UHPC) في أعمدة الطابق الرخو والضعيف.الإطار تم تصميمه تبعاً لتعليمات ASCE7-16 and ACI318-19 يحتوي على طابق رخو بشدّة وطابق ضعيف في الطابق الأرضي. تحليل غير خطي إستاتيكي تم عمله على الإطار بإستخدام برنامج SAP2000. نتائج تحليل الإطار توافقت مع نتائج الدراسة البارامترية، بالإضافة إلى ذلك تصرف الإطار بشكل عام تحسن عندما تمّ إستخدام (UHPC) حيث أنّ الإزاحة والمفصل اللدن لم يتركز في الطابق الرخو أو الضعيف.

في الإجمال، إستبدال مادة الأعمدة في الطابق الرخو والضعيف من (NSC) إلى (UHPC) يمكن استخدامه من أجل التخلص بأمان من الطابق الرخو والضعيف في مراحل التصميم دون التغيير على القيود المعمارية أو الوظيفية.

الكلمات المفتاحية: عدم الإنتظام الرأسي، الصلابة (stiffness)، المقاومة، الطابق الرخو، الطابق الضعيف، صلابة المرونة، معادلات تحليل المقاطع المتشققة، الخرسانة فائثة الأداء (UHPC)، مفصل لدن، التحليل الغير خطي الإستاتيكي.